

University Library



MINERVA
ACCESS

A gateway to Melbourne's research publications

Minerva Access is the Institutional Repository of The University of Melbourne

Author/s:

YUNZAB, MOLIS

Title:

Receptive field properties and dynamics in mammalian primary visual cortex

Date:

2015

Persistent Link:

<http://hdl.handle.net/11343/55546>

File Description:

Receptive Field Properties and Dynamics in Mammalian Primary Visual Cortex

Receptive Field Properties and Dynamics in Mammalian Primary Visual Cortex

Molis Yunzab

Doctor of Philosophy

May 2015

Department of Optometry and Vision Sciences
University of Melbourne, Australia

and

National Vision Research Institute
Australian College of Optometry

*Submitted in total fulfilment of the requirements of the degree of
Doctor of Philosophy*

Abstract

The functional properties and structure of receptive fields in primary visual cortical (V1) neurons represent how visual information is processed in the mammalian neocortex. Cortical receptive fields are diverse and highly dynamic to accommodate the constantly changing visual environment. The mechanisms behind the organisation of different types of receptive fields are still highly debated after David Hubel and Torsten Wiesel first described the fundamental properties of cortical receptive fields half a century ago. These pivotal discoveries were conducted in the classic animal models of vision research: cats and monkeys. In recent years, fuelled by the opportunities for genetic and molecular manipulation, mice have rapidly become a major model for studying cortical visual processing. It is essential to recognise the similarities and differences between mouse V1 and that of the well-established animal models. A major goal in this thesis is to compare the receptive field properties of mouse V1 (area 17) and cat V1 (area 17 and 18).

Cortical neurons are largely composed of excitatory pyramidal cells and GABAergic inhibitory cells. Compared to excitatory neurons, the receptive field properties of inhibitory neurons are poorly understood due to the difficulty in identifying the diverse inhibitory subpopulations. In Chapter 4, by separating inhibitory and excitatory neurons based on their spike waveform shapes, I was able to examine the inhibitory receptive fields in both mouse and cat V1 and demonstrate differences in orientation selectivity and response linearity between these cell types in two species. In addition, I was also able to show that inhibitory cells were significantly over-represented in layer 1 of cat V1 and were less sensitive to low contrasts, as a population, compared to excitatory cells.

Based on receptive field structures and response properties, V1 neurons are classified into simple cells and complex cells. Simple cells are thought to have spatially segregated ON and OFF subfields and are thus highly selective for the

spatial phases of oriented edges. Complex cells have intermingled ON and OFF subfields and are largely phase-insensitive. Recent evidence reveals that some complex cells in cat and monkey V1 show increased phase sensitivity in their spiking activity as stimulus contrast is reduced, which suggests a shift towards a simple-like receptive field at low contrasts. By employing drifting sine-wave gratings (Chapter 5) and contrast-reversing gratings as visual stimuli (Chapter 6), I demonstrated the same effect in mouse V1 neurons. Furthermore, through intracellular recording I also observed contrast-dependent phase-sensitivity in the subthreshold membrane potentials of the cells as well as their spiking responses. This confirmed that the contrast-driven effect was a result of altered synaptic inputs and not the non-linear transformation from membrane potential to spike output.

Declaration

This is to certify that:

- this thesis comprises only my original work towards the PhD except where indicated in the preface,
- due acknowledgement has been made in the text to all other material used,
- this thesis is fewer than *100,000* words in length, exclusive of graphs, tables, bibliographies and footnotes.

Molis Yunzab

May, 2015

Preface

I performed all work involved in extracellular electrophysiological recordings from mouse cortex in Professor Michael Ibbotson's laboratory at the National Vision Research Institute (NVRI). I conducted all intracellular experiments on mouse cortex in the laboratory of Professor Nicholas Priebe at the University of Texas in Austin, U.S.

Experiments in cats were performed by a team of people over the course of 2007-2014 at the Australia National University (until early 2011) and the NVRI. I was directly involved in collecting data from fifteen cats during the period between 2010-2014, six of which were prior to my PhD candidature.

My period of study at The University of Texas in Austin was made possible through a generous scholarship I received from the NVRI (approved by the ACO Council) during the course of my PhD candidature.

Acknowledgements

First and foremost I want to express my deepest gratitude and sincere appreciation to my supervisor, Professor Michael Ibbotson. It has been an honour and pressure to be your PhD student. I have benefited tremendously from your advice and encouragement as a young scientist. Without your support and guidance, this thesis would not be a reality.

Secondly, I would like to extend my special appreciation and thanks to Professor Nicholas Priebe, Ben Scholl and the others from the University of Texas in Austin. Not only did Nicholas and Ben spend most of their valuable time during their visit to Melbourne in 2011 teaching me new experimental techniques, they and the others also welcomed me into their laboratory during my two-month stay in Austin, with the warmest hospitality. They graciously offered me their time, equipment and importantly their remarkable expertise.

I would also like to give special thanks to Dr Shaun Cloherty, Dr Markus Hietanen and Dr Hamish Meffin for their invaluable help with data analysis and experiments during my candidature. I am truly grateful for all of your support, especially your patience during crises such as ‘my Matlab code doesn’t run’ or ‘I hear radio instead of spikes’.

My gratitude also goes to my PhD advisory committee, Professor Trichur Vidyasagar, Professor Andrew Metha and Professor Bang Bui for your brilliant comments and suggestions. I want to specially thank Sagar, who generously lent me experimental equipment on many occasions.

To my colleagues at the National Vision Research Institute, Alex, Yu-Shan (Sherry), Matias, Josephine, Susmita and Priscilla, I appreciate every good conversation and bad joke. Thanks for making my candidature such an enjoyable experience.

To my family both in Australia and overseas, especially my wonderful parents, words cannot express how grateful I am to all of the sacrifices that you have made on my behalf. I am forever grateful for your unconditional love and support.

And finally, I would like to thank all my friends who supported me through my candidature. In particular, I want to thank Andrew Corson, my ‘partner in climb’, for proof reading part of my thesis and being a fantastic ‘adventure buddy’; and Imogen Stafford also for proof reading and for her ‘world’s most terrible’ greeting cards that always arrive to cheer me up when times are hard. I also want to thank Alice Brandli for proof reading and her brilliant suggestions. I am grateful for time spent with my friends, housemates, climbing and hiking buddies. Thank you all for the laughter and adventures - my life would not be as fulfilled and exciting without you.

Table of Contents

| | |
|---|------------|
| Abstract | i |
| Declaration | iii |
| Preface | iv |
| Acknowledgements | v |
| Chapter 1: General Introduction..... | 1 |
| 1.1 Thesis Outline..... | 2 |
| Chapter 2: Literature Review..... | 5 |
| 2.1 An overview of the visual system | 5 |
| 2.2 Cortical visual processing in the form of receptive field construction | 8 |
| 2.2.1 Receptive fields in the early visual pathway..... | 8 |
| 2.2.2 Receptive fields in V1 | 9 |
| 2.2.3 The mechanisms of receptive field formation in V1 | 10 |
| 2.2.3.1 The hierarchical model..... | 10 |
| 2.2.3.2 The parallel model..... | 14 |
| 2.2.3.3 Recurrent models | 15 |
| 2.2.3.4 New approaches for modelling V1 receptive field formation | 18 |
| 2.2.4 Classification of simple and complex cells..... | 20 |
| 2.3 The role of inhibition in cortical visual processing..... | 22 |
| 2.3.1 Identifying inhibitory cells <i>in vivo</i> | 22 |
| 2.3.2 Classification criteria for inhibitory cells | 23 |
| 2.3.2.1 Morphology | 23 |
| 2.3.2.2 Molecular | 23 |
| 2.3.2.3 Physiology | 26 |
| 2.3.2.4 Problems associated with classification of inhibitory cells..... | 27 |
| 2.4 Animal models in vision research | 28 |
| 2.4.1 The cat as a model for vision research | 28 |
| 2.4.2 A shift towards mouse vision | 29 |
| 2.4.3 The mouse as a model for vision research..... | 31 |
| 2.4.3.1 Retina | 31 |
| 2.4.3.2 Lateral Geniculate Nucleus (LGN) | 33 |
| 2.4.3.3 Primary visual cortex (V1)..... | 34 |

| | |
|---|-----------|
| 2.4.3.4 Concluding remarks on mouse as a vision research model | 40 |
| Chapter 3: General Methods..... | 41 |
| 3.1 Animal preparations..... | 41 |
| 3.1.1 Mouse..... | 41 |
| 3.1.2 Cat..... | 42 |
| 3.2 Surgical procedures | 42 |
| 3.2.1 Mouse..... | 42 |
| 3.2.2 Cat..... | 43 |
| 3.3 Extracellular recording and visual stimuli..... | 43 |
| 3.4 Intracellular recording and visual stimuli | 44 |
| Chapter 4: Receptive Field Properties of Inhibitory and Excitatory neurons in V1..... | 47 |
| 4.1 Abstract | 47 |
| 4.2 Introduction..... | 47 |
| 4.3 Methods | 49 |
| 4.3.1 Stimulus protocols | 49 |
| 4.3.2 Analysis of receptive field properties | 50 |
| 4.3.3 Histological reconstruction of recording sites..... | 51 |
| 4.4 Results..... | 52 |
| 4.4.1 Separating putative inhibitory and excitatory cells based on extracellular spike waveforms..... | 52 |
| 4.4.2 Receptive field properties of FS and RS cells..... | 58 |
| 4.4.2.1 Response linearity | 58 |
| 4.4.2.2 Orientation selectivity | 59 |
| 4.4.2.3 Spatial and temporal frequencies | 59 |
| 4.4.2.4 Laminar distribution of inhibitory and excitatory cells in cat V1..... | 64 |
| 4.4.2.5 Correlating contrast response functions and cell type..... | 66 |
| 4.5 Discussion..... | 70 |
| 4.5.1 Inhibitory cells play an important role in visual processing | 70 |
| 4.5.2 Identifying inhibitory cells <i>in vivo</i> | 71 |
| 4.5.3 Receptive field properties of FS and RS cells in mouse and cat V1..... | 74 |
| 4.5.3.1 Orientation selectivity | 75 |
| 4.5.3.2 Response linearity (simple and complex)..... | 76 |
| 4.5.3.3 Laminar locations | 78 |
| 4.5.3.4 Contrast response functions | 78 |
| 4.5.3.5 Discrepancy: a result of different recording electrodes? | 79 |

| | |
|--|----|
| 4.5.3.6 Preferred spatial and temporal frequencies | 80 |
| 4.5.4 Summary | 81 |

| | |
|---|------------|
| Chapter 5: Contrast-Dependent Phase-Sensitivity of V1 Complex Cells | |
| Tested by Drifting Gratings..... | 83 |
| 5.1 Abstract | 83 |
| 5.2 Introduction..... | 83 |
| 5.3 Methods | 85 |
| 5.3.1 Stimulus Protocol..... | 85 |
| 5.3.2 Analysis of extracellular spike responses | 86 |
| 5.3.3 Accommodating for increases in F_1/F_0 ratio resulting from reduced spike counts at low stimulus contrasts..... | 87 |
| 5.3.4 Two-photon imaging setup | 88 |
| 5.4 Results..... | 89 |
| 5.4.1 Measuring extracellular spiking responses of V1 neurons to drifting gratings at different stimulus contrasts | 89 |
| 5.4.1.1 Accommodating for spike number reduction at low contrasts | 94 |
| 5.4.1.2 Population analysis of contrast-dependent spiking responses | 98 |
| 5.4.2 Intracellular membrane potential responses of mouse V1 neurons to drifting gratings at different stimulus contrasts | 106 |
| 5.4.3 Morphologically identifying recorded neurons through intracellular labelling | 119 |
| 5.5 Discussion..... | 122 |
| 5.5.1 Contrast-dependent synaptic inputs of V1 neurons..... | 123 |
| 5.5.2 Laminar consideration of cell classes | 126 |
| 5.5.3 Stimulus-dependent receptive field formation..... | 127 |
| Chapter 6: Contrast-Dependent Phase-Sensitivity in V1 Complex Cells | |
| Tested by Contrast-Reversing Gratings..... | 133 |
| 6.1 Abstract | 133 |
| 6.2 Introduction..... | 133 |
| 6.3 Methods | 135 |
| 6.3.1 Stimulus protocol..... | 135 |
| 6.3.2 Analysis of extracellular spiking responses | 136 |
| 6.4 Results..... | 139 |
| 6.4.1 Extracellular spiking response to contrast-reversing gratings at different stimulus contrasts..... | 139 |

| | |
|---|------------|
| 6.4.2 Intracellular membrane potential responses to contrast-reversing gratings at different stimulus contrasts | 149 |
| 6.5 Discussion..... | 159 |
| 6.5.1 Why use contrast-reversing gratings as visual stimuli? | 159 |
| 6.5.2 Changes in spatial modulation depths of extracellular spiking responses at different stimulus contrast levels | 160 |
| 6.5.3 Membrane potential responses to contrast-reversing gratings..... | 162 |
| 6.5.4 Summary | 164 |
| Chapter 7: General Discussion..... | 167 |
| 7.1 Receptive field properties of inhibitory and excitatory neurons in V1... | 167 |
| 7.2 Contrast-dependent phase-sensitivity in V1 | 168 |
| References | 171 |

List of Figures

| | |
|--|-----|
| Figure 2.1. Laminar organisation and cell types of V1 | 7 |
| Figure 2.2. The hierarchical model of V1 receptive field construction | 12 |
| Figure 2.3. Alternative models for cortical processing | 17 |
| Figure 2.4. Cortical inhibitory subtype anatomy | 24 |
| Figure 2.5. Electrophysiological classes of cortical inhibitory neurons..... | 25 |
| Figure 2.6. Functional organisation of mammalian V1 | 38 |
| Figure 4.1. Separating FS and RS cells in mouse V1 | 54 |
| Figure 4.2. Separating FS and RS cells in cat V1 | 56 |
| Figure 4.3. Receptive field properties of FS and RS cells in mouse..... | 61 |
| Figure 4.4. Receptive field properties of FS and RS cells in cat | 62 |
| Figure 4.5. Layer distributions of FS and RS cells in cat V1..... | 65 |
| Figure 4.6. CRFs of FS and RS cells in mouse and cat V1 | 68 |
| Figure 5.1. Spiking responses to drifting gratings in mouse V1..... | 90 |
| Figure 5.2. Spiking responses to drifting gratings in cat V1..... | 92 |
| Figure 5.3. Accommodating spike number reduction effect at low contrasts..... | 96 |
| Figure 5.4. F_1/F_0 at low and high contrasts for mouse and cat V1 neurons..... | 100 |
| Figure 5.5. Accounting for sample size differences between mouse and cat data | 105 |
| Figure 5.6. Membrane potential responses of a mouse simple cell | 107 |
| Figure 5.7. Membrane potential responses to drifting gratings at different contrasts of three example cells | 108 |
| Figure 5.8. Membrane potential responses to drifting gratings at different contrasts | 112 |
| Figure 5.9. Fitting sine-waves to cycle-averaged membrane potentials | 114 |
| Table 5.1. A summary table of intracellular data (drifting gratings) | 116 |
| Figure 5.10. Membrane potential and spiking activity of intracellular responses to drifting gratings at different contrasts | 118 |
| Figure 5.11. Two-photon image of a Layer 2/3 basket cell in mouse V1 | 121 |

| | |
|--|-----|
| Figure 6.1. Spiking responses to contrast-reversing gratings at 100% contrast | 140 |
| Figure 6.2. Extracting peak modulation depths from period histograms | 142 |
| Figure 6.3. Contrast-dependent changes in a complex cell | 144 |
| Figure 6.4. Contrast-dependent changes in a simple cell | 146 |
| Figure 6.5. Changes in modulation depths from low to high contrast (population data) | 148 |
| Figure 6.6. Membrane potential responses in Layer 4 | 150 |
| Figure 6.7. Membrane potential responses in Layer 2/3 | 151 |
| Figure 6.8. Membrane potential responses in Layer 5 | 152 |
| Figure 6.9. Membrane potential responses at high and low contrasts | 155 |
| Figure 6.10. Fitting sine-waves to cycle-averaged membrane potentials | 157 |
| Table 6.1. A summary table of intracellular data test (contrast-reversing gratings) | 158 |

Chapter 1: General Introduction

Understanding how the brain processes visual information to generate the experience of sight is one of the most important and fundamental areas in neuroscience research. After all, most mammals, including humans, rely primarily on vision to assess their surrounding environment. The primary visual cortex is the first major centre for cortical processing in the visual system. It has been under intense investigation at both system and cellular levels since the pioneering work of David Hubel and Torsten Wiesel half a century ago. The receptive fields of neurons are the building blocks of visual processing in the primary visual cortex. The functional properties and structure of a receptive field represent how visual information is processed at the single cell level. Understanding the formation of different types of receptive fields is important to comprehend the computations taking places in the visual brain.

In their pivotal studies, Hubel and Wiesel (1962, 1968) described many fundamental properties of cortical receptive fields in cats and monkeys. Over the last fifty years, the ideas and concepts proposed by the pair have inspired much controversy within the field of cortical vision research. One of the most significant insights we have gained since is the recognition of the flexibility and diversity of cortical receptive field structures and properties. It has been clearly demonstrated by a substantial body of evidence that the receptive fields of mammalian cortical neurons are highly dynamic. That is, their structures and properties vary considerably to accommodate the constantly changing visual environment. Furthermore, it has been discovered that different cortical cell types exhibit distinct receptive field properties that reflect their computational functions.

Historically, cats and non-human primates, predominantly macaque monkeys, are the primary animal models for cortical vision research. However, fuelled by the abundant opportunities for genetic and molecular manipulation, the mouse is

fast becoming a popular model amongst visual neuroscientists. As a result, it is important to study mouse vision alongside the well-established animal models such as cats.

In this thesis, I examined and compared receptive field properties of neurons in mouse and cat primary visual cortex with various experimental approaches. I investigated the dynamic nature of receptive field structures under different visual stimulus conditions, as well as the receptive field properties of different neuronal cell types. Collectively the results revealed similarities, but also differences between the cat and mouse models. Overall the outcome of this thesis is in support of the mouse primary visual cortex being a suitable model for studying visual processing.

1.1 Thesis Outline

I will present my thesis in the form of a literature review, a general methods chapter, three results chapters and a general discussion chapter.

Chapter 2 reviews a selection of literature that investigates the receptive fields of the mammalian visual pathways. I will begin with a brief overview of the basic anatomical and physiological features of the mammalian visual system. I will then introduce the concept of the receptive field and discuss the validity of several proposed models for the construction of receptive fields in primary visual cortex. In the following section, I will review the receptive field properties of different neuronal cell types in primary visual cortex with the emphasis on inhibitory receptive fields and the problems associated with identifying inhibitory neurons during *in vivo* experiments. The chapter then concludes with a review of animal models used for cortical vision research with a focus on comparing the visual systems of mouse and cat.

Chapter 3 outlines the common experimental methods used for all subsequent results chapters. The chapter includes the anaesthetic and surgical preparations

used in mouse and cat, the extracellular and intracellular recording methods and the various visual stimuli used.

Experimental findings in the primary visual cortex are presented in Chapter 4 - 6. Below is a list of hypotheses that underpinned studies carried out in these chapters:

Chapter 4:

- Inhibitory and excitatory neurons could be identified based on the shape of their extracellular spiking waveforms.
- Inhibitory and excitatory neurons have different basic receptive field properties.
- Mouse and cat V1 neurons have different basic receptive field properties.

Chapter 5:

- Receptive field structures of some neurons in both mouse and cat V1 change according to contrast level of drifting sine-wave grating stimulus.
- Contrast-dependant response linearity could be observed in both extracellular and intracellular recorded responses in mouse V1.

Chapter 6:

- Contrast-reversing grating is a more suitable stimulus for examining changes to response linearity as it separates the influence of spatial and temporal phases.
- Contrast-dependant response linearity measured by contrast-reversing gratings could be observed in both extracellular and intracellular recorded responses in mouse V1.

Chapter 7 summarises the results presented in the preceding chapters in a general discussion. The opportunity is taken to discuss the similarities and differences between mouse V1 and that of other animal models, as well as to speculate upon the functional purposes and cortical mechanisms of contrast-dependent phase-sensitivity in some cortical complex cells.

Chapter 2: Literature Review

2.1 An overview of the visual system

Visual information processing begins with photoreceptors in the retina, which transduce energy from photons (light) into electrical signals (membrane potentials) (Hurley 1994, Lagnado & Baylor 1992). Visual information arising from photoreceptors is passed onto interneurons in the rest of the retina via chemical synapses (Obrien 1982, Wassle 2004). The final processing stage in the retina occurs as retinal ganglion cells assimilate the information from the preceding interneurons and send it along their axons in the form of action potentials (Kuffler 1953). The axons of the retinal ganglion cells, bundled with blood vessels, from the optic nerve. The main target in the brain for retinal signals is the dorsal lateral geniculate nucleus (dLGN) in the thalamus (Ling et al 1998). Although significant early processing occurs in both the retina and the dLGN, the emergence of advanced visual processing occurs in an area of the cerebral cortex known as the visual cortex.

The visual cortex is subdivided into different hierarchical areas. The area that receives the majority of the dLGN projection is the primary visual cortex, also known as V1 or striate cortex due to the stratified appearance of its layers (Rosa & Krubitzer 1999). The physiology of this region of visual cortex is the main concern of this thesis.

The primary visual cortex (henceforth referred to as V1) – in the same way as other areas of cerebral cortex – is organised into six distinct layers (Defelipe & Farinas 1992, Jones 1984, White 1989). As illustrated in Figure 2.1A, from the cortical surface downwards, the layers are identified as 1 to 6. The laminar structure of V1 allows localised processing by specific neuronal types and circuits within layers. Although overly simplified, it is helpful to conceptualise the dissemination of processing and the direction of information flow between

layers within V1 with regard to some general principles. Layer 4 is the geniculo-recipient layer; the projection from dLGN predominately terminates in this layer. From Layer 4, information is then sent into Layers 2/3 before it is then passed down into Layer 5 and Layer 6 (Gilbert & Wiesel 1979). Information leaves V1 from different layers depending on the destination. Feed-forward projections that pass information to other higher order visual cortical areas, predominately leave from Layers 2/3. Feedback projections, which transmit information to subcortical brain areas (dLGN and superior colliculus), originate from deeper layers, such as Layer 5 and Layer 6 (Jones & Wise 1977, Rockland & Pandya 1979). Along the visual pathway, visual information is processed and transformed at each ‘relay cell’ before it is passed on to other nuclei or areas.

The most basic elements of the cortex consist of two general types of neurons: pyramidal neurons and interneurons (or non-pyramidal neurons). Pyramidal neurons are the more common types of neurons in the cortex. Morphologically, they are characterised by a triangular soma, a long axon that leaves the cortex through the white matter, a large single apical dendrite extending from the apex of the soma towards the surface of the cortex, and an array of basal dendrites spread laterally from the soma and ending in the same layer (Elston et al 1997) (Figure 2.1B). Pyramidal neurons are universally excitatory in nature due to the types of neurotransmitters they release, which is most commonly glutamate. Pyramidal neurons are found in all cortical layers except Layer 1 and they are believed to be responsible for long-range intra-cortical and inter-cortical projections (Fitzpatrick 1996, Gilbert & Wiesel 1979).

Interneurons comprise the rest of the neurons in the cortex. They are mainly inhibitory in nature with the majority of the population releasing γ -Aminobutyric acid (GABA) as their neurotransmitter (Obrien 1982). However it should be mentioned that the spiny stellate cells in Layer 4 are excitatory interneuron (DeFelipe 2002). Compared to pyramidal neurons, interneurons are extremely diverse in their morphology. This significant characteristic will be discussed in detail later in the chapter. Despite the diversity, a general feature remains constant amongst the interneuron population: the axons and dendrites

of interneurons do not extend beyond the immediate vicinity of their cell bodies, which strongly suggests that interneurons have a restricted local influence (DeFelipe 2002). Figure 2.1C shows an example drawing of a Chandelier cell, which represents one of the many subtypes of interneuron.

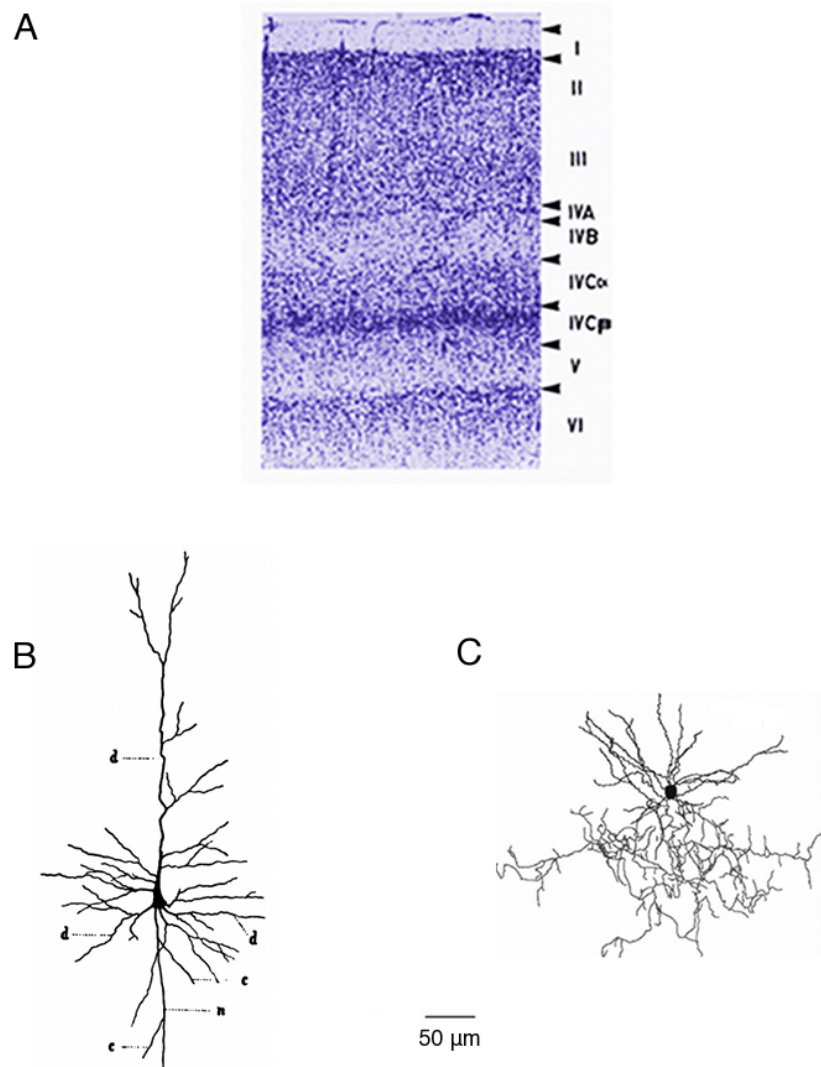


Figure 2.1. Laminar organisation and cell types of V1

A, The laminar organisation of the macaque primary visual cortex shown as a Nissl stain. The primary visual cortex is a six-layered structure (I-VI). Layer IV is further subdivided into sublayers. It is noteworthy that macaque V1 has special features compared to rodent and carnivore V1. For example, macaque Layer 4B does not receive thalamic inputs. Adapted from Lund (1973) with permission from John Wiley and Sons. **B**, A drawing of a pyramidal neuron. From 'Atlas and Epitome of Human Histology and Microscopic Anatomy' by J. Sobotta (1903), sourced from Public Domain US, which is a collection of works with expired copyright. **C**, A drawing of a GABAergic interneuron. From Woodruff and Yuste (2008), open access.

2.2 Cortical visual processing in the form of receptive field construction

2.2.1 Receptive fields in the early visual pathway

The term receptive field was introduced in the visual system over 70 years ago to describe the region of the retina where a change in stimulus brightness alters the firing rate of a retinal ganglion cell (Hartline 1938). Thus, in its narrowest sense, the receptive field simply represents a spatial location amongst sensory receptors. Nowadays the term is used as a broad concept; it generally refers to structures or substructures within a region of sensory space that when stimulated generates responses in a chosen sensory neuron (Bair 2005, Hirsch & Martinez 2006, Martinez 2006).

Receptive fields are universally present in all sensory systems. In the visual system, neurons along the visual pathway can be characterised by their receptive field structures. In the retina, the receptive field structures of ganglion cells were first described by Kuffler (1953) and Barlow (1953) as circular in shape and had two distinct subfields, centre and surround, which have opposite preferences for stimulus polarity. If we consider only the geometry of their receptive fields, retinal ganglion cells can be classified into two groups: one group is excited by bright stimuli in the centre and dark stimuli in the surround (ON cell) and the other group responds to dark stimuli in the centre and bright stimuli in the surround (OFF cell) (Barlow 1953, Hubel & Wiesel 1961). Both subfields are also inhibited by the reciprocal polarity that excites them; this is known as the ‘push-pull’ response.

In the thalamus, dLGN (henceforth referred to as LGN for simplicity) cells that receive input from retinal ganglion cell projections inherit the same centre-surround receptive field structures from the ganglion cells (Figure 2.2A, example a and b are receptive fields for ON and OFF LGN cells, respectively). The geometry of a receptive field can directly account for the spatial response profile of a neuron. For instance, retinal ganglion and LGN cells show minimal changes in their response to uniform stimulus patterns that span their entire receptive

fields. However, they are very sensitive to local changes in stimulus brightness (Barlow & Levick 1976, Hubel & Wiesel 1961, Kuffler 1953).

2.2.2 Receptive fields in V1

Hubel and Wiesel (1959, 1962) were the first to map the receptive field structures of V1 neurons. They discovered that the centre-surround receptive field geometry of retinal and LGN cells was transformed into a variety of different receptive-field structures within V1. These new receptive field characteristics are referred to as ‘cortical emergent properties’. Based on their receptive field structures, Hubel and Wiesel classified V1 neurons into two main groups: simple cells and complex cells. The fundamental difference between receptive field structures of simple and complex cells is the spatial arrangements of ON and OFF subfields. The ON subfield responds to brightness increments, whereas the OFF subfield responds to brightness decrements. Hubel and Wiesel observed that, similar to neurons in the early visual pathway, simple cells had spatially segregated subfields (Figure 2.2A, c - g). Unlike the centre-surround arrangement, the ON and OFF subfields of simple cells were elongated and parallel to each other. On the other hand, complex cells were defined by exclusion. A cell was categorised as a complex cell if it lacked spatially discrete subfields. When mapped, the ON and OFF subfields of complex cells were largely intermingled.

Similar to ganglion and LGN cells, the spatial arrangements of ON and OFF subfields directly resulted in the specific response properties of V1 neurons. For example, the elongated but parallel configuration of the antagonistic ON and OFF subfields of simple cells correlates with the emergence of selectivity for stimulus orientation (Hubel & Wiesel 1968, Hubel & Wiesel 1962). When receptive fields of neurons along the visual pathway were first described, neurons in the retina or LGN did not appear to show response bias towards the specific orientations of edges. In contrast, Hubel and Wiesel (1962) witnessed V1 simple cells responding vigorously to a bright or dark bar moving parallel to the long axis of the polarity-matching subfields, whilst showing no or minimal response when

the bar was moving in any other orientations. Remarkably, complex cells, which had largely circular and overlapped ON and OFF subfields, were also observed to show strong orientation selectivity. The fact that the preferred orientation of a complex cell could not be predicted by the geometry of its receptive field structure suggests that its orientation selectivity might be inherited from its presynaptic cells.

2.2.3 The mechanisms of receptive field formation in V1

2.2.3.1 *The hierarchical model*

The difference in functional response properties between neurons with distinct receptive field structures prompted Hubel and Wiesel (1962) to speculate the mechanism behind the formation of receptive fields along the visual pathway. They proposed the idea of a hierarchical model for receptive field construction based on the feed-forward direction of information flow in the visual pathway. It assumes that simple and complex cells represent two distinct stages of V1 cortical processing. Each subfield of a simple cell is assembled from convergent projections from LGN cells with corresponding polarities, which are aligned in visual space along the long axis of the simple cell subfield (Figure 2.2B). Spatially offset simple cells with similar orientation preferences will in turn converge and form the receptive field of a complex cell (Figure 2.2C).

The arrangement of LGN inputs to a simple receptive field, as suggested by Hubel and Wiesel, potentially, allows for the emergence of orientation selectivity. For instance, a bar of light moving parallel to the long axis of the ON subfield will be simultaneously activated by all presynaptic LGN ON-centre cells, so the strong excitatory inputs will depolarise the simple cell and cause it to spike. If the bar is moving at an angle to the ON subfield, only a subset of presynaptic LGN cells will be activated at any moment in time and the combined excitatory input might not be strong enough to depolarise the simple cell above spike threshold. Here the proposed model assumes that simple cell responses are created through linear summation. The segregation of ON and OFF regions in a simple cell ensures that at any given location in its receptive field, a simple cell will be either excited or

inhibited by the same stimulus polarity but not both. As a result, the spike output of a simple cell is the linear sum of all inputs from their presynaptic LGN cells. On the other hand, complex cells can be described as the non-linear rectification stage of processing. The presentation of an oriented stimulus at any given location in a complex receptive field is likely to elicit a mixture of synaptic inputs from its presynaptic simple cells with possibly overlapping ON and OFF subfields, which means the spike threshold of the complex cell is required to filter out the weak synaptic inputs received from non-optimally tuned simple cells.

The proposed model provides a possible mechanism for the emergence of orientation selectivity in simple cells from non-selective LGN inputs, as well as the observed orientation selectivity that is independent of their receptive field arrangements in complex cells. This was the first theory to reconcile the structure of receptive fields with the functional properties of neurons at various stages of visual processing.

Five decades after Hubel and Wiesel (1962) first proposed the idea of a hierarchical model, the concept is far from being out dated and has evolved into a substantial model with a considerable amount of support from a combination of morphological and physiological data. Several lines of evidence support the existence of direct synaptic and functional connections between LGN relay cells and simple cells.

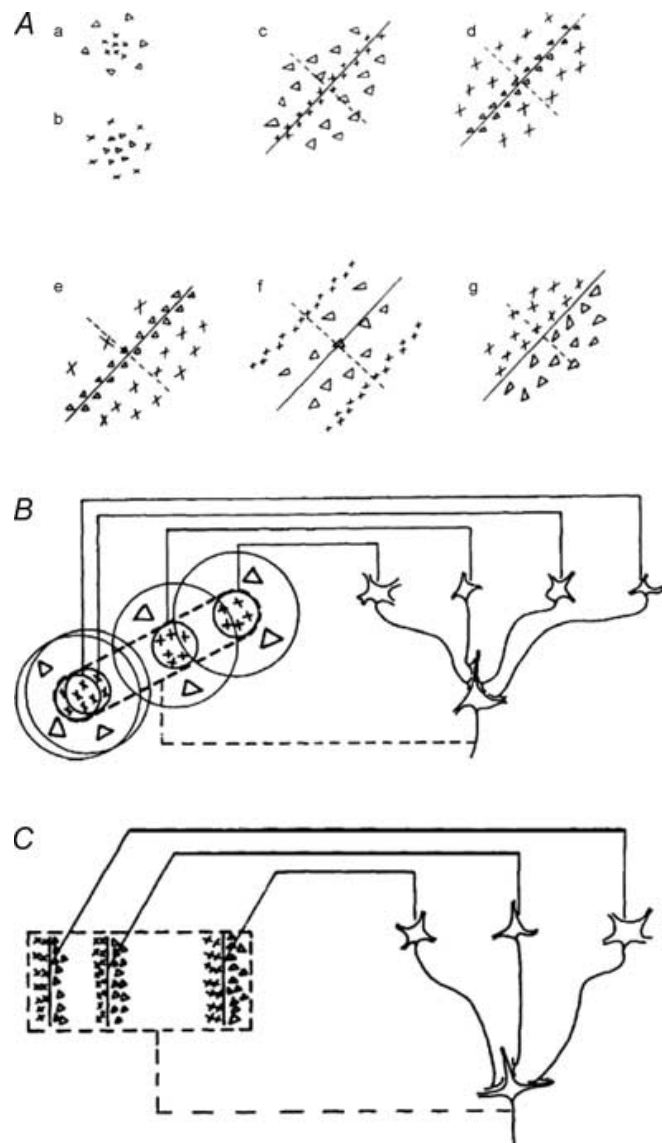


Figure 2.2. The hierarchical model of V1 receptive field construction

The classical hierarchical model of the construction of simple and complex receptive fields proposed by Hubel and Weisel (1962). **A**, LGN cells (ON-centre LGN cells (a); OFF-centre LGN cells (b)) have centre-surround receptive field structures and simple cells (c – g) have segregated ON and OFF subfields. **B** and **C**, The hierarchical model of simple and complex receptive fields. **B**, elongated and segregated ON and OFF subfields of a simple cell were constructed by the convergence of LGN receptive fields that are aligned in space. **C**, A complex receptive field is in turn built by the convergence of several simple cells. Adapted from Hubel and Weisel (1962) with permission from John Wiley and Sons.

Firstly, it has been demonstrated that geniculo-recipient layers (Layer 4 and upper Layer 6) are populated predominately by simple cells in cat and monkey V1 (Crowder et al 2007, Gilbert 1977, Gilbert & Wiesel 1979, Hirsch et al 1998a, Hirsch et al 1998b, Kelly & Vanessen 1974, Martinez et al 2002, Martinez et al 2005, Ringach et al 2002). Secondly, paired recordings from LGN and simple cells show synaptic connections from the former to the latter with overlapping receptive fields of the same polarity. In addition, the strength of the synaptic connectivity was correlated to the degree of overlap of their receptive fields (Reid & Alonso 1995, Tanaka 1983). Using a similar experimental concept but using more advanced paired multi-electrode recordings of LGN and cortex, a recent study demonstrated that a group of LGN cells with overlapping receptive fields projected to a single orientation column in the cortex to form a simple-like receptive field that was parallel to the column's preferred orientation (Jin et al 2011). Thirdly, electrical stimulation of the LGN, coupled with intracellular measurement of excitatory post synaptic potential (EPSP) latency in a simple cell revealed substantial monosynaptic excitation from LGN cells to Layer 4 simple cells (Ferster & Lindstrom 1983, Martin & Whitteridge 1984a). Further confirmation came from a study that pharmacologically silenced cortical cells and recorded from LGN cells with axons terminating within the corresponding areas of Layer 4. It was demonstrated that the receptive fields of LGN cells aligned parallel to the preferred orientation of the silenced cortical cells that had been recorded prior to the silencing (Chapman & Stryker 1991).

The second stage of the hierarchy, in which a complex cell integrates synaptic inputs from a subset of spatially offset simple cells, also received substantial experimental support. Firstly, morphological studies showed that the majority of Layer 4 simple cells project to the superficial layers where complex cells are over-represented (Gilbert & Wiesel 1979, Hirsch et al 1998b, Martin & Whitteridge 1984b, Martinez et al 2002). Secondly, spike-triggered averaging of pair-recorded simple and complex cells showed direct excitatory connections (Alonso & Martinez 1998). Thirdly, pharmacologically silencing simple cells *in vivo* also silences complex cells (Martinez & Alonso 2001).

The above experimental evidence builds a strong and convincing case for a hierarchical model of cortical visual processing. Nonetheless, since Hubel and Wiesel's (1962) proposal, evidence-based scepticism of the model has always existed alongside support for the theory. In the following few paragraphs, I will discuss these criticisms in association with alternative models proposed to reconcile some major flaws of the hierarchical model.

2.2.3.2 The parallel model

The first strong case to argue against the hierarchical model was the discovery of direct synaptic connections between LGN relay cells and cortical complex cells (Bullier & Henry 1979, Ferster & Lindstrom 1983, Hoffmann & Stone 1971, Martin & Whitteridge 1984a). Inspired by this observation and the fact that simple cells also receive direct LGN inputs, Hoffman and Stone (1971) proposed an alternative model hypothesising that receptive fields of simple and complex cells were generated in parallel by separated thalamo-cortical pathways (Figure 2.3A). It was already known that both linear (X-cells) and non-linear (Y-cells) cells existed within LGN and the two cell types receive inputs from two separate but parallel channels in the retina (Shapley & Hochstein 1975). Therefore, it was speculated that simple cells and complex cells were convergent cortical targets of X- and Y- channels, respectively (Hoffmann & Stone 1971, Stone et al 1979).

There was some experimental evidence supporting this theory. Firstly, it was shown that some complex cells seemed to respond to visual stimuli that did not drive simple cells (1977, Hammond & Mackay 1975). Secondly, few studies recorded normal responses in Layer 2/3 complex cells when Layer 4 simple cells were pharmacologically inactivated (Malpeli 1983, Mignard & Malpeli 1991). Interestingly, in cats the superficial complex cells were only affected when inactivation of LGN relay cells were combined with large lesions in area 18 of cat cortex, which receives predominantly Y-cell input (Mignard & Malpeli 1991). This finding suggests a complicated pathway for inputs to area 18 of cat cortex (part of their primary visual cortex). In contrast, a large number of studies have either failed to observe a clear separation of the X and Y parallel pathways

(Bullier & Henry 1979, Ferster & Lindstrom 1983, Martin & Whitteridge 1984a, Singer et al 1975, Tanaka 1983), or have claimed that the impact of the Y pathway was rather weak in V1 (Burke et al 1992, Ferster 1990a, Ferster 1990b, Spitzer & Hochstein 1987).

Overall, the evidence suggests that it is unlikely that simple and complex responses are generated from two completely independent parallel thalamo-cortical pathways. Nevertheless, the notion that some complex receptive fields might be constructed, at least in part, by direct LGN inputs is likely to be true.

2.2.3.3 Recurrent models

Perhaps the strongest argument against the hierarchical model comes from the natural architecture of cortical circuits themselves. The hierarchical model is also referred to as the feed-forward model due to the fact that it only addresses the feed-forward thalamo-cortical and cortical-cortical connections. However, LGN input only constitutes a small proportion of the total synaptic input of a cortical cell. In fact, the majority of synapses on a cortical cell, regardless of functional cell type, are of cortical origin (Ahmed et al 1994, Callaway 1998, Fitzpatrick 1996, Kisvarday et al 1986, Levay & Gilbert 1976, Peters & Payne 1993).

An alternative type of model that accommodates the strong cortical contribution to the synaptic inputs of cortical neurons has gained considerable popularity over the years. These models, collectively known as recurrent models, speculated that simple and complex cells largely share the same basic feed-forward excitatory circuitry. The difference between the two cell types comes from the strength and integrative properties of recurrent cortical-cortical inputs (Chance et al 1999, Debanne et al 1998, Douglas et al 1995, Tao et al 2004, Wielaard et al 2001, Zhu et al 2009) (Figure 2.3B).

Several lines of strong evidence support recurrent models. First of all, early studies have demonstrated that experimental manipulation of recurrent

excitatory and inhibitory inputs could generate pronounced changes in cortical receptive field structures and response properties. Chance et al (1999) demonstrated differential response properties of a V1 neuron when its intra-cortical inputs were manipulated. Strikingly, a cell showed simple-like responses when its recurrent excitation was weak, whereas strong, nonlinear excitatory recurrent inputs resulted in complex-like responses from the same cell. In addition, elimination of cortical inhibitory inputs can result in the loss of orientation selectivity (Rivadulla et al 2001, Sillito 1975, Tsumoto et al 1979), as well as the loss of spatial segregation in simple cell receptive fields (Nelson et al 1994a, Sillito 1975). Secondly, not only are recurrent models a more representative description of realistic neuronal network connections, they also offer a possible resolution for experimental data that cannot be accounted for by feed-forward models. For instance, an outstanding response feature of simple cells is their contrast-invariant orientation tuning, which refers to the observation that the orientation tuning width of a cell does not change with the contrast of the stimulus (Sclar & Freeman 1982, Skottun et al 1987). The hierarchical model could not explain the mechanism behind this response feature, as it predicts a broadening of tuning width with increasing stimulus contrast. This is caused by the increasing LGN input from non-preferred orientations, which results from the increase in overall response strength of all presynaptic LGN cells (Cheng et al 1995). The recurrent model, which proposes a weak feed-forward thalamo-cortical orientation bias, which is subsequently sharpened by recurrent excitation and inhibition from neighbouring cortical neurons, can account for the contrast-invariance of simple cell orientation tuning (Benyishai et al 1995, Carandini & Ringach 1997, Douglas et al 1995, Somers et al 1995) (Figure 2.3B).

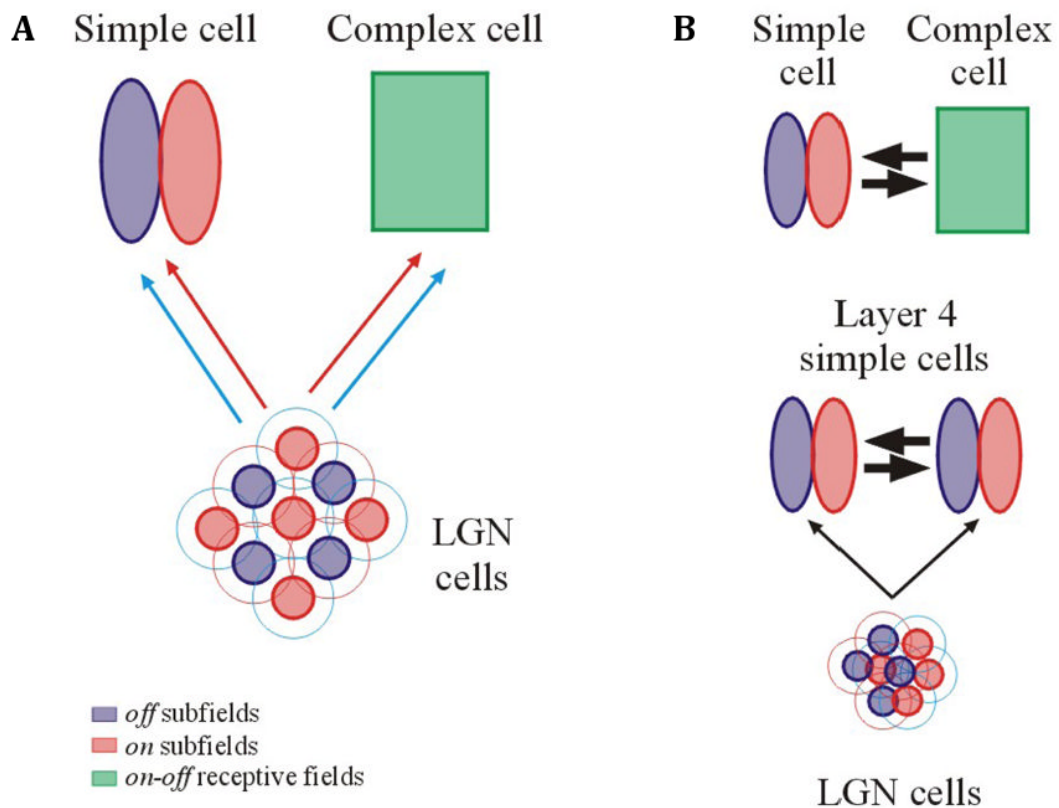


Figure 2.3. Alternative models for cortical processing

General concepts of alternative models to the classic hierarchical model. **A**, Parallel model: simple and complex receptive fields are generated in parallel by different thalamo-cortical pathways. **B**, Recurrent models: simple and complex cells obtain their receptive field from weak thalamic inputs and strong recurrent cortico-cortical inputs. Several versions of recurrent models exist based on different experimental evidence. The two versions illustrated in this feature are the Layer 4 simple-simple recurrent model (Douglas & Martin 1991) and Layers 2/3 simple-complex recurrent model (Chance et al 1999, Debanne et al 1998). From Martinez and Alonso (2003) with permission from Sage Publishing.

Similar to other models, the recurrent model also endures criticism. For instance, its assumption of weak LGN inputs based solely on the number of synaptic contacts is thought to be unrealistic by some authors (Alonso et al 2001, Gil et al 1999, Martinez & Alonso 2003, Martinez & Alonso 2001). In addition, several cortical inactivation experiments failed to observe the effects on cortical response properties that were predicted by the recurrent model (Chung & Ferster 1998, Ferster et al 1996).

2.2.3.4 New approaches for modelling V1 receptive field formation

It is obvious that the three cortical processing models discussed above all have their own strengths and weaknesses. No one model to date can comprehensively account for all response features of cortical neurons. This comes as no surprise as the brain is a highly dynamic and non-homogenous system. Over the years, it has become clear that each model can no longer be considered in isolation.

Instead of building the simplest possible model accounting only for a few features of the system, approaches shifted towards trading simplicity for the ability to explain more experimental data with an integrated model that combines and modifies existing models. This approach seems to be better at representing the complex nature of cortical processing. For instance, by comparing various versions of feed-forward and recurrent models, Teich and Qian (2006) proposed a model, called the Modified Recurrent Model, which claims to provide the best explanation for most data on orientation plasticity in both simple and complex cells. This model adopted a modified version of the feed-forward model to explain simple cell behaviour, in which the orientation selectivity is mainly generated by feed-forward thalamo-cortical inputs but the contrast invariance is maintained by cortical inhibition. The recurrent model, with its inhibition-dominance, was thought to be suitable to explain complex cell orientation tuning.

This general model framework is supported by another study that showed that the best model to explain the development of functional maps in V1 is a strong

feed-forward and weak recurrent integration in simple-cell dominant Layer 4, while the complex-cell dominant Layer 2/3 has strong lateral inputs but very little thalamic input (Antolik & Bednar 2011). In addition, Antolik and Bednar's model also comprises another essential element, which is the feedback connectivity from Layer 2/3 to Layer 4 that ensures the development of matching maps across the cortex. The feedback pathway, which is seen throughout the neocortex (Alitto & Usrey 2003, Binzegger et al 2004), also adds another layer of complexity to modelling cortical processing.

Overall, it is clear that reaching a consensus in modelling cortical processing based on anatomical and physiological data is difficult. However, after years of debate and controversy, there are several main elements in various models that have stood the test of time. With these elements a general framework for cortical processing can largely be agreed upon. The idea of a two stage processing system proposed in the hierarchical model seems to be highly viable (Hubel & Wiesel 1962). In the first stage, the feed-forward convergence of LGN inputs is responsible for Layer 4 simple cell receptive field formation, with limited local recurrent inputs modulating and maintaining response linearity and orientation tuning (Cossell et al 2015, Tao et al 2004, Troyer et al 1998). The second stage happens in Layer 2/3 complex cells where receptive field structures are mainly shaped by intracortical inputs with some feed-forward influence from Layer 4 (Chance et al 1999, Debanne et al 1998, Teich & Qian 2006). In parallel, the receptive field of a small subpopulation of complex cells are created mainly from direct LGN inputs (Mel et al 1998, Spitzer & Hochstein 1987, Tao et al 2004).

Nonetheless, fifty years since Hubel and Weisel proposed the hierarchical model, the debate on how cortical receptive fields are created remains heated. Hopefully, with new physiological and anatomical details, a consensus on models of cortical processing will be achieved.

2.2.4 Classification of simple and complex cells

Historically, the discussion about how the cortex works has been largely centred around how simple and complex cells create their receptive field structures and subsequently their response properties. When Hubel and Weisel (1962) first introduced the concept of V1 simple and complex cells, the descriptions of their receptive fields were mainly qualitative. They derived a set of criteria for identifying simple and complex cells. A cell is classified as simple if it has:

1. spatially segregated ON and OFF subfields;
2. summation within each subfield;
3. antagonism between ON and OFF subfields;
4. predictable responses to any visual stimuli based solely on the arrangement of its ON and OFF subfields.

If any one of the criteria is not met, the cell is classified as complex.

As the theory gained popularity, it became apparent that the qualitative classification criteria were difficult to apply consistently across studies, thus a quantitative metric for classification was required. When it was realised that Hubel and Wiesel's criteria were essentially describing the difference in linearity of spatial summation within simple and complex receptive fields, a quantitative classification system measuring the response linearity of a cell was developed (De Valois et al 1982, Maffei & Fiorenti 1973, Movshon et al 1978b, Skottun et al 1991). When presented with a drifting sinusoidal grating, the linear nature of a simple cell dictates that its spike rate oscillates at the temporal frequency of an optimally oriented and spatially scaled grating. This is because the alternating bars of opposite polarities move in and out of the segregated ON and OFF subfields. On the other hand, a non-linear complex cell would show less response modulation to the alternating light and dark bars of an optimal grating due to its intermingled ON and OFF subfields.

The degree of response modulation to a drifting sinusoidal grating is measured as the ratio between the amplitude of the first harmonic of the response (F_1) and the mean spike rate (F_0). This is commonly referred to as the F_1/F_0 ratio (or modulation ratio). It was established that the F_1/F_0 ratio is bimodally distributed

across the V1 population with the classically defined simple and complex cells corresponding extremely well with cells showing F_1/F_0 ratios > 1 and F_1/F_0 ratios < 1 , respectively (De Valois et al 1982, Maffei & Fiorenti 1973, Movshon et al 1978b, Skottun et al 1991). The F_1/F_0 ratio has since become the standard classification method for simple and complex cells due to its simplicity and effectiveness. One of the most attractive features of this classification system is that almost all cortical cells respond very strongly to moving gratings and the basic classification can be done in a few minutes.

The bimodal distribution of the F_1/F_0 ratio appeared to further confirm the existence of two distinct classes of cells in V1, as proposed by Hubel and Wiesel (1962). However, as the validity of the hierarchical model was challenged, it was suggested by some studies, especially the ones that supported the recurrent model, that simple and complex cells might represent the two ends of a continuum rather than two discrete populations of cells (Abbott & Chance 2002, Chance et al 1999, Mechler & Ringach 2002, Priebe et al 2004). This proposal was inspired by studies that showed interchangeable response properties of simple and complex cells when their synaptic inputs were manipulated (Nelson et al 1994a, Rivadulla et al 2001, Shulz et al 1993, Sillito 1975). If the V1 population indeed sits on a continuum, how does one explain the observed dichotomy of F_1/F_0 ratio within V1? A body of experimental and computational evidence suggests that the bimodal distribution of F_1/F_0 ratio may be the consequence of a non-linear transformation of membrane potential to spike rate in an otherwise unimodal population of cells (Carandini & Ferster 2000, Mechler & Ringach 2002, Priebe et al 2004). Furthermore, it was revealed that the F_1/F_0 ratio of a V1 neuron is not a fixed property. For instance, some complex cells in cat and monkey defined by $F_1/F_0 < 1$ at high stimulus contrast show increased modulation ratios when the contrast of a grating stimulus is decreased (Cloherty & Ibbotson 2015, Crowder et al 2007, van Kleef et al 2010).

It is apparent that the classification into simple and complex cells is more than a mere technical discussion of identifying two cell populations: it may also expose the underlying mechanisms of cortical processing.

2.3 The role of inhibition in cortical visual processing

To understand receptive field formation, it is essential to understand the interplay of excitation and inhibition. Cortical sensory neurons receive both excitatory and inhibitory synaptic inputs, which are both important in shaping the overall response. For instance, when Hubel and Wiesel first speculated the formation of a simple receptive field, they proposed a ‘push-and-pull’ mechanism, which described the simple receptive field as resulting from excitation and inhibition, each arising from the opposite polarity of light (Hubel & Wiesel 1962). Understanding the role of inhibition in cortical visual processing has long been a major goal in vision research.

2.3.1 Identifying inhibitory cells *in vivo*

Inhibition in the cortex comes from neurons that release the neurotransmitter GABA. These neurons, namely GABAergic inhibitory cells, make up approximately 20-30% of cortical neurons (Meinecke & Peters 1987), which are significantly outnumbered by excitatory neurons that comprise the other 70-80% of neocortical cells (Defelipe & Farinas 1992). Despite their small population, GABAergic inhibitory cells are highly diverse in morphology, physiology and molecular composition when compared to the relatively homogenous excitatory population (Beaulieu 1993, Cauli et al 1997, DeFelipe 2002, Defelipe & Farinas 1992, Gupta et al 2000, Markram et al 2004, Peters & Sethares 1991). The diversity amongst the inhibitory population implies a necessity for a wide range of functional capabilities that play different roles in various cortical circuits. Indeed, distinct inhibitory cell types have been found to stabilise, refine, restrain and synchronise activities of neurons and circuits (Foldy et al 2004).

However, the heterogeneity of the GABAergic inhibitory populations make direct investigation of specific neuronal subtypes and their associated neuronal circuits a difficult task. Huge efforts have been dedicated to the classification and

identification of GABAergic subtypes based on their morphology, molecular markers and electrophysiological responses, to facilitate comparison between studies with different experimental approaches (Ascoli et al 2008, DeFelipe et al 2013).

2.3.2 Classification criteria for inhibitory cells

2.3.2.1 Morphology

Morphologically speaking, GABAergic cells vary widely in their somatic, dendritic and axonal appearances, all of which have been used to differentiate the subtypes of inhibitory neurons (Markram et al 2004). However, the most reliable anatomical feature for classification was thought to be axonal morphologies, especially the target of axonal projections. GABAergic cells could be classified into four general categories based on their axon targets: (1) soma- and proximal dendrite-targeting basket cells; (2) dendrite-targeting cells, which include cortical bipolar cells, Boule bouquet cells, Bitufted cells and neurogliaform cells; (3) dendrite- and tuft-targeting Martinotti cells; and (4) axon-targeting chandelier cells (Ascoli et al 2008, DeFelipe 1997, DeFelipe et al 2013, Markram et al 2004, Somogyi et al 1998) (Figure 2.4).

2.3.2.2 Molecular

In addition to morphology, GABAergic cells have also been classified based on the expression of specific molecular markers. In general, there are five classes of GABAergic cells distinguished by characteristic protein expression: (1) those expressing calcium binding protein parvalbumin (PV), including basket and chandelier cells; (2) those expressing peptide hormone somatostatin (SOM), which are mostly Martinotti cells; (3) those expressing neuropeptide Y (NPY); (4) those expressing vasoactive intestinal peptide (VIP); and (5) those expressing cholecystokinin (CCK) (DeFelipe et al 2013, Lee et al 2010, Markram et al 2004, Rudy et al 2011). These five distinct molecular markers account for almost all GABAergic cells with some degree of overlap. Certain groups of GABAergic cells express more than one of the molecular markers described

above (Rudy et al 2011). Consequently, the five classes can be further divided into subgroups based on other molecular signatures such as transcription factors, ion channels and neurotransmitter receptors etc. (Karagiannis et al 2009, Porter et al 1998, Welagen & Anderson 2011).

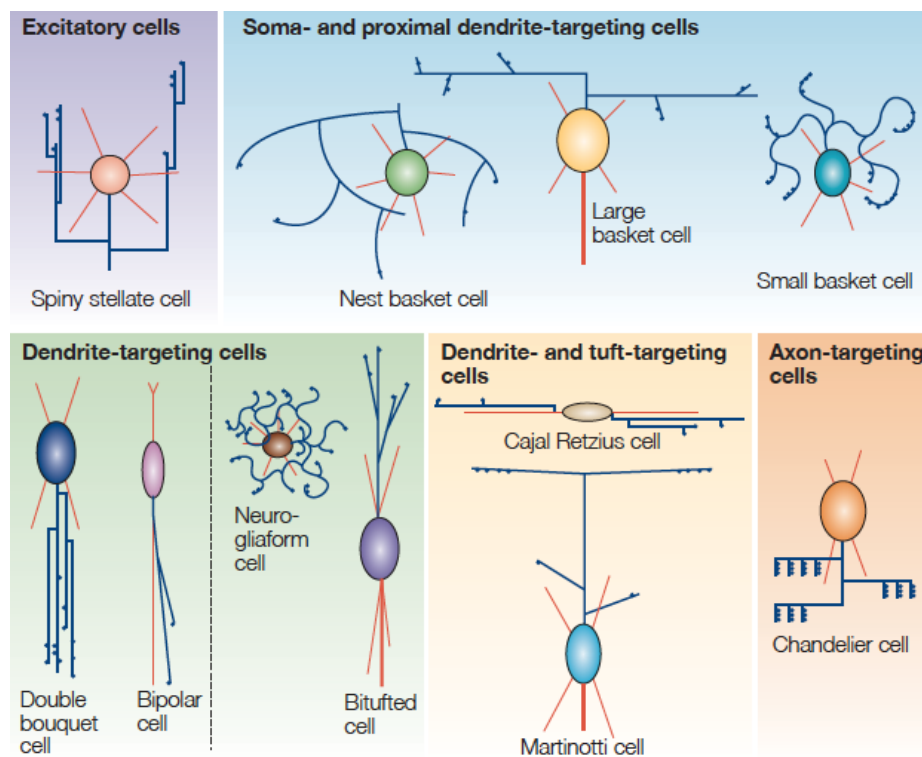


Figure 2.4. Cortical inhibitory subtype anatomy

A cartoon summary of anatomical features of major cortical inhibitory neuron types and an example of an excitatory cell. Each neuron type has a different soma colour. Axons are red lines, dendrites are blue lines and axonal boutons are blue dots. Each neuron is oriented so that the pia is above and white matter is underneath the neuron. Inhibitory interneurons are mainly classified morphologically by their axonal structures and their targeting domain of postsynaptic cells (see text). From Markram et al (2004) with permission from the Nature Publishing Group.

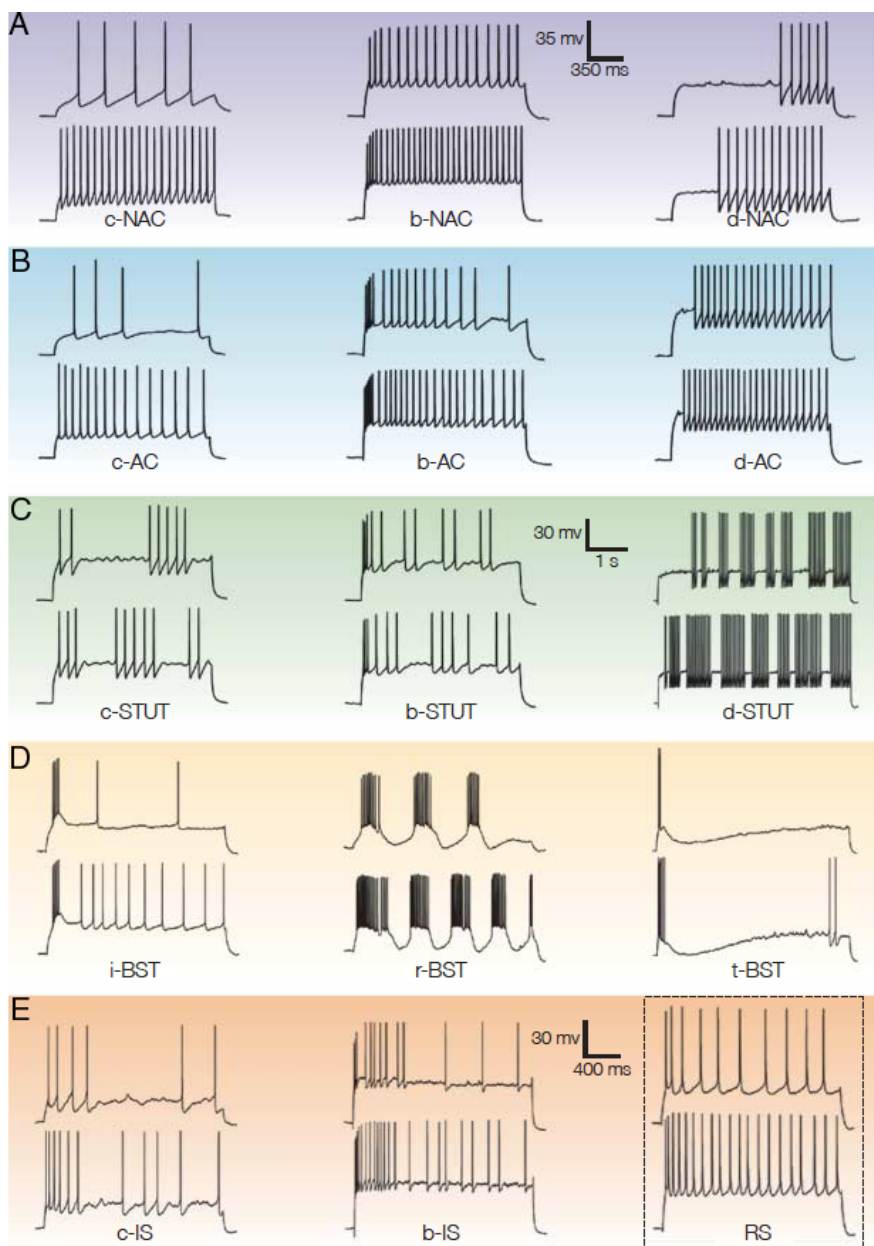


Figure 2.5. Electrophysiological classes of cortical inhibitory neurons

A summary of electrophysiological classes of cortical inhibitory neurons classified based on the responses to a sustained step current injection in the soma: non-accommodating (NAC) (A); accommodating (AC) (B); stuttering (STUT) (C); bursting (BST) (D) and irregular spiking (IS) (E). Most cell classes consist of three subtypes: delay (d); classic (c) and burst (b). For bursting cells, the three subtypes are repetitive (r), initial (i) and transient (t). An example of the regular-firing excitatory cell is also shown. Two examples that differ in their firing rates were shown for each cell type. From Markram et al (2004) with permission from the Nature Publishing Group.

2.3.2.3 Physiology

GABAergic cells have also been identified based on their biophysical responses, more precisely, the shape and pattern of their spiking responses. The physiological approach to classification is heavily dependent on experimental methods and conditions, thus often making it difficult to compare studies without a complete specification of experimental conditions and standardised recording methods. Nonetheless, several distinct types of spiking activities were observed amongst GABAergic cells. Fast spiking cells generally show narrow spike width with large fast after-hyperpolarisations and steady non-adapting spiking patterns (DeFelipe et al 2013, Markram et al 2004, Mountcastle et al 1969, Nowak et al 2003).

Fast spiking cells correspond reasonably well with PV expressing basket and chandelier cells, which constitute the majority of GABAergic cells (Griffen & Maffei 2014, Kawaguchi & Kubota 1993, Rudy et al 2011, Wang et al 2002, Xu & Callaway 2009). As a result, historically, all inhibitory neurons were thought to be fast spiking cells (Connors & Gutnick 1990, McCormick et al 1985). However, subsequent studies have revealed other spiking patterns amongst GABAergic cells.

In the most recent effort to unify the classification scheme, a categorising system based on the onset and steady-state responses to a step current injection into the soma was developed (Gupta et al 2000, Markram et al 2004) (Figure 2.5). GABAergic cells were sorted into the following classes: (1) non-accommodating cells with regular interspike intervals at steady-state (Figure 2.5A); (2) accommodating cells and accelerating neurons show significant increases and decreases in interspike intervals, respectively (an accommodating cell is illustrated in Figure 2.5B); (3) stuttering cells display high-frequency clusters of firing intermingled with irregular periods of silence (Figure 2.5C); (4) intrinsic bursting cells display burst-like discharges riding on a depolarisation envelope followed by a slow after-hyperpolarisation phase (Figure 2.5D); (5) irregular spiking cells have irregular interspike intervals at steady-state (Figure 2.5E) (DeFelipe et al 2013, Markram et al 2004). Each class can be further divided into

subtypes (see Figure 2.5). In this classification scheme, fast spiking cells fall into the non-accommodating group alongside a small population of regular spiking inhibitory cells that have spiking characteristics that resemble those of excitatory pyramidal cells.

2.3.2.4 Problems associated with classification of inhibitory cells

The field of GABAergic neuronal classification has long been controversial and equivocal due to the high heterogeneity within the population and the non-standardised experimental methods and conditions. Furthermore, however comprehensive, each of the classification schemes discussed above only provide partial information on an identified neuron. To study the functional roles of specific GABAergic subtypes meticulously, all neuronal features need to be taken into account. However, it is no small task to match morphological features, molecular markers and electrophysiological responses of a single neuron as these properties are obtained through distinct and time-consuming experimental methods, let alone doing so for a substantial population of neurons.

Our understanding of GABAergic inhibitory contributions have long been hindered by the complication associated with the difficulties of inhibitory neuronal identification. Fortunately, with the recent development in genetic and molecular tools, rapid progress has been made in large-scale identification of GABAergic subtypes, thus addressing the roles of distinct types of inhibition in visual processing. A wide range of experimental approaches such as two-photon calcium imaging, retrospective immunohistochemistry tracing and two-photon guided cell-attached recording have been performed on genetically labelled GABAergic subtypes of Cre-dependent viral mouse lines or green fluorescent reporter mouse lines (Huberman & Niell 2011, Kerlin et al 2010, Ma et al 2010, Runyan et al 2010, Zariwala et al 2011).

Genetic labelling allows instant identification of cell types of interest during experiments, which is unparalleled in its power compared to any other classification scheme. As a result, our knowledge of response properties of

different GABAergic cell types has proliferated dramatically in the last few years. For example, in mouse it was revealed that PV-expressing fast-spiking cells were less orientation selective when compared to excitatory cells, however, a class of SOM expressing Martinotti cells showed high orientation selectivity that was indifferent to excitatory cells (Cardin et al 2007, Ma et al 2010). The difference in selectivity suggests different functional roles in visual processing for the two inhibitory subtypes. Genetics could also be used to manipulate the activity of targeted cells, which allows the observation of the impact of over-activation or silencing of an entire cell type on local circuits and/or cortical function.

2.4 Animal models in vision research

Despite the diverse functional demands of vision, V1 is universally present in all mammals from highly visual primates to blind mole rats with subcutaneous eyes (Cooper et al 1993, Krubitzer & Kaas 2005). On the other hand, driven by evolution, variances in this homologous system were created to accommodate differences in the visual environments of different species. These differences could be observed in functional cell types and network connections across mammalian V1. Comparative studies of V1 in different species enable researchers not only to examine variations in the system that reflect functional necessity, but also investigate the driving force behind the preservation of the core system, both of which are important inquiries in understanding cortical visual processing.

This thesis focuses on two mammalian species that have been two of the principal animal models studied extensively for visual processing: the domestic cat (*Felis catus*) and the house mouse (*Mus musculus*).

2.4.1 The cat as a model for vision research

Studies of cortex in carnivores started in the mid-19th century inspired by the newly discovered structural similarity between the cortex of carnivores and primates. Initially, dogs were preferred as the animal model. However, by the

mid-20th century, cat cerebrum became more favourable largely for practical reasons, such as the modest variability in body size and cerebral gyral and sulcal patterns between different strains (Kawamura & Naito 1978). Permitted by the consistency of size and position of subcortical structures among individual animals, perhaps one of the biggest advances made by shifting to cat cerebrum at the time was the establishment of accurate and replicable stereotaxic coordinates (Berman 1968, Berman & Jones 1982, Sanderso 1971, Winkler & Potter 1914). With information on the precise location of cortical areas, experiments from different research groups became comparable and reproducible.

The pivotal studies by Hubel and Wiesel in the 1960s/1970s that established fundamental concepts in visual neurophysiology, plasticity, development and anatomy were predominately centered on cat V1. Since the 1970s there has been a fast proliferation in the field of cortical research using cat V1 as a model. In fact, more than 5000 articles were published on the topic of cat visual cortex in the second half of the 20th century, which was 10 times higher than the number of publications on monkey and rat visual cortex (Payne & Peters 2002). I will discuss features of cat V1 in detail as a comparison with mouse V1 in later sections.

2.4.2 A shift towards mouse vision

In addition to the cat other mammalian species were also studied. Macaque (Albright 1984, Callaway 1998, Felleman & Van Essen 1991, Hubel & Wiesel 1977, Hubel & Wiesel 1968, Luck et al 1997, Peter 1994, Ringach 2002) and marmoset (Fritsches & Rosa 1996, Rosa et al 1997, Tinsley et al 2003, Usrey & Reid 2000, Webb et al 2002) monkeys were popular primate models. Rodents such as rats (Girman et al 1999, Gonchar & Burkhalter 1997, Ohki et al 2005) and grey squirrels (Harting & Huerta 1983, Van Hooser & Nelson 2006) were also studied. Tree shrew, which is closely related to primates, is also used as a model (Chisum & Fitzpatrick 2004, Fitzpatrick 1996, Veit et al 2014).

Interestingly, although the mouse was the most widely used rodent model in other areas of biological research, it has long been dismissed in the field of vision research. This is partially due to its small body size, which causes experimental fragility. Both the retina and the neuronal visual pathway of the mouse are two orders of magnitude smaller than in cats and monkeys (Remtulla & Hallett 1985), which creates technical challenges for performing targeted electrophysiological recordings and labelling of individual cells, tracing of pathways and lesions of specific subcortical areas. Perhaps more significant than technical concerns, mice were perceived to have poor visual abilities. The mouse eye has particularly low spatial resolution: about 100 times lower than that of a human eye (Prusky & Douglas 2004).

In addition, the mouse was seen as especially unsuitable for studies of systems neuroscience due to the lack of 'organisational complexity' within their neocortex. A distinct organisational scheme within V1 in cats and monkeys is the feature column, which is a vertical column spanning all cortical layers that contains neurons similar in their preferences for particular visual stimulus features such as orientation and ocular-dominance (Hubel & Wiesel 1977, Hubel & Wiesel 1965, Hubel & Wiesel 1962, Hubel & Wiesel 1963). Unlike cats and monkeys, mice (and all other rodents) do not have such columnar organisation of stimulus features (Metin et al 1988b, Ohki et al 2005, Schuett et al 2002a, Van Hooser et al 2005). I will explain this discrepancy in more detail in later paragraphs.

Despite obvious disadvantages, the mouse has emerged as a key model for cortical vision research since the beginning of the 21st century. The change in attitude was mainly initiated by the recent proliferation in mouse genetics, which offered many solutions to long-term obstacles in vision research. Modern genetic tools provide a level of fine-scale manipulation of precise cell types and neuronal circuits that was unparalleled by traditional methods such as pharmacology and visual stimulation. Transgene expression allows investigators to visualise specific cell types for targeted single-cell recording and monitoring large-scale activities, as well as selectively silencing and activating them in a

reversible manner *in vivo*, for the purpose of studying their functional roles in a defined neuronal circuit (Luo et al 2008, Taniguchi et al 2011, Umino et al 2008, Zhuang et al 2013).

The fast reproductive rate of mice allows rapid establishment of various transgenic mouse lines, as well as useful molecular tools, which are readily available. From a practical point of view, mice are simpler and less expensive to work with. Without being constrained by the complexities of maintaining and handling larger mammals, researchers are more likely to experiment with new methods and techniques. Lastly, perhaps more surprisingly, mice are in fact more closely related to primates than carnivores (Arnason et al 2002). This close relationship is becoming increasingly obvious as more and more studies are revealing similarities between the visual systems of primates and rodents than exist between primates and carnivores (Grubb & Thompson 2003, Van den Bergh et al 2010, Veit et al 2014).

2.4.3 The mouse as a model for vision research

Despite new and exciting opportunities offered by the mouse cortex, it has to be kept in mind that our goal is to understand the visual system. Is mouse vision worthy of our time and effort after all? Here I provide a general review of the mouse visual system following the flow of visual information from retina to LGN to V1 with an emphasis on its comparison with the well-known cat visual system.

2.4.3.1 Retina

The composition of cell types is very similar between mouse and cat retina. The retinas of both species are dominated by rod photoreceptors, with approximately 97% of photoreceptors being rods in mouse retina and 95% being rods in cat retina (Jeon et al 1998, Schneider & Zrenner 1986). The high proportion of light sensitive rods is well suited for vision under low light conditions as both mice and cats are active at night (nocturnal), dawn and dusk (crepuscular). Wavelength sensitive cones makeup the rest of the photoreceptors in the retina. Similar to cats, mice are dichromats, meaning their

cones, at most, only express two photopigments: one sensitive to ultraviolet light with short wavelengths (peak at 360 nm) and one sensitive to green light with medium wavelengths (peak at 511 nm) (Calderone & Jacobs 1995). Unlike primates, mice and cats lack the cone photopigment sensitive to long wavelengths of light that would allow them to perceive red hues (Haverkamp et al 2005, Szel et al 1993).

After transduction in photoreceptors, visual information is relayed onto interneurons and then onto retinal ganglion cells. All of the major interneuron types present in monkeys and cats are also found in mice (Masland 2001). In mammals, retinal ganglion cells are functionally and morphologically diverse. For monkeys, there are 20 subtypes of ganglion cells (Field & Chichilnisky 2007). To date, 22 anatomically distinct ganglion cell subtypes have been identified in mouse retina (Volgyi et al 2009).

The level of complexity and capability of mouse ganglion cells is no less than that seen in carnivores and primates. For instance, direction-selective cells, as well as cells that are sensitive to approaching or 'looming' stimuli, are found amongst mouse retinal ganglion cells (Huberman et al 2009, Kim et al 2008, Munch et al 2009, Rivlin-Etzion et al 2011). Interestingly, a subtype of mouse ganglion cell was discovered to express photopigments, thus being capable of phototransduction (Berson et al 2002, Provencio et al 2000). It was confirmed later that photosensitive retinal ganglion cells also exist in some primates including macaques and humans (Dacey et al 2005, Rollag et al 2003). Understanding the functional and anatomical complexity of diverse ganglion cell subtypes, for instance, how ganglion subtypes compare across species are longstanding issues in vision research. Recent identification of subtype-specific genes and molecular markers amongst mouse ganglion cells has begun to answer some of the questions (Huberman et al 2008, Huberman et al 2009, Kay et al 2011, Kim et al 2008, Rivlin-Etzion et al 2011).

2.4.3.2 Lateral Geniculate Nucleus (LGN)

Continuing up the central visual pathway, the LGN is the next major processing and relaying centre after the retina. Compared to its retina and V1, the mouse LGN has not received the same amount of attention. Only a few studies have comprehensively looked at the receptive field properties of mouse LGN cells. Nevertheless, evidence has suggested a high degree of similarity between mouse LGN and that of cats and monkeys and confirmed the capability of the mouse LGN to relay complex information to the cortex. Mouse LGN cells exhibit classic ON and OFF centre-surround receptive field structures (Grubb & Thompson 2003, Zhao et al 2013). The three classes of LGN cells that sent projections to visual cortex are also preserved across all studied species: X, Y and W cells in rodents and carnivores are functionally parallel to parvocellular (P), magnocellular (M), and koniocellular (K) cells in primates, respectively (Grubb & Thompson 2003, Hendry & Reid 2000, Holdefer & Norton 1995, Shapley & Perry 1986, Sherman et al 1976, So & Shapley 1979, Van Hooser et al 2003).

Recent studies have reported the presence of direction-selective LGN cells in mice (Zhao et al 2013). Similar to cats and monkeys, these directionally biased LGN cells are not the result of cortical feedback and their preferred orientations are dependent on the direction of the receptive field elongation (Daniels et al 1977, Smith et al 1990, Vidyasagar & Urbas 1982, Zhao et al 2013).

On the other hand, some differences were observed between rodent and carnivore LGN cells. First of all, the non-linear Y cells found in cats and ferrets were not present in the mouse LGN (Grubb & Thompson 2003, Price & Morgan 1987, So & Shapley 1979, Sur & Sherman 1982). Instead, mouse LGN cells resemble primate LGN cells more closely in that almost all LGN cells show linear spatial summation (Blakemore & Vitaldurdand 1986, Derrington & Lennie 1984, Kaplan & Shapley 1982, Levitt et al 2001, Usrey & Reid 2000, White et al 2001, Xu et al 2001). The linear responses were also observed in LGN cells of grey squirrels (Van Hooser et al 2003). Secondly, the connectivity between the LGN and V1 are different in carnivores compared to rodents and primates. In all species studied, X/P and Y/M cells primarily project to Layer 4 of V1 with some

species-specific sublaminar targeting. For example, in monkeys, M cells target the upper section of Layer 4C (Layer 4C α) and P cells project to the lower section of Layer 4C (Layer 4C β) (Casagrande & Kaas 1994). Conversely, in cat, X and Y cell projections are highly overlapping with some Y cells targeting more superficially than X cells (Humphrey et al 1985, Leventhal 1979a, Leventhal 1979b). Nevertheless, the LGN projection in mice and primates is restricted to area 17 (Billingsgagliar et al 1974, Caviness 1975, Peter 1994, Wang & Burkhalter 2007). However, in cat, some Y cells send major projections to the second topographic area of visual space, area 18 (Lee et al 1998, Mignard & Malpeli 1991, Payne & Peters 2002, Tretter et al 1975).

The comparison between rodent, primate and carnivore LGN again emphasises the close relationship between rodents and primates and suggests that the carnivore visual system might not be as representative as we previously thought.

2.4.3.3 Primary visual cortex (V1)

Mouse V1 has been under intense investigation in the last decade or so; both similarities and differences to V1 in cat and monkey have been observed in mouse V1.

Where is V1?

First of all, the very concept of V1 varies with the species in question. The definition of primary visual cortex has evolved over the years with the development of techniques for defining cerebral cortical areas and the expansion of species studied. The most current and fundamental criteria define V1 as a region in the occipital area of the neocortex that (1) has a retinotopic map, (2) receives substantial inputs from LGN, and (3) has a highly granulated Layer 4 (Payne & Peters 2002, Rosa & Krubitzer 1999).

For primates and rodents, V1 corresponds to area 17 in Brodmann's (Brodmann 1909) cytoarchitectural map of neocortex, where all three criteria to define the region as V1 were fully met (Billingsgagliar et al 1974, Caviness 1975, Peter

1994, Wang & Burkhalter 2007). The definition of V1 in carnivore however, is more controversial. Area 18, which is laterally and rostral-laterally adjacent to area 17, is defined as the second visual area (V2) in monkeys (Allman & Kaas 1971, Rosa et al 1988) and rodents (Montero 1993, Wagoner et al 1980, Wang & Burkhalter 2007). V2 is generally described as the area that predominantly receives topographically organised projections from the supragranular layers of V1, as well as some thalamic inputs from the pulvinar (or lateral posterior) complex (Livingstone & Hubel 1983, Malach 1989, Rosa & Krubitzer 1999, Rosa et al 1994, Sincich & Horton 2002) and it is functionally distinct from V1 (Burkhalter & Vanessen 1986, Foster et al 1985, Maruko et al 2008, Van den Bergh et al 2010). On the other hand, area 18 as well as area 17 in the cat cortex were found to receive significant LGN inputs, therefore it was debated whether area 18 in carnivores should be included in the primary visual cortex (Lee et al 1998, Mignard & Malpeli 1991, Payne & Peters 2002, Tretter et al 1975). Subsequent studies that compared afferent and efferent connections, neuronal cell type composition and distribution, as well as neuronal response properties between cat area 17 and 18 have reached the consensus that cat V1 should include both areas (Payne & Peters 2002).

In the subsequent discussion and the following chapters, unless otherwise stated, cat V1 refers to both areas 17 and 18. Nevertheless, in terms of the general neural organisation within V1, mouse V1 is similar to that of cats and monkeys: neurons in mouse V1 are characteristically organised into six distinct layers and the general direction of information flow across layers is also conventional. All major subtypes of inhibitory and excitatory neurons identified in V1 of cats and monkeys are also found in mouse V1 (Drager 1975, Mangini & Pearlman 1980b).

Receptive field properties

A study by Niell and Stryker (2008) provided the most comprehensive quantitative survey of receptive field properties of mouse V1 neurons to date. Through extracellular electrophysiological recordings, the response properties

of a large population of mouse V1 neurons with regard to their morphological identities and laminar locations were examined. It was demonstrated that all basic, as well as some higher-order receptive field properties observed in neurons of cat and monkey V1 were also present in mouse V1 neurons. The study showed that mouse V1 neurons are sharply tuned to specific spatial and temporal frequencies, as well as orientations (Huberman & Niell 2011, Niell & Stryker 2008, Van den Bergh et al 2010). Higher-order properties such as contrast gain control and contrast-invariant tuning were also observed. Mouse V1 neurons could be classified as either simple or complex cells according to their response linearity; however, this required the removal of substantial spontaneous activities, which is not a feature in cats and monkeys. Moreover, the size and shape of the spatial structures of ON and OFF subfields were indistinguishable between simple cells of mouse and monkey V1, except for very obvious differences in the sizes of the subfields, which were much larger in mice (Liu et al 2010, Niell & Stryker 2008, Ringach 2002).

The comprehensive receptive field properties suggest that mouse V1 neurons operate at a similar level to higher visual species in computing complex visual information. However, it needs to be kept in mind that they are doing so at much lower spatial resolution, which is reflected in larger receptive fields and lower preferred spatial and temporal frequencies when compared to cats and monkeys (Niell & Stryker 2008, Van den Bergh et al 2010, Van Hooser 2007).

Columnar organisation

Perhaps the biggest difference in the primary visual cortex between mouse and other higher order mammals is the lack of large-scale functional organisation. All mammals examined so far have some degree of columnar structure in visual cortex: vertical columns spanning all cortical layers that contain neurons similar in their functional properties, and these properties tend to change smoothly from column to column across the cortical surface. Retinotopic maps of spatial arrangement of the visual field is universally present in all mammalian V1 studied (Kaas 1997).

The V1 areas of carnivores and primates also have columnar organisation for specific visual stimulus preferences such as orientation and ocular-dominance, which is evidently lacking in the V1 of rodents including mice, rats and highly visual grey squirrels, which have large V1s (Blasdel & Salama 1986, Drager 1975, Girman et al 1999, Hubel & Wiesel 1977, Hubel & Wiesel 1963, Mangini & Pearlman 1980a, Metin et al 1988a, Ohki et al 2005, Schuett et al 2002a, Van Hooser et al 2005, Zariwala et al 2011) (Figure 2.6). Neurons in an orientation column have similar orientation preferences, and the preferred angle of orientation selectivity changes smoothly across the cortical surface (Figure 2.6A-D). In cat and ferrets, orientation maps repeat at 800-900 μm intervals throughout the cortex. In addition, each orientation map also comprises a map of direction selectivity: in each orientation map, orientation domains are divided equally into two direction domains with an abrupt boundary where direction preference reverses (Ohki et al 2005, Weliky et al 1996) (Figure 2.6D).

It was previously thought that functional architecture was important in generating and maintaining the selectivity of individual neurons because the maps provided physical proximity for maximising connections between neurons that share the same selective preferences (Hubel & Wiesel 1963, Sompolinsky & Shapley 1997). The discovery of sharply tuned orientation selective neurons in mouse V1 demonstrates that cortical orientation maps are not always necessary to obtain highly selective responses (Figure 2.6E). However, recent studies have demonstrated that mouse V1 is not completely devoid of any functional architecture. Two-photon calcium imaging across the whole of V1, which was made possible by the small overall size of rodent V1, revealed salt-and-pepper organisation of subnetworks of neurons with similar orientation preferences exhibiting strong connections in rats and mice (Ohki et al 2005, Sohya et al 2007, Wang et al 2006). Furthermore, by utilising transgenic mice to target specific subtypes, some neurons with sharp orientation tuning were demonstrated to have small dendritic fields sampling uniformly from nearby neurons with similar orientation preferences (Runyan & Sur 2013). This study, in conjunction with electrophysiology studies that show response correlation between neurons with

similar orientation selectivity (Cossell et al 2015, Denman & Contreras 2014), suggests that functional organisation exists in mouse V1 in the form of very small-scale, local coherence of orientation preferences.

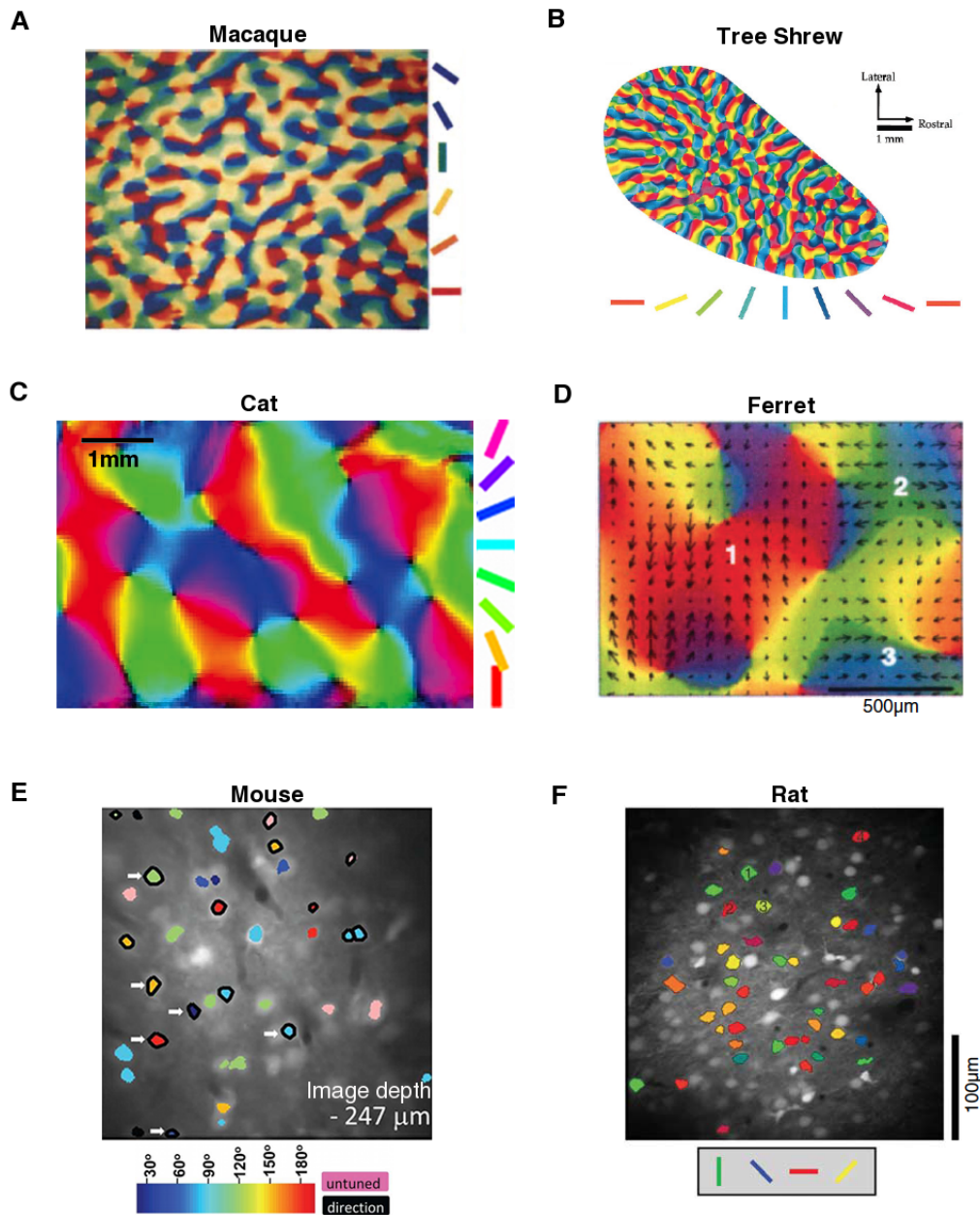


Figure 2.6. Functional organisation of mammalian V1

Functional organisation of orientation selectivity of various visual cortices in mammalian species. Colours in each image are false and correspond to specific orientations shown in the associated keys. **A**, Map of orientation preference in macaque monkey striate cortex obtained by voltage sensitive dye imaging. From Blasdel and Salama (1986) with permission of the Nature Publishing Group. **B**, Orientation map in tree shrew V1 revealed by optical imaging. From Bosking et al (1997) with permission from the Society for Neuroscience. **C** and **D**, Optical imaging maps of orientation preference in carnivores: cat area 17 and 18 (**C**) and ferret area 17 (**D**). **C**, From unpublished data collected at the National Vision Research Institute by Shaun Cloherty and Michael Ibbotson (2014), with permission. **D**, Carnivores have an additional direction map superimposed on the orientation map. Key as in **C**. Arrows indicate the preferred direction. Numbers indicate locations of abrupt fractures in direction preference (see text). From Weliky et al (1996) with permission from the Nature Publishing Group. **E** and **F**, Two-photon images of orientation selectivity of individual neurons in rodent V1: mouse (**E**) and rat (**F**). Coloured cells show significant response bias towards the corresponding orientation. Rodent V1 in general lacks the functional organisation seen in primates and carnivores, e.g. orientation maps (see text). In both **E** and **F**, many neighbouring neurons show different orientation preferences. **E**, Reproduced from Zariwala et al (2011) with open access. **F**, adapted from Ohki et al (2005) with permission from the Nature Publishing Group.

2.4.3.4 Concluding remarks on mouse as a vision research model

Overall, it is apparent that the central visual system of mouse is much more sophisticated and similar to higher-order mammals than previously thought. The pathway that relays complex visual information from retina to V1 is highly conserved from mice to primates. The intricacy of receptive field properties of mouse V1 neurons suggests that they are executing similar computations as in cats and monkeys. Even though mouse V1 lacks ordered maps of orientation, it is still capable of producing highly orientation selective neurons relying on sparse and local sampling of inputs with similar orientation preferences. It is important to be cautious when making cross-species comparisons of any biological system. The nature of evolution often results in the same functional outcome from different mechanisms and structures (Van Hooser 2007). In more ways than one, mouse visual system is not like that of cats and monkeys, but it does not mean we should discount the value of the mouse visual system.

It has been proven beyond doubt that mouse V1 is a powerful model for investigating certain fundamental questions in visual processing. In recent years, a fast proliferation of knowledge in the structural and functional circuits of mammalian visual cortex has been achieved by shifting our attention to mouse vision. With the rapid development of mouse molecular-genetic tools, combined with new recording and imaging techniques, the trend is set to continue. At the same time, the obvious differences in the structure of mouse V1 compared to cat and monkey, requires that we also investigate the unique features in those species, as they perhaps have more relevance to the human condition.

Chapter 3: General Methods

Recordings were made from anaesthetised C57BL/6 mice aged five to twelve weeks and adult cats of either sex weighing between 2.8 and 4.2 kg (also see, (Crowder et al 2007, Tan et al 2011). All experiments were performed according to the National Health and Medical Research Council's Australian Code of Practice for the Care and Use of Animals for Scientific Purposes. Ethics were approved by Animal Ethics Committee of the Australian National University and the Melbourne University, as well as the University of Texas at Austin Institutional Animal Care and Use Committee. Mice were acquired from several different sources: the Monash Animal Research Platform, the Animal Resources Centre, Western Australia and the Walter and Eliza Hall Institute and the University of Texas in Austin Animal Resources Centre. Cats were acquired from the Australian National University, the Royal Victorian Eye and Ear Hospital Biological Research Centre and from a cat supplier in the Australian Capital Territory.

3.1 Animal preparations

3.1.1 Mouse

Before surgery, mice were anesthetised with intraperitoneal injections of chlorprothixene (10mg/kg) followed by Urethane (1g/kg). For intracellular recording experiments, an injection of dexamethasone (20mg/kg) was also admitted to reduce brain edema. Anaesthesia was deemed sufficient by the lack of toe-pinch reflexes from the animals. The level of anaesthesia was monitored using the electrocardiogram (ECG) and repeated Toe-Pinches throughout the experiment. The animal's body temperature was maintained at approximately 37°C by a feedback controlled heating pad. To ensure a clear airway for each mouse, a tracheotomy was performed and a glass capillary tube was inserted into the trachea.

3.1.2 Cat

Cats were initially anaesthetised with ketamine HCL (20 mg/kg, Ilium, Smithfield, NSW, Australia) delivered intramuscularly. Once the animal was deeply anaesthetised, as determined by the lack of withdrawal and corneal reflexes, the animal was intubated and connected to the anaesthesia machine. Anaesthesia was maintained throughout surgery and the entire experiment by inhalation of gaseous halothane (1-2% during surgery, 0.5% during unit recordings) in a 2:1 mix of O₂ and N₂O. The health of the animal and the depth of anaesthesia were continuously monitored by acquiring respiration rate, end-tidal CO₂ concentration, specific oxygen concentration, the electrocardiogram (ECG), electroencephalogram (EEG) and blood pressure. The body temperature of the animal was monitored and maintained by a feedback controlled heating blanket. After initial surgery, neuromuscular blockage was induced with an intravenous injection of 50 mg of gallamine triethiodide (Flaxedil; Sigma, St. Louis, MO) in 2 ml of Hartmann's solution and thereafter continuously delivered through intravenous infusion containing Hartmann's solution (25% by volume), 5% glucose with 0.9% NaCl solution (25% by volume) and 8% animal acid solution (50% by volume) at a rate of 10 mg/kg/h. The intravenous infusion of fluid was delivered through the cephalic vein at 2.5 ml/kg/h. The animal was also given daily intramuscular injections of atropine (0.2 mg/kg; Apex Laboratories, Somersby NSW, Australia) to reduce salivation, dexamethasone phosphate (1 ml; Ilium) to prevent cerebral oedema and Clavulox to control infection (1 ml, Pfizer, West Ryde, NSW, Australia). Animals were ventilated to maintain end-tidal CO₂ between 3.5 and 4.5%.

3.2 Surgical procedures

3.2.1 Mouse

The mouse's head was fixed to a custom-built stereotaxic holder. After the scalp was retracted, V1 in the left hemisphere was exposed by a craniotomy and a durotomy. The cranial window was approximately 1mm × 2.5 mm in size. The

surface of the cortex was kept moist by frequent applications of 4% agarose in normal saline. The right eye was lubricated with frequent applications of silicon oil drops. The pupil was not dilated. The left eye was covered throughout the experiment. At the end of the experiment the animal was euthanized with an overdose of Pentobarbitone sodium (150mg).

3.2.2 Cat

The head of the cat was fixed in a stereotaxic frame using ear bars, a mouth bar and head bolt which was attached to the skull at the midline 3 cm anterior to interaural zero (Crowder et al 2006). A craniotomy was performed 0-8 mm posterior and 2-8 mm lateral to interaural zero to allow access to areas 17 and 18 (collectively V1) spanning both hemispheres. A durotomy was then performed to expose the brain. The surface of the brain was kept moist by frequent applications of 4% agarose in normal saline. The pupils were dilated and accommodation was paralysed with 1% atropine sulphate eye drops (Sigma). The nictitating membranes were retracted with 0.01% phenylephrine HCl eye drops (Sanofi-Synthelabo, New York, NY). The corneas were protected with zero-power rigid gas-permeable contact lenses. Corrective lenses were placed in front of the eyes to focus the stimulus on the retina. Three millimetre diameter artificial pupils were placed between the eyes and the corrective lenses to prevent spherical and chromatic aberrations.

3.3 Extracellular recording and visual stimuli

Recordings were made with gold tipped, lacquer coated tungsten microelectrodes with impedance between 1 to 2 M Ω s (FHC, Bowdoinham, ME). Signals were amplified and band-pass filtered at between 300 Hz and 6 kHz, then sampled at 40 kHz using a CED 1401 interface and Spike2 software (Cambridge Electronic Designs, Cambridge, UK). To assess online spike analysis, a Schmitt trigger was used to trigger TTL pulses that were passed to Spike2.

The tip of the electrode was lowered to approximately 200 μm beneath the surface of the cortex before neurons were isolated. The locations of the receptive fields of single neurons were identified using a hand-driven light spot against a white background. A neuron was isolated based on its responsiveness to the stimulus, as well as the consistency and shape of its spike waveforms.

All visual stimuli was generated with a VSG Series 2/5 Stimulus generator (Cambridge Research Systems, Cambridge, UK) and displayed on a calibrated CRT monitor (Clinton monoray monitor, 1024 by 768 pixels). The viewing distance was kept at approximately 30 cm for mice and 57 cm for cats. The test stimulus was a sine-wave grating presented in a circular aperture against a grey background of mean luminance (57 cd/m^2). The contrast of the grating was defined as: Michelson contrast = $[(\text{Lum}_{\max} - \text{Lum}_{\min})/\text{Lum}_{\max} + \text{Lum}_{\min}] \times 100$ where Lum_{\max} and Lum_{\min} are the maximum and minimum luminance of the grating. For each neuron, the preferred temporal frequency (TF), Spatial frequency (SF) and Orientation, as well as the location and size of the receptive field at 100% contrast were determined by the maximum response evoked by moving gratings for each parameter at 100% contrast.

3.4 Intracellular recording and visual stimuli

Intracellular responses were obtained via blind recordings with a whole-cell configuration *in vivo* (Margrie et al 2002, Priebe et al 2004, Tan et al 2011). A silver chloride wire was inserted into the muscle in the animal's neck as a reference electrode. Patching pipettes with tip resistance of 8 to 10 $M\Omega$ were pulled from 1.2 mm outer diameter and 0.7 mm inner diameter KG-33 borosilicate glass capillaries (King Precision Glass) on a P-97 micropipette puller (Sutter Instruments). A silver chloride wire was inserted into the pipette that was filled with 135mM K-gluconate, 4mM NaCl, 0.5mM EGTA, 2mM MgATP, 10mM phosphocreatine disodium, and 10mM HEPES, pH adjusted to 7.3 with KOH (Sigma-Aldrich).

Current clamping was performed with an Axoclamp 2B patch-clamp amplifier to record from neurons 150 – 600 μm below the surface of the cortex. The voltage was digitised and recorded with custom software (labVIEW, National Instruments), which also sent instructions to a separate stimulus-generating computer. The resting membrane potential (V_{rest}) of a patched cell, measured as the responses to a blank screen, ranged from -40 mV to -80 mV.

Visual stimuli were generated using Psychophysics toolbox libraries for Matlab (The Mathworks Inc. Natick, MA, USA) and were presented on a Sony GDM f-250 video monitor placed approximately 30 cm in front of the animal's eye. The monitor used to present the stimuli is different to that used during the extracellular experiments. The monitor used for intracellular experiments has a non-interlaced refresh rate of 120 Hz. It has a spatial resolution of 1280 x 1024 pixels, which subtended 38 cm horizontally and 30 cm vertically. The mean luminance of the monitor was 25 cd/cm².

Chapter 4: Receptive Field Properties of Inhibitory and Excitatory neurons in V1

4.1 Abstract

In the primary visual cortex of mammals, GABAergic inhibitory neurons have a range of important roles in visual processing. Historically, studying inhibitory receptive field properties has been often problematic due to the difficulty in identifying inhibitory neurons *in vivo*. In this chapter, I classified inhibitory and excitatory neurons based on the shape of their extracellular spike waveforms in both mouse and cat V1, which made it possible to examine and compare the receptive field properties between inhibitory and excitatory neurons within each species as well as between the two species. In mouse V1, fast-spiking (FS) inhibitory cells are evenly distributed amongst complex and simple cells and exhibit a broad range of orientation selectivity, whereas the majority of regular-spiking (RS) cells were non-selective complex cells. Compared to mouse V1, FS and RS cells in cat V1 exhibit fewer differences in their receptive field properties. Histological analysis showed that FS cells are substantially over-represented in Layer 1 of cat V1.

4.2 Introduction

In mammalian primary visual cortex (V1), GABAergic inhibitory cells are morphologically and functionally different to excitatory pyramidal cells. It is increasingly apparent that cortical inhibitory neurons are capable of much more than regulating circuit excitability - they have been found to play many essential roles in shaping cortical receptive fields (see reviews by Griffen & Maffei 2014, and Isaacson & Scanziani 2011).

Surprisingly, the fundamental properties of inhibitory neuron receptive fields are not well understood. This is largely due to the difficulty in efficiently identifying inhibitory cells *in vivo* as the inhibitory subpopulations are morphologically, molecularly and physiologically diverse. It has been demonstrated in several mammalian species, when compared to excitatory neurons, a large proportion of inhibitory neurons have narrower spike waveforms (rat: Kawaguchi & Kubota 1993; rat somatosensory cortex: Wang et al 2002; mouse: Rudy et al 2011; mouse somatosensory cortex: Xu & Callaway 2009; Guinea pig: McCormick et al 1985; cat: Nowak et al 2003). These inhibitory neurons are known as fast spiking (FS) cells and the excitatory neurons are referred to as regular spiking (RS) cells. As a result, many electrophysiological studies have utilised this difference in spike waveform shapes to separate inhibitory and excitatory cortical neurons after recordings (Andermann et al 2011, Atencio & Schreiner 2008, Bartho et al 2004, Bruno & Simons 2002, Hasenstaub et al 2005, Lee et al 2007, Mitchell et al 2007, Niell & Stryker 2008, Swadlow 2003).

Soon after the mouse became a popular model for cortical vision research, Niell and Stryker (2008) conducted an extensive survey on the receptive field properties of mouse V1, in which they classified all recorded cells as either inhibitory or excitatory based on the shapes of their extracellular spike waveforms. In more ways than one, mouse is a valuable model for cortical vision research, thus it is essential to examine the similarity and differences of their receptive field properties to those of longer-established animal models for visual cortical research, such as cats. To my best knowledge, all investigations of inhibitory neurons in cat have consisted of intracellular studies with population sizes ranging from 11 to 73 cells (Azouz et al 1997, Cardin et al 2007, Hirsch 2003, Nowak et al 2003). There has not been any large-scale extracellular examination of FS (inhibitory) and RS (excitatory) neuron receptive field properties in cat V1¹.

¹ Cat V1 refers to both areas 17 and 18 of cat cortex, whereas mouse V1 refers only to area 17 (for detailed description see Chapter 2)

To make direct comparisons between mouse and cat V1, I classified neurons recorded in mouse and cat V1 into FS inhibitory cells and RS excitatory cells based on the shape of their extracellular spike waveforms and examined and compared their receptive field properties. In this chapter, I present the findings of this comparison. The results demonstrate that the shape of extracellular spike waveforms is a reliable and consistent feature for separating FS and RS cells in both mice and cats. I have also demonstrated many novel similarities and differences between the receptive field properties in mouse and cat V1. Moreover, I have shown for the first time a comparison of some receptive field properties, such as preferred spatial and temporal frequencies, between inhibitory and excitatory cells as well as their laminar locations for cat V1 neurons.

4.3 Methods

Experiments were performed on both mice and cats. General procedures can be found in Chapter 3. Here I present specific protocols for the data in this chapter.

4.3.1 Stimulus protocols

Stimuli were presented in a circular aperture the size of the excitatory receptive field. The size of the excitatory field was established using an expanding circular patch of moving grating. In some cells the responses saturated as the stimulus expanded and the point at which this occurred was taken to be the maximum extent of the excitatory receptive field (an assumption was made that there was no surround suppression in these cases). In some cells the response was maximal at a certain stimulus diameter and then decreased as it was enlarged further (it is assumed that these cells had surround suppression). In these cases the size of the receptive field was taken as the peak of the size tuning function.

Drifting sine-wave gratings presented at 100% contrast were used to determine various receptive field properties of the recorded neurons, including orientation

selectivity, spatial frequency, temporal frequency and response linearity. To measure orientation selectivity, sine-wave gratings were set to drift at eight different orientations (in angle): 0, 22.5, 45, 67.5, 90, 112.5, 135 and 157.5. After 0.5 s presentation of each orientation, gratings moving in the opposite direction were presented and followed with 0.5 s of grey screen (at the mean luminance of the prior grating). Optimal spatial and temporal frequencies were tested with 2s long drifting gratings of eight different temporal frequencies (in Hz): 0.25, 0.5, 1, 2, 4, 8, 16 and 24 and several different spatial frequencies (in cycles/degree): 0.005 - 0.1 for mice and 0.05-1.6 for cats. Optimal orientation, spatial frequency and temporal frequency were first determined by calculating on-line tuning functions for each stimulus parameter using customised MatlabTM programs (The Mathworks Inc. Natick, MA, USA). The stimulus for measuring response linearity was a moving sine-wave grating presented at the optimal orientation, spatial frequency and temporal frequency in a circular aperture the size of the excitatory receptive field at 100% contrast. Interleaved with 1 s of a blank (mean luminance) screen, each grating was presented for 3 s with the first and last 0.5 s stationary and the 2 s in between drifting. Trials were repeated as often as the stability of the recording would allow. On average, 10 trials were recorded for each cell for every stimulus condition.

4.3.2 Analysis of receptive field properties

The extracellular signals from individual units recorded from mouse or cat V1 were amplified, filtered and acquired by a CED 1401 interface and Spike2 software (Cambridge Electronic Designs, Cambridge, UK) (see general methods). The recorded spikes were sorted off-line using a Spike2 waveform isolating program, which selects for single cell responses based on voltage threshold crossing and spike waveform template matching.

Tuning curves were generated for each of the receptive field properties. The preferred orientation, spatial frequency and temporal frequency were determined as the test stimuli that generated the maximum response for each stimulus parameter. Orientation selectivity of individual units was measured as

an orientation index, which was calculated as the depth of modulation from the preferred orientation to its orthogonal orientation. The orthogonal orientation is defined as $\theta_{ortho} = \theta_{pref} + \pi/2$. The orientation selectivity index is calculated as:

$$\frac{R_{pref} - R_{ortho}}{R_{pref} + R_{ortho}}$$

where R_{pref} is the response recorded with preferred orientation and R_{ortho} is the response recorded with the orthogonal orientation. Response linearity was measured as the relative modulation (F_1/F_0) of the response, which was the ratio between the amplitude of the Fourier coefficient at the fundamental frequency of the stimulus grating (F_1) and the increase in mean firing rate above the spontaneous baseline (F_0). Fourier coefficients were calculated using the FFT function in Matlab™ (The Mathworks Inc. Natick, MA, USA).

4.3.3 Histological reconstruction of recording sites

For three cats, histological analysis was carried out to examine the laminar locations of recorded cells. Their brains were extracted immediately after electrophysiological experiments for histological reconstruction of recording locations. Brains were then cryoprotected in sucrose (30% in 0.1 M PB) before being processed. For each brain, the section between 0 and 8 mm posterior to interaural zero was cut into slices that were 45 μ m thick in the coronal plane. Slices were then mounted onto gelatin chrome aluminum coated slides and counterstained with thionin for Nissl substance. The tissue was then examined under light microscopy to retrieve the locations of the electrode tracks. Laminar locations of recorded cells were reconstructed by correlating the electrode depths with the bottom of the electrode track, the location was documented during recordings and marked in some penetrations with a microlesion.

4.4 Results

4.4.1 Separating putative inhibitory and excitatory cells based on extracellular spike waveforms

Extracellular recordings were made from areas 17 and 18 of 8 anaesthetised cats ($n = 368$) and the V1 of 22 anaesthetised mice ($n = 78$). For simplicity, cat areas 17 and 18 will be referred to collectively as V1 (both of which are primary geniculo-recipient areas). I preformed all mouse cortical experiments. The cat data presented in this chapter was collected by various people over the course of 2007-2014. Each cat experiment was performed by a team of investigators. I was directly involved in collecting data from 5 cats between 2010 and 2014. The cat data is stored and organised on a server. I used a custom-designed program to extract spike trains for each individual cell from the server and analysed it for presentation in this chapter.

The extracellular spikes used for waveform analysis were recorded during the presentation of a sine-wave grating moving at the optimal orientation, spatial frequency and temporal frequency at 100% contrast. For each cell, average spike waveforms were generated by aligning all recorded spikes at their most negative values (the trough value). Each waveform in Figure 4.1A and Figure 4.2A represents the average spike waveform of a recorded cell in mouse and cat cortex, respectively. These waveforms are aligned and normalized to their trough values.

For both mouse (Figure 4.1A) and cat (Figure 4.2A), waveforms can be seen to fall into two general populations: fast-spiking (red) and regular-spiking (blue). Figure 4.1B and 4.2B show averages for the fast and slow spiking units across each population using corresponding colours. Several key parameters of the shape of the spike waveforms have been used to separate fast-spiking (FS) and regular-spiking (RS) cells quantitatively, by several studies (Andermann et al 2004, Atencio & Schreiner 2008, Bartho et al 2004, Bruno & Simons 2002, Hasenstaub et al 2005, Mitchell et al 2007).

The most comprehensive survey of mouse V1 neurons using extracellular responses was conducted by Niell and Stryker (2008). In this study, trough-to-peak time, slope-after-peak and peak-to-trough height ratios were used to separate FS and RS cells. ‘Trough’ refers to the most negative point on the waveform, whereas ‘peak’ refers to the most positive point. For the sake of comparison, we used the same separation parameters as Niell and Stryker’s study.

For each waveform in Figure 4.1A and 4.2A, we measured the time difference between trough and peak (Figures 4.1C and Figure 4.2C) and the slope of the waveform 700 μ s after the trough (Figures 4.1D and Figure 4.2D) and plotted those values against the trough to peak height ratios (i.e. ratio between the normalized amplitude of the trough and the peak). Using cluster analysis, points in each scatter plot were separated into two groups, represented by blue and red symbols. All red symbols in Figures 4.1C and 4.1D correspond to FS (red) units in Figure 4.1A. Except for one unit in Figure 4.2D, which is indicated as the black symbol, all red symbols in Figures 4.2C and 4.2D correspond to FS units in Figure 4.2A. As in Niell and Stryker’s study, these three parameters proved to be effective in distinguishing FS from RS cells. From my data, in mouse, 12% of all recorded units were FS cells (FS cells: $n = 9$, RS cells: $n = 69$), and in cat 5% of all recorded units were FS cells (FS cells: $n = 18$, RS cells: $n = 350$).

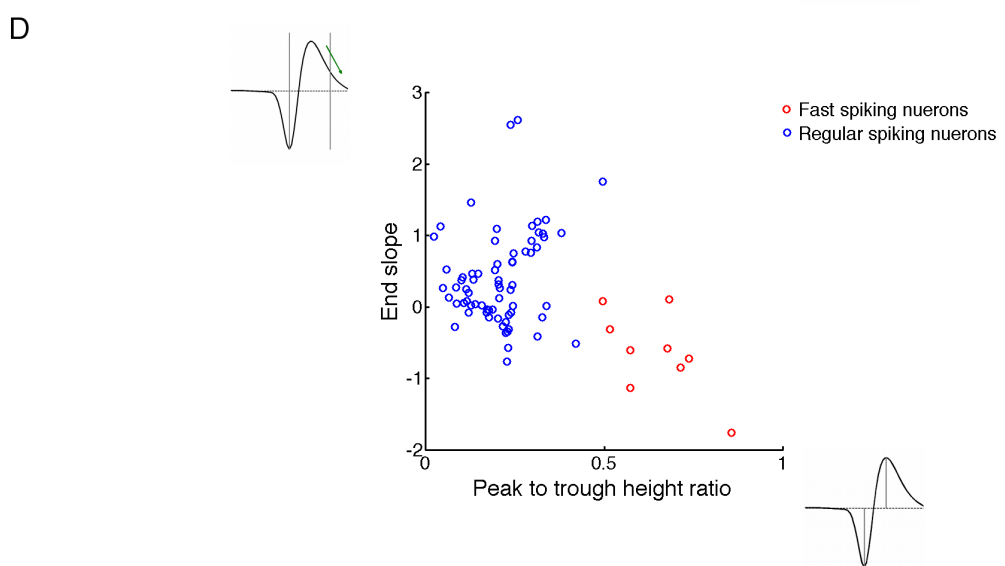
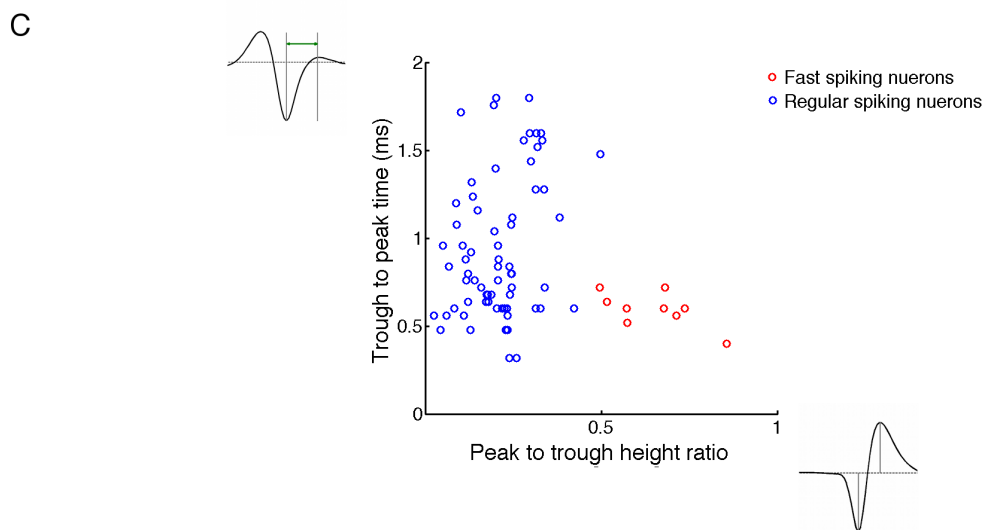
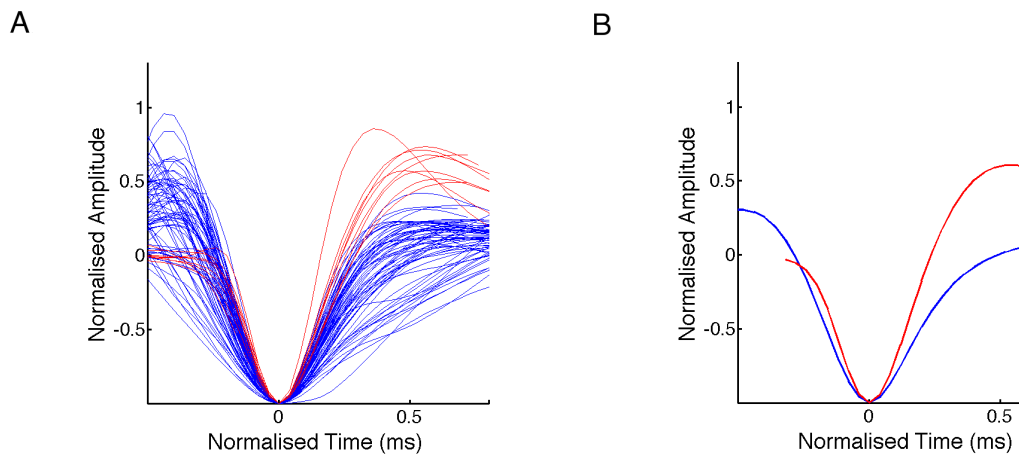


Figure 4.1. Separating FS and RS cells in mouse V1

Separating FS and RS cells in mouse V1 Separating fast-spiking (FS) and regular-spiking (RS) units in mouse V1 based on extracellular spike waveform shapes. **A**, Average spike waveforms for all analysed units, aligned and normalised by the trough depth. Red waveforms represent FS units ($n = 9$) and blue waveforms represent RS units ($n = 69$). **B**, Average of all FS (red) and RS (blue) waveforms. **C** and **D**, Scatter plots of spike waveform shape parameters that are used to separate FS and RS units. Cluster analysis is used to statistically separate points in scatter plots into FS and RS populations with corresponding colours.

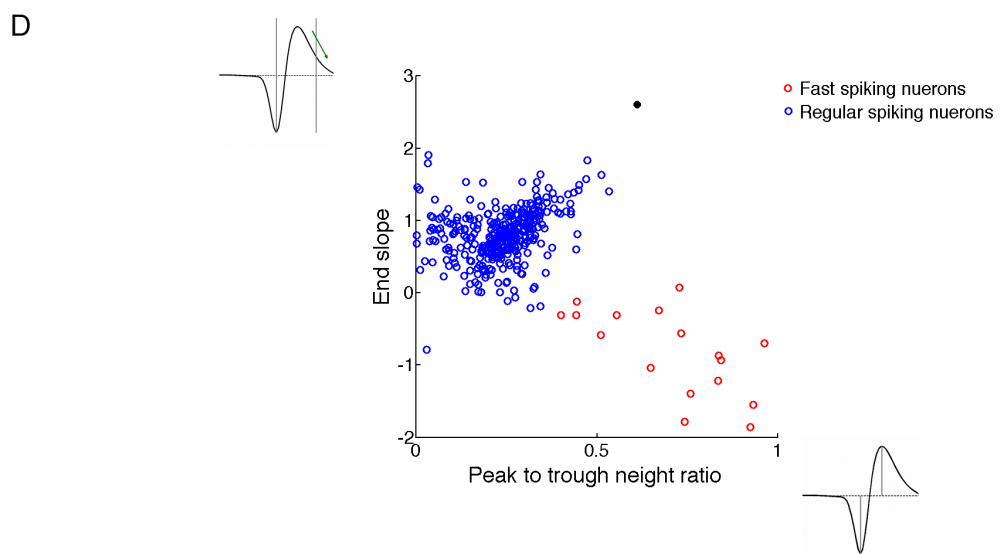
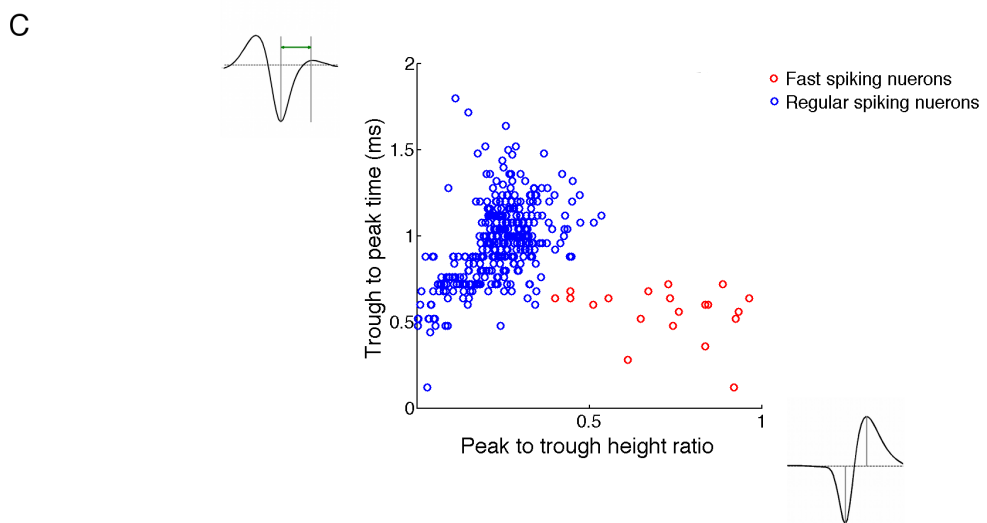
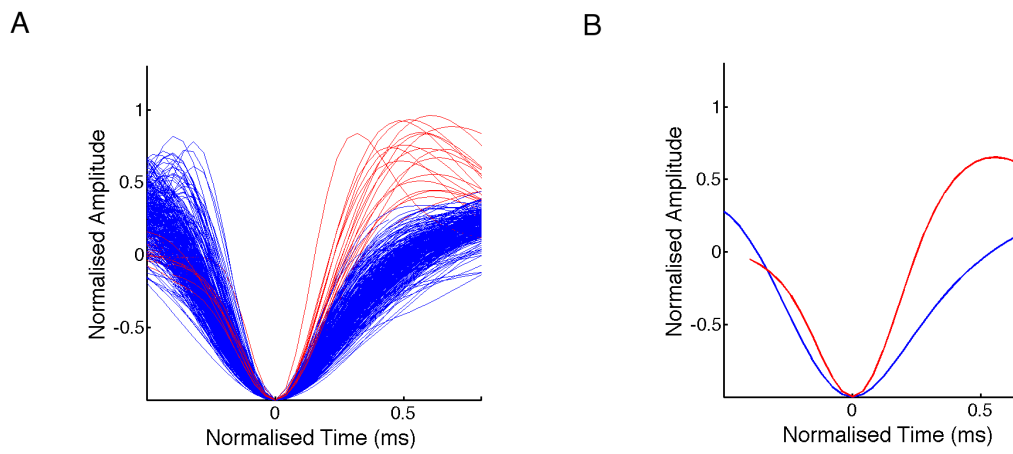


Figure 4.2. Separating FS and RS cells in cat V1

Separating fast-spiking (FS) and regular-spiking (RS) units in catV1 based on extracellular spike waveform shapes. **A**, Average spike waveforms for all analysed units, aligned and normalised by the trough depth. Red waveforms represent FS units ($n = 18$) and blue waveforms represent RS units ($n = 350$). **B**, Average of all FS (red) and RS (blue) waveforms. **C** and **D**, Scatter plots of spike waveform shape parameters that are used to separate FS and RS units. Cluster analysis is used to statistically separate points in scatter plots into FS and RS populations with corresponding colours.

4.4.2 Receptive field properties of FS and RS cells

Previous studies in several species and brain areas have established that FS cells correspond to a subset of GABAergic interneurons and RS cells are predominantly excitatory pyramidal neurons (turtle: Connors & Kriegstein 1986, rat: Kawaguchi & Kubota 1993, Guinea pig: McCormick et al 1985, cat: Nowak et al 2003, mouse: Rudy et al 2011, rat somatosensory cortex: Wang et al 2002, mouse somatosensory cortex: Xu & Callaway 2009). By identifying the recorded cells as FS or RS, we examined and compared the response properties and (for the cat) the laminar locations of the two neuronal populations. Figure 4.3 and Figure 4.4 illustrate the distribution of F_1/F_0 ratio, orientation index, peak spatial frequency and preferred temporal frequency amongst FS (red bars) and RS (blue bars) neurons of mouse and cat, respectively. The arrowhead with a value on each graph indicates the mean of the distribution. Figure 4.5 shows the analysis of laminar locations of FS and RS cells in three cats. The descriptions below outline the findings.

4.4.2.1 Response linearity

Response linearity was measured in the form of F_1/F_0 ratios. A cell is classified as a simple cell if it has an $F_1/F_0 > 1$, whereas an $F_1/F_0 < 1$ signifies a complex cell. The distributions of F_1/F_0 ratios in both mouse (Figure 4.3B) and cat (Figure 4.4B) V1 suggest that the majority of RS cells (90% for both mouse and cat) are complex cells with $F_1/F_0 < 1$ (two-sided Wilcoxon signed rank test, mouse: $p < 0.001$, cat: $p < 0.001$). The median F_1/F_0 ratio of the mouse RS population is 0.56, whereas the median F_1/F_0 ratio of the cat RS population is 0.27. The F_1/F_0 ratios of mouse FS cells are evenly distributed amongst simple (44%) and complex (56%) cell types (two-sided Wilcoxon signed rank test, $p = 0.125$). In fact, the average F_1/F_0 ratio (0.93) of mouse FS cells sits on the boundary between simple and complex cells, suggesting that no particular cell type is favoured in the FS spiking categories. Cat FS cells are mainly complex cells with 85% of the FS population having $F_1/F_0 < 1$ (Figure 4.4A, two-sided Wilcoxon signed rank test, $p < 0.001$). The median F_1/F_0 ratio of FS cells (0.23) in cat is very similar to the value for RS cells (0.27), showing that there is no difference in the distribution of

simple and complex cells amongst RS and FS spiking types (Wilcoxon rank sum test, $p = 0.145$).

4.4.2.2 Orientation selectivity

Orientation selectivity is quantified as an Orientation Index (OI), of which $OI = 0$ represents a cell that responds equally to all orientations, $OI = 1$ represents a very selective cell and a ratio of 3:1 corresponds to $OI = 0.5$. For mouse V1, both FS (median OI: 0.33, two-sided Wilcoxon signed rank test, $p = 0.125$) and RS (median OI: 0.2, two-sided Wilcoxon signed rank test, $p = 0.065$) populations show none-significant bias toward the low end of the orientation selectivity spectrum (Figure 4.3C and 4.3D). However, compared to RS cells, FS cells are more evenly distributed over a wide range of orientation selectivity. Approximately 67% of RS cells and 86% of FS cells show $OI < 0.5$. For cat V1, OI distributions of FS cells (Figure 4.4C) and RS cells (Figure 4.4D) show similar distribution, which exhibits a slight biases towards the higher end of the orientation selectivity spectrum (Wilcoxon rank sum test, $p = 0.008$). The median OIs for FS and RS cells are identical (0.82). As a population, cat FS cells are slightly less orientation selective than RS cells with 32% of FS cells and 22% of RS cells having an $OI < 0.5$.

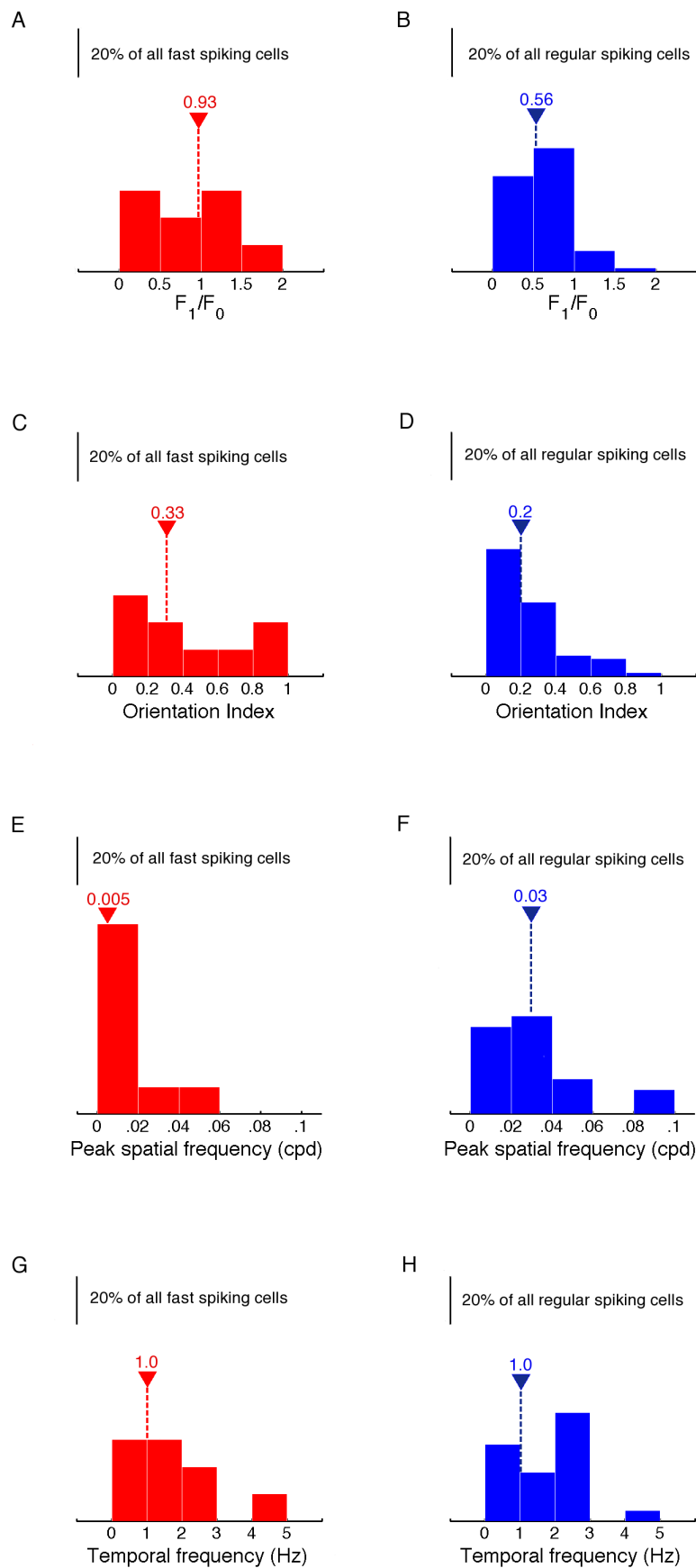
4.4.2.3 Spatial and temporal frequencies

Apart from a small proportion of mouse RS cells with peak spatial frequencies (PSFs) higher than 0.08, the majority of PSFs for mouse RS cells are distributed between 0 and 0.06 cpd, with a median PSF of 0.03 cpd (Figure 4.3F). In contrast, mouse FS cells show a highly skewed distribution towards the very low end of PSF with a median value of 0.005 cpd and 78% of the population having PSFs of 0.01 cpd (Figure 4.3E, two-sided Wilcoxon signed rank test, $p < 0.001$). For cat, both FS (median PSF: 0.4 cpd, two-sided Wilcoxon signed rank test, $p < 0.05$) and RS (median PSF: 0.2 cpd, two-sided Wilcoxon signed rank test, $p < 0.01$) cells are skewed toward the lower end of the PSF distribution (Figures 4.4E and 4.4F).

The peak temporal frequencies of FS and RS cells show similar distributions with the same medians in mouse (Figures 4.3G and 4.3H, Wilcoxon rank sum test, $p = 0.29$) and in cat (Figures 4.4G and 4.4H, Wilcoxon rank sum test, $p = 0.4$). It is noteworthy that the range of PSF and peak temporal frequencies for mouse V1 cells are significantly lower than those of cat V1 cells. The majority of mouse V1 cells have PSFs between 0 - 0.06 cpd (Figures 4.3E and 4.3F) and peak temporal frequencies between 0 – 3 Hz (Figures 4.3G and 4.3H), whereas most cat V1 cells show PSFs between 0 – 0.9 cpd (Figures 4.3E and 4.3F) and peak temporal frequencies of 0 – 9 Hz (Figures 4.4G and 4.4H).

Figure 4.3. Receptive field properties of FS and RS cells in mouse

Histograms of F_1/F_0 ratios (**A** and **B**), orientation index (**C** and **D**), peak spatial frequency (**E** and **F**) and temporal frequency (**G** and **H**) for FS and RS cells recorded from mouse V1. Red histograms represent FS cells and blue histograms represent RS cells. The arrow on each graph indicates the median value for the corresponding receptive field property.



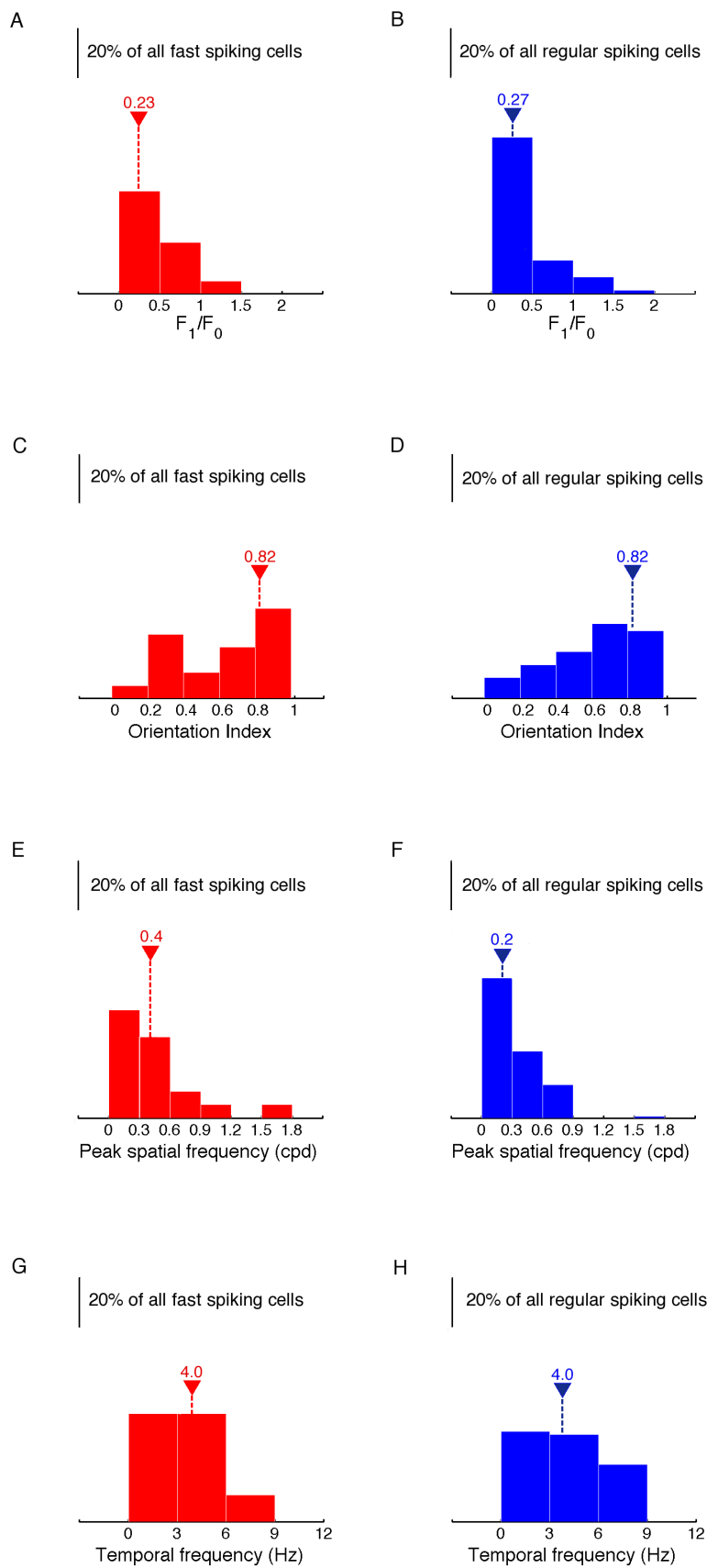


Figure 4.4. Receptive field properties of FS and RS cells in cat

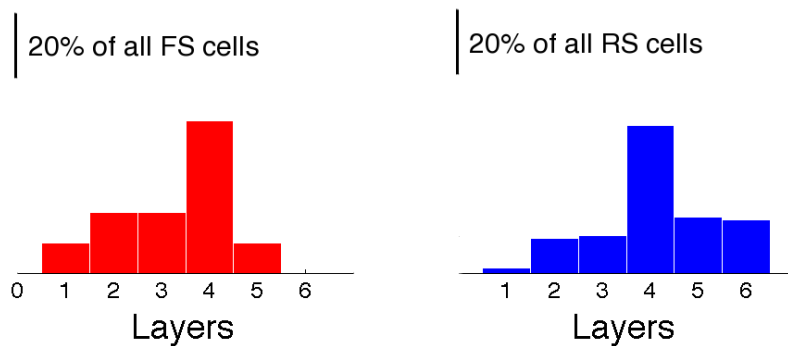
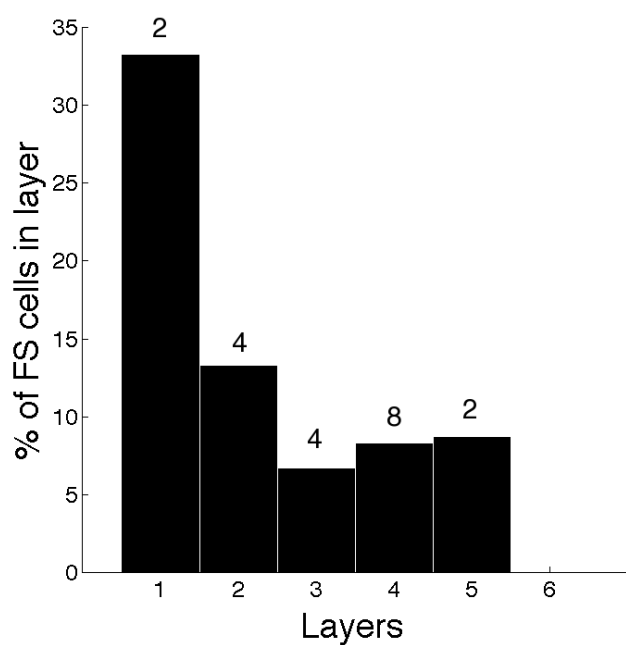
Histograms of F_1/F_0 ratios (**A** and **B**), orientation index (**C** and **D**), peak spatial frequency (**E** and **F**) and temporal frequency (**G** and **H**) for FS and RS cells recorded from cat V1. Red histograms represent FS cells and blue histograms represent RS cells. The arrow on each graph indicates the median value for the corresponding receptive field property.

4.4.2.4 Layer distribution of inhibitory and excitatory cells in cat

V1

For three cats ($n = 172$), we examined the laminar locations for every recorded cell. Figure 4.5A shows the distribution of FS cells (red bars on the left) and RS cells (blue bars on the right) amongst the six layers of V1. For both FS and RS spiking cells, there is an overrepresentation of Layer 4 neurons. No FS cells were recorded in Layer 6, and a very small proportion of RS cells were found in Layer 1. Figure 4.5B demonstrated the percentage of FS cells out of all recorded cells in each layer. It clearly shows that FS cells are over-represented in the most superficial layers (i.e. Layer 1) compared to the other layers, which all show similarly low percentages of FS compared to Layer 1.

It was not possible to establish the layer distributions of mouse cells as tissue damage during long recordings made it difficult to locate recording locations.

A**B****Figure 4.5. Layer distributions of FS and RS cells in cat V1**

A, Histograms of laminar locations of FS (red histogram on the left) and RS cells (blue histogram on the right). **B**, Population histogram shows the percentage of FS cells in all recorded cells in each layer. The number above each bar indicates the number of FS cells in each layer.

4.4.2.5 Correlating contrast response functions and cell type

All cortical visual neurons have a characteristic contrast response function (CRF). Figure 4.6A illustrates a CRF of a mouse V1 neuron. Typically, the CRF is sigmoidal in shape, with low contrasts generating very few spikes, a steep increase in spike rate with increasing contrast in a mid-contrast range and then a saturation, where increases in contrast do not lead to further increases in spike rate. I fit the CRFs for all recorded cells in mouse and cat using a sigmoidal function of the form:

$$R(c) = \frac{R_{\max} \times c^n}{c^n + C_{50}^n} + M$$

where $R(c)$ is the amplitude of the evoked response at contrast c , M is the spontaneous rate, n is the exponent that determines the steepness of the curve, R_{\max} is the maximum elevation in response above the spontaneous rate, and C_{50} is the contrast that generates a response elevation of half R_{\max} (the dotted line in figure 4.6A). C_{50} is also referred to as the semi-saturation contrast. Goodness of fit to the curves was measured with R^2 values, and across all fits this measure formed a highly skewed distribution with a mean of 0.9, and a median of 0.96. Rarely, contrast response functions did not show saturation at higher contrasts; in these cases the upper and lower R_{\max} bounds for the fit were set at $\pm 10\%$ of the maximum measured neuronal response above spontaneous.

Figure 4.6B and 4.6D show the distribution of C_{50} s for FS and RS cells in mouse cortex. For the nine FS cells the C_{50} s were between 0.2 and 0.6. For the 61 RS cells the distribution was highly skewed towards contrasts in the same range (0.2 - 0.6) (two-sided Wilcoxon signed rank test, $p = 0.01$), with a small percentage of cells with $C_{50} > 0.6$. In the cat, as shown in Figure 4.6C and 4.6E, the FS cells were distributed between contrasts of 0 and 1, with a non-significant bias towards lower contrasts (Figure 4.6C, two-sided Wilcoxon signed rank test, $p = 0.125$). Cells with C_{50} s at high contrasts (> 0.6) represented 24% of the population. The 320 RS cells had C_{50} s that spanned the entire contrast range, but there was a very highly skewed distribution (Figure 4.6C, two-sided Wilcoxon

signed rank test, $p < 0.01$). Low contrasts were over-represented, while high contrasts were under-represented. Cells with $C_{50S} > 0.6$ represented only 7% of the cat population.

I was interested in the differences between the distributions of C_{50} for the FS and RS cells in relation to contrast. Therefore, I subtracted the percentage of RS cells in each contrast bin from the percentage of FS cells. For the mouse, this calculation revealed little because the distribution of FS cells was so narrow (Figure 4.6F). However, for the cat data, this simple difference calculation emphasised the observation made in the previous paragraph (Figure 4.6F), i.e. FS cells with high C_{50S} are over-represented, while those with low C_{50S} are under-represented.

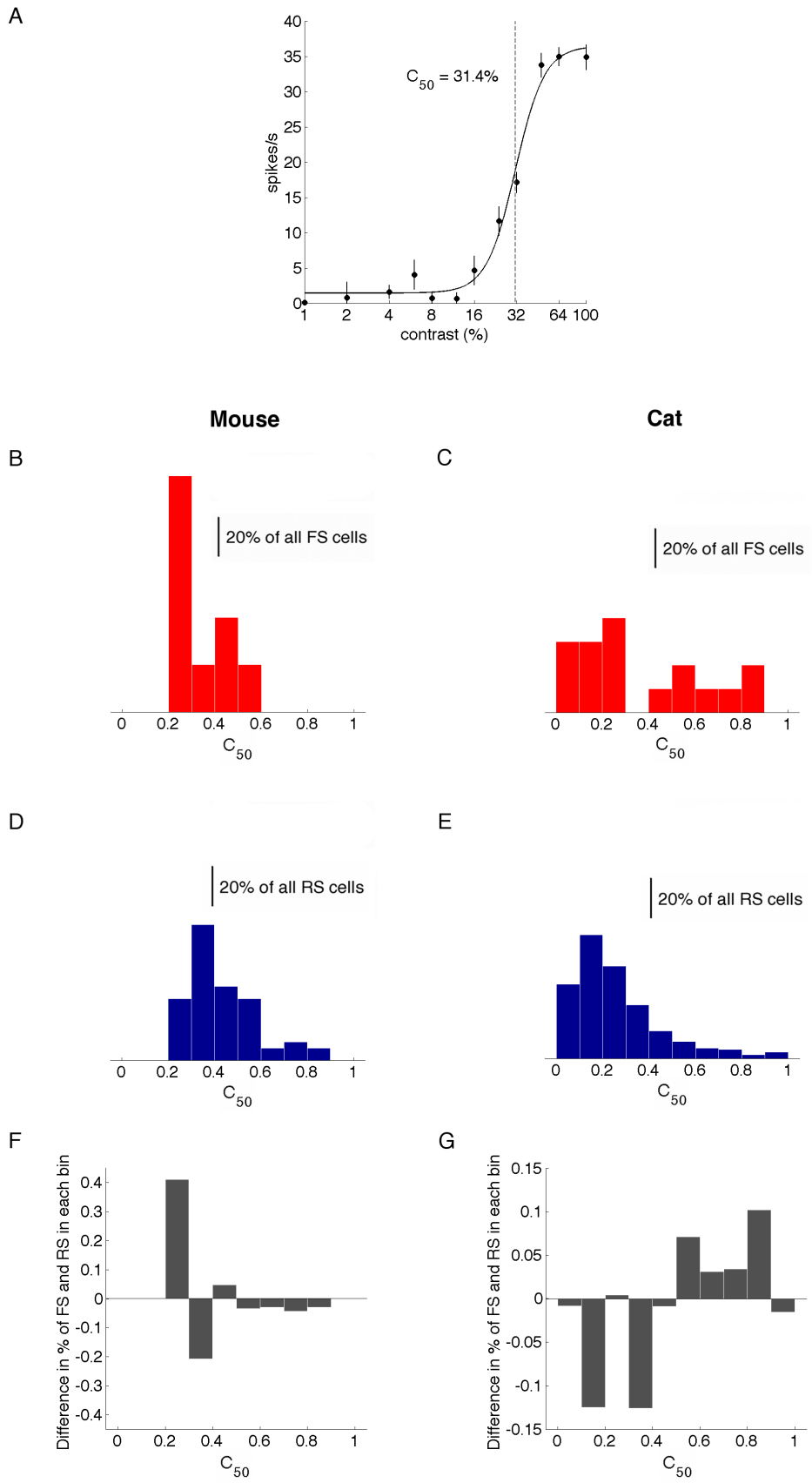


Figure 4.6. CRFs of FS and RS cells in mouse and cat V1

Contrast response functions (CRFs) of FS and RS cells in mouse and cat V1. **A**, a CRF of a mouse V1 neuron, which is the best fit to the spike rate of the cell at various contrast levels. The CRF is classically sigmoidal in shape with low spike rates at low contrasts, a steep increase in spike rate with increasing contrast in a mid-contrast range and a saturation phase where increases in contrast no longer result in further spike rate increases. The dotted line indicates the C_{50} or semi-saturation contrast, which is the contrast that generates a response elevation at half of the maximum elevation in response above the spontaneous rate. C_{50} is used as a measurement for the saturation contrast level of neuronal responses. **B – E**, Histograms of C_{50} for FS and RS cells recorded from mouse (**B** and **D**) and cat (**C** and **E**) V1. Red histograms represent FS cells (**B** and **C**) and blue histograms represent RS cells (**D** and **E**). **F – G**, The distribution of the percentage of RS cells in each contrast bin showed in B-E from the percentage of FS cells for mouse (**F**) and cat (**G**) populations. A Bar above zero indicates that the proportion of FS cells is higher than the proportion of RS cells in that particular C_{50} bin, whereas a bar below zero suggests a higher proportion of RS cells compared to the proportion of FS cells.

4.5 Discussion

4.5.1 Inhibitory cells play an important role in visual processing

Cortical GABAergic inhibitory neurons, which here onwards will be referred to as inhibitory cells, are morphologically, physiologically and molecularly different to excitatory cells. They have different but equally important roles to excitatory neurons in cortical processing. With recent advances in developing and applying genetic and molecular tools, our understanding of their roles in neuronal network computations is just beginning. Nevertheless, it has long been recognised that cortical inhibition is more than just a regulator of circuit excitability. The highly interconnected networks of inhibitory neurons are very diverse in their anatomical, molecular and physiological properties, which are well suited for a wide range of cortical functions such as circuit refinements, stabilisation, restrain and synchronization (Foldy et al 2004).

Although the V1 is one of the most extensively researched cortical areas, receptive field properties of inhibitory cells in various species remains relatively obscure due to the difficulty in identifying them *in vivo*. To comprehensively identify an inhibitory cell, its morphological, molecular and physiological properties all need to be acquired. The receptive field properties of individual V1 neurons could be obtained through *in vivo* extracellular electrophysiological recordings, however, to identify the recorded neuron morphologically and molecularly *in vivo*, intracellular access is necessary. Not only is intracellular recording more difficult than extracellular recording, the cell also needs to be labelled and examined post-mortem. Although informative and thorough, these labour intensive investigations have limited the range of observations and the recording conditions under which neurons have been studied. It would be, therefore, beneficial if neurons could be identified through their physiological responses alone.

4.5.2 Identifying inhibitory cells *in vivo*

A field of cortical research is dedicated to the classification of inhibitory subtypes. It has long been established that inhibitory cells have distinct electrophysiological responses, which are different to those of excitatory cells (Bartho et al 2004, Connors & Kriegstein 1986, Griffen & Maffei 2014, McCormick et al 1985, Nowak et al 2003, Simons 1978). Mountcastle et al. (1969) first described the extracellular discharge of a class of somatosensory neurons as ‘thin-spikes’, referring to the narrow spike waveform, and speculated that those neurons were thalamic-afferent-targeting interneurons. Later, several intracellular studies confirmed that neurons with narrow spike widths corresponded well with parvalbumin (PV)-expressing interneurons. These cells comprise the basket cells and chandelier cells in cortex, whereas excitatory pyramidal neurons exhibit spikes with broader widths (Connors & Kriegstein 1986, Kawaguchi & Kubota 1993, McCormick et al 1985, Nowak et al 2003, Rudy et al 2011, Wang et al 2002, Xu & Callaway 2009). The two classes of neurons were referred to as fast spiking (FS) cells and regular spiking (RS) cells. The likely cause for the difference in spiking duration is the expression of different classes of K^+ and Na^+ channels, which differ in their kinetics and their distributions on the neurons (Erisir et al 1999, Martina & Jonas 1997, Martina et al 1998).

Although accurate, due to the scarcity of interneurons and the time-consuming nature of the recording methods, identifying cell types through intracellular whole cell recording yields very few cells. It would be beneficial to identify cell types and obtain response properties through highly efficient extracellular recording. Studies have shown that the duration of extracellular spike waveforms directly correspond to intracellular spike widths, which suggests that it is possible to distinguish FS and RS cells based only on the shape of extracellular spike waveforms (Gold et al 2006, Henze et al 2000).

Subsequent studies have derived a set of classification criteria based on the shape of extracellular spike waveforms. Bartho et al. (2004) demonstrated that the trough-to-peak duration of unfiltered extracellular spikes was a reliable

measurement for distinguishing GABAergic interneurons and pyramidal neurons in rat frontal cortex. Mitchell et al. (2007) further confirmed that extracellular trough-to-peak duration was bimodally distributed amongst neurons in Macaque V1. The ratio of trough and peak amplitude (Andermann et al 2004, Hasenstaub et al 2005), the duration of spike after-hyperpolarisation, measured as time between two zero crossings after the initial peak (Atencio & Schreiner 2008, Bruno & Simons 2002), and the slope-after-peak (Niell & Stryker 2008) have all been waveform shape parameters used to distinguish FS and RS neurons.

Many studies have utilised the above classification scheme to identify recorded neurons in different cortical areas of various species (rat somatosensory cortex: Andermann et al 2004, Lee et al 2007; cat: Atencio & Schreiner 2008, Macaque: Mitchell et al 2007, mouse: Niell & Stryker 2008, rabbit: Swadlow 2003). In their comprehensive survey of mouse V1 receptive field properties, Niell and Stryker (2008) classified units as either FS or RS neurons based on the trough-to-peak duration, the ratio of trough and peak amplitude and the slope-after-peak of their extracellular spike waveforms. For comparison, we used identical parameters in the present study to separate FS and RS neurons in mouse and cat cortex. Our results show that 13% of all recorded units in mouse were fast-spiking, which was similar to but slightly lower than Neill and Stryker's result of 19%. A study that identified inhibitory cells through histochemically labelling GAD, a marker protein found in all GABAergic inhibitory cells, also showed that 19% of the mouse V1 neuronal population were GAD-expressing inhibitory cells (Tamamaki et al 2003).

I used the same waveform parameters to separate recorded units in cat V1 in the present study. A smaller proportion of FS cells (5%) were observed amongst cat V1 cells than amongst mouse cells. Intracellular studies that have looked for FS cells in cat cortex have reported percentages in the range 10 to 33% (Cardin et al 2007, Nowak et al 2003). These studies conducted intracellular recording from Layers 2-6, with an over-emphasis on Layer 4. None of the studies recorded any responses from Layer 1. It is possible that the extracellular electrodes I used favoured RS cells (probably large pyramid cells), while the intracellular

electrodes used in previous studies were better at isolating FS cells (see below for a longer discussion of electrode issues).

It is important to keep in mind that there are significant limitations associated with using extracellular spike waveforms to separate inhibitory and excitatory cells. First of all, it has been established that other spike waveform shapes and discharge patterns exist amongst inhibitory cells (Cauli et al 1997, Cauli et al 2000, Hu et al 2014, Kawaguchi 1995, Kawaguchi & Kondo 2002, Kawaguchi & Kubota 1993, Kawaguchi & Kubota 1997, Kawaguchi & Kubota 1998, Povysheva et al 2008, Wang et al 2002, Zaitsev et al 2005, Zaitsev et al 2009). Especially, some inhibitory cells have been shown to display regular spiking waveforms that are indistinguishable from excitatory cells; namely basket cells expressing cholecystokinin and/or vasoactive intestinal peptide (Kawaguchi 1995, Kawaguchi & Kubota 1997, Wang et al 2002, Zaitsev et al 2009) and a subgroup of somatostatin-expressing Martinotti cells (Ali & Thomson 2008, Kawaguchi & Kubota 1997, Thomson et al 2002, Wang et al 2004). FS cells are thought to be predominately PV-expressing GABAergic inhibitory neurons (Kawaguchi & Kubota 1993, Povysheva et al 2008, Rudy et al 2011, Wang et al 2002, Woodruff et al 2009, Xu & Callaway 2009).

However, some studies suggest that a small proportion of PV-expressing neurons were found to have regular spiking or other firing patterns (Blatow et al 2003, Han 1994, Kawaguchi & Kubota 1997, Kawaguchi & Kubota 1998, Krimer et al 2005, Markram et al 2004) and spike width (Nowak et al. 2003, Gray & McCormick 1996, Haider et al. 2010). As a result, it is possible that some RS cells identified in this study might in fact be inhibitory in nature. Along similar lines, several recent studies showed that some excitatory cells in both rodents and primates exhibit spike waveforms that resemble FS cells (Sohya et al 2007, Vigneswaran et al 2011).

Taken together, it is evident that this classification scheme is prone to ambiguity and errors (Gold et al 2006, Gonzalez-Burgos et al 2005, Henze 2000). On the other hand, fast spiking PV-expressing cells are the dominant inhibitory subtype

in the cortex; it comprises 50-74% of all inhibitory cells depending on the study and the species in question (Chow et al 1999, Demeulemeester et al 1991, Gonchar & Burkhalter 1997, Kawaguchi & Kubota 1997, Schwark & Li 2000). In addition, compared to the large number of RS excitatory cells in the cortex, the small outlier groups of RS inhibitory cells and FS excitatory cells are likely to be minimal (Defelipe & Farinas 1992). Overall, the advantage of extracellular recordings seems to outweigh the uncertainties of the classification scheme, especially in studies that focus on large population surveys of electrophysiological properties, which demand rapid and straightforward indication of neuronal identity.

In the present study, I used the shape of extracellular spike waveforms as a means to identify recorded units as inhibitory or excitatory. With the rapid development of genetic and imagining tools, there are now more sophisticated and accurate methods for classification of cell types and examining their stimulus preferences (Hofer et al 2011, Kerlin et al 2010, Liu et al 2009, Ma et al 2010, Runyan et al 2011, Runyan & Sur 2013, Sohya et al 2007, Zariwala et al 2011). However, most of these new experimental techniques were exclusively available for mouse cortex, which makes it difficult to compare new findings with other species. In the current study, we had the opportunity to examine a large population of cortical neurons in two major animal models, in parallel. The identical recording and classification methods ensure a credible comparison between the two species.

4.5.3 Receptive field properties of FS and RS cells in mouse and cat V1

After identifying all recorded units as either FS or RS cells, we examined and compared receptive field properties, specifically the orientation selectivity, response linearity, peak spatial frequency and peak temporal frequency, of FS and RS populations in mouse and cat V1.

4.5.3.1 Orientation selectivity

Orientation selectivity is one of the most extensively studied receptive field properties in visual neurons. My results show that FS cells in mouse V1 exhibit a broad range of orientation tuning. To date, the orientation tuning of mouse V1 inhibitory neurons was examined in several studies. Including the present study, several studies have described a broad range of orientation selectivity amongst inhibitory cells (Ma et al 2010, Niell & Stryker 2008, Runyan et al 2011, Runyan & Sur 2013, Zariwala et al 2011), whereas other studies have only found weakly or non-selective inhibitory cells (Atallah et al 2012, Hofer et al 2011, Kerlin et al 2010, Liu et al 2009, Sohya et al 2007).

New experimental techniques such as genetic labeling of specific cell types and functional two-photon imaging were recently utilised in the survey of receptive field properties in mouse V1 (Hofer et al 2011, Kerlin et al 2010, Liu et al 2009, Ma et al 2010, Runyan et al 2011, Runyan & Sur 2013, Sohya et al 2007, Zariwala et al 2011). It is likely that differences in targeting and recording methods could have resulted in the latter studies missing the highly tuned subclass of inhibitory cells that have smaller soma (Hasenstaub & Callaway 2010).

Variations in receptive field properties amongst the same group of cells imply that these neurons might sample and integrate their inputs in different ways. A recent study in mouse V1 supports this notion. It was demonstrated that PV-positive inhibitory neurons with a range of orientation selectivities differ in their dendritic morphology: highly selective cells have short proximally branched dendrites, which were thought to sample sparsely from a homogenous local area, whereas weakly selective cells have longer and distally branched dendrites that possibly sample from a more distant and heterogeneous population (Runyan & Sur 2013). Even though mouse V1 lacks the highly organised orientation maps found in carnivores (Metin et al 1988b, Ohki et al 2005, Schuett et al 2002b, Van Hooser et al 2005), recent studies have found local clustering of orientation preferences and strong reciprocal connections between neighboring neurons with similar stimulus preferences (Bock et al 2011, Cossell et al 2015, Hofer et al 2011, Kerlin et al 2010).

Similar to mouse, studies in cat V1 also seem to be in favour of FS cells showing a diverse range of orientation selectivity (Azouz et al 1997, Cardin et al 2007, Hirsch et al 2003, Nowak et al 2008), which is in agreement with my observations. Evidence suggests that orientation selectivity of FS cells in cat V1 varies with laminar locations: Layer 4 FS cells are either broadly tuned or untuned (Cardin et al 2007, Hirsch et al 2003, Nowak et al 2008); FS cells outside Layer 4 are sharply tuned (Cardin et al 2007), but this study did not include any cells from Layer 1.

The laminar difference in tuning properties suggests that inhibition may contribute to shaping receptive field properties in a laminar-specific fashion. In my study, the higher proportion of FS cells (as a percentage of cells in that layer) were found in Layer 1. Given that previous studies have not included cells from this layer, my study is the first to show that Layer 1 has a high proportion of FS cells compared to other cortical striations. These cells showed a range of orientation tuning, so no particular sharpness or broadness of tuning can be assigned to FS cells in Layer 1 of cat.

4.5.3.2 Response linearity (simple and complex)

Response linearity, which is measured as an F_1/F_0 ratio, is another key receptive field property examined in the current study. A V1 neuron can be classified as either a simple cell, whose predictable responses are the result of linear summation of overall inputs, or a complex cell, which exhibits non-linear input summation. FS cells recorded in the current study showed an even distribution of F_1/F_0 ratios with perhaps marginally more complex cells than simple cells. On the other hand, the majority of FS cells in Niell and Stryker's (2008) study were complex cells. It is not clear why this inconsistency between the two studies exists.

For cat V1, the majority of FS cells were complex cells. The few studies that have investigated response linearity of inhibitory neurons in cat V1 are mostly

intracellular studies of Layer 4 neurons, usually with limited sample sizes, typically around ten cells recorded in total. Two studies found more simple cells than complex cells (Azouz et al 1997, Nowak et al 2003) in layer 4, whereas one study recorded from equal numbers of simple and complex cells (Hirsch 2003). To the best of our knowledge, the present study is the first large-scale study to show the simple and complex cell composition of the FS population in cat V1. A recent large-scale survey (109 cells) in awake rabbit V1 also showed a larger proportion of complex cells amongst Layer 4 FS cells (Zhuang et al 2013).

In the present study, the majority of RS cells in both mouse and cat V1 were found to be non-linear complex cells. This observation is different to Niell and Stryker's (2008) study, which showed that RS cells in mouse V1 were predominantly simple cells. In cat V1, Nowak et al. (2003) also showed more simple cells ($n = 24$) than complex cells ($n = 9$) amongst RS cells. There is a clear over-representation of complex cells amongst recorded units in the present study. It has been noticed from past studies conducted in our laboratory that we tend to record from more complex cells than simple cells in cat V1 (Crowder et al 2006, Crowder et al 2007, van Kleef et al 2010). The fact that experiments performed on many animals by different researchers over many years all showed a tendency towards recording from more complex cells suggests that the discrepancy is unlikely a result of laminar bias during recording; it is more likely to be caused by differences in experimental methods, most probably the electrode types used (see heading below).

If we consider the distribution of orientation selectivity again, although not the majority, a considerable number of cat V1 neurons showed low orientation selectivity. It is well established that cat V1 neurons are highly orientation selective, with some studies showing as much as 95-99% of cells exhibiting high levels of orientation selectivity (reviewed by Van Hooser 2007). Therefore, compared to the general consensus, our cat V1 population exhibits a higher proportion of non- or weakly-selective cells. Interestingly, studies have confirmed that Layer 4 FS cells are either broadly tuned or untuned (Cardin et al 2007, Hirsch et al 2003, Nowak et al 2008) and our results clearly showed that

the majority of the cells in the cat V1 population were recorded in Layer 4. At the same time, we observed a significant bias towards complex cells amongst the same population. Hirsch et al. (2003) showed that cat V1 neurons with little or no orientation selectivity in Layer 4 seem to have complex receptive fields, which suggests that this subpopulation may be over-represented in the data presented here. However, in contrast, Cardin et al. (2007) claimed that they had failed to observe any un-tuned complex cells in Layer 4. It appears that the type of electrode used may bias the data towards certain cell types.

4.5.3.3 Laminar locations

Among studies that investigated the FS and RS receptive field properties of cat V1, Hirsch et al. (2003) and Nowak et al. (2008) only investigated the orientation selectivity of Layer 4 FS and RS cells, whilst Cardin et al. (2007) and Azouz et al. (19997) examined neurons in Layers 2-6 and Layers 2-4, respectively. Our results have shown a significant over-representation of FS cells in Layer 1, which was not examined in other studies. It has been demonstrated that neurons in Layer 1 of rat V1 are almost exclusively inhibitory, with the majority of cells exhibiting fast-spiking waveforms (Anderson et al 1992, Hestrin & Armstrong 1996, Zhou & Hablitz 1996a, Zhou & Hablitz 1996b). Layer 1 cells were found to receive both excitatory and inhibitory inputs and serve in an inhibitory intracortical feedback circuit. This subpopulation of FS cells is missing in the previous cat studies.

4.5.3.4 Contrast response functions

In Figure 4.6 I showed that for cats, the semi-saturation (C_{50}) points for the CRFs of FS cells had a different distribution across contrast than the C_{50} s for RS cells. Cells with $C_{50} > 0.6$ were common for FS cells (24%) but uncommon for RS cells (7%). This observation means that amongst the FS cell population, fewer cells are sensitive to low contrasts than is the case for RS cells. Another study that examined the C_{50} of FS and RS cell responses also showed a higher C_{50} in FS cell than RS cells (Contreras & Palmer 2003). However, this observation was observed in the membrane potential instead of spiking activity. The implication

is that as a population inhibitory FS cells may exert less influence at low contrasts. In following chapters I discuss the influence of stimulus contrast on receptive field structures in visual cortex. It is shown that the sensitivity to the spatial phase of a moving or contrast-reversing grating stimulus increases in cat and mouse cortex as stimulus contrast declines (see Chapters 5 and 6, also see Crowder et al. 2007; Hietanen et al. 2013; Cloherty and Ibbotson 2015).

The present observation suggests that at the population level, at low contrasts there will be less inhibition from FS cells. Therefore, it is plausible that the inability of 24% of FS (inhibitory) cells to respond at low contrasts may influence the receptive field organisations of the excitatory population. Of course, this is speculative and the observations are based on relatively few FS cells. It should also be noted that a similar assertion could not be formed about mouse cortex. However, the theory in cat cortex is worth further investigation.

4.5.3.5 Discrepancy: a result of different recording electrodes?

A likely explanation for the discrepancy in percentages of FS cells is the difference in electrodes used for extracellular recordings in various studies. In our laboratory, single tungsten electrodes coated with laquer were used for all recordings. Niell and Stryker (2008) used silicon multi-electrode arrays that were embedded in mouse V1. Other studies using single tungsten electrodes also showed some discrepancies in receptive field properties of mouse V1 neurons to that of Niell and Stryker's study (Mangini & Pearlman 1980b, Metin et al 1988b, Van den Bergh et al 2010). Similar to our results, the proportion of orientation selective neurons (both FS and RS cells) recorded in two early studies using single tungsten electrodes was lower compared to Niell and Stryker's study: 34% orientation selective cells were reported by Mangini and Pearlman (1980b) and 41% by Metin et al. (1980b), as compared to 74% shown by Niell and Stryker. Moreover, a recent study using tungsten electrodes recorded from a higher proportion of complex cells (62%) than simple cells (38%) (Van den Bergh et al 2010).

In their study, Niell and Stryker suggested that these discrepancies were related to the differences in recording electrodes. They suspected that sharp tungsten electrodes have the tendency to selectively isolate afferents of LGN cells, which were thought to have non-oriented responses. In addition, even with the same type of electrodes, the electrode impedance could have an effect on the type of cells recorded. It is obvious that for both mouse and cat, we recorded from many more RS cells than FS cells. A study that segregated inhibitory and excitatory cells based on the extracellular spike waveform in rat V1 recorded almost equal numbers of FS and RS cells (54 RS cells and 45 FS cells) (Bruno & Simons 2002). Single tungsten electrodes were used for recording in Bruno and Simons' study, however, the impedance of their electrodes ($5\text{-}12\text{ M}\Omega$) were much higher than the ones used in the current study ($1\text{-}2\text{ M}\Omega$). With similar electrode impedances (less than $1\text{ M}\Omega$), Niell and Stryker also recorded from many more RS cells than FS cells (190 RS cells and 45 FS cells).

The difference in morphological features between inhibitory and excitatory cells, such as soma size, could potentially result in differential recording preferences with various types of electrodes and/or differences in electrode impedance.

4.5.3.6 Preferred spatial and temporal frequencies

We also looked at some basic receptive field properties such as preferred spatial and temporal frequencies. The ranges of preferred spatial and temporal frequencies observed in all recorded units of mouse V1 agree with previous studies (Gao et al 2010, Niell & Stryker 2008, Van den Bergh et al 2010). Compared to RS cells, FS cells have lower peak spatial frequencies. This difference was also demonstrated in Niell and Stryker's study (2008), where the median peak spatial frequencies for the FS population was significantly lower than the RS population. Here, little difference was observed in the distributions of preferred temporal frequencies between FS and RS cells in mouse V1, which is also similar to Niell and Stryker's (2008) observation.

The FS and RS cells in cat V1 show similar distributions in their preferred spatial and temporal frequencies in the present study. The similarity in preferred spatial frequency distributions between FS and RS cells is in agreement with the intracellular study of cat cortex by Cardin et al. (2007). However, to our best knowledge, the present study was the first to examine the preferred temporal frequencies of FS and RS cells separately.

4.5.4 Summary

It has been clearly demonstrated in this chapter that FS inhibitory and RS excitatory cells in both mouse and cat V1 could be effectively separated based on the shape of extracellular spike waveforms. In mouse V1, FS cells were evenly distributed amongst complex and simple cells and exhibit a broad range of orientation selectivity, whereas the majority of RS cells were non-selective complex cells. Compared to mouse V1, FS and RS cells in cat V1 exhibit fewer differences between their receptive field properties. In addition, it was revealed that FS cells are significantly over-represented in Layer 1 of cat V1 and are less sensitive to low contrasts as a population compared to RS cells. Since similar recording and analysis procedures were performed in both mice and cats in this study, the comparison between the two species is credible. In agreement with general consensus, my findings have demonstrated some major differences between mouse and cat V1 neurons, which suggest that direct comparison between the receptive field properties of the two species should be undertaken with caution.

Chapter 5: Contrast-Dependent Phase-Sensitivity of V1 Complex Cells Tested by Drifting Gratings

5.1 Abstract

Neurons in mammalian primary visual cortex (V1) are classified into simple and complex cells. Simple cells strongly modulate their responses according to the position of oriented edges in their receptive fields, whereas complex cells respond relatively evenly wherever the edge is located in their receptive fields. This difference reflects the distinct receptive field structures of simple and complex cells and can be measured quantitatively as the degree of sensitivity to the spatial phases of a moving sinusoidal grating. Specifically, simple cells respond only when the grating is in-phase and don't respond when it is out of phase, whereas complex cells are phase insensitive. Recent evidence has shown that some complex cells in cat areas 17 and 18 (collectively V1) and monkey V1 exhibit increased phase sensitivity in their extracellular spiking responses as the stimulus contrast is reduced. I present in this chapter data from a subset of mouse V1 complex cells that also display contrast-dependant phase sensitivity in their extracellular spiking responses. I also present data based on intracellularly recorded membrane potentials that support the extracellular results. These findings demonstrate that the dynamic phase sensitivity in V1 complex cells is preserved across mammalian species. More importantly, it is a fundamental physiological property resulting from altered synaptic inputs rather than simply a non-linear transformation between membrane potential and spike outputs.

5.2 Introduction

One of the most fundamental response properties of V1 neurons is their selectivity for the spatial phases of moving sinusoidal gratings presented within

their receptive fields. Some cells are selective for the spatial phase of the grating (simple cells), whereas other cells are phase-insensitive (complex cells) (De Valois et al 1982, Maffei & Fiorentini 1973, Movshon et al 1978a, Movshon et al 1978b). The difference in spatial phase sensitivity is thought to reflect the differences in the rudimentary receptive field structures between simple and complex cells (Hubel & Wiesel 1962). It has been demonstrated in cat areas 17 and 18 (henceforth referred to as V1) as well as primate V1 (only area 17), that a subpopulation of complex cells show increased phase sensitivity as the stimulus contrast is reduced (cat: Bardy et al 2006a, Crowder et al 2007, van Kleef et al 2010; monkey: Cloherty & Ibbotson 2015, Durand et al 2012, Henry & Hawken 2013, Romo et al 2011).

The effect of stimulus contrast on phase sensitivity of complex cells has only been observed through recording extracellular spiking responses. Several studies have proposed the idea that the observed difference in spiking responses to drifting gratings between simple and complex cells is a result of a non-linear transformation between membrane potentials and spike outputs (Carandini & Ferster 2000, Mechler & Ringach 2002, Priebe et al 2004). Therefore, there are two obvious explanations for phase sensitivity changes in complex cells. It could be either a change in the fundamental receptive field structures resulting from altered synaptic inputs at low stimulus contrasts, or the transformation between membrane potential and spikes. To test these competing theories, the effect of stimulus contrast on intracellular membrane potentials of V1 neurons will be studied in parallel to their extracellular spiking responses.

In this chapter, I examined both extracellular and intracellular responses of mouse V1 neurons to moving gratings under different stimulus contrasts. Compared to larger mammals, mice are more practical for technically demanding intracellular recordings. Moreover, it has recently become an established model for cortical vision research (Huberman & Niell 2011). The results demonstrate that, similar to cat and monkeys, a subset of complex cells in mouse V1 show increased phase sensitivity as the stimulus contrast is reduced. This effect was observed in both extracellular spiking responses and intracellular membrane

potentials. This finding not only confirmed the dynamic phase sensitivity as an intrinsic property of a proportion of mammalian V1 neurons, but also further demonstrated the relevance of mouse V1 as a useful model for studying cortical visual processing.

It was recently established that the analysis of spiking responses is universally sensitive to the number of spikes available (Cloherty & Ibbotson 2015, Crowder et al 2007, Hietanen et al 2013). The unavoidable effect of decreasing stimulus contrast is the reduction in spiking rate. To solve this problem, a statistical model was used to examine extracellular spiking responses in both mouse and cat neurons to exclude the effect of reduced spike counts at low stimulus contrast levels. My results have clearly shown significant increases in phase sensitivity beyond what is expected from the reduction in spike count at low stimulus contrast levels. Furthermore, I attempted to morphologically identify intracellular recorded neurons in mice *in vivo* with two-photon imaging.

5.3 Methods

Extracellular experiments were performed on both mice and cats. All intracellular recordings were done exclusively with mice. General procedures can be found in Chapter 3. Here I present specific protocols for the data in this chapter.

5.3.1 Stimulus Protocol

The experimental stimulus was a moving sine-wave grating presented at the optimal temporal frequency (TF), spatial frequency (SF) and orientation of the recorded cell in a circular aperture the size of its excitatory receptive field. For each trial, gratings were displayed at 12 different contrast levels in pseudorandom order. The contrast levels used for extracellular recordings were 0, 2, 4, 6, 8, 12, 16, 24, 32, 48, 64 and 100%. For intracellular recording the same series was used but with the addition of 82% contrast (13 contrast values). Interleaved with 1 s of blank (mean luminance) screen, each grating was

presented for 3 s with the first and last 0.5 s stationary and 2 s in between the drifting phases. Trials were repeated as often as the stability of the recording would allow. On average, 10 trials were obtained per contrast level for each extracellularly recorded cell. Due to less stability in recording, approximately 4 trials per contrast level were obtained for each intracellular recording.

5.3.2 Analysis of extracellular spike responses

The recorded spikes were sorted off-line using Spike2 to select for single cell responses based on spike waveform shapes. Spike arrival times were determined through action potential template matching in Spike2. For each cell, the spiking rate was computed and presented as a spike density function (SDFs) with 1 kHz resolution generated by convolution of a Gaussian kernel of unit area and $\sigma = 10$ ms, with a train of Dirac delta functions; one delta function corresponding to the arrival time of each spike (van Kleef et al 2010). The mean firing rate for each stimulus condition was calculated by trial averaging SDFs for the duration of the drifting grating presentation (2 s). I estimated the spontaneous activity of each cell by averaging the firing rate over a period of 500 ms immediately prior to each stimulus presentation, during which a grey screen of mean luminance was displayed.

Fourier analysis was used to quantify the phase sensitivity of the responses at different stimulus contrast levels. Phase sensitivity was quantified using the relative modulation (F_1/F_0) of the response, which was the ratio between the amplitude of the Fourier coefficient at the fundamental frequency of the stimulus grating (F_1) and the increase in mean firing rate above the spontaneous baseline (F_0). Fourier coefficients were calculated using the FFT function in Matlab™ (The Mathworks Inc. Natick, MA, USA).

For each cell, I compared the relative modulation of the responses at high and low stimulus contrasts. The high contrast condition was defined as the stimulus contrast that evoked the highest firing rate (most often 100% contrast, occasionally a lower contrast at 64% - 82%). The low contrast condition was

defined as the lowest stimulus contrast that evoked a response significantly higher than the cell's spontaneous firing rate. Due to differences in contrast gain, which were apparent in comparing the individual contrast response functions, low contrast conditions varied between cells. To determine the low contrast condition for each cell, I used Poisson analysis to provide a response threshold. Specifically, a Poisson distribution was calculated from the spontaneous firing rate. A response threshold was determined based on the 99% confidence limit of the Poisson distribution (Crowder et al 2007). The lowest stimulus contrast that evoked an F_0 response above the Poisson threshold was considered as the low contrast condition.

5.3.3 Accommodating for increases in F_1/F_0 ratio resulting from reduced spike counts at low stimulus contrasts

It has been demonstrated that the relative modulation of the spike response calculated by Fourier analysis is sensitive to the number of recorded spikes (Crowder et al 2007, Hietanen et al 2013). To account for the changes in F_1/F_0 ratio due to the reduction in the number of spikes at low stimulus contrast, I compared the observed F_1/F_0 ratio with an empirical distribution of F_1/F_0 values from a simulated complex cell (Cloherty and Ibbotson, 2015). We assigned the model complex cell to produce n spikes over a response equivalent to the full cycle of a sine-wave grating. The spike arrival times, $t_i \in (-\pi, \pi)$, $i = 1 \dots n$, were assumed to be independent and identically distributed values randomly drawn from a raised cosine distribution defined by,

$$f(t_i; A, B) = \frac{1}{2\pi} [1 + A \cos(t_i - B)] \quad B - \pi \leq t < B + \pi \quad (1),$$

where A ($0 \leq A \leq 1$) represents the assumed true or asymptotic value of F_1/F_0 as $n \rightarrow \infty$ and B defines the position of the distribution. For each cell, we simulated responses (i.e., spike arrival times (t_i)) using Equation 1 for a chosen asymptotic F_1/F_0 ratio and the position of a standard raised cosine distribution (i.e., $A = (F_1/F_0)_\infty$ and $B = 0$). The asymptotic F_1/F_0 ratio was estimated for

each cell by maximizing the likelihood of the observed data. The log likelihood (L) of the data for a given asymptotic F_1/F_0 ratio was computed as follows:

$$\log L = \log \prod_j f(A_n|A) \quad (2),$$

where A_n is the observed F_1/F_0 value based on the actual spike count (n) of the cell, A is the assumed asymptotic F_1/F_0 ratio for the simulation and j indicates the stimulus contrast, which is set to the stimulus that evokes the maximal response.

With the appropriate asymptotic F_1/F_0 ratio maximizing the likelihood of the observed data at the high contrast condition, we simulated responses with spike count (n) observed at the low contrast condition using Equation 1 and computed an empirical distribution of F_1/F_0 ratio for each cell. To eliminate the effect of the reduction in spike count, the increase in observed F_1/F_0 ratio at the low contrast condition was only considered significant if the value exceeded the 99% confidence limit of the empirical distribution.

5.3.4 Two-photon imaging setup

For two-photon imaging experiments *in vivo*, 100 μM Alexa Fluor 488 fluorescent dye was added to the intracellular solution that fills the recording pipettes. After electrophysiology experiments, positive pressure was applied to fill the patched cell with fluorescent dye-containing intracellular solution. Neurons were typically allowed to fill with dye for 10 minutes before imaging. Imaging was performed using a custom built two-photon microscope (Waters et al 2003) fitted with a pulsed Ti:sapphire laser with a repetition rate of 80 MHz and 100–150 fsec pulse width (Mira 900; Coherent, Santa Clara, CA). Excitation light with a wavelength of 840 nm was focused onto the brain using a water immersion , 40 \times , 0.8 NA objective (Zeiss). Emitted light was collected in the epifluorescence configuration through a 680 nm long-pass dichroic mirror and an infrared-blocking emission filter (Schott BG39) using a photomultiplier tube (Hamamatsu). Scanning and image acquisition were controlled using custom software (R. Stepnoski and M. Müller, Lucent Technologies, NJ; and MPImF, Heidelberg, Germany). The

fluorescence intensities within a $200 \times 200 \mu\text{m}$ region of interest centred around the soma were sampled at 40 Hz. Starting from the surface of the brain, 200 to 300 stacks of the region of interest were scanned at $1 \mu\text{m}$ apart. Images were compiled and processed with a custom build Matlab™ Gui program (The Mathworks Inc. Natick, MA, USA).

5.4 Results

I conducted all experiments in mouse cortex. Each cat experiment was performed by a team of investigators. The cat data presented in this chapter was collected by various people over the course of 2007-2014. I was directly involved in collecting data from fifteen cats during the period between 2010-2014. The cat data was stored and organised on a server. I used a custom-designed program to extract spike trains for each individual cell from the server and analysed it for presentation in this chapter.

5.4.1 Measuring extracellular spiking responses of V1 neurons to drifting gratings at different stimulus contrasts

Extracellular recordings were made from areas 17 and 18 of 25 anaesthetised cats ($n = 416$) and area 17 of 22 anaesthetised mice ($n = 80$) that were stimulated by optimal drifting sine-wave gratings at different contrast levels. For each cell, the relative modulations, represented as F_1/F_0 , were calculated for each stimulus contrast level. I classified the cell as simple or complex based on its F_1/F_0 ratio at the stimulus contrast that evoked the maximum response. A cell was considered simple if $F_1/F_0 > 1$ and complex if $F_1/F_0 < 1$. Figure 5.1A and Figure 5.2A show examples of simple cells from mouse and cat V1, respectively. Both cells exhibit strong response modulations to sine-wave gratings at different tested contrast levels as shown by the spike density function plots (mouse: Figure 5.1A; cat: Figure 5.2A). In comparison, the spike density function plots for example complex cells show a relatively weak modulation level at all tested contrasts for both mouse (Figure 5.1C) and cat (Figure 5.2C). Simple and

complex cells exhibit consistency in the level of response modulation across all stimulus contrasts in both species.

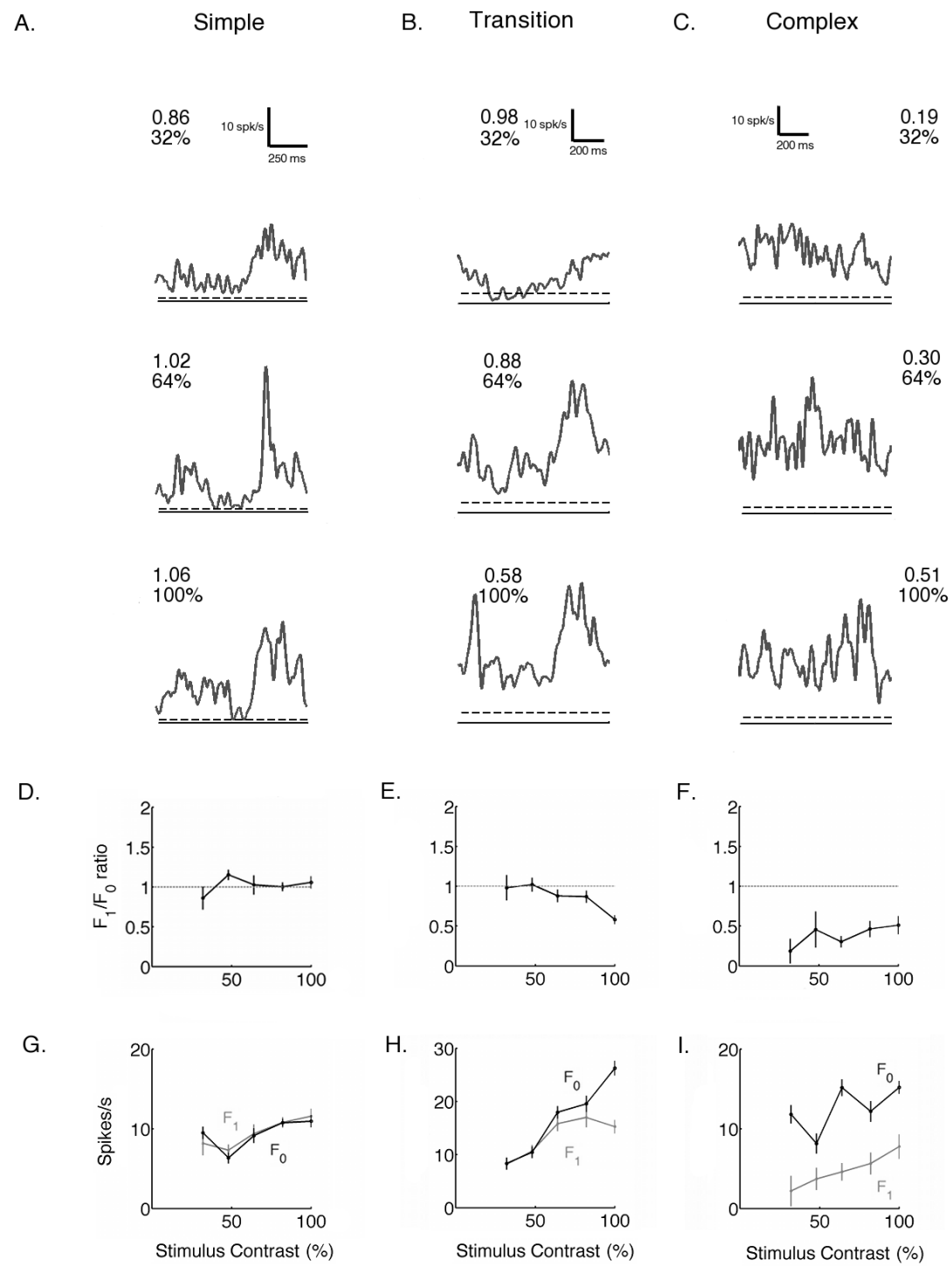


Figure 5.1. Spiking responses to drifting gratings in mouse V1

Relative modulation responses of three Mouse V1 cells (a simple cell, a phase sensitive complex or transition cell and a complex cell) to drifting sine-wave gratings. Spike density function plots of cycle-averaged responses for three test stimulus contrasts for the simple cell (**A**), the phase sensitive complex cell (**B**) and the complex cell (**C**). The values on each plot indicate the F_1/F_0 ratio (top number) observed at the corresponding stimulus contrast (bottom number). **D, E and F**, Relative modulation of responses, measured as F_1/F_0 ratios, plotted against stimulus contrasts for the simple cell, the phase sensitive complex cell and the complex cell, respectively. The dotted lines in **D, E** and **F** indicate $F_1/F_0 = 1$. An F_1/F_0 ratio >1 suggests the response is phase sensitive, whereas a F_1/F_0 ratio <1 suggests the response is phase insensitive. **G, H and I**, Amplitudes (spikes/s) of the modulated component of the responses (F_1 , grey line) and the mean responses (F_0 , black line) as functions of stimulus contrast for the simple cell, the phase sensitive cell and the complex cell, respectively. In **D** through to **I**, the symbols indicate the mean (cycle-averaged) values of the respective response parameter at 32%, 48%, 64%, 82% and 100% stimulus contrasts (from left to right) and error bars show bootstrap estimates of standard errors. The lowest stimulus contrast (32%) shown on each plot is the lowest stimulus contrast that evoked responses above the spontaneous activity in each cell.

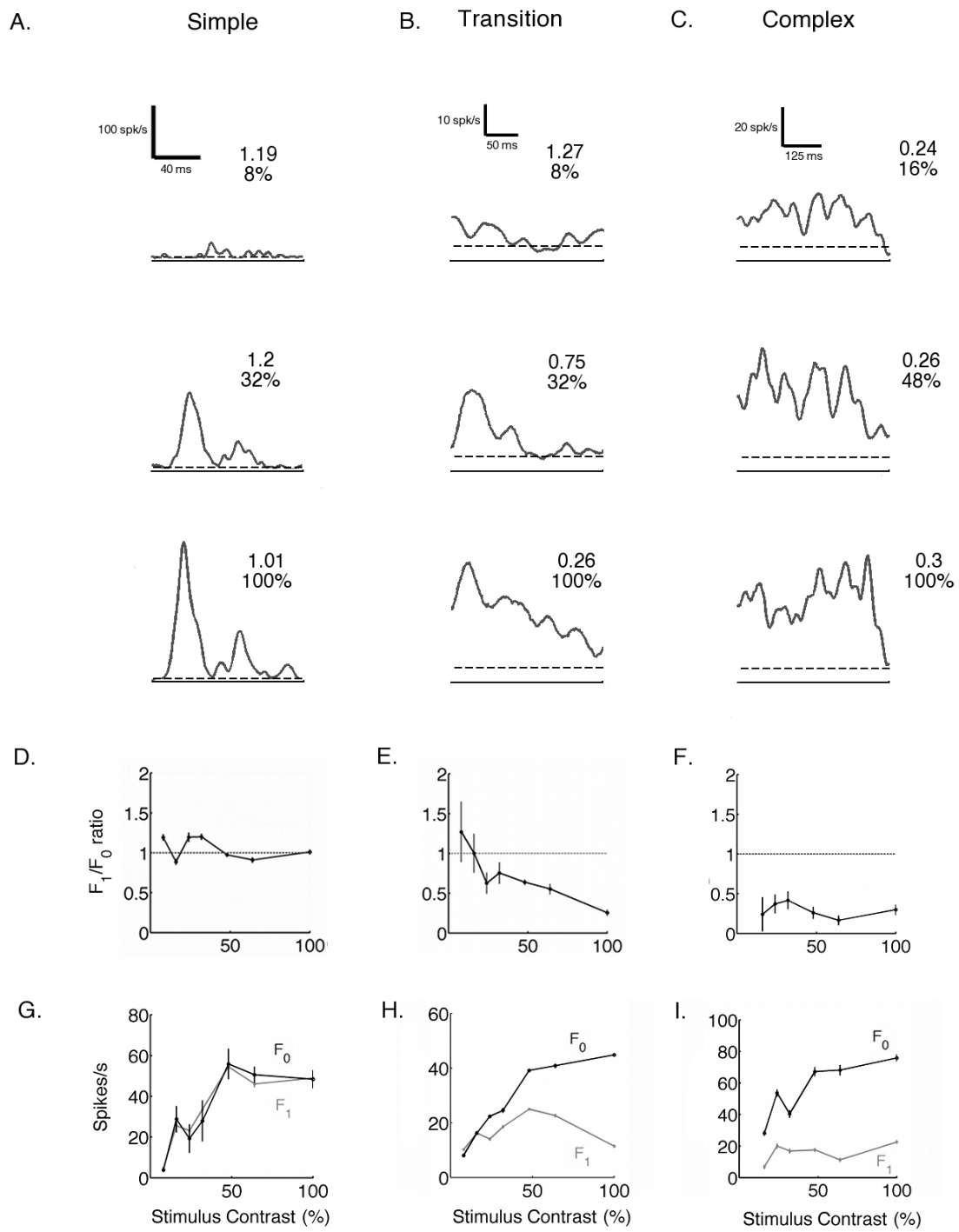


Figure 5.2. Spiking responses to drifting gratings in cat V1

Relative modulation responses of three Cat V1 cells (a simple cell, a phase sensitive complex or transition cell and a complex cell) to drifting sine-wave gratings. Spike density function plots of cycle-averaged responses for three test stimulus contrasts for the simple cell (**A**), the phase sensitive complex cell (**B**) and the complex cell (**C**). The values on each plot indicate the F_1/F_0 ratio (top number) observed at the corresponding stimulus contrast (bottom number). **D, E and F**, Relative modulation of responses, measured as F_1/F_0 ratios, plotted against stimulus contrasts for the simple cell, the phase sensitive complex cell and the complex cell, respectively. The dotted lines in **D, E and F** indicate $F_1/F_0 = 1$. An F_1/F_0 ratio <1 suggests the response is phase insensitive, whereas an F_1/F_0 ratio >1 suggests the response is phase sensitive. **G, H and I**, Amplitudes (spikes/s) of the modulated component of the responses (F_1 , grey line) and the mean responses (F_0 , black line) as functions of stimulus contrasts of the simple cell, the phase sensitive cell and the complex cell, respectively. In **D** through to **I**, the symbols indicate the mean (cycle-averaged) values of the respective response parameter at 32%, 48%, 64%, 82% and 100% stimulus contrasts (from left to right) and error bars show bootstrap estimates of standard errors. The lowest stimulus contrast (32%) shown on each plot is the lowest stimulus contrast that evoked responses above the spontaneous activity in each cell.

The example cells shown in Figure 5.1B and Figure 5.2B exhibit a moderate level of response modulation at 100% contrast (mouse: $F_1/F_0 = 0.58$, Figure 5.1B; cat: $F_1/F_0 = 0.26$, Figure 5.2B), which is characteristic of a classic complex cell (Hietanen et al 2013, Hubel & Wiesel 1962). However, as the stimulus contrast is reduced (Figure 5.1B and Figure 5.2B; top and middle plots), the response oscillation starts to become more prominent and the responses become phase-locked to the sine-wave grating. The significant increase in F_1/F_0 with the reduction of stimulus contrast is apparent in Figure 5.1E (student t-test, $P < 0.001$) and Figure 5.2E (student t-test, $P < 0.001$). The amplitude of the fundamental Fourier component (F_1) and the mean response (F_0) are plotted against stimulus contrasts in Figure 5.1H and Figure 5.2H. In both mouse and cat cells, the mean response (F_0) decreases monotonically with reduced contrast levels, whereas the modulated components (F_1) are relatively constant down to contrasts of 48%. Consequently, the relative modulation of the response (F_1/F_0) increases monotonically as stimulus contrast is reduced, despite the decrease in the overall firing rate.

5.4.1.1 Accommodating for spike number reduction at low contrasts

It has been established that Fourier analysis of spiking responses is universally sensitive to the number of spikes available (Cloherty & Ibbotson 2015, Hietanen et al 2013): F_1/F_0 increases as the number of spikes is reduced. The unavoidable effect of decreasing stimulus contrast is the reduction in spiking rate. Consequently, any observed increase in F_1/F_0 at low stimulus contrast levels is confounded by the influence of reduced spike counts. Therefore, it is necessary to control for this effect. To demonstrate the effect of spike counts on F_1/F_0 , consider the case of an ideal phase-invariant complex cell with a true or asymptotic F_1/F_0 of 0.

Figure 5.3A illustrates the empirical distribution of F_1/F_0 simulated with spike counts of 50, 100 and 500 under the assumption that the spike arrival times are uniformly distributed over the response interval of a single cycle of a sine-wave

grating. The expected F_1/F_0 at a given spike count is defined as the mean of the distribution (solid lines in Figure 5.3A). As the spike count decreases, the distribution becomes more spread out. Consequently the expected F_1/F_0 deviates more from the asymptotic F_1/F_0 . Figure 5.3B demonstrates the relationship between the expected F_1/F_0 and the spike count derived from simulating empirical distributions of F_1/F_0 for a range of asymptotic F_1/F_0 values, including the phase-invariant model complex cell which has an asymptotic $F_1/F_0 = 0$ (the green line). It is evident that the expected F_1/F_0 is dependent on the number of spikes. As the spike count (n) approaches the low bound of $n = 1$, the expected F_1/F_0 of all asymptotic F_1/F_0 values approaches 2. Subsequently, a cell with lower asymptotic F_1/F_0 ratios tends to have larger increases in the expected F_1/F_0 at low spike count. As illustrated in Figure 5.3B, the steepest curve occurs when the asymptotic $F_1/F_0 = 0$ (i.e. the ideal phase-invariant complex cell) (the green line).

The asymptotic F_1/F_0 for each recorded cell was determined by maximising the likelihood of the observed data (see methods). Consider the example cell shown in Figure 5.1B, a total of 984 spikes were recorded throughout all repeats at 100% contrast and the observed F_1/F_0 at that contrast was 0.58. Figure 5.3C shows the likelihood of the observed data for the example cell as a function of assumed asymptotic F_1/F_0 values. The likelihood peaks at $F_1/F_0 = 0.58$, which suggests that the asymptotic F_1/F_0 is the observed F_1/F_0 of the data. This is expected, as demonstrated by the red curve in Figure 5.3B, given the relatively high spike count recorded at 100% contrast and the flat slope as the curve approaches the high end of the spike count.

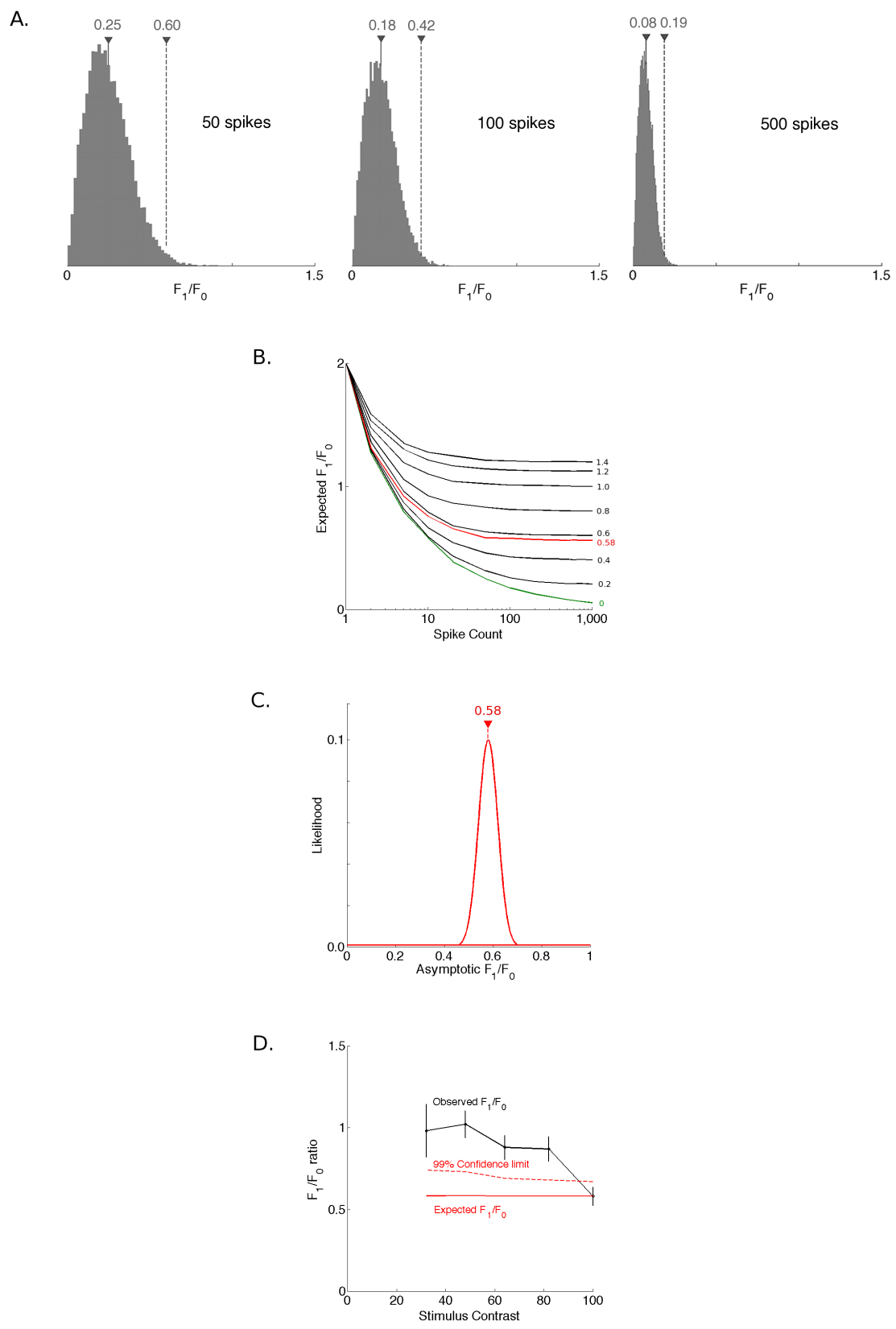


Figure 5.3. Accommodating spike number reduction effect at low contrasts

Simulation of the effect of spike count reduction at low stimulus contrast levels on the expected F_1/F_0 ratio. **A**, The empirical distributions of simulated F_1/F_0 for a model complex cell with $F_1/F_0 = 0$ for 50, 100 and 500 spikes (left to right). With each distribution, the expected F_1/F_0 for the corresponding spike count, i.e., the mean of the distribution, is indicated with solid grey lines. The broken grey line indicates the 99% confidence limit of each distribution. The empirical distributions demonstrate the increase in expected F_1/F_0 as the spike count reduces. **B**, Curves illustrate relationships between the expected F_1/F_0 and spike counts, derived from empirical distributions of simulated F_1/F_0 for a range of assumed asymptotic values. The asymptotic value for each curve is shown on the right. The red curve shows the relationship between expected F_1/F_0 and spike count that is simulated with the asymptotic F_1/F_0 of the example phase sensitive complex cell shown in Figure 1 (asymptotic $F_1/F_0 = 0.58$). The curve illustrates the expected F_1/F_0 and spike count relationship for the model complex cell (asymptotic $F_1/F_0 = 0$) in A. As demonstrated for various asymptotic F_1/F_0 values, as the spike count decreases, the expected F_1/F_0 increases. **C**, The likelihood of the observed F_1/F_0 at 100% stimulus contrast for the phase sensitive complex cell as a function of asymptotic F_1/F_0 values. The likelihood peaks at 0.58 (red broken line), which is identical to the observed F_1/F_0 at 100% contrast for this cell. **D**, A comparison between the observed F_1/F_0 and the expected F_1/F_0 according to the spike count plotted against stimulus contrasts for the example phase sensitive complex cell. The black line shows the observed F_1/F_0 as a function of stimulus contrast. The symbols indicate the mean (cycle-averaged) values of the respective response parameter at 32%, 48%, 64%, 82% and 100% stimulus contrasts (from left to right) and error bars show bootstrap estimates of standard errors. The red solid line indicates the expected F_1/F_0 derived from the simulated empirical distributions for spike counts observed at different stimulus contrasts. The broken red line indicates the 99% confidence limit of the empirical distributions for corresponding stimulus contrasts. It is apparent that the expected increases in F_1/F_0 due to the reduction of spike count fails to account for the increase in observed F_1/F_0 as stimulus contrast decreases.

With the estimated asymptotic F_1/F_0 for each recorded cell, we generated the empirical distributions of F_1/F_0 with the spike count of each stimulus contrast that had response rates above the spontaneous activity. The mean (the expected F_1/F_0) and a 99% confidence limit were calculated for each distribution as illustrated in Figure 5.3A (mean: solid line; 99% confidence limit: broken line). Figure 5.3D shows the observed F_1/F_0 ratio, the expected F_1/F_0 and the 99% confidence limit at each stimulus contrast for the example cell. The lowest contrast that evoked a response is 32% for this cell. It is apparent that the increase in the observed F_1/F_0 as the contrast is reduced far exceeds the expected F_1/F_0 due to the reduction spike count reduction.

5.4.1.2 Population analysis of contrast-dependent spiking responses

The observed F_1/F_0 ratios for the high contrast condition (i.e. the stimulus contrast that evoked the maximum response) plotted against the observed F_1/F_0 ratio for the low contrast conditions (i.e. the lowest stimulus contrast that evoked responses above the spontaneous firing rate) for each cell from mouse and cat V1 are shown in Figures 5.4A and 5.4B, respectively. The red (mouse) and blue (cat) symbols indicate cells that exhibit significant increases in F_1/F_0 ratio in the low contrast conditions, which are defined by an increase in F_1/F_0 ratio that exceeds the 99% confidence limit of their corresponding empirical distributions. Both figures demonstrate that all significant cells are complex (i.e. $F_1/F_0 < 1$ at High contrast). Amongst mouse V1 complex cells, 13/63 cells (21%) exhibited significant increases in F_1/F_0 (Figure 5.4A). A slightly larger proportion of significant cells (114/365; 31%) were observed in the cat V1 complex population (Figure 5.4B).

I quantified the changes in F_1/F_0 ratio between low and high contrast conditions for individual cells. Simple cells in mouse (dark symbols, Figure 5.4A) showed a small but significant difference at the 95% confidence level in F_1/F_0 ratio at low and high contrasts (Mouse: -0.22, two-sided Wilcoxon signed rank test, $p = 0.04$). Simple cells in cat (dark symbols, Figure 5.4B) showed no significant difference

in F_1/F_0 ratio at low and high contrasts (Cat: 0.08, two-sided Wilcoxon signed rank test, $p = 0.14$). It should be noted that the team deliberately selected complex cells during some of the cat experiments (but not the mouse experiments), which biased the cat population towards far larger numbers of complex cells.

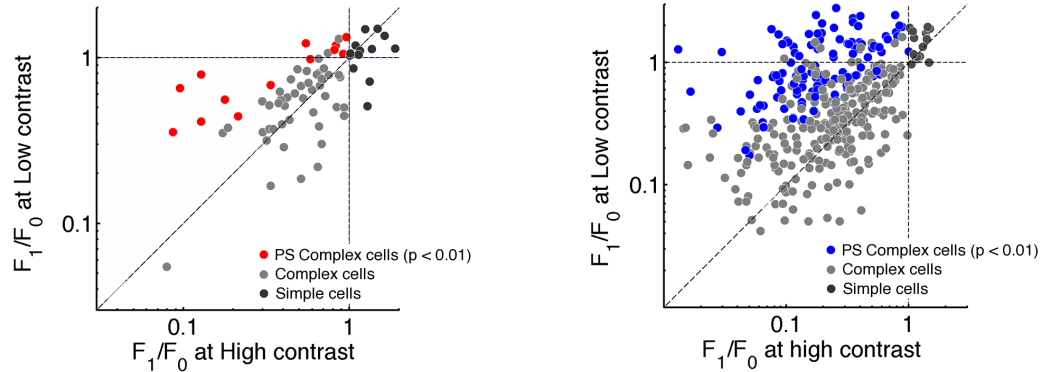
The histogram distributions of the change in F_1/F_0 ratio between low and high contrast conditions for complex cells in mouse and cat V1 are shown in Figures 5.4C and 5.4D, respectively. The complex cells in mouse and cat V1 collectively both showed a significant increase in F_1/F_0 ratio for the low contrast condition (mouse: 0.1, two-sided Wilcoxon signed rank test, $p = 0.003$; cat: 0.34, two-sided Wilcoxon signed rank test, $p < 0.001$). When a subset of mouse V1 complex cells that showed significant increases for the low contrast condition (red symbols in Figure 5.4A) were then quantified separately, a highly significant difference between low and high contrast conditions was apparent (0.38, two-sided Wilcoxon signed rank test, $p < 0.001$, red bars in Figure 5.4C). This subset of complex cells in cat V1 not only exhibited a significant change in F_1/F_0 ratio between low and high contrast conditions (0.84, two-sided Wilcoxon signed rank test, $p < 0.001$, blue bars in Figure 5.4D), but also showed a considerably larger change in F_1/F_0 compared to mouse V1 cells (Wilcoxon rank sum test, $p < 0.001$).

A.

Mouse

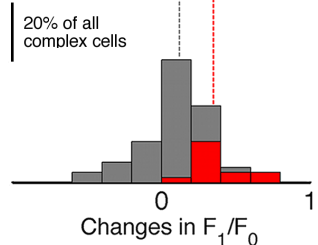
B.

Cat



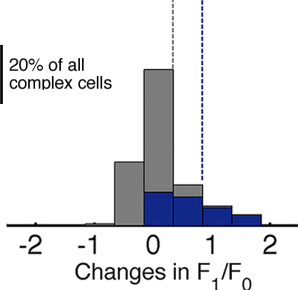
C.

0.12 0.35



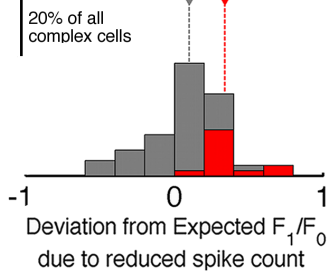
D.

0.34 0.84



E.

0.1 0.34



F.

0.25 0.76

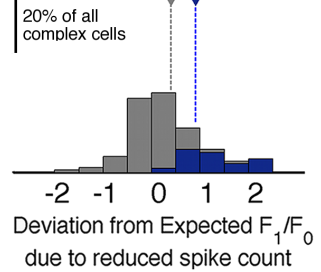


Figure 5.4. F_1/F_0 at low and high contrasts for mouse and cat V1 neurons

Comparing the relative modulation of responses (F_1/F_0) at low and high stimulus contrasts in mouse and cat V1 cells. **A**, Scatter plot of F_1/F_0 observed at low and high contrasts for 73 mouse V1 cells. **B**, Scatter plot of F_1/F_0 observed at low and high contrasts for 416 cat V1 cells. For each cell on either plot, the low contrast is defined as the lowest stimulus contrast that evoked responses above spontaneous activity and the high contrast is the stimulus contrast that evoked the maximum responses. In **A** and **B**, the complex cells that exhibit a significant increase ($p < 0.001$) in F_1/F_0 at low contrasts are indicated with red (mouse) and blue (cat) symbols respectively. Light grey symbols represent the remaining complex cells and dark grey symbols indicate simple cells in both plots. **C** and **D**, histograms of the quantified difference in observed F_1/F_0 between low and high contrasts for complex cells in mouse and cat V1, respectively. Coloured bars show the distribution of the subset of complex cells that showed significant changes in F_1/F_0 at low contrast. The broken lines indicate the mean of distributions of the corresponding colours. **E** and **F**, distributions of changes in observed F_1/F_0 between low and high contrasts after subtracting the expected changes in F_1/F_0 due to the reduction of the spike count in mouse and cat V1, respectively. Similar to **C** and **D**, the coloured bars represent the same subset of complex cells and the broken lines indicate the mean for the distributions.

Data presented for absolute changes in F_1/F_0 between low and high contrast conditions has not been adjusted according to the influence of the spike count reduction at lower contrast levels. To address this matter, I quantified the changes in the observed F_1/F_0 ratio at high and low stimulus contrasts after subtracting the expected changes in F_1/F_0 ratio purely due to spike count reduction for each complex cell. The expected change was defined by the difference between the F_1/F_0 ratio observed in the high contrast condition and the expected F_1/F_0 ratio for the corresponding spike count for the low contrast condition. Figures 5.4E and 5.4F show the distribution of this metric for mouse and cat V1 complex cells, respectively. On a population level, the difference between the observed and the expected changes in F_1/F_0 ratio for mouse complex cells is significantly different from zero at the 95% confidence level (difference=0.08, two-sided Wilcoxon signed rank test, $p = 0.026$; Figure 5.4E), which suggests that a physiological mechanism is in operation. In cat, as demonstrated in Figure 5.4F, the average differences also lie significantly away from zero (difference=0.25, two-sided Wilcoxon signed rank test, $p < 0.001$).

The coloured bars in Figures 5.4E and 5.4F show the distribution of the subset of complex cells that exhibited significant increases in modulation ratio at low contrast conditions (indicated in correspondingly coloured symbols in Figures 5.4A and 5.4B). This subset of complex cells showed significant changes between the observed and the expected changes in F_1/F_0 ratio in both mouse and cat V1 (mouse: 0.38, two-sided Wilcoxon signed rank test, $p < 0.001$; Cat: 0.76, two-sided Wilcoxon signed rank test, $p < 0.001$). Moreover, when compared to mouse V1, the observed change in F_1/F_0 ratio shows a greater deviation from the expected change in F_1/F_0 ratio, which was due to the reduction in spike count in the subset of cat V1 complex cells (Wilcoxon rank sum test, $p < 0.001$).

It is apparent that the number of cells recorded from cat V1 is significantly larger than that of mouse V1 (mouse: 73 cells in total, 63 complex cells; cat: 416 cells in total, 365 complex cells). Figure 5.5A shows the distribution for the number of complex cells recorded from mouse (red bars) and cat V1 (blue bars) that exhibit specific spike counts at high contrast conditions. It is possible that the relatively

small sample size of the mouse V1 cells might skew the results, thus contributing to the different observations between cat and mouse V1 complex cells. To make an informative comparison between the two populations of cells, I randomly sampled cat V1 complex cells according to the number of complex cells recorded from mouse V1 for each spike count bin (Figure 5.5A).

Figure 5.5B shows the distributions of the average change in F_1/F_0 ratio between low and high contrast conditions for 10,000 samples of cat V1 complex cells for each spike count bin (the last two bins are combined in Figure 5.5B-V due to the small number of mouse V1 complex cells with spike counts between 800 and 1200 spikes). The means of the distributions (grey broken lines) are reasonably consistent across all spike count bins (student t-test, $P = 0.03$). Furthermore, they are consistent with the average change in F_1/F_0 ratio measured across all complex cells in cat V1 (0.34, grey broken lines in Figure 5.4D).

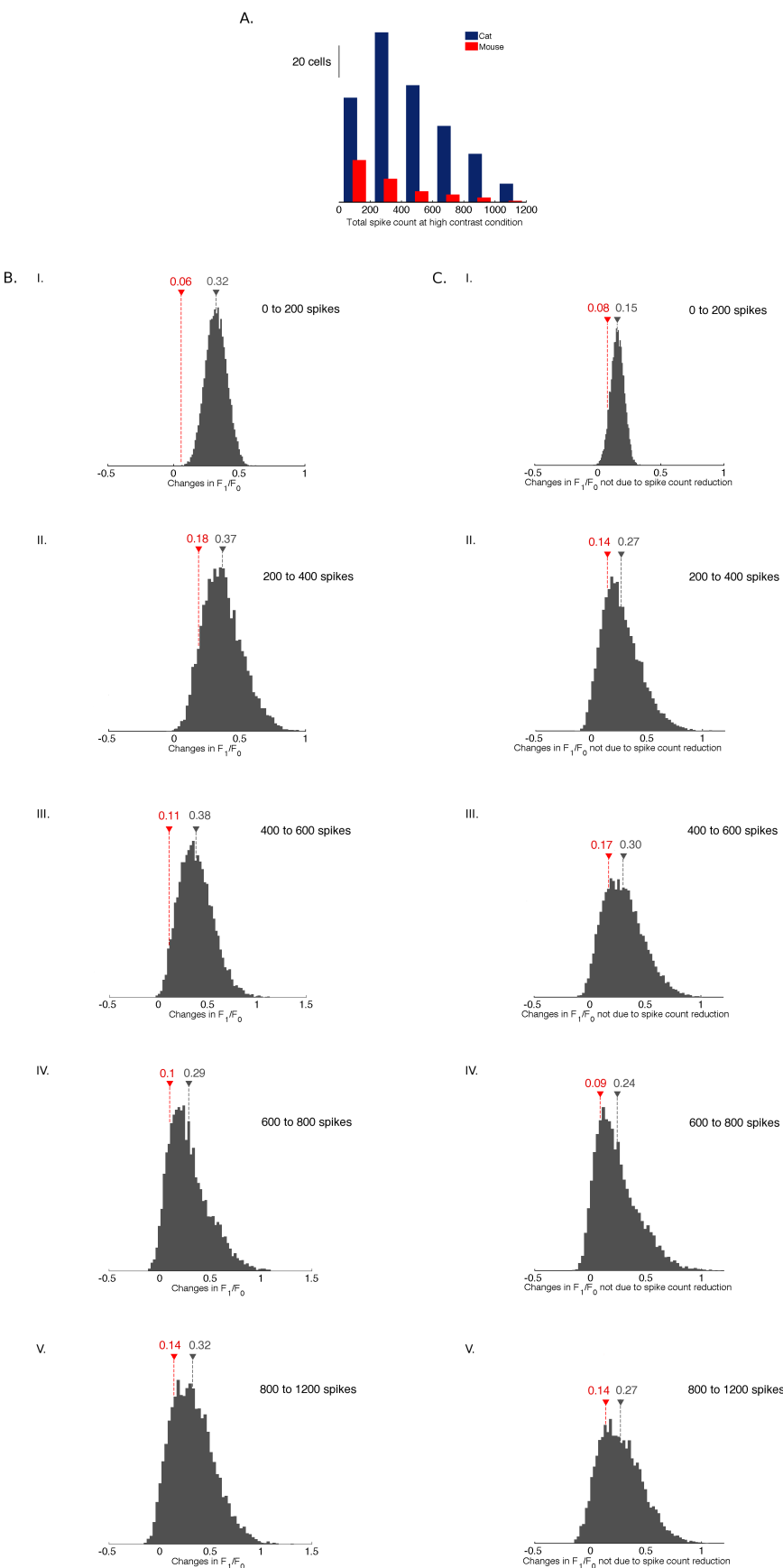
The red arrow on each distribution in Figure 5.5B indicates the average change in F_1/F_0 ratio of mouse V1 complex cells with corresponding spike counts. The difference between the mouse complex cells and the sampled cat cells are relatively consistent across all distributions and are similar to the differences between the population results (mouse: 0.11, grey broken lines in Figure 5.4D; cat: 0.34, grey broken lines in Figure 5.4D).

Figure 5.5C shows the sampling results for the changes in F_1/F_0 ratio after subtracting the expected change due to the reduction of spike count. Similar to the sampling results of the absolute change in F_1/F_0 ratio, the means (grey broken lines in Figure 5.5C) are relatively consistent between distributions, as well as when compared to the population result (0.25, grey broken line in Figure 5.4F). Furthermore, the difference between the mouse complex cells (red broken line in Figure 5.5C) and the sampled cat complex cells (grey broken lines in Figure 5.5C) are consistent across spike count bins and are all comparable to the population results (mouse: 0.08, grey broken line in Figure 5.4E; cat: 0.38, grey broken line in Figure 5.4F).

Overall, the sampling results indicate that the difference in population sizes does not influence the findings reported for the mouse and cat V1 complex cells.

Figure 5.5. Accounting for sample size differences between mouse and cat data

Sampling cat V1 complex cells according to the number of mouse V1 complex cells using similar spike counts, as observed at high stimulus contrast. **A**, distributions of total spike count observed at stimulus contrasts that evoked maximum responses for mouse (red bars) and cat (blue bars) complex cells. Complex cells with spike count higher than 1200 spikes are not shown on the histogram. Clearly, we have recorded more complex cells in cat than in mouse for all spike counts. **B**, Distributions of average changes in observed F_1/F_0 at low contrast for 10,000 random samples of cat V1 according to the number of mouse complex cells with spike counts ranging from 0 to 200 spikes (I), 200 to 400 spikes (II), 400 to 600 spikes (III), 600 to 800 spikes (IV) and 800 to 1200 spikes (V). **C**, Similar distribution histograms as **B** for average changes in observed F_1/F_0 at low contrast after subtracting the expected changes in F_1/F_0 due to spike count reduction. In **B** and **C**, the mean of each distribution is indicated by the grey broken line and the mean of the respective response metric for mouse V1 complex cells with the corresponding spike count range is indicated by the red broken line. The mean of the distribution represents the sampling result of the respective response metric of the cat complex cells with specific spike count.



5.4.2 Intracellular membrane potential responses of mouse V1 neurons to drifting gratings at different stimulus contrasts

In addition to the extracellular recordings described above, twenty intracellular recordings were made from eleven mice to examine the subthreshold responses of V1 neurons to drifting gratings at different stimulus contrasts. However, only ten of these recordings from seven mice generated a complete physiological data set. The following data presented in this chapter are from these ten cells. Figure 5.6 shows an example of intracellular recordings from a mouse V1 cell to drifting gratings with preferred orientation, spatial and temporal frequencies at 100% stimulus contrast. The raw intracellular membrane potential responses to four cycles of the drifting sine-wave grating (Figure 5.6C) are shown in Figure 5.6A. To study sub-threshold membrane potential responses, all spikes were removed prior to averaging across trials (Figure 5.6B). Both the raw response and the trial-averaged voltage trace for this simple cell clearly demonstrate that the responses are highly modulated and phase-locked to the sine-wave grating stimulus.

In a similar way to the extracellular experiments, I examined the intracellular responses of mouse V1 cells to different stimulus contrast levels. Figure 5.7 illustrates cycle-averaged membrane potentials to a cycle of a drifting sine-wave grating presented at different contrast levels for three example cells. From left to right, the response traces for each example cell are shown from the lowest to the highest stimulus contrast. Illustrations of a single cycle of a sine-wave grating is presented above each response trace alongside the stimulus contrast values.

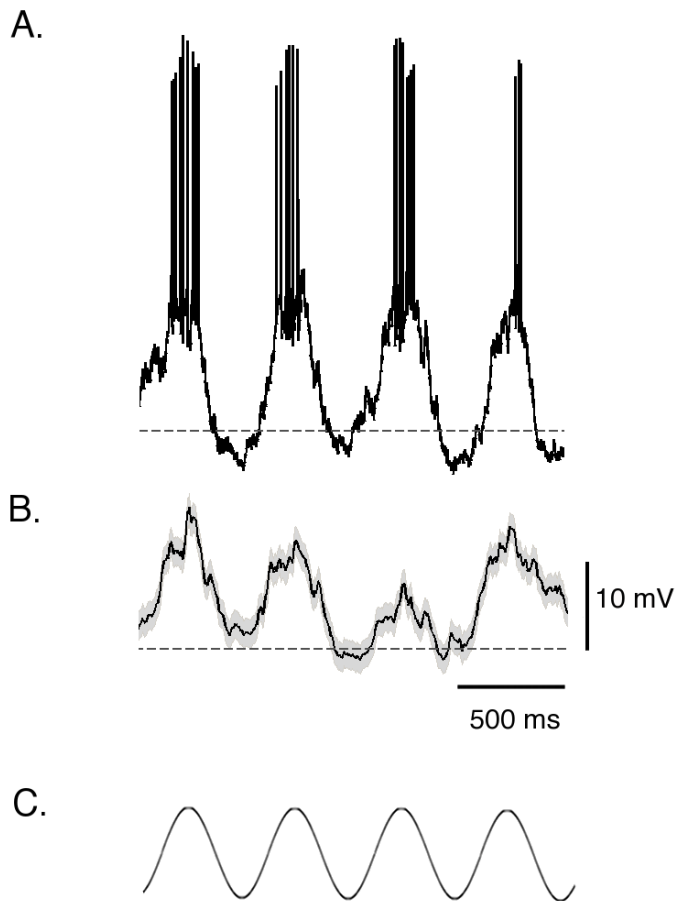


Figure 5.6. Membrane potential responses of a mouse simple cell

Intracellular responses of an example Mouse V1 simple cell to drifting sine-wave gratings. **A**, Responses to a sine-wave grating moving at 2 Hz and 100% contrast. The trace includes 2 s of stimulus after 0.5 s of black screen (blank screen responses not shown). The broken line indicates the resting membrane potential (V_{rest}) of the cell: -48.5mV. **B**, Trial-averaged ($n = 5$) voltage trace for the same stimulus shown in **A**. Spikes are removed from voltage traces prior to averaging by calculating the derivative (dmV) of the membrane potential and excluding rapid voltage excursions based on a derivative threshold. The threshold was set by eye for each cell. **C**, A visual representation of 4 cycles of the sine-wave grating stimulus moving at 2 Hz for 2 s.

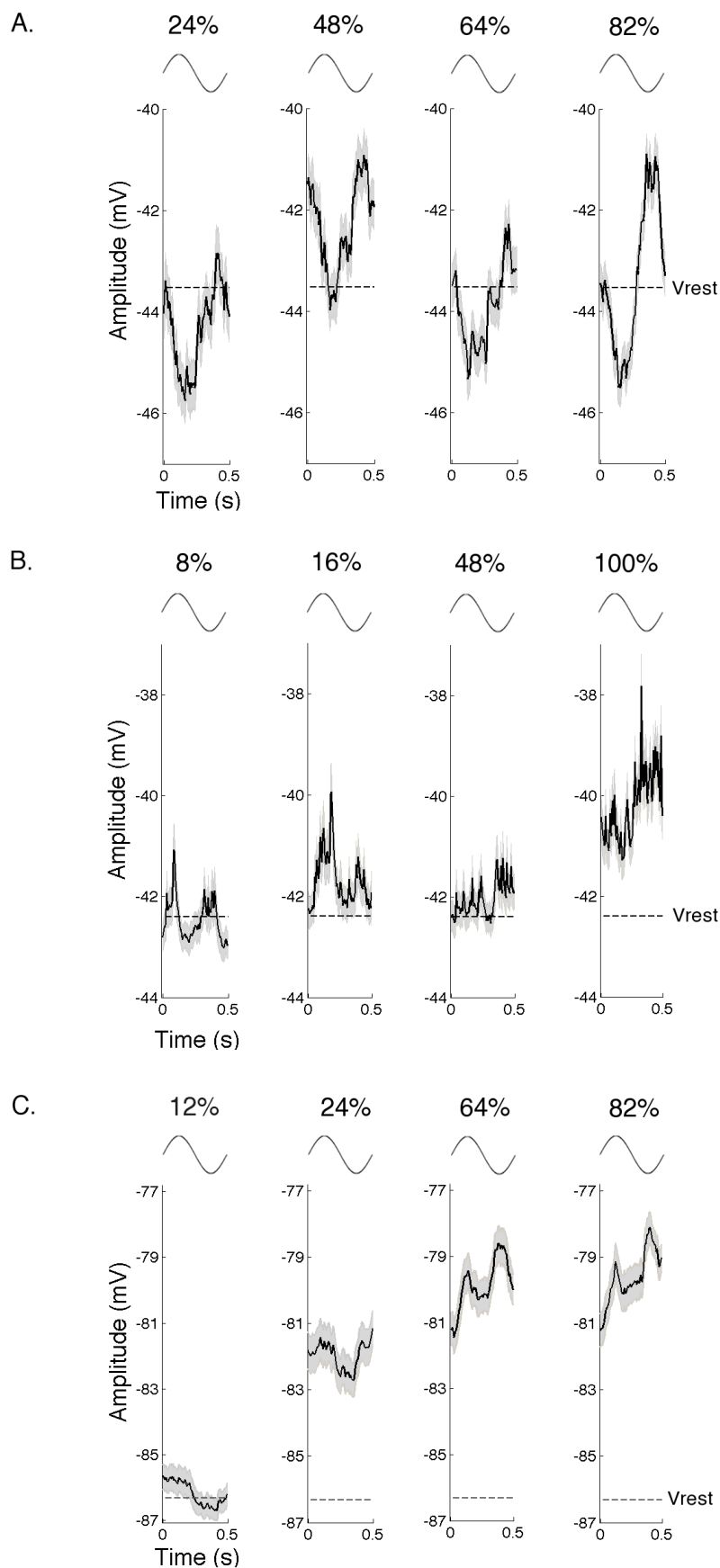


Figure 5.7. Membrane potential responses to drifting gratings at different contrasts of three example cells

Cycle-averaged membrane potentials to drifting sine-wave gratings at different stimulus contrast levels for a simple cell (**A**), a complex cell (**B**) and a phase-sensitive complex cell (**C**). For each example cell, responses to four different stimulus contrast levels are shown from the lowest stimulus contrast that elicits significant responses to the contrast that evoked the maximum response (from left to right). The contrast levels are shown above each membrane potential trace along with the visual representation of one cycle of the sine-wave grating stimulus. The grey shaded area surrounding the voltage traces are the estimated standard errors across cycles. The broken lines indicate resting membrane potentials (V_{rest}).

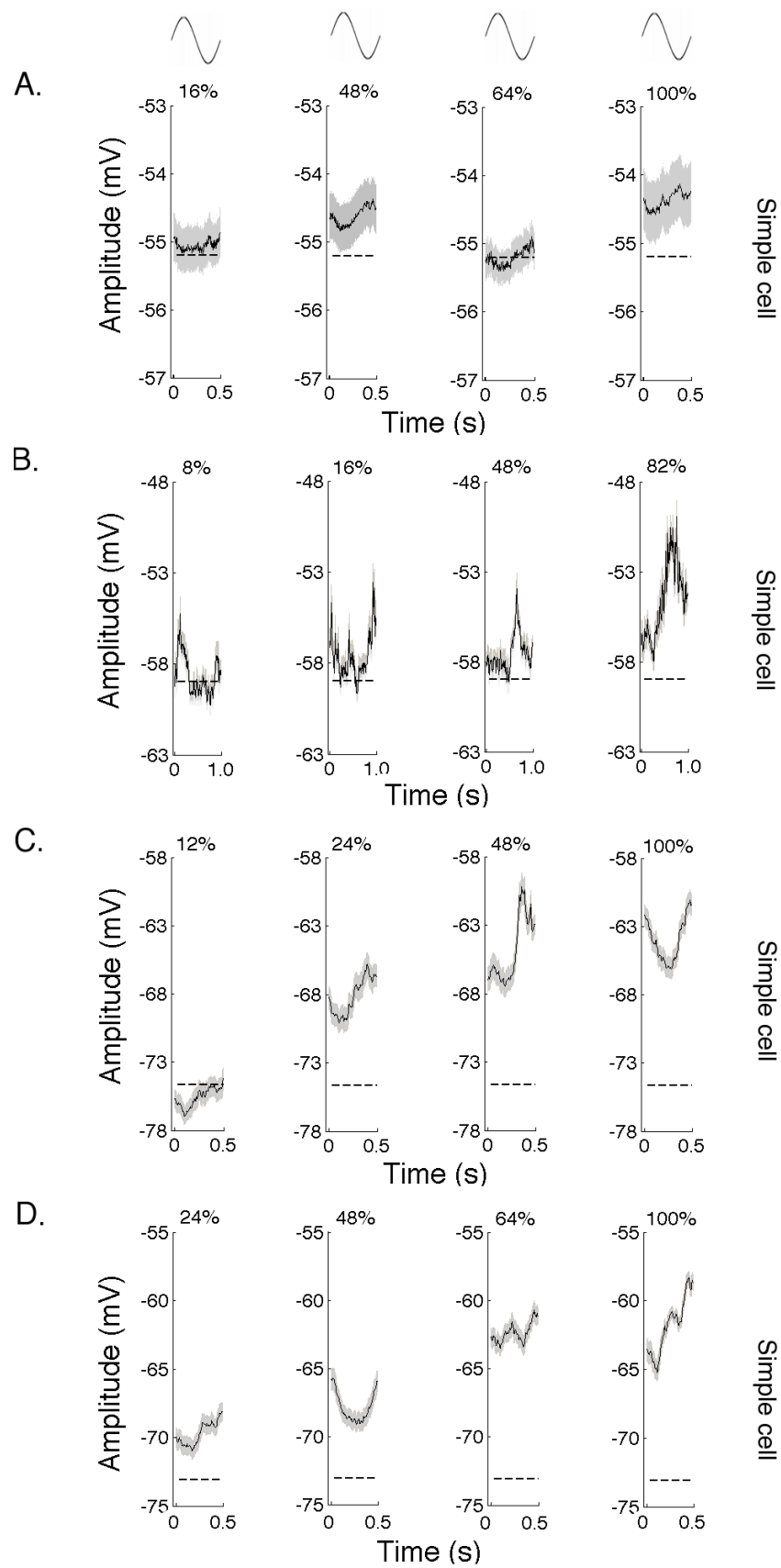
At high stimulus contrast (82%), the membrane potential of the example cell in Figure 5.7A oscillates in-phase with the sine-wave grating around the resting membrane potential, which is a strong indication of a simple cell. As the contrast level decreases, the strong phase-locked modulation of the membrane potential remains unchanged (Figure 5.7A). This observation is similar to the extracellular result, in which the modulation in the firing rate of simple cells does not show large changes with stimulus contrast levels.

The example cell in Figure 5.7B exhibits a membrane potential modulation at twice the temporal frequency of the sine-wave grating. This frequency doubling response is especially pronounced at low stimulus contrasts (8% and 16%). Overall, regardless of the stimulus contrast, the example cell does not show a phase-locked oscillation at the fundamental frequency of the sine-wave grating stimulus. Instead, it responds throughout most of the stimulus cycle, which is characteristic of a complex cell.

Another example cell is shown in Figure 5.7C. At high contrast (82% and 64%), the cell shows clear complex-like, frequency-doubled responses. However, as the stimulus contrast reduces, the response displays phase-locked membrane potential fluctuations at the fundamental frequency of the input stimulus.

Alongside the changes in response modulation, the amplitude of mean membrane potential also shifted towards the resting membrane potential as the stimulus contrast is reduced. At 12% contrast, the cell oscillates in-phase with the sine-wave around the resting membrane potential, which is similar to the observation of the simple cell response in Figure 5.7A. Comparable to extracellular investigation, sub-threshold membrane potentials of some complex cells also exhibit increased phase-sensitivity at the fundamental frequency of drifting grating low stimulus contrast level.

Figure 5.8 shows responses of the other seven intracellularly recorded cells, presented in the same layout as the example cells in Figure 5.7. The three cells illustrated in Figures 5.8A - 5.8C oscillate in-phase with the sine-wave grating at the highest contrast levels, as expected from simple cells. Similar to the example simple cell in Figure 5.7A, as the contrast level decreases, the phase-locked modulation of the membrane potential remains unchanged. Figures 5.8E and 5.8F mostly show frequency doubling responses across different stimulus contrasts in a similar fashion to the example complex cell in Figure 5.7B. The cell shown in Figure 5.8G seems to have a frequency doubling response of a complex cell at high contrast and the phase-locked responses of a simple cell at low contrast, which places this cell in the same category as the example cell in Figure 5.7C. These seven cells fall into one of the three response profiles demonstrated in Figure 5.7. The responses of the cell in Figure 5.8D are more difficult to interpret but might represent the responses of a noisy simple cell.



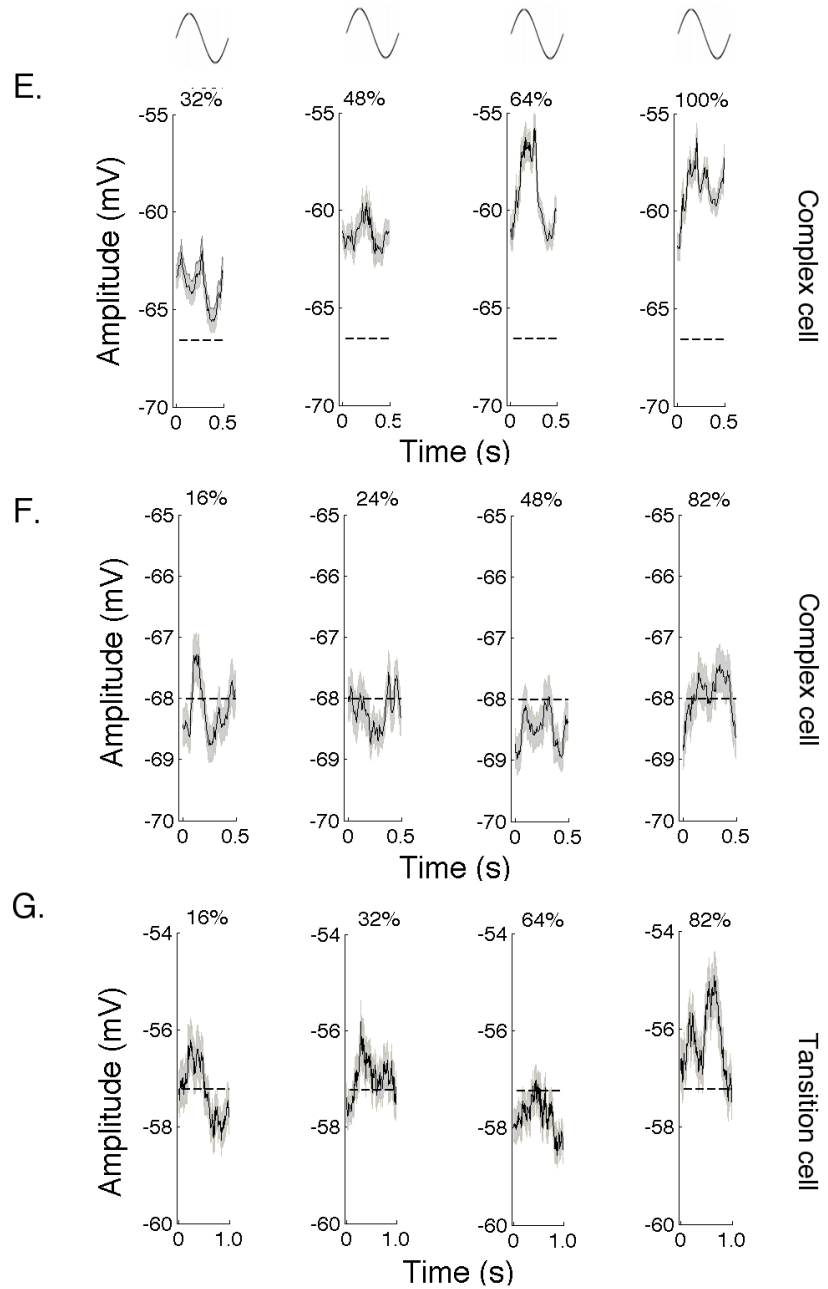


Figure 5.8. Membrane potential responses to drifting gratings at different contrasts

Cycle-averaged membrane potentials to drifting sine-wave gratings at different stimulus contrast levels for all recorded cells that are not shown in Figure 7. **A – G**, For each example cell, responses to four different stimulus contrast levels are shown from the lowest stimulus contrast that elicits significant responses to the contrast that evoked the maximum response (from left to right). The contrast levels are shown above each membrane potential trace along with the visual representation of one cycle of the sine-wave grating stimulus. The grey shaded areas surrounding the voltage traces are the estimated standard errors across cycles. The broken lines indicate resting membrane potentials (V_{rest}).

To measure the phase-sensitivity of the membrane potential responses at different stimulus contrast levels, I fitted sine-waves to cycle-averaged membrane responses at low and high stimulus contrasts. Table 5.1 lists the 10 intracellular recordings along with the goodness of fits for the high and low contrast sine-waves. The low contrast is defined as the lowest stimulus contrast eliciting a membrane potential that was significantly higher than the response to a blank screen. The high contrast is the stimulus contrast level that evoked the maximum response.

Figure 5.9 shows the cycle-averaged responses (black lines) and the fitted sine waves (red lines) for three example cells, one a simple cell and the other two cells that show contrast-dependent changes in phase sensitivity. The goodness of the fit is measured with R^2 , which ranges between 0 and 1. $R^2 = 1$ indicates a perfect fit and $R^2 = 0$ indicates the complete failure of the fit. For the example simple cell (Figure 5.9A), high R^2 values of 0.89 and 0.94 occurred at low and high contrasts, respectively, indicating that the cycle-averaged membrane potential responses oscillate in-phase with the sine-wave grating stimulus at both low and high contrasts. A similar pattern was observed for most recordings from simple cells, except for two cells that had relatively poorer fits at low contrast – most likely due to noise (Table 5.1). Interestingly, for the second and third example cells, R^2 values of 0.33 and 0.44 indicate a poor fit between the cycle-averaged membrane potential and a sine-wave at high contrast. However, fits of $R^2 = 0.95$ and $R^2 = 0.89$ were obtained for the responses at low contrast, which signifies a strong correlation with the strong sine-wave-like oscillation of the membrane potential.

The changes in the fit between the cycle-averaged response and the sine-wave further demonstrate the increase in phase-locked modulation as the stimulus contrast is reduced. Complex cells consistently showed poorer fits to a sine-wave grating at both high and low contrasts (Table 5.1).

Examination of the subthreshold membrane potential recorded through intracellular recording reveals that 2/10 (20%) of cortical cells recorded in this

project exhibited increased phase-locked membrane potential modulations at the fundamental frequency of the stimulus at low contrasts. This proportion matches the 21% of cells that were observed to show the same effect using extracellular recording.

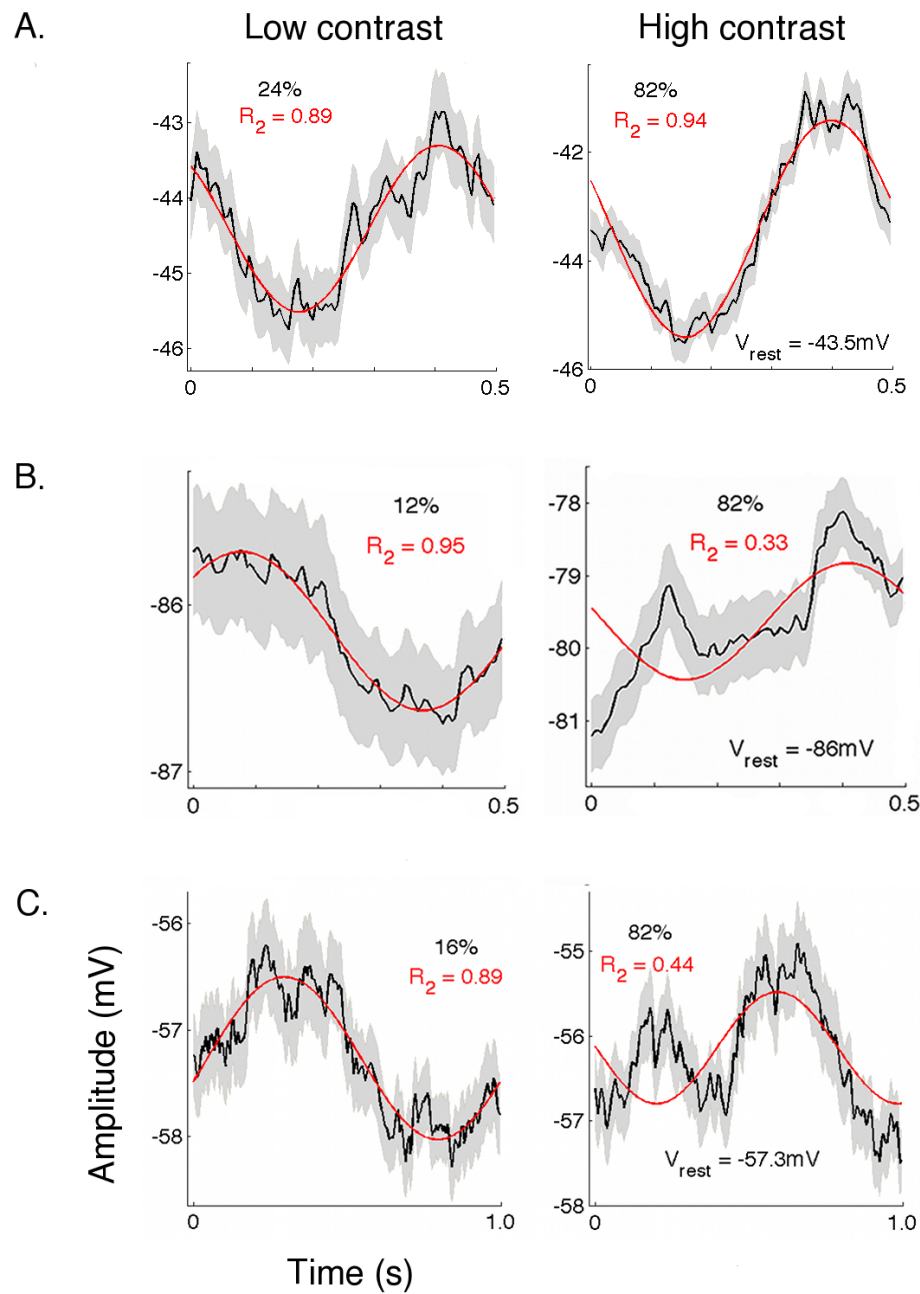


Figure 5.9. Fitting sine-waves to cycle-averaged membrane potentials

Cycle-averaged membrane potentials to drifting sine-wave gratings at the lowest (left) and the highest (right) contrast level for a simple cell (**A**) and two phase-sensitive complex cells or transition cells (**B** and **C**). The amplitude of each voltage trace is scaled individually to optimise the presentation of the response. A sine-wave (the red line on each trace) is fitted to each voltage trace and the goodness of the fit is measured with R^2 , where $R^2 = 1$ indicates a perfect fit and $R^2 = 0$ signifies a complete failure to fit the sine-wave to the voltage trace. Note that for **B** and **C** the fits are poor at high contrasts but excellent at low contrasts. Based on the intracellular membrane potentials, these cells transition from having a frequency doubled response (indicative of non-linear rectification) at high contrast to a phase-sensitive response that oscillates at the same frequency as the stimulus at low contrasts (indicative of linear summation).

| Cell number | Figure number | R ² at low contrast | R ² at high contrast | Cell types | Depth (μm) | Laminar location | Recording method* |
|-------------|---------------|--------------------------------|---------------------------------|------------|------------|------------------|-------------------|
| 1 | 5.7A/5.9A | 0.89 | 0.94 | Simple | 311 | L4 | EP |
| 2 | 5.8A | 0.4 | 0.79 | Simple | 200 | L2/3 | EP |
| 3 | 5.8B | 0.6 | 0.85 | Simple | 525 | L5 | EP |
| 4 | 5.8C | 0.85 | 0.96 | Simple | 190 | L2/3 | TPI |
| 5 | 5.8D | 0.87 | 0.87 | Simple | 154 | L2/3 | TPI |
| 6 | 5.7B | 0 | 0.62 | Complex | 520 | L5 | EP |
| 7 | 5.8E | 0.41 | 0.45 | Complex | 195 | L2/3 | TPI |
| 8 | 5.8F | 0.67 | 0.5 | Complex | 470 | L5 | EP |
| 9 | 5.7C/5.9B | 0.95 | 0.33 | Transition | 152 | L2/3 | TPI |
| 10 | 5.8G/5.9C | 0.89 | 0.44 | Transition | 523 | L5 | EP |

*EP: electrode position as indicated by the micromanipulator that drives the electrode, which was set to zero when the electrode touched the brain surface.

*TPI: two-photon imaging of fluorescent dye filled soma, the depth of which was determined through incremented scanning from the brain surface. This technique was used to confirm depth measured by the electrode position.

Table 5.1. A summary table of intracellular data (drifting gratings)

Data presented in the table are obtained from the 10 intracellularly recorded cells. For each cell, from left to right, the table shows the figures displaying its responses, the goodness fit, the R² for the fit, the sine-wave fit to the cycle-averaged membrane responses at low and high stimulus contrasts, the cell classification, the depth, the laminar location and the experimental methods used to obtain and confirm the depth information.

Attempts were also made to examine the correlation between membrane potentials and spiking responses of intracellularly recorded cells at different contrast levels. Out of the ten recorded cells, three cells exhibited spiking activity. Examples of a simple cell (A and B) and a complex cell (C and D) are shown in Figure 5.10. From left to right, membrane potential traces (above) and spike rate (below) for each example cell are shown from the lowest to the highest stimulus contrast that elicited spiking activities. As showing in the example simple cell, membrane potentials oscillated in-phase with sine-wave grating stimuli around the resting membrane potential (Figure 5.10A). Spiking responses roughly correlated with the modulation of membrane potentials (Figure 5.10B). However, for 24% contrast level, spikes were elicited at the lowest point of membrane potential trace. Moreover, the least amount of spikes was elicited for the highest contrast level (64%). For the example complex cell, membrane potential (Figure 5.10C) fluctuation correlated well with spiking responses (Figure 5.10D), both of which were not phase-locked to sine-wave grating stimuli. Unfortunately, cells that showed contrast-dependent changes in phase sensitivity did not produce spikes.

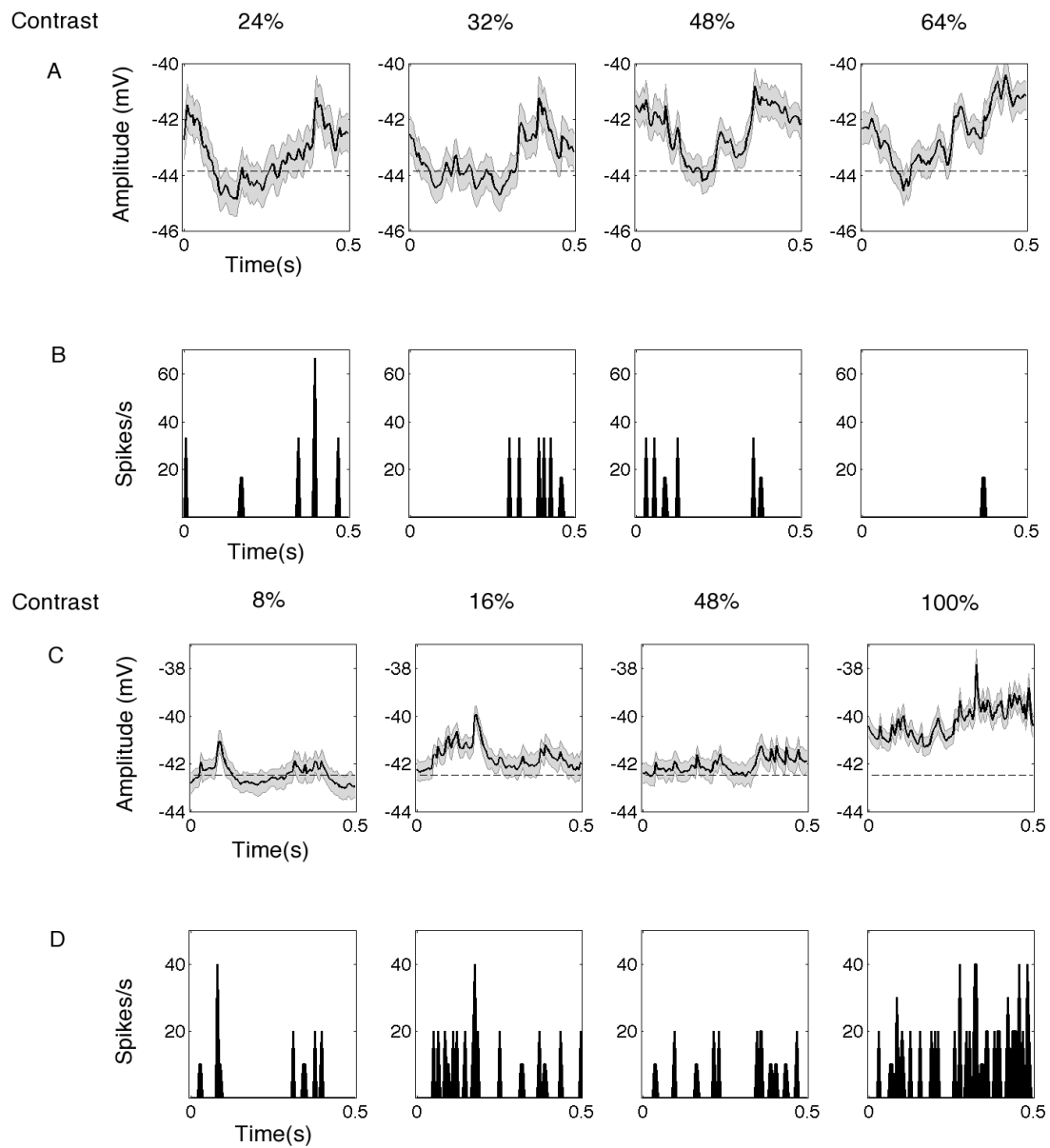


Figure 5.10. Membrane potential and spiking activity of intracellular responses to drifting gratings at different contrasts

Correlating cycle-averaged membrane potentials and spiking responses to drifting gratings at different stimulus contrast levels for an intracellularly recorded simple cell (**A** and **B**) and complex cell (**C** and **D**). For each example cell, responses to four different stimulus contrast levels are shown from the lowest stimulus contrast that elicits spiking responses to the contrast that evoked the maximum response (from left to right). Membrane potential responses (**A** and **C**) are shown above spiking responses (**B** and **D**) for the same stimulus contrast level. The contrast levels are shown above each membrane potential trace. The grey shaded areas surrounding the voltage traces are the estimated standard errors across cycles. The broken lines indicate resting membrane potentials.

5.4.3 Morphologically identifying recorded neurons through intracellular labelling

Table 5.1 summarises the types of anatomical information collected from the ten cells in which I obtained the full set of moving grating data using intracellular electrodes. Using the depth from the brain surface of which the cells were located (Table 5.1), the layers of the ten cells were deduced based on comparisons with Neil and Stryker (2008). As part of the intracellular investigation, I attempted to label individual cells to reveal their morphological identity and confirm their laminar location. I first tried labelling with Biocytin (a neuronal labelling dye) and Alexa Fluor 488 fluorescent dye through intracellular injection followed by post-mortem immuno-histochemical staining of brain slices. Unfortunately, this approach was fruitless as the staining was never successful.

This technique was attempted on four mice and seven recorded cells. The low number of recorded cells per animal was a deliberate effort to eliminate the possible mismatch between labelled cells and the physiological data in post-mortem staining. Out of the seven recordings, four generated a complete physiological data set, while the other three only led to partial data collection. The data from the four successful experiments are presented in Figures 5.7 and 5.8, along with two other cells in which anatomical analysis was not attempted (see Table 5.1 to locate the anatomical information that corresponds to the physiological data in Figures 5.7 and 5.8).

Following the failure of the post-mortem identification technique, I attempted *in vivo* two-photon microscope imaging of neurons filled with Alexa Fluor 488 fluorescent dye during intracellular recording. This technique was successful with five cells in two mice. From these experiments, four cells were filled sufficiently to identify enough morphological features to locate their laminar locations (Table 5.1). The two-photon imaging was conducted while I was visiting Professor Priebe's laboratory in the University of Texas in Austin, US and the short tenure of the trip (two-months) prevented further imaging of this type. It took me several months to get the technique optimised. All four of the

anatomically located cells had their cell bodies in Layers 2/3, which exactly matched the predictions made based on their depths from the brain surface.

Importantly, all four of the localised cells had complete physiological data sets, which are presented in Figures 5.7 and 5.8 (see Table 5.1 to locate specific cell data). Figure 5.11 shows a neuron that was filled and imaged using the two-photon technique (the physiological data for this cell is presented in Figure 5.8H). The soma of this cell was located 154 μm beneath the cortical surface, which corresponds to Layer 2/3. The observed dendritic morphology suggests that it is an inhibitory basket cell (Markram et al 2004).

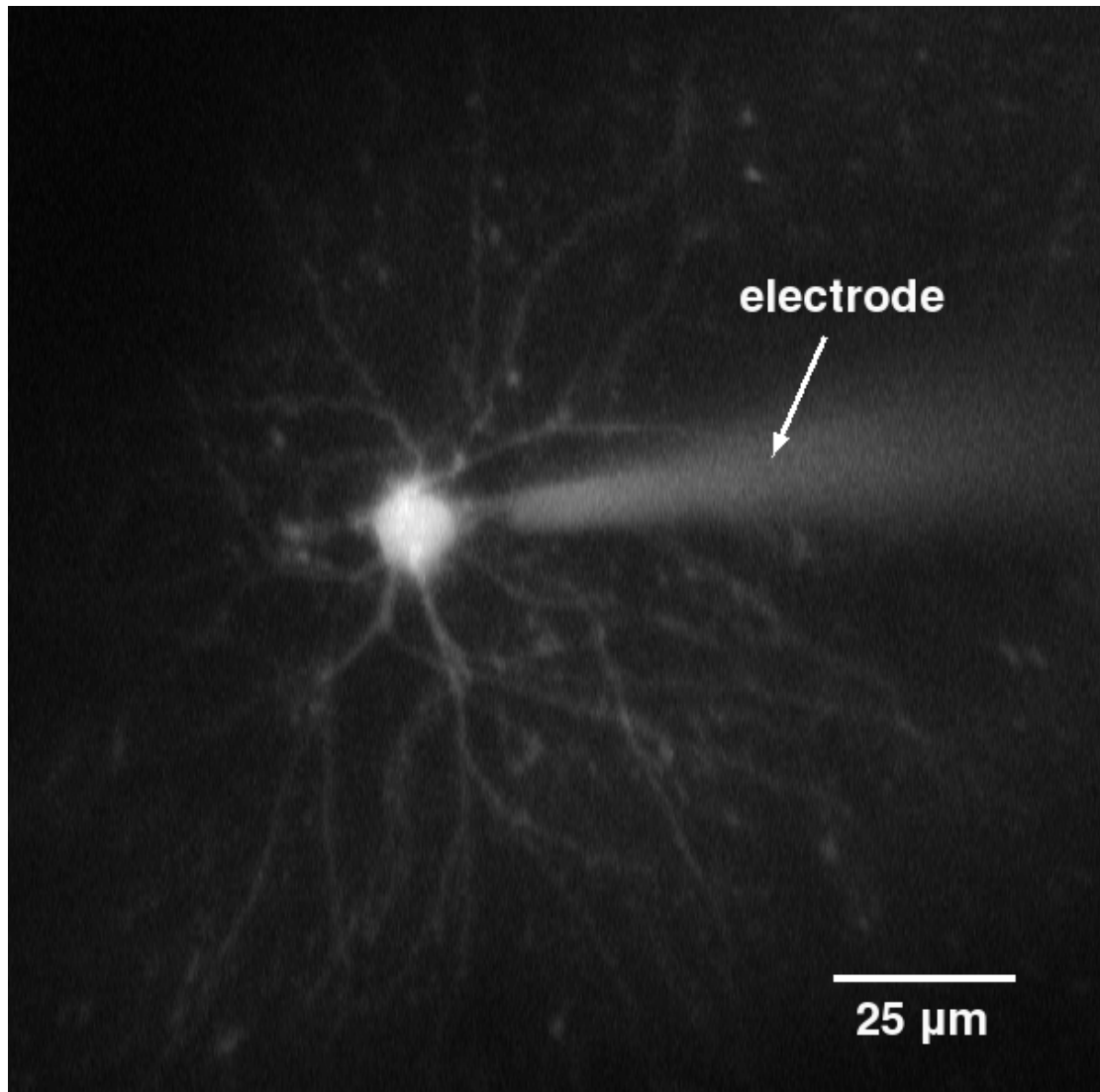


Figure 5.11. Two-photon image of a Layer 2/3 basket cell in mouse V1

The cell was filled with Alexa Fluor 488 fluorescent dye through an intracellular recording pipette (indicated by the arrow in the image). The soma of the cell was 154 μm beneath the cortical surface.

5.5 Discussion

It was first discovered in cat primary visual cortex (V1) that a proportion of complex cells showed significant increases in the relative modulation ratio (F_1/F_0 ratio) of their responses when the stimulus contrast was reduced, whereas the modulation ratios of simple cells remained unaffected (Crowder et al 2007). In addition, reduction in stimulus contrast results in a decrease in the spike rate of neurons. As the contrast of the stimulus decreases, a neuron's response in the form of spike rate also decreases. Recent studies demonstrated that the reduction in the number of spikes results in increased F_1/F_0 values due to the nature of Fourier analysis (Hietanen et al 2013, van Kleef et al 2010). Crowder and colleagues established statistical bounds outside of which this analysis limitation could not be accounted for by the reduction in spike count, therefore it was concluded to result from a physiological phenomenon. Cloherty and Ibbotson (2015) have further developed and improved this statistical model, and shown that a subclass of complex cells in macaque monkey V1 exhibit significant increases in F_1/F_0 ratio beyond what is expected from the reduction in spike count at low stimulus contrast. This data suggests that the phase-sensitivity of a subset of complex cells in monkey V1 is significantly altered between high and low stimulus contrasts. The present study demonstrates that a similar subset of phase-sensitive V1 complex cells also exist in both cat and mouse.

To the best of our knowledge, the present study was the first to demonstrate the existence of contrast-dependant phase-sensitive complex cells in mouse V1. It is also the first time that the new analysis technique developed to study monkey cortex has been applied to data from cat V1. The end result is a very rigorous proof that cat cortex contains contrast-dependent phase sensitive cells, as previously reported using other analysis techniques (Crowder et al. 2007). The findings suggest commonality in visual processing mechanisms amongst rodents, carnivores and primates. Thus further validating the relevance of mouse V1 in visual cortical research.

5.5.1 Contrast-dependent synaptic inputs of V1 neurons

The majority of mouse V1 neurons recorded in this study have F_1/F_0 ratios less than 1 (84%, 67 cells out of 80 cells in total). The median of the F_1/F_0 ratio distribution across the population is 0.59. Both results indicate that the majority of the neurons recorded have complex receptive fields, which is consistent with previous surveys of mouse V1 (Gao et al 2010).

Measuring the F_1/F_0 ratio of a cell's spiking rate to a moving sine-wave grating is the conventional method for identifying simple and complex cells. This quantitative classification system is closely based on the linearity of spatial summation within the receptive field proposed by Hubel and Wiesel (1962) (De Valois et al 1982, 1962, Maffei & Fiorenti 1973, Movshon et al 1978b, Skottun et al 1991). When the receptive field is presented with a drifting sine-wave grating in which the spatial frequency matches its preferred spatial frequency, a simple cell will display linearly modulated responses due to the spatially segregated ON and OFF subfields. On the other hand, as the drifting sine-wave encounters overlapped ON and OFF subfields, a complex cell will respond in a relatively steady and unmodulated fashion. The linearity was measured as the ratio between the first fundamental frequency and the mean spike rate (F_1/F_0 ratios). In the V1 population F_1/F_0 ratios are bimodally distributed in cat and monkey with simple cells having $F_1/F_0 > 1$ and complex cells $F_1/F_0 < 1$ (Skottun et al. 1991). The F_1/F_0 ratio quickly became the standard method to identify recorded V1 neurons due to it being relatively easy to use (Skottun et al. 1991).

An ongoing concern of this identification method is that it was established based on Hubel and Wiesel's (1962) hierarchical model of cortical processing, which argues for the existence of two discrete patterns of synaptic inputs that represent two distinct classes of functional units as simple and complex cells. Over the years as more evidence emerged, the complexity of cortical visual processing was realised. In turn, the clear distinction of two cell classes that represent two distinct stages of cortical processing was questioned. Several studies have shown that the observed dichotomy of F_1/F_0 ratios does not

necessarily suggest the presence of two separate cell classes with distinct patterns of synaptic inputs (e.g. Mechler & Ringach 2002).

The transformation between membrane potential and spikes is a non-linear process. An earlier study showed that the non-linear spike threshold enhanced the distinction between simple and complex responses (Carandini & Ferster 2000). Mechler and Ringach (2002) first put forward an alternative account for the bimodality in modulation ratio (F_1/F_0). Through modelling, they suggested that the non-linear threshold for spike generation is responsible for the bimodality of the modulation ratio of spiking rate. Moreover, they proposed that the distribution of the modulation ratio of the membrane potential of V1 neurons was actually unimodal. Lastly, they suggested that only small proportions of cells on each end of the distribution received pure simple or complex-like inputs as described in the hierarchical model, but the majority of cells sit somewhere in the middle of the modulation ratio distribution and receive a mixture of synaptic inputs.

Mechler and Ringach's model was later examined experientially by Priebe et al. (2004) using *in vivo* intracellular recording in cat V1. They confirmed that the modulation ratio of the membrane potential of V1 neurons was indeed unimodally distributed with the distribution highly skewed to the lower end. In addition, they revealed that V1 neurons formed two discrete populations when the ON and OFF subfield segregation was mapped using spiking responses. On the other hand a continuously distributed, single population was observed when the segregation was based on membrane potential responses. This study convincingly demonstrated that the dichotomy of simple and complex cells in V1 is, at least in part, a result of the non-linear mechanism of spike generation from a unimodal distribution of synaptic connectivity.

Including the present study, to our best knowledge, all literature that showed contrast-dependent changes in response linearity was quantified with F_1/F_0 ratios calculated from the extracellular response to drifting gratings. Our findings showed that some cells with $F_1/F_0 < 1$ at high stimulus contrasts

displayed increased F_1/F_0 ratios when the contrast was reduced. As shown by Priebe et al. (2004), measuring F_1/F_0 ratios based on spike frequency could not directly test for the spatial organisation of the membrane potential receptive fields, which reflects the synaptic inputs of the cells. Therefore, it is unclear if the increased F_1/F_0 ratio indicates a change in receptive field structure as a result of changes in synaptic inputs or results from the transformation between membrane potential and spikes. In addition, Carandini and Ferster (2000) demonstrated that stimulus contrast levels did not affect spike threshold.

Here, to address the influence of stimulus contrast levels on the synaptic receptive fields of V1 neurons, intracellular recordings to drifting sine-wave gratings at different contrasts were performed. As mentioned earlier, unlike the bimodal distribution of modulation ratios of extracellular responses, modulation ratios of membrane potential of V1 neurons are unimodally distributed. Consequently, changes in modulation ratio, measured as V_1/V_0 (V_1 : changes in membrane potential; V_0 : mean membrane potential), is not a strong indication of the change in membrane potential under different stimulus contrast levels. Alternatively, I fitted sine-waves to cycle-averaged membrane responses at low and high stimulus contrasts and measured the goodness of fits. The results demonstrated that the membrane potential oscillated in synchrony with the phase of the grating for simple cells, whereas complex cells responded in a phase-invariant or frequency doubled fashion. More importantly, some cells that showed complex-like intracellular responses at high contrast exhibited phase-locked membrane potential fluctuations, which are simple-like at low contrast. This finding confirmed that the contrast-dependant response linearity could also be observed in the membrane potentials of some V1 complex cells at low contrast. This in turn, demonstrated that synaptic inputs for some complex cells were different at high and low stimulus contrast levels.

Intracellular recording also provides an opportunity to examine the correlation between membrane potential and spiking responses. Interestingly, very few intracellularly recorded neurons produced spikes. This might be due to the fact that some cells were not perfectly healthy as indicated by the variability in

resting membrane potentials amongst recorded cells. Considering the difficulty in acquiring intracellular recordings, I did not reject any cell that responded to visual stimuli. Unfortunately, cells showed significant changes in membrane potential modulation under different contrast levels did not spike. Amongst neurons that exhibited spiking activities, it is evident that fluctuation in membrane potential does not necessarily reflect spiking activity, which further confirmed the necessity of intracellular examination of neuronal responses.

5.5.2 Laminar consideration of cell classes

The immediate investigations should be focused on the laminar locations of the contrast-dependent receptive fields in mouse V1. It was shown that phase-sensitive complex cells were found in high-proportions in Layer 4C and 6 of Macaque monkey V1, which receive direct afferent excitations (Cloherty & Ibbotson 2015, Henry & Hawken 2013). The experimental tools provided by recent advances in mouse genetics have allowed for detailed identification and manipulation of distinct neuronal types, which are unachievable in cat and monkey cortex. Further investigation should concentrate on isolating individual excitatory or inhibitory inputs to specific neuronal types under different stimulus contrast levels, as well as studying the effect on receptive field structures through elimination of singular excitatory or inhibitory sources.

The next major step following the physiological investigation of receptive field dynamics in V1 is to morphologically identify the group of neurons that exhibit contrast-dependant response linearity. However, linking physiology with anatomy has always been difficult in an experimental context.

In the present study, I attempted various methods to label recorded cells through intracellular dye injections. For unknown reasons, either Biocytin or Alexa Fluor 488 labelling coupled with post-mortem immunohistochemical staining were unsuccessful. To eliminate the complication associated with post-mortem brain slicing and immunohistochemical staining, which were prone to errors, I attempted to image fluorescent dye-filled neurons *in vivo* using a two-photon microscope. I had some success with this labelling method in that I was able to

identify the laminar locations of four cells and clearly identify a Layer 2/3 basket cell.

There are both advantages and limitations associated with this labelling method. To our advantage, the dye injection is done through the recording pipette immediately after intracellular recording of the physiological responses of the neuron. This allows the identification of the recorded neuron in real time, which avoids issues associated with post-mortem examination such as mismatching labelled cells and physiological data, and accidental labelling of neighbouring cells due to dye spillage. Several limitations are also associated with this method. First of all, imaging is limited to neurons above the depth of approximately 300 µm since the laser cannot penetrate below this depth, which means we are unable to image Layer 4-6 neurons. Secondly, the high-power laser damages the brain tissue, which limits the number of cells that could be recorded and imaged. Thirdly, unlike labeling preparations involving post-mortem processing, *in vivo* imaging is not suitable for detailed anatomical analysis, e.g. 3-dimensional reconstruction of the neuron. Overall, *in vivo* imaging of dye-filled neurons is a good method for fast and rough identification of intracellular recorded neurons in superficial layers, which proved suitable for the purpose of this study.

5.5.3 Stimulus-dependent receptive field formation

Cortical visual processing in mice has been studied extensively in the past decade (Huberman & Niell 2011). The abundant opportunities for genetic manipulation have made mouse visual cortex a model more preferable than carnivores and primates for studying receptive field properties. The feed-forward visual processing in mouse is largely similar to that of carnivores and primates, in which visual inputs generated in the retina are sent to V1 through the dorsal lateral geniculate nucleus (LGN) of the thalamus (Van Hooser 2007).

V1 neurons transform the centre-surround LGN receptive fields into elongated receptive fields that are selective for multiple visual parameters such as orientation, direction, temporal frequency and spatial frequency (Andermann et

al 2011, Bonin et al 2011, Gao et al 2010, Lien & Scanziani 2013, Niell & Stryker 2008, Roth et al 2012, Smith & Häusser 2010, Van den Bergh et al 2010). Also similar to other species, the feed-forward visual information is modified and fine-tuned by feedback inputs within V1 and/or from higher extra-striate cortical areas (Callaway 1998, Douglas et al 1995, Gilbert & Wiesel 1989, Li et al 2013, Liu et al 2010).

The mechanisms behind the formation of cortical receptive fields have long been the centre of debate in visual processing. Several models have been proposed to explain the construction of complex receptive fields (reviewed by Martinez & Alonso 2003). Here I discuss the validity of these models in light of the contrast-dependant receptive field structures observed in mouse V1. The hierarchical model proposed by Hubel and Wiesel (1962) states that simple cells in geniculo-recipient layers combine geniculate inputs to form spatially segregated ON and OFF subfields, and several spatially offset simple cell outputs are then combined to generate a complex receptive field with overlapping ON and OFF subfields. This model could potentially explain the contrast-dependent response modulation of some complex cells if their simple cell inputs have different contrast thresholds. As the contrast reduces, the inputs with higher contrast thresholds will start to ‘drop-out’ and the complex cell will in turn exhibit phase-sensitive responses due to the smaller number of remaining simple cell inputs (van Kleef et al 2010).

This model requires a specific laminar distribution of simple and complex cells, of which simple cells are located in geniculo-recipient layers and complex cells in subsequent afferent layers. Some studies in cats and macaque monkeys have shown that simple cells are over-represented in geniculo-recipient layers (Layer 4C and upper Layer 6) (Cat: Cloherty & Ibbotson 2015, Crowder et al 2007, Martinez et al 2005, Macaque: Ringach et al 2002). However, this is not entirely the case in mouse V1: simple cells are found throughout both geniculo-recipient Layer 4 and its main output layers, i.e. Layers 2/3 (Gao et al 2010, Niell & Stryker 2008, Van den Bergh et al 2010). Moreover, a recent study, which isolated thalamic excitation by optogenetically silencing cortical inputs, revealed that

thalamic inputs to Layer 4 neurons in mouse V1 were organized into spatially offset, yet highly overlapping ON and OFF receptive fields (Lien & Scanziani 2013).

Overall, the organisation of the receptive fields in mouse V1 does not appear to directly support the feed-forward mechanism of the hierarchical model. Moreover, LGN-afferent complex receptive fields have also been observed in cat and monkey V1(Bullier & Henry 1980, for review: Stone et al 1979, Tanaka 1985). A study in macaque monkey V1 has shown an over-representation of contrast-dependant phase sensitive complex cells in geniculo-recipient layers (Layer 4C and upper Layer 6), which further question the validity of the hierarchical model (Cloherty & Ibbotson 2015, Henry & Hawken 2013).

Regardless of species, V1 neurons not only receive afferent excitatory inputs, they also receive intracortical excitatory and inhibitory inputs (reviewed by Harris & Mrsic-Flogel 2013). The hierarchical model is based entirely on feed-forward connections; it does not consider the contributions of lateral cortical inputs to the receptive field structures. An alternative model proposed that both simple and complex cells share the same basic cortical circuitry, but the difference in their receptive field structures are created by adjusting the strength of the recurrent intracortical inputs (Chance et al 1999, Tao et al 2004, Wielaard et al 2001, Zhu et al 2009). This alternative model overcomes some problems associated with the feed-forward model such as the non-specific laminar distribution of simple and complex cells (Gao et al 2010, Martinez et al 2005, Ringach et al 2002) and the non-linearity of thalamic inputs (Lien & Scanziani 2013, Tolhurst & Dean 1990, Wielaard et al 2001).

Modeling studies based on Macaque V1 Layer 4 circuits demonstrated that recurrent excitation is important in determining the linearity of receptive field summation (Chance et al 1999, Tao et al 2004). Recent evidence from mouse V1 supports this claim. By eliminating intracortical inputs, it has been shown that Layer 4 receptive fields resulting purely from thalamic excitation are smaller in size than receptive fields measured with total excitatory inputs, which suggests

that recurrent excitation plays a part in shaping classic receptive fields (Lien & Scanziani 2013, Liu et al 2010). Moreover, Layer 4 neurons that receive non-linear thalamic inputs are found to also receive phase-sensitive cortical excitation, which is tuned to the same orientation as their thalamic inputs (Li et al 2013).

In more superficial layers of mouse V1, distinct neuronal types are recruited unequally by afferent and lateral excitation. In addition, pyramidal cells and parvalbumin expressing (PV) inhibitory cells are largely driven by direct excitation from Layer 4, whereas the major excitatory inputs of somatostatin expressing (SOM) inhibitory neurons are from horizontal axons within Layer 2/3 (Adesnik et al 2012, Xu & Callaway 2009). The differential excitatory recruitment of neuronal types might in part be responsible for the diverse receptive field structures in mouse V1.

Across species, V1 neurons also receive lateral inhibition, which is thought to shape their receptive field structures (Borg-Graham et al 1998, Ferster 1988, Hirsch et al 2003, Liu et al 2010, Sillito 1975). As pointed out in Chapter 4, it was noticed that cells identified as FS (inhibitory) neurons in cat cortex tended to have higher proportions that were insensitive to low contrasts. It is possible that the changes to the receptive field structures of the neurons seen at low contrasts are related to the reduced number of inhibitory inputs from such cells at low contrasts.

Early studies in cat V1 revealed that by blocking GABA receptors extracellularly or intracellularly, simple receptive fields could be transformed into complex-like receptive fields (Nelson et al 1994b, Sillito 1975). A recent study in mouse V1 has demonstrated that the specific spatial arrangement of inhibitory inputs were responsible for generating segregated ON and OFF subfields of Layer 2/3 simple cells with overlapping excitatory ON/OFF inputs (Liu et al 2010). Although it should be stated that both simple and complex receptive fields receive overlapped excitatory and inhibitory ON/OFF inputs to various degrees. The

authors suggested it was the spatial arrangement of excitatory and inhibitory inputs that gave rise to the dichotomy of receptive field structures.

Recent evidence in mouse V1 has also suggested involvement of inhibitory circuits in the contrast-dependent spatial summation of receptive fields (Adesnik et al 2012, Nienborg et al 2013, Vaiceliunaite et al 2013). It was discovered in monkey V1 that the size of classic receptive fields in superficial layers increase significantly at low stimulus contrast (Kapadia et al 1999, Levitt & Lund 1997, Sceniak et al 1999).

Further studies demonstrate that the same phenomenon is also observed in the superficial layers of mouse V1 and that inhibitory neurons might be responsible for contrast-dependent spatial integration (Nienborg et al 2013, Vaiceliunaite et al 2013). By selectively activating individual neuronal types using optogenetic techniques it was shown that depolarization of PV and SOM inhibitory neurons increased the size of classic receptive fields, which resembled the effect of reducing stimulus contrast. However, SOM activation tends to increase receptive field sizes in superficial and intermediate layers, whereas PV activation results in size increases in receptive fields across all V1 laminar depths (Nienborg et al 2013). As mentioned before PV and SOM cells are recruited differently in superficial layers: PV cells are driven by feed-forward excitatory inputs from geniculo-recipient Layer 4 and SOM cells receive lateral excitation within Layer 2/3 (Adesnik et al 2012, Xu & Callaway 2009).

The difference in excitation sources indicates that the two populations of inhibitory neurons might play different roles in shaping receptive fields in mouse V1. The effect of activating PV cells is consistent with the idea that they are responsible for global feed-forward inhibition, which rapidly adjusts the excitability of postsynaptic pyramidal cells according to the strength of the stimulus (Nienborg et al 2013, Pouille et al 2009). In contrast, SOM cells operate more locally through feedback inhibition driven either by intracortical lateral connections or long-distance axons from extrastriate cortex (Adesnik et al 2012).

In support of the possible role of cortical-cortical inhibition in receptive field formation, a study that inactivated the 'higher-order' visual cortex in cat observed that about 30% of complex cells in V1 increase their phase-sensitivity (F_1/F_0) whereas simple cells were not affected (Bardy et al 2006b). Differences between cat and mouse visual cortex are known (see Chapter 2), nevertheless it will be beneficial to investigate the effect of optogenetic inactivation of extrastriate cortex in mouse to test the linearity of the receptive fields in V1.

Alongside the present finding of stimulus feature dependent receptive field structures, it is apparent from increasing volumes of evidence that a single mechanism might not be sufficient to explain the diverse and flexible structures of V1 receptive fields. The formation of receptive fields is more likely the interplay of strength and spatial arrangements of feed-forward geniculate inputs versus both excitatory and inhibitory lateral cortical inputs. Recent works in mouse V1 have clearly shown the diversity in both excitatory and inhibitory recruitment of distinct neuronal types within and across cortical layers (Markram et al 2004).

Chapter 6: Contrast-Dependent Phase-Sensitivity in V1 Complex Cells Tested by Contrast-Reversing Gratings

6.1 Abstract

The receptive field structures of neurons in primary visual cortex (V1) create the foundation for all higher-level visual processing. Based on receptive field structures, V1 neurons are classified into simple cells, which are phase-sensitive, and complex cells, which are significantly less phase-sensitive. In the previous chapter, I have used drifting sine-wave gratings to show that the phase sensitivities of complex cells in mouse V1 increase at low contrast and after contrast adaptation, while those of simple cells remain the same at all contrasts. However, drifting gratings confound the influence of spatial and temporal summation, so in this chapter I have stimulated mouse V1 cells with static contrast-reversing gratings at optimal spatial and temporal frequencies. I varied the spatial phase and contrast of the reversing gratings to establish if contrast-dependent phase sensitivity in complex cells results from changes in spatial or temporal processing, or both. I demonstrated in both extracellular spiking and intracellular membrane potential responses that most of the increased phase sensitivity at low contrasts could be attributed to changes in the spatial structures of the receptive fields.

6.2 Introduction

The receptive field properties of mammalian primary visual cortex are dynamic. Various aspects of visual stimuli can influence the structure of cortical receptive fields. The contrast level is one of many stimulus features shown to influence the response properties of V1. The widths of the orientation tuning functions are

invariant to contrast changes (Sclar & Freeman 1982, Skottun et al 1987) but receptive field size and spatial tuning are contrast dependent (Sceniak et al 1999). Contrast tuning is also influenced by prior stimulus history, such that sensitivity is dynamically enhanced at the prevailing stimulus contrast and reduced at low contrasts (Crowder et al 2008, Ohzawa et al 1985). These contrast-related characteristics impose important restrictions on the types of models that can account for the tuning properties of the neurons.

Another important characteristic of receptive field properties in cortex is that cells can be classified as either simple or complex cells based on the spatial structures of their receptive fields (Hubel & Wiesel 1962, Skottun et al 1991). Simple cells have segregated subfields made up of oriented patches that detect either brightness increments (ON) or decrements (OFF) (Hubel & Wiesel 1962). This gives them the capacity to code the locations of oriented borders in the image, i.e. the cells are sensitive to spatial phase. Complex cells show a range of receptive field characteristics, some with moderate segregation of ON and OFF regions and others with no evidence of segregation, leading to a range of spatial phase sensitivities, from moderate to phase invariant (Gilbert 1977, Hammond & Ahmed 1985, Henry 1977, Hietanen et al 2013, Hubel & Wiesel 1962, Mechler & Ringach 2002, Spitzer & Hochstein 1988).

Regardless of precise classification, it has been generally accepted that a given cell fits permanently into a particular location in the phase sensitivity spectrum. However, recent studies using drifting sinusoidal gratings have shown that some complex cells increase their phase sensitivities as contrast is reduced (mouse: Chapter 5; cat: Crowder et al. 2007; van Kleef et al. 2010; monkey: Henry & Hawken 2012; Cloherty & Ibbotson 2015). In cat, Crowder et al. (2007) also revealed that exposure to an adapting stimulus, which causes a virtual reduction in image contrast, also leads to increased phase sensitivity. These findings, in combination with the contrast-related issues introduced above, have further complicated the requirements for models that explain receptive field organisation in cortex (e.g. van Kleef et al 2010).

While recent work has revealed that reduced contrast leads to increased phase sensitivity in some complex cells, all of the studies have used drifting sine-wave gratings. As drifting gratings are unable to separate the effects of spatial and temporal phase summation, it has been difficult to establish the origin of the contrast-dependent phase sensitivity. In this chapter, I measure the phase sensitivities of neurons in mouse V1 at multiple contrasts using temporally modulated but stationary gratings presented at many different spatial phases within each cell's receptive field. I examined the effect of stimulus contrasts in both the extracellular spiking and the intracellular membrane potential responses. I demonstrated that there was a trend towards increased spatial phase sensitivity of a subset of V1 neurons in both spiking rates and subthreshold membrane potentials.

6.3 Methods

Extracellular and intracellular experiments were performed in mice. General procedures can be found in Chapter 3. Here I present specific protocols for the data in this chapter.

6.3.1 Stimulus protocol

For each cell presented I measured the spiking responses or membrane potentials to sinusoidally modulated contrast-reversing gratings that were presented at 8 different spatial phases (0, 45, 90, 135, 180, 225, 270, & 315 in degrees). I intended to test ten different peak contrast levels for every phase (contrasts: 6, 8, 12, 16, 24, 32, 48, 64, 82 and 100%). Depending on the stability of recording, various combinations of contrast levels were tested. Due to the less stable nature of intracellular recordings, some cells were only presented with contrast-reversing gratings at 100% contrast. Gratings with different contrasts were presented in random order at the optimal temporal frequency (TF), spatial frequency (SF) and orientation of the recorded cell, in a circular aperture the size of its excitatory receptive field. Each stimulus consisted of the grating presented

for 0.5 s with stationary peak contrast, 2 s presented with sinusoidally modulated contrast, and another 0.5 s with stationary peak contrast.

6.3.2 Analysis of extracellular spiking responses

To analyse the combined spatial and temporal tuning properties of each extracellularly recorded cell, two-dimensional spatio-temporal period histograms were constructed from the spiking response to the contrast-reversing portion of the stimulus. This involved assigning each spike to one of 64 bins in an 8×8 grid corresponding to the combinations of 8 spatial and 8 temporal phases (0, 45, 90, 135, 180, 225, 270 & 315 degrees in each case). By plotting these histograms over the range of contrasts presented, any changes in the spatial and temporal tuning of the cell with contrast could be visualised.

To quantitatively summarise the spatio-temporal tuning of cells and how this changed with contrast, the period histograms were smoothed by fitting to an appropriate function, and the smoothed version was used to extract a variety of tuning measures. As the great majority of period histograms appeared bimodal, we chose to fit to a function which was the sum of two von Mises distributions (the von Mises distribution is a unimodal distribution for periodic variables, such as phase, analogous to the Gaussian distribution for non-periodic variables).

$$P(\varphi_t, \varphi_s) = \sum_{n=1}^2 B_n \frac{e^{K_{t,n} \cos(\varphi_t - \hat{\varphi}_{t,n}) + K_{s,n} \cos(\varphi_s - \hat{\varphi}_{s,n})}}{4\pi^2 I_0(K_{t,n}) I_0(K_{s,n})}$$

Here φ_t and φ_s are variables for the temporal and spatial phases; $\hat{\varphi}_{t,n}$ and $\hat{\varphi}_{s,n}$ are the corresponding peak (or preferred) phases for the two modes $n=1,2$; $K_{t,n}$ and $K_{s,n}$ are parameters that are inversely related to the temporal or spatial width of the distribution of each mode n , and B_n is the total number of spikes belonging to mode n (across all spatial and temporal phases). The parameters $\hat{\varphi}$ and $1/K$ are analogous to the mean and variance of a Gaussian distribution, and B is the area underneath the distribution. I_0 is the modified Bessel function of the

first kind of order 0 and is required in the denominator to normalise the integral of the distribution.

The measures extracted from this fitted function to characterise each cell's tuning were the preferred spatial and temporal phases, $\hat{\varphi}_{s,n}$, $\hat{\varphi}_{t,n}$, the peak spike rate A_n of each mode ($= \frac{B_n}{4\pi^2 T I_0(K_{t,n}) I_0(K_{s,n})}$, where T is the duration of the temporal phase bind, which varied depending on the cells optimal temporal frequency) and the spatial and temporal modulation depths, $D_{s,n}$ and $D_{t,n}$. These latter quantities are defined as the relative change in spike rate between the peak of each mode and an appropriately defined trough; for example $D_{s,1}$ is the relative change in spike rate from the peak of mode 1, at $(\hat{\varphi}_{t,1}, \hat{\varphi}_{s,1})$, to the trough at $(\check{\varphi}_{t,1}, \check{\varphi}_{s,1})$, as φ_s is varied keeping φ_t fixed at its peak value $\hat{\varphi}_{t,1}$ (see Figure 6.2 for a graphical illustration). $D_{t,n}$ etc. are defined analogously. The relative change is referenced to the peak rate, and lies between 0 and 1.

The fitting was performed by a least-squares optimisation on the parameters B_n , $\hat{\varphi}_{t,n}$, $\hat{\varphi}_{s,n}$, $K_{t,n}$ and $K_{s,n}$ using the `lsqnonlin` function in Matlab™ (The Mathworks Inc. Natick, MA, USA), which employs the trust region reflective algorithm. As the period histogram at 100% contrast typically had the greatest signal-to-noise ratio, this was fit first with random initial estimates of the parameters provided to `lsqnonlin`. The best fit over 100 runs with random initial parameter estimates was used to avoid fits that were only local optima. For subsequent lower contrast levels, the best parameter estimate for the contrast above was used as the estimate to initialise `lsqnonlin`. This process made it possible to continuously trace the parameters corresponding to each distinct mode across descending contrasts. For some cells, one of the two modes became indistinct at low contrasts. To avoid fitting the second peak to noise in this case, the bimodal fit was rejected if the number of spikes B_n belonging to the smaller mode was less than 10% of the total. In this case the period histogram was refitted with a unimodal von Mises distribution.

In addition, to gauge the statistical significance of the parameter estimates, the following three-fold analysis was performed for each cell. First, to ensure that we were measuring reliable stimulus evoked spiking, for each contrast we excluded any parameter estimates for which the mean spike-rate across the period-histogram was not above the mean spontaneous rate by at least twice the sum of both standard errors. Second, a standard error for each of the fitted parameters was calculated by refitting the von Mises distribution to period-histograms obtained from each single repetition of the stimulus ($n=10$ or 20), instead of the pooled data. The resulting set of parameter estimates across repetitions was then used to calculate a standard error of the mean. Third, some parameters, such as modulation depth and peak spike rate were subject to biased estimates when the total number of spikes used to estimate them was low (i.e. the mean value of the parameter estimate using a subsample of the data was systematically either above or below the parameter estimate obtained from using all the data).

To determine if any given parameter estimate was biased, Monte Carlo simulations were performed, to examine how the number of spikes in the associated period histogram affected the parameter estimate. N spikes were randomly sampled from the period-histogram and used to re-estimate the parameters as described above. This was repeated 100 times, with independent resampling to obtain estimates for the mean and standard deviation of the parameter estimates as a function of the number of spikes, N , ranging from 64 to 65,536 in powers of 2. This range was chosen to span the number of recorded spikes, N_{exp} , in the experimentally obtained histograms, which ranged from around 100 to over 10,000 depending on cell and contrast. For the great majority of parameters it was found that the simulated parameter estimate converged to the experimentally obtained estimate at high spike counts, but in some cases a systematic discrepancy between the two estimates was observed at low spike counts. The experimentally obtained parameter estimate was deemed unbiased if it differed from the simulated parameter estimate with $N = N_{\text{exp}}$ simulated spikes, by less than two standard errors of its mean.

6.4 Results

6.4.1 Extracellular spiking response to contrast-reversing gratings at different stimulus contrasts

Extracellular recordings were made from V1 of six anaesthetised mice ($n = 13$) that were presented with contrast-reversing gratings at their optimal orientations, and spatial and temporal frequencies at different contrast levels. I recorded from both simple ($n = 4$) and complex cells ($n = 9$), which were classified by their F_1/F_0 ratio to optimal drifting gratings at 100% contrast (see Chapter 5 for methods).

The raster plot in Figure 6.1A shows responses from a simple cell when stimulated by contrast-reversing gratings at 100% contrast. The different spatial phases are arranged along the y-axis delimited by horizontal thin grey lines; vertical thick grey lines delimit consecutive cycles during the sinusoidal modulation of the stimulus and vertical thin grey lines delimit different temporal phases within this. The corresponding spatio-temporal period-histogram obtained by pooling the data from the raster plot across cycles and trials is shown in Figure 6.1B. The position of the standing wave in the receptive field is given in degrees of spatial phase, with one entire spatial cycle being 360° .

As is typical of simple cells, at two spatial phases ($\varphi_s = 90^\circ$ and $90^\circ+180^\circ$) the response is small. At a spatial phase of $\varphi_s = 180^\circ$ and temporal phase of $\varphi_t = 0^\circ$, there is a robust peak in response which clearly demonstrates a half-wave rectification. A second similar response peak occurs at a spatial phase of $\varphi_s = 180^\circ+180^\circ$ (360° or 0°) but displaced in time to $\varphi_t = 0^\circ+180^\circ$, reflecting the 180° phase shift of the standing wave. This typical simple cell response-characteristic acts as a baseline for comparison with complex cell behaviour. The key features of the simple cell are that there are clear spatial and temporal null phases, where responses are small (black in Figure 6.1B). When the grating is spatially ‘in-phase’, the temporal form of the response is a half-wave rectified version of the sinusoidally modulated input. This results in two response peaks separated from each other by 180° in space and time by deep troughs with little or no response.

Figures 6.1C and 6.1D show the response in the same format for a complex cell. The raster plot and period-histogram reveal similar response amplitudes at all spatial phases (Y-axis) and a frequency doubled temporal response (X-axis), resulting from full-wave rectification, regardless of the polarity of the contrast change. Similar to the simple cell shown above, two response peaks are evident, however in this case they show little spatial modulation, while in the temporal domain the peaks are once again separated by 180°, but with shallower intervening troughs (grey rather than black in Figure 6.1D).

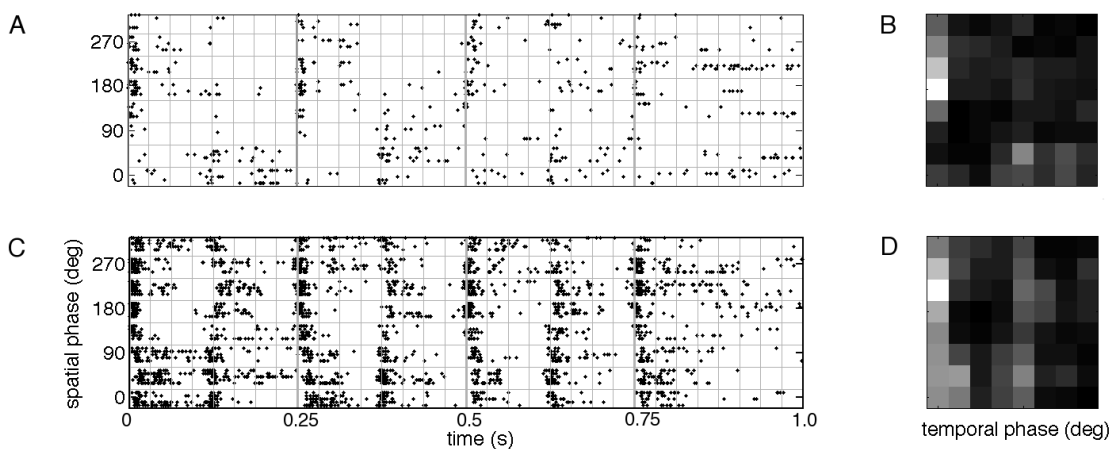


Figure 6.1. Spiking responses to contrast-reversing gratings at 100% contrast

Response of an example simple cell (top) and complex cell (bottom) to a contrast reversing grating stimulus presented at 100% contrast. **A** and **C** show spike rastergrams from 5 repeats of the stimulus at each of 8 spatial phases, delimited by the horizontal feint-grey lines. Vertical bold-grey lines separate four consecutive cycles of the stimulus, and vertical feint-grey lines delimit 8 temporal phases within each period. **B** and **D** are period-histograms corresponding to the rastergrams, formed by pooling spike responses over all cycles of the stimulus; white indicates the bin(s) with maximal spike count in the histogram and black a zero spike count.

To quantify these space-time tuning characteristics at a range of contrasts, the modulation depth and phase-separation of the two response peaks were calculated from the period-histograms in both spatial and temporal dimensions. This process is illustrated in Figure 6.2 for a simple and a complex cell at 100% contrast. The histograms were first smoothed, by fitting them to double-peaked, two-dimensional “periodic-Gaussian” functions (von Mises distributions): this allowed the two main peaks to be identified that account for most of the response variation with stimulus condition (see Methods).

For each peak (denoted by green or blue in the figure) the spatial and temporal modulation depths, D_s and D_t , and peak-phases, $\hat{\phi}_s$ and $\hat{\phi}_t$, were obtained as illustrated in the figure (and described in greater detail in the Methods). The modulation depth measures the relative change in response from peak to trough along a given dimension and varies from 0, for a completely unmodulated response, to 1 for a completely modulated response. The phase-separation of the peaks in the spatial and temporal dimensions, $\Delta\hat{\phi}_s$ and $\Delta\hat{\phi}_t$, was calculated as the difference in the peak phases, and varies between 0° and 180°. The process also gave the peak response rate of both peaks.

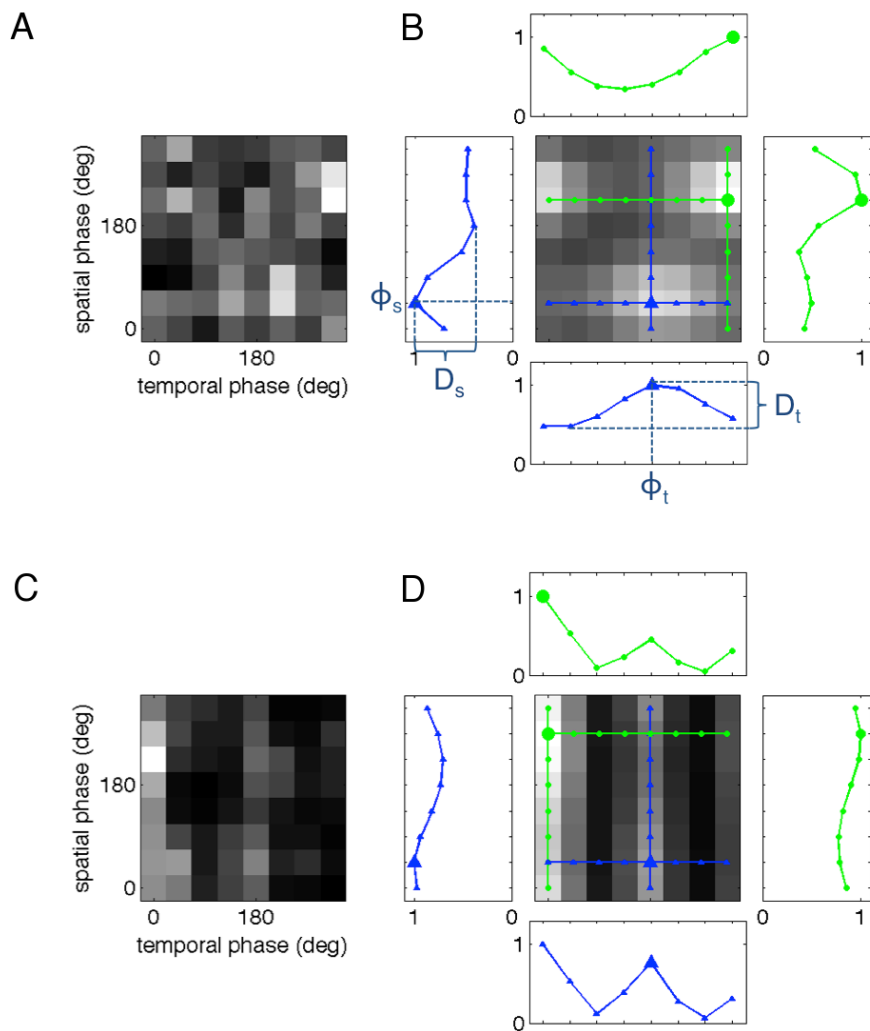


Figure 6.2. Extracting peak modulation depths from period histograms

Illustration of the procedure for extracting the peak-phase and spatial and temporal modulation depth from period histograms for a simple (top) and a complex (bottom) cell. The raw period histograms, **A** and **C**, are first smoothed by fitting to a double peak von Mises distribution (see Methods) to give the histograms shown in **B** and **D**, respectively. For each peak (green or blue) the corresponding spatial and temporal phases are extracted, ϕ_s and ϕ_t . The spatial modulation depth of each peak, D_s , is obtained along the cross-sections through the peak indicated by the overlaid vertical coloured line of the appropriate colour. The modulation depth is the change between peak and trough response, relative to the peak. Similarly the temporal modulation depth, D_t , of each peak is obtained from the appropriately colored horizontal cross-sections. The peak spike rate is the spike rate at each peak.

Figure 6.3 summarises the outcomes of this characterisation of tuning properties as a function of contrast for the complex cell introduced in Figure 6.1 and Figure 6.2. The top row of period-histograms shows the unfitted data arranged by contrast level (Figure 6.3A), and the row underneath shows the corresponding fit (Figure 6.3B). The measured spatial modulation depth of both peaks (green and blue) tended to increase as the contrast was reduced (Figure 6.3C); it varied from a minimum of $D_s = 0.24$ at 100% contrast (mean across the two peaks) to a maximum of $D_s = 0.68$ at 24% contrast, which was the lowest contrast level that evoked responses significantly above the spontaneous activity (see Figure 6.3H).

In comparison, the measured temporal modulation depth was generally high, but showed no consistent change with contrast level except at 24% contrast level (Figure 6.3D). Both the spatial and temporal phase-separation of the response peaks remained consistently around 180° across all contrasts tested (spatial: Figure 6.3E and temporal: Figure 6.3F). As expected, both the peak (Figure 6.3G) and overall mean spike rate (Figure 6.3H) increased as a function of contrast.

For comparison, in Figure 6.4, data for the simple cell introduced in Figure 6.2 is presented in the same format. In this cell, both the spatial and temporal modulation depths were high, but not completely saturated, and did not change markedly with contrast level (Figures 6.4C and 6.4D). Similarly, both the spatial and temporal phase-separation of the peaks were around 180° and did not change markedly with contrast level (Figures 6.4E and 6.4F). As with the complex cell shown in Figure 6.3, the mean and peak spike rate tended to increase with contrast level (Figures 6.4H and 6.4G).

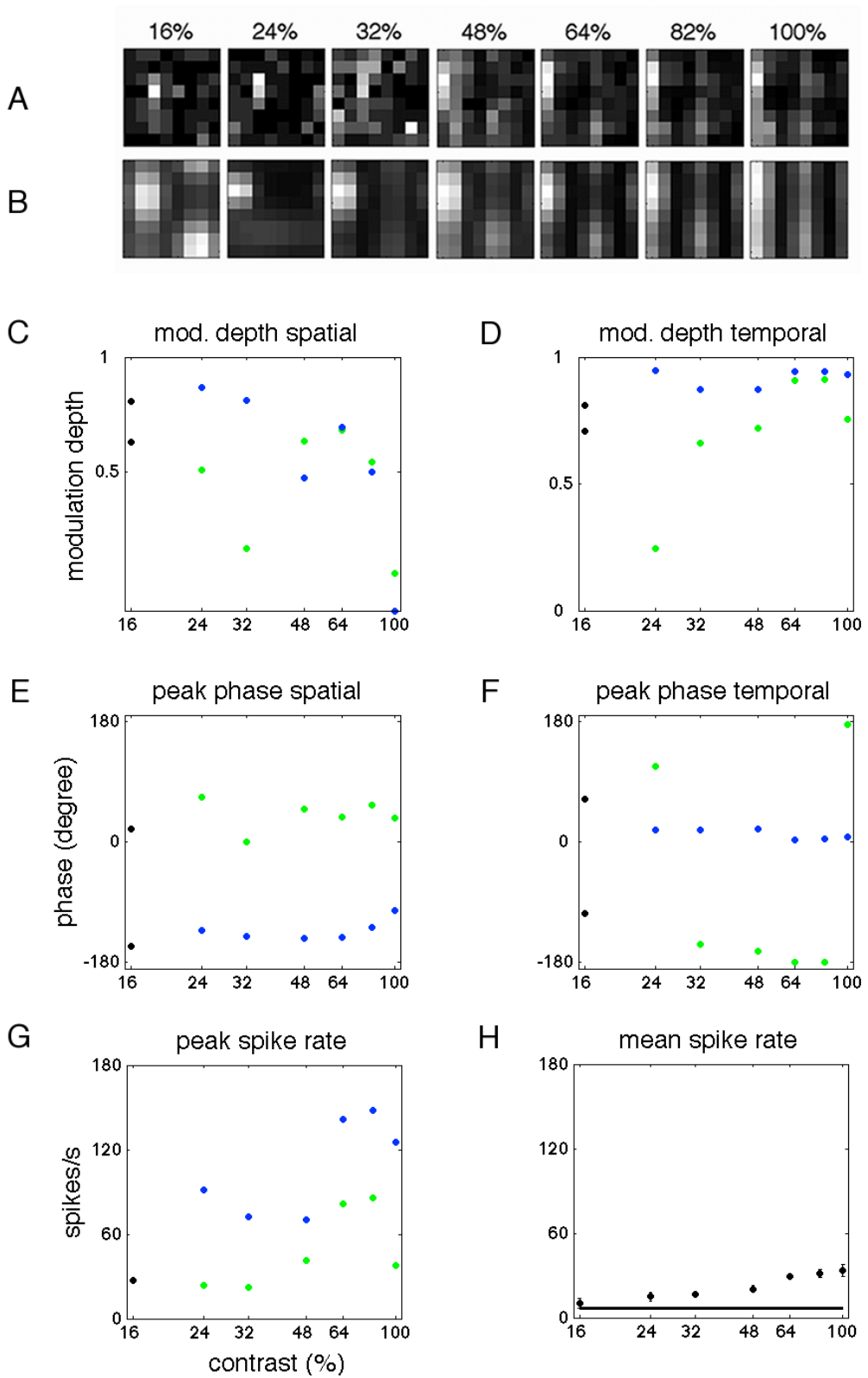


Figure 6.3. Contrast-dependent changes in a complex cell

A shows the raw period histograms as a function of contrast level, and **B** shows the corresponding smoothed versions. From these the following measures are extracted at each contrast level: spatial modulation depth (**C**); temporal modulation depth (**D**); peak spatial phase (**E**); peak temporal phase (**F**); peak spike rate (**G**). At each contrast, measures from both peaks are shown (blue and green), except when only a single peak could be fitted, and/or the response was not significantly driven and/or the measure was assessed to be biased (see Methods) (black). **H** shows the mean spike rate across all stimuli, with the horizontal black line indicating the spontaneous rate. Error bars show ± 1 standard error.

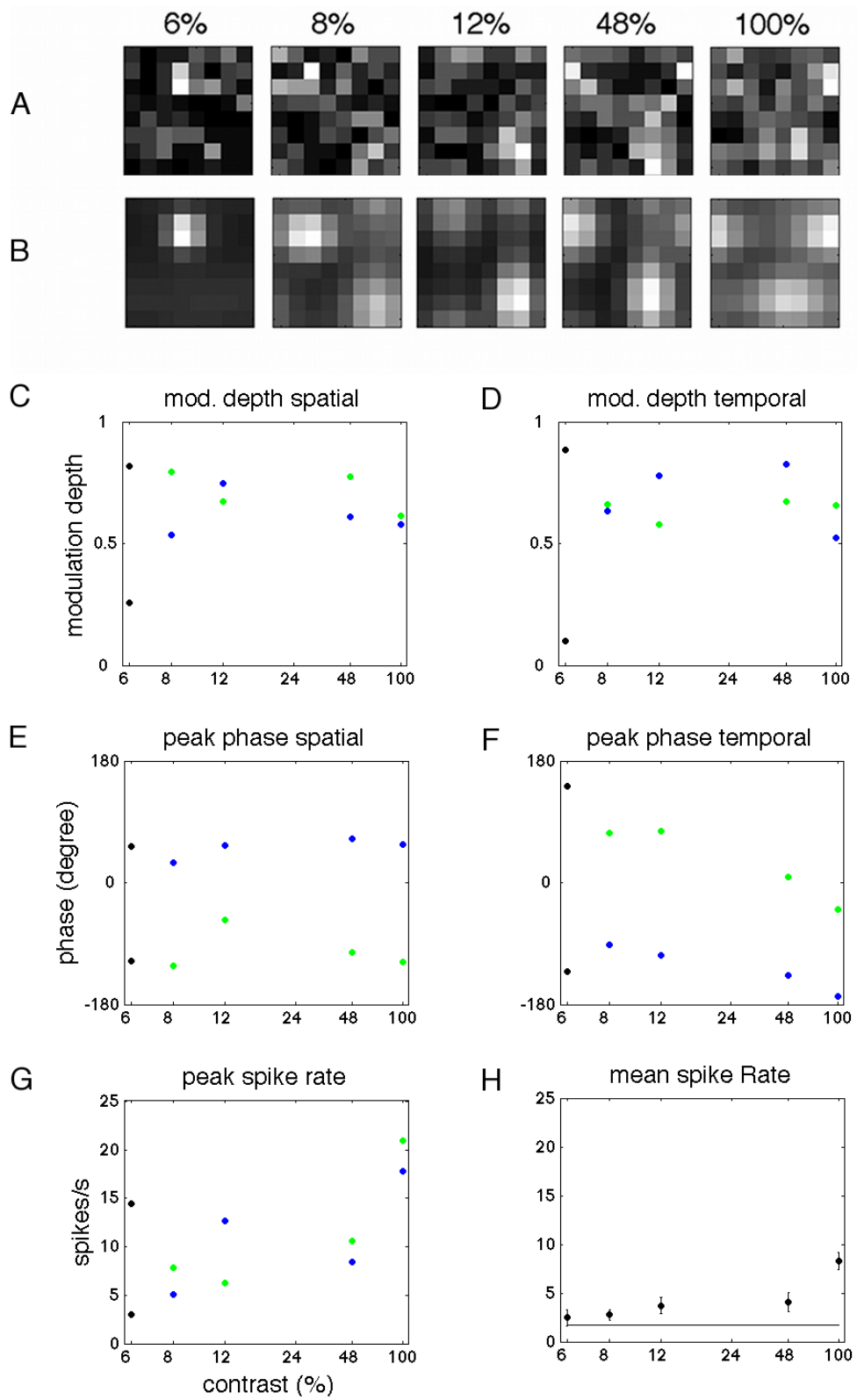


Figure 6.4. Contrast-dependent changes in a simple cell

Figure format is identical to Figure 6.3.

The trend to greater spatial modulation depth as contrast decreased was common amongst the complex cell population. The population results are summarised in Figure 6.5. Figure 6.5A shows a scatterplot of mean modulation depth at low contrast (the two lowest contrasts that evoked significant responses) versus mean modulation depth at high contrast (the two highest contrasts tested).

Out of the thirteen recorded cells, five cells showed significantly greater spatial modulation depth at low than at high contrast (black points above the red diagonal line; grey points are within two standard errors of the diagonal and are not considered significantly different). These data are also presented as a histogram of the change in spatial modulation depth, ΔD_s , from low to high contrast (Figure 6.5B). Over 30% of cells showed a significant increase in spatial modulation depth of 0.15 or more. Nevertheless, this population of cells is not the majority of the population. Moreover, four cells also showed the significant decrease in spatial modulation depth at low contrast level. However, all cells in the population that exhibited greater spatial modulation depth at low contrast level are classified as complex at 100% contrast. Therefore, out of the nine complex cells, five show increases in spatial modulation depth as contrast reduces.

Figures 6.5C and 6.5D present the population data for temporal modulation depth in the same format. As with the population data for spatial modulation depth, while some cells showed significant changes in temporal modulation depth between low and high contrasts by up to 0.25, this could be in either direction and there was no clear trend.

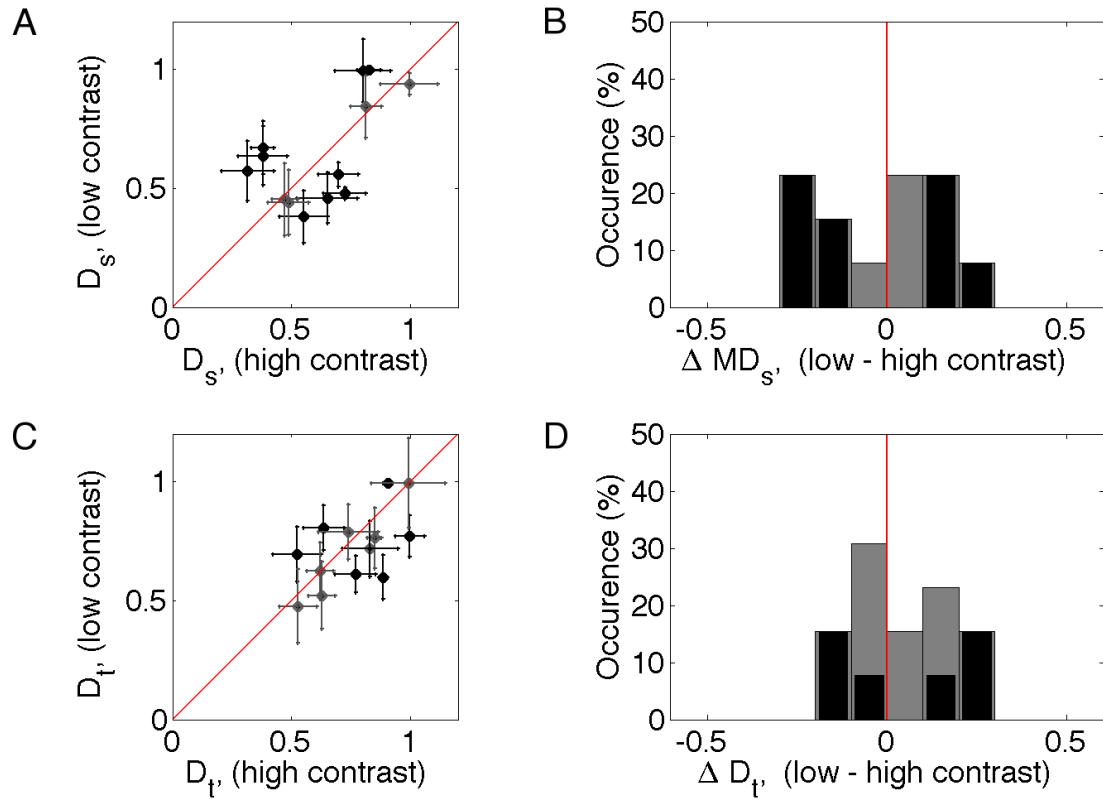


Figure 6.5. Changes in modulation depths from low to high contrast (population data)

Change in spatial (top) and temporal (bottom) modulation depth from low (the two lowest contrasts presented) to high (the two highest contrasts presented) contrast. **A** and **C** represent the data as scatterplots for spatial and temporal modulation depth, respectively, where each data point corresponds to a cell. The red line indicates no change between low and high contrasts; data points above it showed increased modulation depth at low compared to high contrast. Error bars indicate 2 standard errors, and black symbols indicate cells that showed a significant change of more than two standard errors between low and high contrast conditions (either an increase or decrease), while grey symbols indicate cells that showed no significant change. **B** and **D** represent the same data as in **A** and **C**, respectively, shown as histograms of the change in modulation depth from high to low contrast. Again black indicates a significant change and grey an insignificant change, while the red line indicates no change.

6.4.2 Intracellular membrane potential responses to contrast-reversing gratings at different stimulus contrasts

In addition to the extracellular recordings described above, sixteen intracellular recordings were made from nine mice to examine the subthreshold responses of V1 neurons to contrast reversing gratings at different stimulus contrasts. Spikes were removed from raw voltage traces before they were trial- and cycle-averaged (see Chapter 5, Figure 5.6 and related text for more details on this process).

Organised according to laminar locations, Figures 6.6, 6.7, and 6.8 show membrane potentials to contrast-gratings at 100% contrast levels for cells recorded from Layer 4, Layer 2/3 and Layer 5, respectively. For each cell, the averaged membrane potential to one cycle of a sine-wave grating (0.5 s) is shown for four different spatial phases of the contrast-reversing gratings (from left to right: 0, 90, 180 and 270 in degrees). Illustrations of a single cycle of a sine-wave grating of the corresponding phase is shown above the response traces. By analysing the stationary contrast-reversing gratings, I am able to examine the spatial (responses at 4 different spatial phases) and temporal (the response as a function of time at each spatial phase) components of the membrane potentials separately.

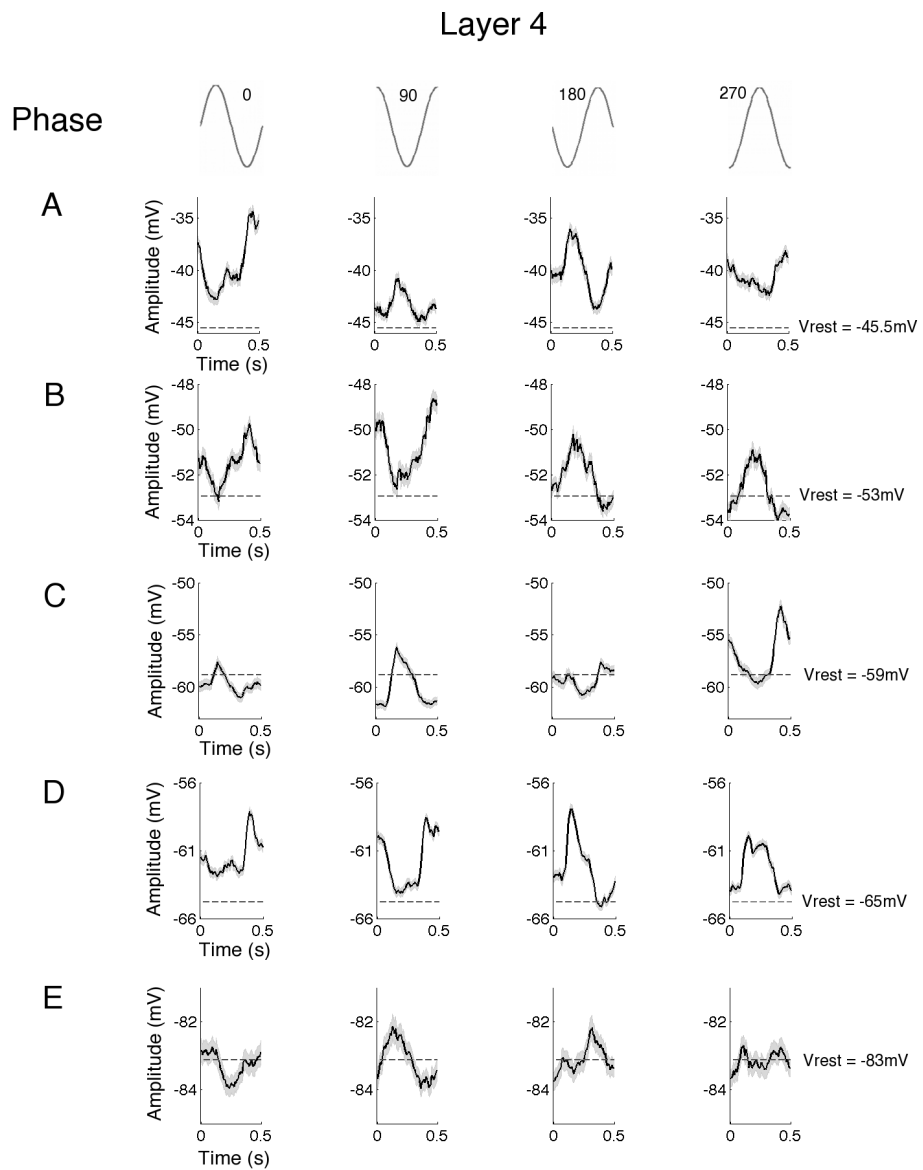
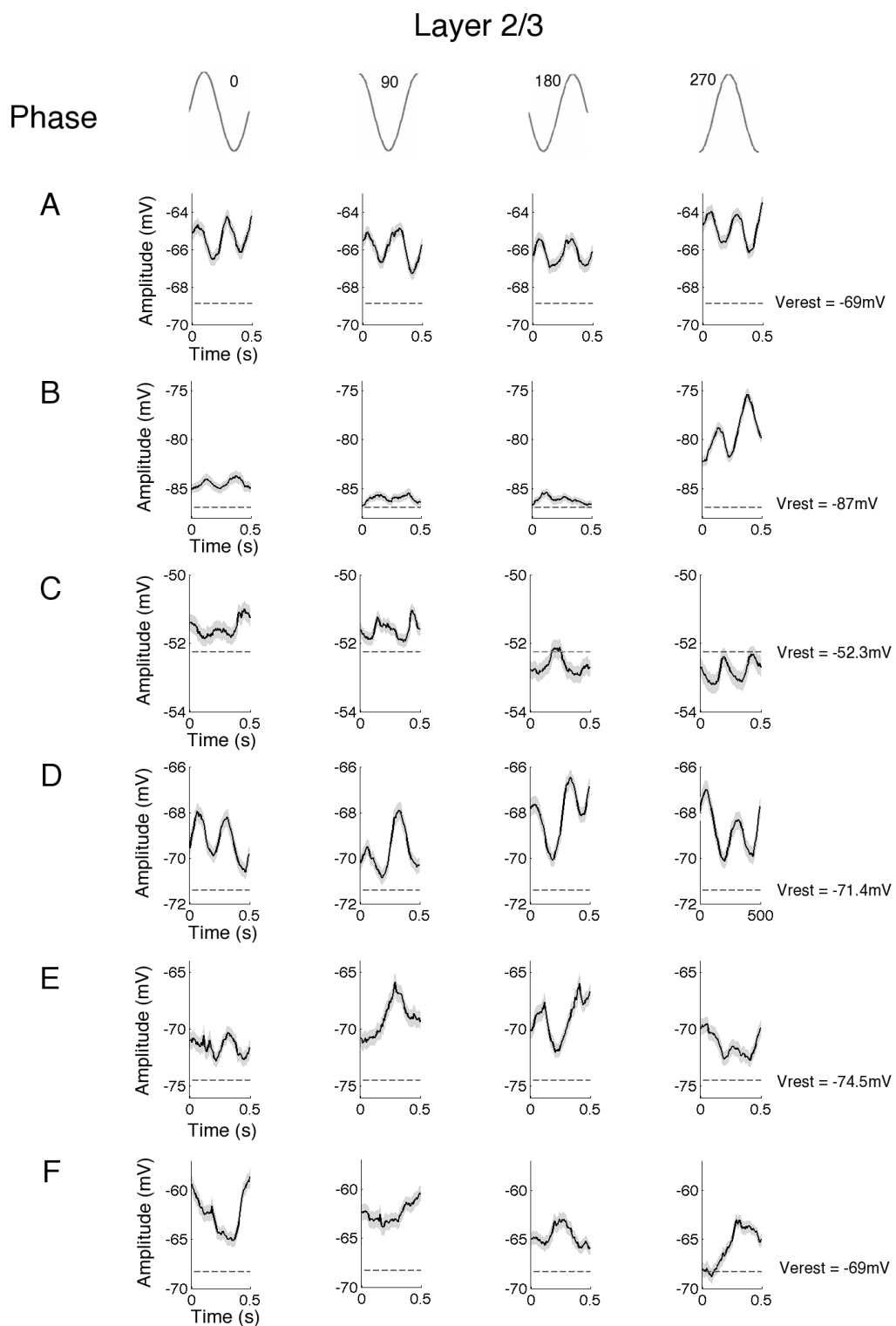


Figure 6.6. Membrane potential responses in Layer 4

Cycle-averaged membrane potentials to contrast reversing gratings at highest stimulus contrast levels for five cells (**A - E**) recorded from Layer 4. For each cell, responses to four different phases are presented with the corresponding phases shown above each membrane potential trace along with the visual representation of one cycle of the sine-wave grating stimulus. The grey shaded area surrounding the voltage traces are the estimated standard errors across cycles. The broken lines indicate resting membrane potentials (V_{rest}).

**Figure 6.7. Membrane potential responses in Layer 2/3**

Cycle-averaged membrane potentials to contrast reversing gratings at highest stimulus contrast levels for six cells (**A - F**) recorded from Layer 2/3. Figure format is identical to Figure 6.6.

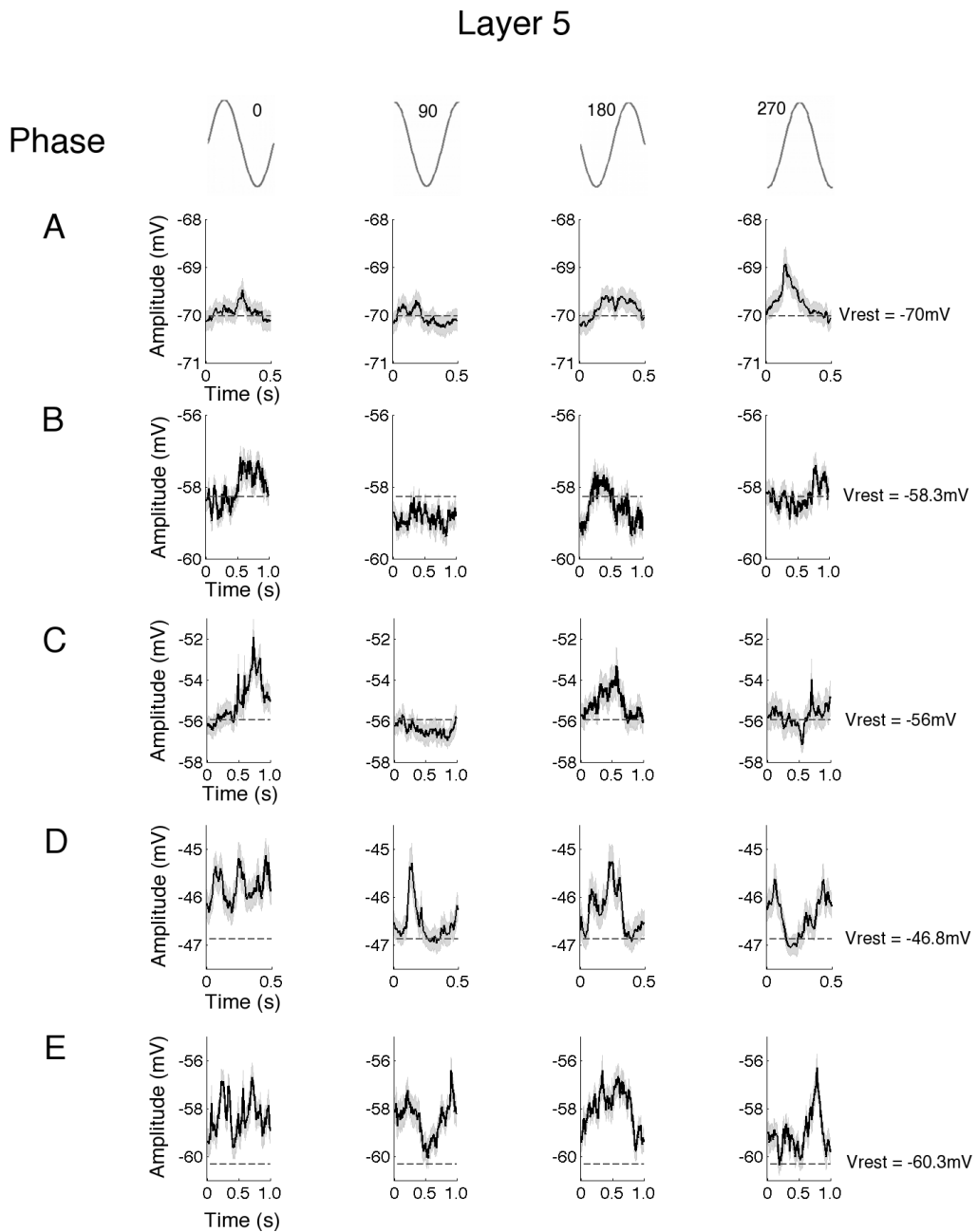


Figure 6.8. Membrane potential responses in Layer 5

Cycle-averaged membrane potentials to contrast reversing gratings at high stimulus contrast levels for five cells (**A - E**) recorded from Layer 5. Figure format is identical to Figure 6.6.

Some layer-specific characteristics were observed. First of all, all Layer 4 cells show in-phase oscillations with the sine-wave grating at each spatial phase. Both spatial and temporal responses reflect the oscillation of the stimulus, which is a strong indication of a simple cell (Figure 6.6). Secondly, pronounced frequency-doubling responses, were only observed in Layer 2/3 cells. Figures 6.7A – 6.7D show membrane potentials modulating at twice the temporal frequency of the sine-wave grating regardless of the spatial phases presented. The lack of phase selectivity in both the spatial and temporal components of the responses is a hallmark of complex cells. Thirdly, unlike cells in other layers, the membrane potentials of Layer 5 cells are noisy and largely independent of both the spatial and temporal phases of the grating stimuli, suggesting that they are complex cells, but with characteristically different properties to those in Layer 2/3 (Figure 6.8).

Another interesting observation is that some cells show frequency-doubling responses that to various degrees are temporally modulated. The two cells shown in Figures 6.7A and 6.7B have two peaks in their membrane potential fluctuations at each spatial phase and they are similar in amplitude. On the other hand, although the two cells in Figures 6.7C and 6.7D show frequency-doubled responses, the amplitude of the two peaks varies in-phase with the sine-wave gratings, which suggests that these cells are sensitive to the temporal phases of the gratings.

In a similar way to the extracellular experiments, I examined the intracellular responses of mouse V1 cells to different stimulus contrast levels. Out of the 16 recorded cells, I was able to obtain a full set of data (both low and high contrasts) in only 8 cells due to the instability of intracellular recording and the long stimulus presentation.

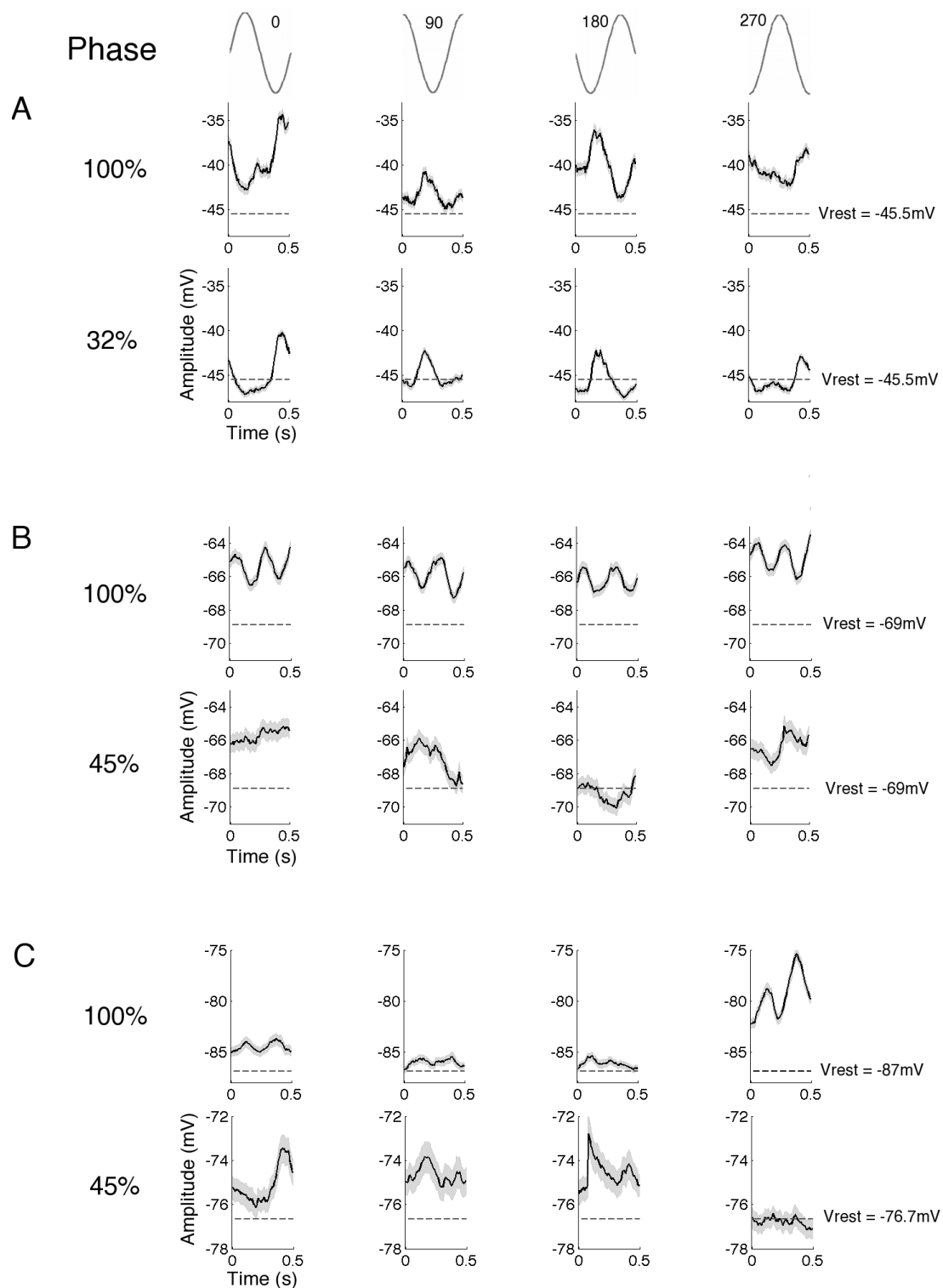
Figure 6.9 shows the averaged membrane potentials to a cycle of a contrast-reversing grating presented at high (top) and low (bottom) contrast levels for three example cells in the same format as Figures 6.6 – 6.8. At 100% contrast (top), the membrane potential of the cell in Figure 6.9A oscillates in-phase with

the sine-wave grating at each spatial phase, as well as exhibiting the opposite response polarity to sine-wave gratings that are 180° out of phase (0° and 180° or 90° and 270°). These response features strongly resemble a simple cell. At a lower contrast level (32%, bottom), although the amplitude of the membrane potential fluctuation is smaller, the strong phase-locked response modulation remains unchanged. This observation is similar to the extracellular result, in which the modulation in the firing rate of simple cells does not show large changes with stimulus contrast levels.

Conversely, the two example cells presented in Figure 6.9B and 6.9C both show clear complex-like, frequency-doubled temporal responses at 100% contrast (top) regardless of the spatial phases of the sine-wave gratings. However, at a lower contrast (45%, bottom), the response displays phase-locked membrane potential fluctuations at the fundamental frequency of the grating stimulus, which is similar to the observation of the simple cell response in Figure 6.9A. It is evident that the sub-threshold membrane potentials of these two ‘transitional’ complex cells become more phase-sensitive as the stimulus contrast is reduced.

Figure 6.9. Membrane potential responses at high and low contrasts

Cycle-averaged membrane potentials to contrast reversing gratings at high and low stimulus contrast levels for a simple cell (**A**) and two phase-sensitive complex cells or transition cells (**B** and **C**). For each cell, responses to four different phases are presented at the highest contrast tested (top) and lowest stimulus contrast (bottom) that elicited a significant response. The phases of the grating stimulus are shown above each membrane potential trace along with the visual representation of one cycle of the sine-wave grating stimulus. The grey shaded areas surrounding the voltage traces are the estimated standard errors across cycles. The broken lines indicate resting membrane potentials (V_{rest}).



To quantitatively measure the changes in phase-sensitivity, I fitted sine-waves to cycle-averaged membrane responses at low and high stimulus contrasts. Figure 6.10 shows the cycle-averaged responses (black lines) and the fitted sine waves (red lines) for the three example cells introduced in Figure 6.9 in the same order. For the fit, I chose the response to the spatial phase of stimulus gratings that elicited the largest response at 100% contrast for cells shown in Figure 6.10A and 10B. For the cell in Figure 6.10C, the optimal spatial phase (270°) at 100% did not evoke a significant response at 45% contrast (Figure 6.9C right most voltage traces). Instead, I used the response to the spatial phase that elicited the second highest response at 100% contrast for sine-wave fitting. The goodness of the fit is measured with R^2 , which ranges between 0 and 1. $R^2 = 1$ indicates a perfect fit and $R^2 = 0$ indicates the complete failure of the fit.

For the simple cell (Figure 6.10A), high R^2 values of 0.86 and 0.89 occurred at low and high contrasts, respectively, indicating that the cycle-averaged membrane potential responses oscillate in-phase with the sine-wave grating stimulus at both low and high contrasts. A similar pattern was observed for most recordings from simple cells as summarised in Table 6.1. In contrast, for the second (Figure 6.10B) and third example cells (Figure 6.10C), R^2 values of 0.16 and 0.29 indicate a poor fit between the cycle-averaged membrane potential and a sine-wave at high contrast. However, fits of $R^2 = 0.76$ and $R^2 = 0.77$ were obtained for the responses at low contrast, which signifies a strong correlation with the strong sine-wave-like oscillation of the membrane potential.

The changes in the fit between the cycle-averaged response and the sine-wave further demonstrate the increase in phase-locked modulation as the stimulus contrast is reduced. I also recorded from a complex that showed poor fits to a sine-wave grating at both low and high contrasts (Table 6.1). Interestingly, this complex cell was one of two cells that were shown to have temporally modulated frequency-doubled responses at 100% contrast (Figure 6.7C). In contrast, the two complex cells that showed phase-sensitivity at low contrasts are the two cells that have temporally invariant frequency-doubled responses at 100% contrast (Figure 6.7A and 6.7B).

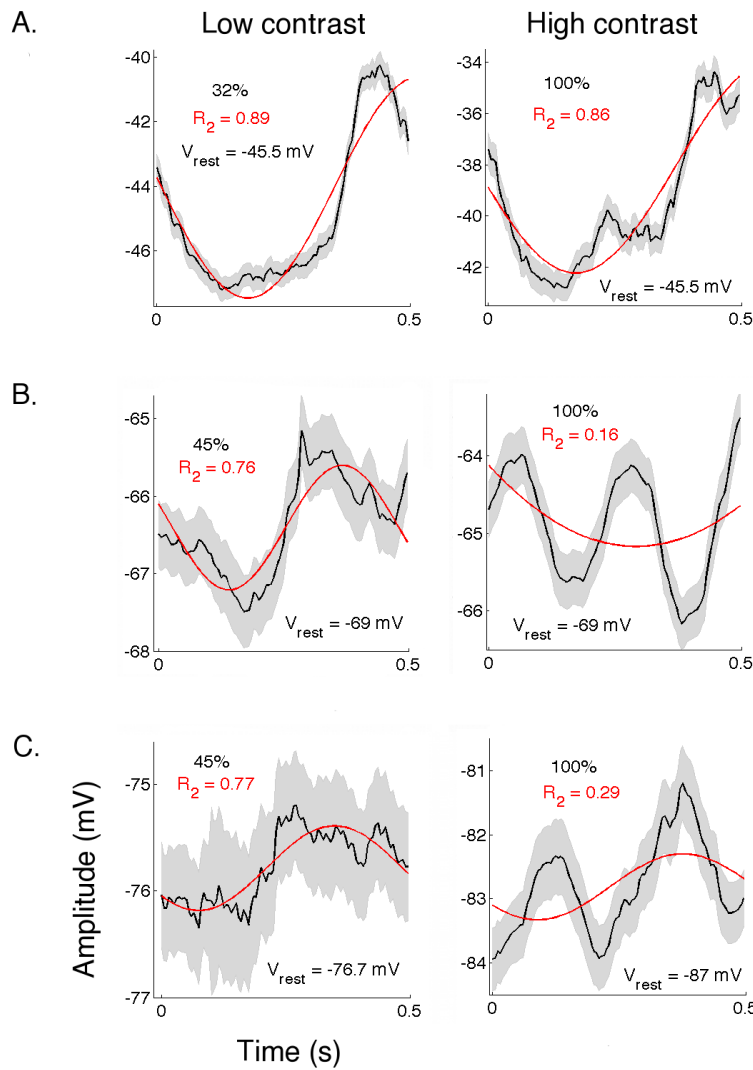


Figure 6.10. Fitting sine-waves to cycle-averaged membrane potentials

Cycle-averaged membrane potentials to the phase of contrast reversing gratings that elicited the maximum response at the lowest (left) and the highest (right) contrast level for a simple cell (**A**) and two phase-sensitive complex cells or transition cells (**B** and **C**). The membrane potentials in **C** were to the grating phase that elicited the second highest response because the optimal phase that generated the maximum responses at 100% contrast did not evoke significant responses at 45% contrast (see Figure 9C right most membrane potential traces). The amplitude of each voltage trace is scaled individually to optimise the presentation of the response. A sine-wave (the red line on each trace) is fitted to each voltage trace and the goodness of the fit is measured with R^2 , where $R^2 = 1$ indicates a perfect fit and $R^2 = 0$ signifies a complete failure to fit the sine-wave to the voltage trace. Note that for **B** and **C** the fits are poor at high contrasts but excellent at low contrasts. Based on the intracellular membrane potentials, these cells transition from having a frequency doubled response (indicative of non-linear rectification) at high contrast to a phase-sensitive response that oscillates at the same frequency as the stimulus at low contrasts (indicative of linear summation).

Overall, examination of the subthreshold membrane potential through intracellular recording reveals that 2/8 (25%) cortical cells recorded in this study exhibited increased phase-locked membrane potential modulations at the fundamental frequency of the stimulus at low contrasts. This proportion matches the 20% of cells that were observed to show the same effect using drifting gratings as visual stimuli (data presented in Chapter 5).

| Cell number | Figure number | R ² at low contrast | R ² at high contrast | Phase at max. response | Classification | Depth (μm) | Laminar location | Recording method* |
|-------------|---------------|--------------------------------|---------------------------------|------------------------|----------------|------------|------------------|-------------------|
| 1 | 6.6A/6.9A | 0.89 | 0.86 | 0 | Simple | 388 | L4 | EP |
| 2 | 6.6B | 0.85 | 0.79 | 45 | Simple | 311 | L4 | EP |
| 3 | 6.7F | 0.89 | 0.96 | 180 | Simple | 195 | L2/3 | TPI |
| 4 | 6.7D | 0.73 | 0.83 | 45 | Simple | 154 | L2/3 | TPI |
| 5 | 6.7E | 0.96 | 0.96 | 45 | Simple | 190 | L2/3 | TPI |
| 6 | 6.7C | 0.42 | 0.61 | 315 | Complex | 200 | L2/3 | EP |
| 7 | 6.7A/6.9B | 0.76 | 0.16 | 270 | Transition | 190 | L2/3 | EP |
| 8 | 6.7B/6.9C | 0.77 | 0.29 | 135 | Transition | 152 | L2/3 | TPI |

*EP: electrode position as indicated by the micromanipulator that drives the electrode, which was set to zero when the electrode touched the brain surface.

*TPI: two-photon imaging of fluorescent dye filled soma, the depth of which was determined through incremented scanning from the brain surface. This technique was used to confirm depth measured by the electrode position.

Table 6.1. A summary table of intracellular data test (contrast-reversing gratings)

A summary of data obtained from the 8 intracellularly recorded cells that were presented with stimuli at both high and low contrast levels. For each cell, from left to right, the table shows the figures displaying its responses, the goodness fit, the R² for the fit, the sine-wave fit to the cycle-averaged membrane responses at low and high stimulus contrasts, the stimulus phase that elicited the maximum response that was used to fit the sine-wave, the cell classification, the depth, the laminar location and the experimental methods used to obtain and confirm the depth information.

6.5 Discussion

6.5.1 Why use contrast-reversing gratings as visual stimuli?

Recent findings using drifting sine-wave gratings as visual stimuli have revealed that a large proportion of complex cells in the primary visual cortical areas of mice (V1), cat (areas 17 and 18) and monkey (V1) increase their phase sensitivities at low contrasts (mouse: Chapter 5; (monkey: Cloherty & Ibbotson 2015, Henry & Hawken 2013; cat: Crowder et al 2007, van Kleef et al 2010). The discovery of contrast-dependent phase sensitivity in the primary visual cortex adds to the list of contrast-related phenomena that impact cortical receptive fields (see Introduction). As with the other effects, this finding needs to be incorporated into future computational models.

However, there is a problem with all the work done with drifting gratings as stimuli. The phase sensitivity measured with drifting gratings combines the influences of spatial and temporal phase (Wielgaard et al 2001). To address this problem, I used contrast-reversing gratings as visual stimuli in this chapter. Contrast-reversing gratings remain fixed in space but are modulated in time. Consequently, by testing at multiple spatial phases, it is possible to assess the influence of the spatial and temporal components of the responses separately.

In response to visual stimulation by contrast-reversing gratings, simple cells have linear-like spatial summation properties (Movshon et al 1978b). That is, they are spatial phase (position) selective and their response is primarily a half-wave rectified version of the sinusoidal stimulus. Consequently, the response in most simple cells is nearly 100% modulated by the spatial phase of the grating. Conversely, in response to contrast-reversing gratings, complex cells exhibit spatial phase insensitivity and, in the time domain, show effects ranging from frequency doubling to near complete phase insensitivity. In the temporal domain, frequency-doubled responses arise because all regions of the receptive field respond to brightness increments and decrements. As contrast changes twice per cycle with a contrast-reversing grating, a frequency-doubled response is expected.

In this chapter, I have observed contrast-dependent spatial phase sensitivity in a subset of complex cells in both extracellular spiking activity and intracellular sub-threshold membrane potentials.

6.5.2 Changes in spatial modulation depths of extracellular spiking responses at different stimulus contrast levels

When examined extracellularly, for few complex cells, robust spiking responses at high contrasts are generated whatever the spatial phase of an optimally oriented, stationary grating, but at low contrasts only gratings with particular spatial phases generate large responses. This latter behaviour is reminiscent of simple cells, which show a clear preference for a particular spatial phase (Movshon et al 1978a, Movshon et al 1978b, Williams & Shapley 2007).

The same analysis using contrast-reversing gratings was also performed in cat V1 (area 17 and 18) neurons (unpublished data from our laboratory). A larger proportion of cells in cat V1 showed a significant increase in the depth of spatial modulation ratio (cat: 44%, mouse: 33%). The difference in proportion of complex cells that exhibit contrast-dependent phase sensitivity is consistent with the observation in Chapter 5 using drifting grating stimuli (cat: 31%, mouse 21%). However, it should be noted that the sample size of the present study is relatively small ($n = 13$). As well as cells that showed opposite behaviour were also present. Therefore, no strong conclusion should be drawn from this set of study.

In Chapter 5, I speculated the validity of various models of cortical receptive field formation based on the contrast-dependent receptive fields observed in some complex cells. Here I re-evaluate existing models with some additional insights obtained in this chapter. The hierarchical model of complex cell receptive field formation posits that spatial phase invariance in complex cells arises from multiple simple cells arranged to span several spatial phases (Hubel & Wiesel 1962). As contrast is reduced, the number of simple cell subunits that provide input to a given complex cell may be reduced because they no longer provide

synaptic drive sufficient for the recorded cell to attain spiking threshold. The end result would be that one remaining simple cell subunit would provide the suprathreshold drive (e.g. van Kleef et al 2010).

As this one simple cell has a distinct spatial phase location within the complex cell receptive field, only stimulation close to that phase will generate spiking responses at low contrast. If this were the case, we would expect complex-like response characteristics at high contrasts (i.e. weak spatial phase sensitivity, small spatial modulation depth and temporally full-wave rectified responses with peaks separated by 180° in time), but simple-like response characteristics at low contrast (i.e. high spatial phase sensitivity, large spatial modulation depth and temporally half-wave rectified responses with peaks separated by 180° jointly in time and space). Our result suggests this might be the case. The spatial phase-separation of response peaks of these complex cells at low contrast is typically 180° , which is similar to simple cells. As well as the depth of response modulation with spatial phase in these complex cells at low contrasts is generally similar to that of simple cells.

Our findings are also consistent with a model in which one phase sensitive region of the complex cell's excitatory receptive field (e.g. ON or OFF) becomes dominant, leading to greater spatial phase sensitivity at low contrasts when using both moving and contrast-reversing gratings. This suggestion does not contradict the earlier finding that the total area of the receptive field that generates spiking activity expands at low contrasts (Sceniak et al 1999). It is possible for the total excitatory area to increase while at the same time one ON or OFF patch exhibits relatively high gain. It has been known since the very first descriptions of complex cell receptive fields that some cells have discrete zones that are selective for ON or OFF (Henry 1977, Hubel & Wiesel 1962, Mata & Ringach 2005). It might be that these segregated light and dark zones are accentuated or the separation between them increases at low contrasts. Durand et al. (2012) used mapping techniques to plot the spatial structures of receptive fields in monkey primary visual cortex. They applied the technique at a range of contrasts and found that reducing contrast moderately decrease the overlap

between receptive field subregions due to changes in subregion width at low contrast.

These findings support our observations that reducing contrast leads to changes in the spatial receptive field structures of complex cells. It is possible, therefore, that the observations presented here and in previous experiments, including Chapter 5 (Crowder et al. 2007; van Kleef et al. 2010; Henry and Hawken 2013; Cloherty and Ibbotson 2015), relate to the fact that certain complex cells have more uneven ON and OFF zones in their receptive fields, which are particularly sensitive to changes in contrast.

6.5.3 Membrane potential responses to contrast-reversing gratings

The segregation of cortical cells into simple and complex types, based on the modulation ratio (F_1/F_0), may be as much to do with the nonlinearities of the spiking threshold as it is to do with the spatial structure of the receptive fields (Mechler & Ringach 2002, Priebe et al 2004). Given this observation, it is reasonable to ask if the increased modulation depth as contrast is reduced (Crowder et al. 2007; Henry and Hawken 2013) might be due to the nonlinear spiking behaviour of the cells. If one assumes that the subthreshold response comprises a sum of components, one modulated by spatial phase and the other invariant to it, one can envisage a number of interactions that could give rise to reduced modulation depth at low contrast. For example, it could be that at low contrast only the peaks of the modulation are suprathreshold (an “iceberg effect”), leading to large modulation depth, while at high contrast the invariant component of the response is driven above threshold so that the modulating component only causes a ‘ripple’ on top of the unmodulated response.

To investigate the impact of stimulus contrast under spiking threshold, I examined the membrane potentials of mouse V1 neurons to contrast-reversing gratings through intracellular recording. The phase-sensitive responses were also observed in membrane potential responses of some complex cells. Similar to

drafting grating responses, some cells show typical frequency-doubling responses to a single cycle of contrast-reversing sine-wave grating at high contrasts, whilst they show temporally full-wave rectified and spatially phase-locked responses (as for simple cells) at low contrasts. Therefore, for the cells recorded here, it is clear that the contrast-dependent spiking responses observed extracellularly are not a result of spiking threshold on different response components. Instead, the phase-modulated membrane potential suggests changes in synaptic inputs at different contrast levels.

In addition to the observation of ‘transition’ cells, several other interesting and noble observations were made in membrane potential responses to contrast-reserving gratings. First of all, the responses of two recorded cells could be described as a mixture of simple and complex cells at 100% contrast. These ‘in-between’ cells show frequency-doubled responses like a complex cell, but the amplitude of the two peaks varies in-phase with the sine-wave gratings, as expected from a simple cell. It is not surprising that these ‘in-between’ cells were not observed in extracellular recordings or intracellular recording with drifting gratings. When their spiking responses are examined extracellularly, the smaller peaks might not rise above spiking threshold, thus these cells will be classified as simple cells. The ‘in-between’ cells will not be detected by using drifting gratings, as the temporal component of the responses could not be observed separately from the spatial component and they will appear as frequency-doubling complex cells. This observation supports the theory that the non-linear spiking threshold enhanced the separation between simple and complex spiking responses and the V1 neurons sit on a continuum rather than being separated into two discrete populations of cells (Carandini & Ferster 2000, Priebe et al 2004).

More interestingly, the responses of one of the ‘in-between’ cells were examined at low contrast levels and its response remained complex-like. The two complex cells that showed contrast-depended phase-sensitivity (‘transition’ cells) have ‘true’ phase-invariant complex cell responses at 100% contrast, of which frequency-doubled temporal responses were observed regardless of the spatial phases. This phenomenon further suggests that ‘transition’ cells and ‘in-between’

cells might have different combinations of input sources. It is possible that ‘in-between’ cells receive a combination of inputs from both phase-sensitive simple cells and phase-invariant complex cells. As the contrast drops, the robust complex-cell input remains while the simple cell inputs ‘drops off’. On the other hand, transition cells are likely to source their inputs from a uniform simple cell population, as described in the hierarchical model.

The observation of the two types of complex cells is helpful in reconciling some contradictions between different cortical processing models. Recurrent models support the idea that simple and complex receptive fields are largely results of different intra-cortical inputs (Chance et al 1999, Tao et al 2004, Wielaard et al 2001, Zhu et al 2009), whereas the hierarchical model argues that feed-forward LGN inputs build simple receptive fields, which then send feed-forward inputs to complex receptive fields in more superficial layers (Hubel & Wiesel 1962, Reid & Alonso 1995, Tanaka 1983). ‘In-between’ cells are more likely to receive lateral inputs from other complex cells as proposed by the recurrent model. At the same time, ‘Transition’ cell receptive fields seem to be the result of feed-forward simple cell inputs. Both types of complex cells are found in Layer 2/3, which are in agreement with experimental evidence for both models (Antolik & Bednar 2011, Chance et al 1999, Debanne et al 1998, Teich & Qian 2006). The layer-specific intracellular responses also expand to Layer 4 and Layer 5 in this study. I noticed that Layer 4 cells largely show simple-like responses and Layer 5 cells are noisy and generally do not show either full-wave rectified complex cell responses or half-wave rectified simple cell responses. It is possible that Layer 5 cells receive input combinations that are distinct from both Layer 2/3 and Layer 4 cells.

6.5.4 Summary

Overall, contrast-dependent phase-sensitivity is evident in a subset of mouse V1 complex cells. This receptive field property is a result of altered synaptic inputs, rather than the non-linear transformation between membrane potential and spike rate. I am not able to provide a clear model to explain the contrast-

dependent phase sensitivity that I observe, but it is clear that future cortical models must account for a range of contrast-dependent effects such as changes in receptive field size, changes in spatial frequency tuning, contrast adaptation and increased plasticity at low contrasts.

Chapter 7: General Discussion

Half a century after David Hubel and Torsten Wiesel described the receptive field structures of neurons in mammalian primary visual cortex, the debate centred on the function and formation of different types of receptive fields is still heated. In recent years, mice have become a major animal model for cortical vision research largely due to opportunities for genetic and molecular manipulation (reviewed by Huberman & Niell 2011). As a result, new insights into receptive field properties have been emerging rapidly from mouse visual cortex at both the circuit and single-cell levels. However, any new findings in mouse based on knowledge accumulated from other animal models needs to be accepted with caution as the difference between mouse cortex and that of other well-studied animal models, predominantly cats and monkeys, are prominent (e.g. Niell & Stryker 2008, Van den Bergh et al 2010, Zariwala et al 2011). Consequently, it is important to study cortical receptive fields of different animal models in parallel.

In this thesis, I examined and compared receptive field properties of neurons in mouse and cat primary visual cortex, as well as further investigating specific receptive field properties in mouse V1 with novel experimental approaches.

7.1 Receptive field properties of inhibitory and excitatory neurons in V1

With the advances in genetic labelling of specific cell types and imaging techniques, the inhibitory neurons in mouse V1 have been extensively studied in recent years (e.g. Hofer et al 2011, Kerlin et al 2010, Liu et al 2009). However, these new experimental approaches cannot be easily applied to other animal models. To compare the receptive field properties of inhibitory and excitatory neurons in mice and cats, I recorded extracellularly from both animals using the same experimental procedures and putatively identified inhibitory and excitatory cells based on their characteristic spike waveform shapes. With the

limitations of this classification technique in mind, it is a quick and reliable means to provide a general guideline to the identities of large numbers of electrophysiologically recorded neurons.

The outcomes of this study demonstrated some major differences in receptive field properties between mouse and cat V1 neurons. Compared to cat V1 neurons, which exhibit very few differences between putative inhibitory and excitatory neurons, mouse inhibitory neurons exhibit a wide range of response linearity and orientation selectivity, whereas the majority of mouse excitatory cells were non-selective complex cells. This study adds to the general consensus that receptive field properties of specific cell types are not uniform amongst species, thus any direct comparison across species should proceed with caution (e.g. Niell & Stryker 2008, Van den Bergh et al 2010, Zariwala et al 2011). This observation comes as no surprise as it is sometimes the case in evolution that the same functional outcome can arise from different mechanisms and structures if driven by the environment (Van Hooser 2007). Nonetheless this is not saying mouse V1 is less capable than that of cats and monkeys. Quite the contrary, as discussed in my literature review and clearly demonstrated in this thesis, neurons in mouse V1 have sophisticated receptive field properties that are comparable with that of cat and monkey.

7.2 Contrast-dependent phase-sensitivity in V1

In this thesis, I especially focused on a specific V1 receptive field property that has been recently discovered in both cats and monkeys. It has been demonstrated in cat V1 (areas 17 and 18) and macaque V1 (only area 17), that a subpopulation of complex cells show increased phase sensitivity as the stimulus contrast is reduced (cat: Bardy et al 2006a, Crowder et al 2007, van Kleef et al 2010; monkey: Cloherty & Ibbotson 2015, Durand et al 2012, Henry & Hawken 2013, Romo et al 2011.). This effect is V1 specific; it rarely occurs in the second hierarchically arranged visual area (V2) in macaque (Cloherty & Ibbotson 2015). This finding suggests that changes to the level of contrast-dependent feed-forward drive to the primary visual cortex alters the phase sensitivities of the

neurons, while further spatial phase averaging appears to remove this property in higher cortical areas (V2).

I have shown that this contrast-dependent property is also common amongst mouse V1 complex cells. More importantly, I have demonstrated this effect in the subthreshold membrane potential responses for the first time, whereas it was only seen in extracellular spiking responses in previous studies. This is significant as it confirms that contrast-dependent phase-sensitivity is a result of altered synaptic inputs at different stimulus contrasts rather than a side effect of the non-linear transformation from membrane potential to spike rate. It is likely that in some complex cells, certain sources of synaptic input are contrast-dependent. At low contrast levels, these inputs are lost and the remaining inputs resemble that of a simple cell.

The dynamic nature of cortical visual neurons has been established with observations such as adaption to prevailing contrast (e.g. Crowder et al 2006, Stroud et al 2012). The distribution of contrast levels in natural scenes peak at low contrasts ranging between 0 – 25% (Balboa & Grzywacz 2000, Chirumuuta et al 2003, Ruderman & Bialek 1994, Tadmor & Tolhurst 2000, Vu et al 1997). Shifting towards simple-like responses at low stimulus contrast might be functionally advantageous because simple cells are known to transmit information at faster rates and carry more edge-like information than complex cells under certain circumstances (Mechler et al 2002, Reich et al 2001). It is evident that cortical responses to visual input are heavily modulated by attention and behavioural state (e.g. Andermann et al 2011, Fu et al 2014, Kagan et al 2002, McAdams & Reid 2005, Niell & Stryker 2010). Therefore, to test this theory, contrast-dependent phase-sensitivity needs to be studied in awake and behaving animals. Electrophysiological recordings and two-photon calcium imaging is now common practise in awake mouse cortex (e.g. Andermann et al 2011, Fu et al 2014, Margrie et al 2002, Niell & Stryker 2010, Polack & Contreras 2012).

A model for cortical receptive field formation is still yet to be agreed by the majority of studies. Popular models such as the hierarchical and recurrent

models demand specific laminar locations of receptive field types (Chance et al 1999, Hubel & Wiesel 1962). Therefore, the immediate step following the physiological investigation of receptive field dynamics in V1 is to identify the laminar locations of neurons that exhibit contrast-dependant phase-sensitivity.

It has been demonstrated in cat V1 (in the laboratory where I conducted my work) that this class of complex cells are located in supragranular (Layers 1-3) or granular (Layer 4) layers, while subgranular layers (5-6) contain few such cells (Meffin et al in press). These observations were based on more than 700 neurons, so the statistical analysis is highly reliable. In monkey V1, an over-representation of contrast-dependent cells was seen among complex cells in Layer 4C and 6 (Henry & Hawken 2013). However, while those layers had a higher proportion, they found such cells in all layers. Cloherty and Ibbotson (2015) did not find a clustering of contrast-dependent phase sensitive cells in any layers of primate cortex. Thus, in monkeys the laminar organisation of the cells is not clear.

With intracellular recordings in mouse V1, I have shown that this class of complex cells are located in both Layer 2/3 and Layer 5. However, the sample size in the present study is small compared to previous studies in cats and monkeys. It is important to further the laminar investigation in mouse as the distribution of the contrast-dependent complex cells is critical in determining whether feed-forward or recurrent connectivity were responsible for the contrast-dependent inputs. In addition, differences in the laminar distributions across species might reveal species-specific receptive field features.

References

- Abbott LF, Chance FS. 2002. Rethinking the taxonomy of visual neurons. *Nat. Neurosci.* 5: 391-392
- Adesnik H, Bruns W, Taniguchi H, Huang ZJ, Scanziani M. 2012. A neural circuit for spatial summation in visual cortex. *Nature* 490: 226-231
- Ahmed B, Anderson JC, Douglas RJ, Martin KAC, Nelson JC. 1994. Polyneuronal Innervation of Spiny Stellate Neurons in Cat Visual-Cortex. *J. Comp. Neurol.* 341: 39-49
- Albright TD. 1984. Direction and Orientation Selectivity of Neurons in Visual Area MT of the Macaque. *J. Neurophysiol.* 52: 1106-1130
- Ali AB, Thomson AM. 2008. Synaptic alpha 5 subunit-containing GABA(A) receptors mediate IPSPs elicited by dendrite-preferring cells in rat neocortex. *Cereb. Cortex* 18: 1260-1271
- Alitto HJ, Usrey WM. 2003. Corticothalamic feedback and sensory processing. *Curr. Opin. Neurobiol.* 13: 440-445
- Allman JM, Kaas JH. 1971. Representation of Visual Field in Striate and Adjoining Cortex of Owl Monkey (*Aotus-Trivirgatus*). *Brain Res.* 35: 89-95
- Alonso JM, Martinez LM. 1998. Functional connectivity between simple cells and complex cells in cat striate cortex. *Nat. Neurosci.* 1: 395-403
- Alonso JM, Usrey WM, Reid RC. 2001. Rules of connectivity between geniculate cells and simple cells in cat primary visual cortex. *J. Neurosci.* 21: 4002-4015
- Andermann ML, Kerlin AM, Roumis DK, Glickfeld LL, Reid RC. 2011. Functional Specialization of Mouse Higher Visual Cortical Areas. *Neuron* 72: 1025-1039
- Andermann ML, Ritt J, Neimark MA, Moore CI. 2004. Neural correlates of vibrissa resonance: Band-pass and somatotopic representation of high-frequency stimuli. *Neuron* 42: 451-463
- Anderson JC, Martin KAC, Picancodiniz CW. 1992. The Neurons in Layer-1 of Cat Visual-Cortex. *P Roy Soc B-Biol Sci* 248: 27-33
- Antolik J, Bednar JA. 2011. Development of maps of simple and complex cells in the primary visual cortex. *Front. Comput. Neurosci.* 5, article number 17
- Arnason U, Adegoke JA, Bodin K, Born EW, Esa YB, et al. 2002. Mammalian mitogenomic relationships and the root of the eutherian tree. *Proc. Natl. Acad. Sci. U. S. A.* 99: 8151-8156
- Ascoli GA, Alonso-Nanclares L, Anderson SA, Barrionuevo G, Benavides-Piccione R, et al. 2008. Petilla terminology: nomenclature of features of GABAergic interneurons of the cerebral cortex. *Nature Reviews Neuroscience* 9: 557-568

- Atallah BV, Bruns W, Carandini M, Scanziani M. 2012. Parvalbumin-Expressing Interneurons Linearly Transform Cortical Responses to Visual Stimuli. *Neuron* 73: 159-170
- Atencio CA, Schreiner CE. 2008. Spectrotemporal processing differences between auditory cortical fast-spiking and regular-spiking neurons. *J Neurosci* 28: 3897-3910
- Azouz R, Gray CM, Nowak LG, McCormick DA. 1997. Physiological properties of inhibitory interneurons in cat striate cortex. *Cereb. Cortex* 7: 534-545
- Bair W. 2005. Visual receptive field organization. *Curr. Opin. Neurobiol.* 15: 459-464
- Balboa RM, Grzywacz NM. 2000. Occlusions and their relationship with the distribution of contrasts in natural images. *Vision Res.* 40: 2661-2669
- Bardy C, Huang JY, Wang C, FitzGibbon T, Dreher B. 2006a. 'Simplification' of responses of complex cells in cat striate cortex: suppressive surrounds and 'feedback' inactivation. *J Physiol* 574: 731-750
- Bardy C, Huang JY, Wang C, FitzGibbon T, Dreher B. 2006b. 'Simplification' of responses of complex cells in cat striate cortex: suppressive surrounds and 'feedback' inactivation. *J. Physiol.-London* 574: 731-750
- Barlow HB. 1953. Summation and Inhibition in the Frogs Retina. *J. Physiol.-London* 119: 69-88
- Barlow HB, Levick WR. 1976. Threshold Setting by Surround of Cat Retinal Ganglion-Cells. *J. Physiol.-London* 259: 737-757
- Bartho P, Hirase H, Monconduit L, Zugaro M, Harris KD, Buzsaki G. 2004. Characterization of neocortical principal cells and Interneurons by network interactions and extracellular features. *J. Neurophysiol.* 92: 600-608
- Beaulieu C. 1993. Numerical Data on Neocortical Neurons in Adult-Rat, with Special Reference to the Gaba Population. *Brain Res.* 609: 284-292
- Benyishai R, Baror RL, Sompolsky H. 1995. Theory of Orientation Tuning in Visual-Cortex. *Proc. Natl. Acad. Sci. U. S. A.* 92: 3844-3448
- Berman AL. 1968. The brain stem of the cat. A cytoarchitectonic atlas with stereotaxic coordinates. Madison, University of Wisconsin Press.
- Berman AL, Jones EG. 1982. The thalamus and basal telencephalon of the cat, a cytoarchitectonic atlas with stereotaxic coordinates. Madison, University of Wisconsin Press.
- Berson DM, Dunn FA, Takao M. 2002. Phototransduction by retinal ganglion cells that set the circadian clock. *Science* 295: 1070-1073
- Billingsgagliar S, Chanpalay V, Palay SL. 1974. Review of Lamination in Area 17 of Visual-Cortex of Macaca-Mulatta. *J Neurocytol* 3: 619-629
- Binzegger T, Douglas RJ, Martin KAC. 2004. A quantitative map of the circuit of cat primary visual cortex. *J. Neurosci.* 24: 8441-8453

- Blakemore C, Vitalduran F. 1986. Organization and Postnatal-Development of the Monkeys Lateral Geniculate-Nucleus. *J. Physiol.-London* 380: 453-491
- Blasdel GG, Salama G. 1986. Voltage-Sensitive Dyes Reveal a Modular Organization in Monkey Striate Cortex. *Nature* 321: 579-585
- Blatow M, Rozov A, Katona I, Hormuzdi SG, Meyer AH, et al. 2003. A novel network of multipolar bursting interneurons generates theta frequency oscillations in neocortex. *Neuron* 38: 805-817
- Bock DD, Lee WC, Kerlin AM, Andermann ML, Hood G, et al. 2011. Network anatomy and in vivo physiology of visual cortical neurons. *Nature* 471: 177-182
- Bonin V, Histed MH, Yurgenson S, Reid RC. 2011. Local Diversity and Fine-Scale Organization of Receptive Fields in Mouse Visual Cortex. *J. Neurosci.* 31: 18506-18521
- Borg-Graham LJ, Monier C, Fregnac Y. 1998. Visual input evokes transient and strong shunting inhibition in visual cortical neurons. *Nature* 393: 369-373
- Bosking WH, Zhang Y, Schofield B, Fitzpatrick D. 1997. Orientation selectivity and the arrangement of horizontal connections in tree shrew striate cortex. *J. Neurosci.* 17: 2112-2127
- Brodmann K. 1909. Vergleichende Lokalisationslehre der Großhirnrinde in ihren Prinzipien dargestellt auf Grund des Zellenbaues. Barth, Leipzig.
- Bruno RM, Simons DJ. 2002. Feedforward mechanisms of excitatory and inhibitory cortical receptive fields. *J Neurosci* 22: 10966-10975
- Bullier J, Henry GH. 1979. Ordinal Position of Neurons in Cat Striate Cortex. *J. Neurophysiol.* 42: 1251-1263
- Bullier J, Henry GH. 1980. Ordinal Position and Afferent Input of Neurons in Monkey Striate Cortex. *J. Comp. Neurol.* 193: 913-935
- Burke W, Dreher B, Michalski A, Cleland BG, Rowe MH. 1992. Effects of Selective Pressure Block of Y-Type Optic-Nerve Fibers on the Receptive-Field Properties of Neurons in the Striate Cortex of the Cat. *Visual Neurosci* 9: 47-64
- Burkhalter A, Vanessen DC. 1986. Processing of Color, Form and Disparity Information in Visual Areas Vp and V2 of Ventral Extrastriate Cortex in the Macaque Monkey. *J. Neurosci.* 6: 2327-2351
- Calderone JB, Jacobs GH. 1995. Regional Variations in the Relative Sensitivity to Uv-Light in the Mouse Retina. *Visual Neurosci* 12: 463-468
- Callaway EM. 1998. Local circuits in primary visual cortex of the macaque monkey. *Annual Review of Neuroscience* 21: 47-74
- Carandini M, Ferster D. 2000. Membrane potential and firing rate in cat primary visual cortex. *The Journal of neuroscience : the official journal of the Society for Neuroscience* 20: 470-484
- Carandini M, Ringach DL. 1997. Predictions of a recurrent model of

- orientation selectivity. *Vision Res.* 37: 3061-3071
- Cardin JA, Palmer LA, Contreras D. 2007. Stimulus feature selectivity in excitatory and inhibitory neurons in primary visual cortex. *J Neurosci* 27: 10333-10344
- Casagrande VA, Kaas JH. 1994. The afferent, intrinsic, and efferent connections of primary visual cortex in primates In *Cerebral cortex, vol. 10: primary visual cortex of primates*, ed. P A., R K., pp. 201-59. New York: Plenum Press
- Cauli B, Audinat E, Lambolez B, Angulo MC, Ropert N, et al. 1997. Molecular and physiological diversity of cortical nonpyramidal cells. *J. Neurosci.* 17: 3894-3906
- Cauli B, Porter JT, Tsuzuki K, Lambolez B, Rossier J, et al. 2000. Classification of fusiform neocortical interneurons based on unsupervised clustering. *Proc. Natl. Acad. Sci. U. S. A.* 97: 6144-6149
- Caviness VS. 1975. Architectonic Map of Neocortex of Normal Mouse. *J. Comp. Neurol.* 164: 247-263
- Chance FS, Nelson SB, Abbott LF. 1999. Complex cells as cortically amplified simple cells. *Nat Neurosci* 2: 277-282
- Chapman B, Stryker MP. 1991. Development of Orientation-Specific Neuronal Responses in Ferret Primary Visual-Cortex. *Nato Adv Sci Inst Lif* 222: 375-377
- Cheng H, Chino YM, Smith EL, Hamamoto J, Yoshida K. 1995. Transfer characteristics of lateral geniculate nucleus X neurons in the cat: Effects of spatial frequency and contrast. *J. Neurophysiol.* 74: 2548-2557
- Chirimutu M, Clatworthy PL, Tolhurst DJ. 2003. Coding of the contrasts in natural images by visual cortex (V1) neurons: a Bayesian approach. *J Opt Soc Am A* 20: 1253-1260
- Chisum HJ, Fitzpatrick D. 2004. The contribution of vertical and horizontal connections to the receptive field center and surround in V1. *Neural Netw.* 17: 681-693
- Chow A, Erisir A, Farb C, Nadal MS, Ozaita A, et al. 1999. K⁺ channel expression distinguishes subpopulations of parvalbumin-and somatostatin-containing neocortical interneurons. *J. Neurosci.* 19: 9332-9345
- Chung S, Ferster D. 1998. Strength and orientation tuning of the thalamic input to simple cells revealed by electrically evoked cortical suppression. *Neuron* 20: 1177-1189
- Cloherty SL, Ibbotson MR. 2015. Contrast-dependent phase sensitivity in V1 but not V2 of macaque visual cortex. *J. Neurophysiol.* 113: 434-444
- Connors BW, Gutnick MJ. 1990. Intrinsic Firing Patterns of Diverse Neocortical Neurons. *Trends Neurosci.* 13: 99-104
- Connors BW, Kriegstein AR. 1986. Cellular Physiology of the Turtle Visual-Cortex - Distinctive Properties of Pyramidal and Stellate Neurons. *J. Neurosci.* 6: 164-177
- Contreras D, Palmer L. 2003. Response to contrast of

- electrophysiologically defined cell classes in primary visual cortex. *J. Neurosci.* 23: 6936-6945
- Cooper HM, Herbin M, Nevo E. 1993. Visual-System of a Naturally Microphthalmic Mammal - the Blind Mole Rat, *Spalax-Ehrenbergi*. *J. Comp. Neurol.* 328: 313-350
- Cossell L, Iacaruso MF, Muir DR, Houlton R, Sader EN, et al. 2015. Functional organization of excitatory synaptic strength in primary visual cortex. *Nature*. 518: 399 - 403
- Crowder NA, Hietanen MA, Price NSC, Clifford CWG, Ibbotson MR. 2008. Dynamic contrast change produces rapid gain control in visual cortex. *J. Physiol.-London* 586: 4107-4119
- Crowder NA, Price NSC, Hietanen MA, Dreher B, Clifford CWG, Ibbotson MR. 2006. Relationship between contrast adaptation and orientation tuning in V1 and V2 of cat visual cortex. *J. Neurophysiol.* 95: 271-283
- Crowder NA, van Kleef J, Dreher B, Ibbotson MR. 2007. Complex cells increase their phase sensitivity at low contrasts and following adaptation. *J Neurophysiol* 98: 1155-1166
- Dacey DM, Liao HW, Peterson BB, Robinson FR, Smith VC, et al. 2005. Melanopsin-expressing ganglion cells in primate retina signal colour and irradiance and project to the LGN. *Nature* 433: 749-754
- Daniels JD, Norman JL, Pettigrew JD. 1977. Biases for Oriented Moving Bars in Lateral Geniculate-Nucleus Neurons of Normal and Stripe-Reared Cats. *Exp. Brain Res.* 29: 155-172
- De Valois RL, Albrecht DG, Thorell LG. 1982. Spatial frequency selectivity of cells in macaque visual cortex. *Vision Res.* 22: 545-559
- Debanne D, Shulz DE, Fregnac Y. 1998. Activity-dependent regulation of 'on' and 'off' responses in cat visual cortical receptive fields. *J. Physiol.-London* 508: 523-548
- DeFelipe J. 1997. Types of neurons, synaptic connections and chemical characteristics of cells immunoreactive for calbindin-D28K, parvalbumin and calretinin in the neocortex. *J Chem Neuroanat* 14: 1-19
- DeFelipe J. 2002. Cortical interneurons: from Cajal to 2001. *Changing Views of Cajal's Neuron* 136: 215-238
- Defelipe J, Farinas I. 1992. The Pyramidal Neuron of the Cerebral-Cortex - Morphological and Chemical Characteristics of the Synaptic Inputs. *Prog Neurobiol* 39: 563-607
- DeFelipe J, Lopez-Cruz PL, Benavides-Piccione R, Bielza C, Larranaga P, et al. 2013. New insights into the classification and nomenclature of cortical GABAergic interneurons. *Nature Reviews Neuroscience* 14: 202-216
- Demeulemeester H, Arckens L, Vandesande F, Orban GA, Heizmann CW, Pochet R. 1991. Calcium-Binding Proteins and Neuropeptides as Molecular Markers of Gabaergic Interneurons in the Cat Visual-Cortex. *Exp. Brain Res.* 84: 538-544

- Denman DJ, Contreras D. 2014. The Structure of Pairwise Correlation in Mouse Primary Visual Cortex Reveals Functional Organization in the Absence of an Orientation Map. *Cereb. Cortex* 24: 2707-2020
- Derrington AM, Lennie P. 1984. Spatial and Temporal Contrast Sensitivities of Neurons in Lateral Geniculate-Nucleus of Macaque. *J. Physiol.-London* 357: 219-240
- Douglas RJ, Koch C, Mahowald M, Martin KAC, Suarez HH. 1995. Recurrent Excitation in Neocortical Circuits. *Science* 269: 981-985
- Douglas RJ, Martin KAC. 1991. A Functional Microcircuit for Cat Visual-Cortex. *J. Physiol.-London* 440: 735-769
- Drager UC. 1975. Receptive fields of single cells and topography in mouse visual cortex. *The Journal of comparative neurology* 160: 269-290
- Durand JB, Girard P, Barone P, Bullier J, Nowak LG. 2012. Effects of contrast and contrast adaptation on static receptive field features in macaque area V1. *J. Neurophysiol.* 108: 2033-2050
- Elston GN, Pow DV, Calford MB. 1997. Neuronal composition and morphology in layer IV of two vibrissal barrel subfields of rat cortex. *Cereb. Cortex* 7: 422-431
- Erisir A, Lau D, Rudy B, Leonard CS. 1999. Function of specific K⁺ channels in sustained high-frequency firing of fast-spiking neocortical interneurons. *J. Neurophysiol.* 82: 2476-2489
- Felleman DJ, Van Essen DC. 1991. Distributed Hierarchical Processing in the Primate Cerebral Cortex. *Cereb. Cortex* 1: 1-47
- Ferster D. 1988. Spatially Opponent Excitation and Inhibition in Simple Cells of the Cat Visual-Cortex. *J. Neurosci.* 8: 1172-1180
- Ferster D. 1990a. X-Mediated and Y-Mediated Current Sources in Area-17 and Area-18 of Cat Visual-Cortex. *Visual Neurosci* 4: 135-145
- Ferster D. 1990b. X-Mediated and Y-Mediated Synaptic Potentials in Neurons of Area-17 and Area-18 of Cat Visual-Cortex. *Visual Neurosci* 4: 115-133
- Ferster D, Chung S, Wheat H. 1996. Orientation selectivity of thalamic input to simple cells of cat visual cortex. *Nature* 380: 249-252
- Ferster D, Lindstrom S. 1983. An Intracellular Analysis of Geniculo-Cortical Connectivity in Area 17 of the Cat. *J. Physiol.-London* 342: 181-215
- Field GD, Chichilnisky EJ. 2007. Information processing in the primate retina: Circuitry and coding. *Annual Review of Neuroscience* 30: 1-30
- Fitzpatrick D. 1996. The functional organization of local circuits in visual cortex: Insights from the study of tree shrew striate cortex. *Cereb. Cortex* 6: 329-341
- Foldy C, Aradi I, Howard A, Soltesz I. 2004. Diversity beyond variance: modulation of firing rates and network coherence by GABAergic subpopulations. *European Journal of Neuroscience* 19: 119-130

- Foster KH, Gaska JP, Nagler M, Pollen DA. 1985. Spatial and Temporal Frequency-Selectivity of Neurons in Visual Cortical Areas V1 and V2 of the Macaque Monkey. *J. Physiol.-London* 365: 331-363
- Fritsches KA, Rosa MGP. 1996. Visuotopic organisation of striate cortex in the marmoset monkey (*Callithrix jacchus*). *J. Comp. Neurol.* 372: 264-282
- Fu Y, Tucciarone JM, Espinosa JS, Sheng NY, Darcy DP, et al. 2014. A Cortical Circuit for Gain Control by Behavioral State. *Cell* 156: 1139-1152
- Gao E, DeAngelis GC, Burkhalter A. 2010. Parallel input channels to mouse primary visual cortex. *The Journal of neuroscience : the official journal of the Society for Neuroscience* 30: 5912-5926
- Gil Z, Connors BW, Amitai Y. 1999. Efficacy of thalamocortical and intracortical synaptic connections: Quanta, innervation, and reliability. *Neuron* 23: 385-397
- Gilbert CD. 1977. Laminar Differences in Receptive-Field Properties of Cells in Cat Primary Visual-Cortex. *J. Physiol.-London* 268: 391-421
- Gilbert CD, Wiesel TN. 1979. Morphology and Intracortical Projections of Functionally Characterized Neurons in the Cat Visual-cortex *Nature* 280: 120-125
- Gilbert CD, Wiesel TN. 1989. Columnar Specificity of Intrinsic Horizontal and Corticocortical Connections in Cat Visual-Cortex. *J. Neurosci.* 9: 2432-2442
- Girman SV, Sauve Y, Lund RD. 1999. Receptive field properties of single neurons in rat primary visual cortex. *J Neurophysiol* 82: 301-311
- Gold C, Henze DA, Koch C, Buzsaki G. 2006. On the origin of the extracellular action potential waveform: A modeling study. *J. Neurophysiol.* 95: 3113-3128
- Gonchar Y, Burkhalter A. 1997. Three distinct families of GABAergic neurons in rat visual cortex. *Cereb. Cortex* 7: 347-358
- Gonzalez-Burgos G, Krimer LS, Povysheva NV, Barrionuevo G, Lewis DA. 2005. Functional properties of fast spiking interneurons and their synaptic connections with pyramidal cells in primate dorsolateral prefrontal cortex. *J. Neurophysiol.* 93: 942-953
- Gray CM, McCormick DA. 1996. Chattering cells: Superficial pyramidal neurons contributing to the generation of synchronous oscillations in the visual cortex. *Science* 274: 109-113
- Griffen TC, Maffei A. 2014. GABAergic synapses: their plasticity and role in sensory cortex. *Front Cell Neurosci* 8: article number 91
- Grubb MS, Thompson ID. 2003. Quantitative characterization of visual response properties in the mouse dorsal lateral geniculate nucleus. *J. Neurophysiol.* 90: 3594-3607
- Gupta A, Wang Y, Markram H. 2000. Organizing principles for a diversity of GABAergic interneurons and synapses in the neocortex. *Science* 287: 273-278

- Haider B, Krause MR, Duque A, Yu YG, Tournyan J, et al. 2010. Synaptic and Network Mechanisms of Sparse and Reliable Visual Cortical Activity during Nonclassical Receptive Field Stimulation. *Neuron* 65: 107-121
- Hammond P, Ahmed B. 1985. Length Summation of Complex Cells in Cat Striate Cortex - a Reappraisal of the Special Standard Classification. *Neuroscience* 15: 639-649
- Hammond P, Mackay DM. 1975. Response of Cat Visual Cortical-Cells to Kinetic Contours and Static Noise. *J. Physiol.-London* 252: 43-44
- Hammond P, Mackay DM. 1977. Differential Responsiveness of Simple and Complex Cells in Cat Striate Cortex to Visual Texture. *Exp. Brain Res.* 30: 275-296
- Han ZS. 1994. Electrophysiological and Morphological-Differentiation of Chandelier and Basket Cells in the Rat Hippocampal-Formation - a Study Combining Intracellular-Recording and Intracellular Staining with Biocytin. *Neurosci Res* 19: 101-110
- Harris KD, Mrsic-Flogel TD. 2013. Cortical connectivity and sensory coding. *Nature* 503: 51-58
- Harting JK, Huerta MF. 1983. The Geniculostriate Projection in the Grey Squirrel - Preliminary Autoradiographic Data. *Brain Res.* 272: 341-349
- Hartline HK. 1938. The Response of Single Optic Nerve Fibers of the Vertebrate Eye to Illumination of the Retina. *Am J Physiol* 121: 400-415
- Hasenstaub A, Shu Y, Haider B, Kraushaar U, Duque A, McCormick DA. 2005. Inhibitory postsynaptic potentials carry synchronized frequency information in active cortical networks. *Neuron* 47: 423-435
- Hasenstaub AR, Callaway EM. 2010. Paint It Black (or Red, or Green): Optical and Genetic Tools Illuminate Inhibitory Contributions to Cortical Circuit Function. *Neuron* 67: 681-684
- Haverkamp S, Wassle H, Duebel J, Kuner T, Augustine GJ, et al. 2005. The primordial, blue-cone color system of the mouse retina. *J. Neurosci.* 25: 5438-5445
- Hendry SHC, Reid RC. 2000. The koniocellular pathway in primate vision. *Annual Review of Neuroscience* 23: 127-153
- Henry CA, Hawken MJ. 2013. Stability of simple/complex classification with contrast and extraclassical receptive field modulation in macaque V1. *J. Neurophysiol.* 109: 1793-1803
- Henry GH. 1977. Receptive-Field Classes of Cells in Striate Cortex of Cat *Brain Res.* 133: 1-28
- Henze DA. 2000. Hippocampal sharp waves and associated high frequency ripple oscillations. *J. Physiol.-London* 523: 83-84
- Henze DA, Borhegyi Z, Csicsvari J, Mamiya A, Harris KD, Buzsaki G. 2000. Intracellular features predicted by extracellular recordings in the hippocampus in vivo. *J. Neurophysiol.* 84: 390-400
- Hestrin S, Armstrong WE. 1996. Morphology and physiology of

- cortical neurons in layer I. *J. Neurosci.* 16: 5290-5300
- Hietanen MA, Cloherty SL, van Kleef JP, Wang C, Dreher B, Ibbotson MR. 2013. Phase Sensitivity of Complex Cells in Primary Visual Cortex. *Neuroscience* 237: 19-28
- Hirsch JA. 2003. Synaptic physiology and receptive field structure in the early visual pathway of the cat. *Cereb Cortex* 13: 63-69
- Hirsch JA, Alonso JM, Reid RC, Martinez LM. 1998a. Synaptic integration in striate cortical simple cells. *The Journal of neuroscience : the official journal of the Society for Neuroscience* 18: 9517-9528
- Hirsch JA, Gallagher CA, Alonso JM, Martinez LM. 1998b. Ascending projections of simple and complex cells in layer 6 of the cat striate cortex. *The Journal of neuroscience : the official journal of the Society for Neuroscience* 18: 8086-801394
- Hirsch JA, Martinez LM. 2006. Circuits that build visual cortical receptive fields. *Trends Neurosci.* 29: 30-39
- Hirsch JA, Martinez LM, Pillai C, Alonso JM, Wang QB, Sommer FT. 2003. Functionally distinct inhibitory neurons at the first stage of visual cortical processing. *Nat. Neurosci.* 6: 1300-08
- Hofer SB, Ko H, Pichler B, Vogelstein J, Ros H, et al. 2011. Differential connectivity and response dynamics of excitatory and inhibitory neurons in visual cortex. *Nat. Neurosci.* 14: 1045-1146
- Hoffmann KP, Stone J. 1971. Conduction Velocity of Afferents to Cat Visual Cortex - Correlation with Cortical Receptive Field Properties. *Brain Res.* 32: 460-471
- Holdefer RN, Norton TT. 1995. Laminar Organization of Receptive-Field Properties in the Dorsal Lateral Geniculate-Nucleus of the Tree Shrew (*Tupaia glis-Belangeri*). *J. Comp. Neurol.* 358: 401-413
- Hu H, Gan J, Jonas P. 2014. Fast-spiking, parvalbumin(+) GABAergic interneurons: From cellular design to microcircuit function. *Science* 345: 529-536
- Hubel DH, Wiesel TN. 1959. Receptive fields of single neurones in the cat's striate cortex. *The Journal of physiology* 148: 574-591
- Hubel DH, Wiesel TN. 1961. Integrative Action in Cats Lateral Geniculate Body. *J. Physiol.-London* 155: 385-398
- Hubel DH, Wiesel TN. 1962. Receptive fields, binocular interaction and functional architecture in the cat's visual cortex. *The Journal of physiology* 160: 106-154
- Hubel DH, Wiesel TN. 1963. Shape and Arrangement of Columns in Cats Striate Cortex. *J. Physiol.-London* 165: 559-568
- Hubel DH, Wiesel TN. 1965. Receptive Fields and Functional Archichitecture in 2 Nonstriate Visual Areas (18 and 19) of Cat. *J. Neurophysiol.* 28: 229-289
- Hubel DH, Wiesel TN. 1968. Receptive fields and functional architecture of monkey striate cortex. *The Journal of physiology* 195: 215-243

- Hubel DH, Wiesel TN. 1977. Functional Architecture of Macaque Monkey Visual-Cortex. *Proc R Soc Ser B-Bio* 198, No. 1130: 1-59
- Huberman AD, Manu M, Koch SM, Susman MW, Lutz AB, et al. 2008. Architecture and activity-mediated refinement of axonal projections from a mosaic of genetically identified retinal ganglion cells. *Neuron* 59: 425-438
- Huberman AD, Niell CM. 2011. What can mice tell us about how vision works? *Trends Neurosci.* 34: 464-473
- Huberman AD, Wei W, Elstrott J, Stafford BK, Feller MB, Barres BA. 2009. Genetic Identification of an On-Off Direction-Selective Retinal Ganglion Cell Subtype Reveals a Layer-Specific Subcortical Map of Posterior Motion. *Neuron* 62: 327-334
- Humphrey AL, Sur M, Uhlrich DJ, Sherman SM. 1985. Projection Patterns of Individual X-Cell and Y-Cell Axons from the Lateral Geniculate-Nucleus to Cortical Area-17 in the Cat. *J. Comp. Neurol.* 233: 159-189
- Hurley JB. 1994. Termination of photoreceptor responses. *Curr. Opin. Neurobiol.* 4: 481-487
- Isaacson JS, Scanziani M. 2011. How Inhibition Shapes Cortical Activity. *Neuron* 72: 231-243
- Jeon CJ, Strettoi E, Masland RH. 1998. The major cell populations of the mouse retina. *The Journal of neuroscience : the official journal of the Society for Neuroscience* 18: 8936-8946
- Jin JZ, Wang YS, Swadlow HA, Alonso JM. 2011. Population receptive fields of ON and OFF thalamic inputs to an orientation column in visual cortex. *Nat. Neurosci.* 14: 232-233
- Jones EG. 1984. Cellular Components of the Cerebral Cortex. pp. 521-554. Plenum, New York.
- Jones EG, Wise SP. 1977. Size, Laminar and Columnar Distribution of Efferent Cells in Sensory-Motor Cortex of Monkeys. *J. Comp. Neurol.* 175: 391-437
- Kaas JH. 1997. Topographic maps are fundamental to sensory processing. *Brain Res Bull* 44: 107-112
- Kagan I, Gur M, Snodderly DM. 2002. Spatial organization of receptive fields of V1 neurons of alert monkeys: Comparison with responses to gratings. *J. Neurophysiol.* 88: 2557-2574
- Kapadia MK, Westheimer G, Gilbert CD. 1999. Dynamics of spatial summation in primary visual cortex of alert monkeys. *Proc. Natl. Acad. Sci. U. S. A.* 96: 12073-12078
- Kaplan E, Shapley RM. 1982. X-Cell and Y-Cell in the Lateral Geniculate-Nucleus of Macaque Monkeys. *J. Physiol.-London* 330: 125-143
- Karagiannis A, Gallopin T, David C, Battaglia D, Geoffroy H, et al. 2009. Classification of NPY-Expressing Neocortical Interneurons. *J. Neurosci.* 29: 3642-3659
- Kawaguchi Y. 1995. Physiological Subgroups of Nonpyramidal Cells with Specific Morphological-Characteristics in Layer II/III of Rat

- Frontal-Cortex. *J. Neurosci.* 15: 2638-2655
- Kawaguchi Y, Kondo S. 2002. Parvalbumin, somatostatin and cholecystokinin as chemical markers for specific GABAergic interneuron types in the rat frontal cortex. *J. Neurocytol* 31: 277-287
- Kawaguchi Y, Kubota Y. 1993. Correlation of Physiological Subgroupings of Nonpyramidal Cells with Parvalbumin-Immunoreactive and Calbindin(D28k)-Immunoreactive Neurons in Layer-V of Rat Frontal-Cortex. *J. Neurophysiol.* 70: 387-396
- Kawaguchi Y, Kubota Y. 1997. GABAergic cell subtypes and their synaptic connections in rat frontal cortex. *Cereb. Cortex* 7: 476-486
- Kawaguchi Y, Kubota Y. 1998. Neurochemical features and synaptic connections of large physiologically-identified GABAergic cells in the rat frontal cortex. *Neuroscience* 85: 677-701
- Kawamura K, Naito J. 1978. Variations of the Dog Cerebral Sulci, Compared in Particular with Those of the Cat. *J Hirnforsch* 19: 457-467
- Kay JN, De la Huerta I, Kim IJ, Zhang YF, Yamagata M, et al. 2011. Retinal Ganglion Cells with Distinct Directional Preferences Differ in Molecular Identity, Structure, and Central Projections. *J. Neurosci.* 31: 7753-7762
- Kelly JP, Vanessen DC. 1974. Cell Structure and Function in Visual-Cortex of Cat. *J. Physiol.-London* 238: 515-521
- Kerlin AM, Andermann ML, Berezovskii VK, Reid RC. 2010. Broadly tuned response properties of diverse inhibitory neuron subtypes in mouse visual cortex. *Neuron* 67: 858-871
- Kim IJ, Zhang YF, Yamagata M, Meister M, Sanes JR. 2008. Molecular identification of a retinal cell type that responds to upward motion. *Nature* 452: 478-482
- Kisvarday ZF, Martin KAC, Freund TF, Magloczky Z, Whitteridge D, Somogyi P. 1986. Synaptic Targets of Hrp-Filled Layer-Iii Pyramidal Cells in the Cat Striate Cortex. *Exp. Brain Res.* 64: 541-552
- Krimer LS, Zaitsev AV, Czanner G, Kroner S, Gonzalez-Burgos G, et al. 2005. Cluster analysis-based physiological classification and morphological properties of inhibitory neurons in layers 2-3 of monkey dorsolateral prefrontal cortex. *J. Neurophysiol.* 94: 3009-3022
- Krubitzer L, Kaas J. 2005. The evolution of the neocortex in mammals: how is phenotypic diversity generated? *Curr. Opin. Neurobiol.* 15: 444-453
- Kuffler SW. 1953. Discharge Patterns and Functional Organization of Mammalian Retina. *J. Neurophysiol.* 16: 37-68
- Lagnado L, Baylor D. 1992. Signal Flow in Visual Transduction. *Neuron* 8: 995-1002
- Lee C, Weyand TG, Malpeli JG. 1998. Thalamic control of cat area-18 supragranular layers: Simple cells, complex cells, and cells projecting to

- the lateral suprasylvian visual area. *Visual Neurosci* 15: 27-35
- Lee S, Hjerling-Leffler J, Zagha E, Fishell G, Rudy B. 2010. The Largest Group of Superficial Neocortical GABAergic Interneurons Expresses Ionotropic Serotonin Receptors. *J. Neurosci.* 30: 16796-16808
- Lee SH, Land PW, Simons DJ. 2007. Layer- and cell-type-specific effects of neonatal whisker-trimming in adult rat barrel cortex. *J. Neurophysiol.* 97: 4380-4385
- Levay S, Gilbert CD. 1976. Laminar Patterns of Geniculocortical Projection in Cat. *Brain Res.* 113: 1-19
- Leventhal AG. 1979a. Evidence That the Different Classes of Relay Cells of the Cats Lateral Geniculate-Nucleus Terminate in Different Layers of the Striate Cortex. *Exp. Brain Res.* 37: 349-372
- Leventhal AG. 1979b. Evidence That W, X, and Y Cells of the Cats Lateral Geniculate-Nucleus Terminate in Different Layers of the Striate Cortex. *Invest Ophthalmol Vis Sci*: 156-157
- Levitt JB, Lund JS. 1997. Contrast dependence of contextual effects in primate visual cortex. *Nature* 387: 73-76
- Levitt JB, Schumer RA, Sherman SM, Spear PD, Movshon JA. 2001. Visual response properties of neurons in the LGN of normally reared and visually deprived macaque monkeys. *J. Neurophysiol.* 85: 2111-2129
- Li YT, Ibrahim LA, Liu BH, Zhang LI, Tao HW. 2013. Linear transformation of thalamocortical input by intracortical excitation. *Nat. Neurosci.* 16: 1324-1330
- Lien AD, Scanziani M. 2013. Tuned thalamic excitation is amplified by visual cortical circuits. *Nat. Neurosci.* 16: 1315-1323
- Ling CY, Schneider GE, Jhaveri S. 1998. Target-specific morphology of retinal axon arbors in the adult hamster. *Visual Neurosci* 15: 559-579
- Liu BH, Li P, Li YT, Sun YJ, Yanagawa Y, et al. 2009. Visual receptive field structure of cortical inhibitory neurons revealed by two-photon imaging guided recording. *J Neurosci* 29: 10520-10532
- Liu BH, Li P, Sun YJ, Li YT, Zhang LI, Tao HW. 2010. Intervening inhibition underlies simple-cell receptive field structure in visual cortex. *Nat Neurosci* 13: 89-96
- Livingstone MS, Hubel DH. 1983. Specificity of Cortico-Cortical Connections in Monkey Visual-System. *Nature* 304: 531-534
- Luck SJ, Chelazzi L, Hillyard SA, Desimone R. 1997. Neural mechanisms of spatial selective attention in areas V1, V2, and V4 of macaque visual cortex. *J. Neurophysiol.* 77: 24-42
- Lund JS. 1973. Organization of Neurons in Visual-Cortex, Area 17, of Monkey (Macaca-Mulatta). *J. Comp. Neurol.* 147: 455-495
- Luo L, Callaway EM, Svoboda K. 2008. Genetic dissection of neural circuits. *Neuron* 57: 634-660
- Ma WP, Liu BH, Li YT, Huang ZJ, Zhang LI, Tao HZW. 2010. Visual

- Representations by Cortical Somatostatin Inhibitory Neurons- Selective But with Weak and Delayed Responses. *J. Neurosci.* 30: 14371-14379
- Maffei L, Fiorenti A. 1973. Visual-Cortex as a Spatial Frequency Analyzer. *Vision Res.* 13: 1255-1267
- Malach R. 1989. Patterns of Connections in Rat Visual-Cortex. *J. Neurosci.* 9: 3741-3752
- Malpeli JG. 1983. Activity of Cells in Area-17 of the Cat in Absence of Input from Layer-a of Lateral Geniculate-Nucleus. *J. Neurophysiol.* 49: 595-610
- Mangini NJ, Pearlman AL. 1980a. Laminar distribution of receptive field properties in the primary visual cortex of the mouse. *The Journal of comparative neurology* 193: 203-222
- Mangini NJ, Pearlman AL. 1980b. Laminar Distribution of Receptive-Field Properties in the Primary Visual-Cortex of the Mouse. *J. Comp. Neurol.* 193: 203-222
- Margrie TW, Brecht M, Sakmann B. 2002. In vivo, low-resistance, whole-cell recordings from neurons in the anaesthetized and awake mammalian brain. *Pflugers Arch* 444: 491-498
- Markram H, Toledo-Rodriguez M, Wang Y, Gupta A, Silberberg G, Wu C. 2004. Interneurons of the neocortical inhibitory system. *Nat Rev Neurosci* 5: 793-807
- Martin KAC, Whitteridge D. 1984a. Form, Function and Intracortical Projections of Spiny Neurons in the Striate Visual-Cortex of the Cat. *J. Physiol.-London* 353: 463-504
- Martin KAC, Whitteridge D. 1984b. The Relationship of Receptive-Field Properties to the Dendritic Shape of Neurons in the Cat Striate Cortex. *J. Physiol.-London* 356: 291-302
- Martina M, Jonas P. 1997. Functional differences in Na⁺ channel gating between fast-spiking interneurones and principal neurones of rat hippocampus. *J. Physiol.-London* 505: 593-603
- Martina M, Schultz JH, Ehmke H, Monyer H, Jonas P. 1998. Functional and molecular differences between voltage-gated K⁺ channels of fast-spiking interneurons and pyramidal neurons of rat hippocampus. *J. Neurosci.* 18: 8111-8125
- Martinez LM. 2006. The generation of receptive-field structure in cat primary visual cortex. *Visual Perception, Part 1, Fundamentals of Vision: Low and Mid-Level Processes in Perception* 154: 73-92
- Martinez LM, Alonso JM. 2001. Construction of complex receptive fields in cat primary visual cortex. *Neuron* 32: 515-525
- Martinez LM, Alonso JM. 2003. Complex receptive fields in primary visual cortex. *Neuroscientist* 9: 317-331
- Martinez LM, Alonso JM, Reid RC, Hirsch JA. 2002. Laminar processing of stimulus orientation in cat visual cortex. *J. Physiol.-London* 540: 321-333
- Martinez LM, Wang Q, Reid RC, Pillai C, Alonso JM, et al. 2005. Receptive field structure varies with layer in the primary visual cortex. *Nat. Neurosci.* 8: 372-379

- Maruko I, Zhang B, Tao X, Tong J, Smith EL, Chino YM. 2008. Postnatal Development of Disparity Sensitivity in Visual Area 2 (V2) of Macaque Monkeys. *J. Neurophysiol.* 100: 2486-2495
- Masland RH. 2001. The fundamental plan of the retina. *Nat. Neurosci.* 4: 877-886
- Mata ML, Ringach DL. 2005. Spatial overlap of ON and OFF subregions and its relation to response modulation ratio in macaque primary visual cortex. *J. Neurophysiol.* 93: 919-928
- McAdams CJ, Reid RC. 2005. Attention modulates the responses of simple cells in monkey primary visual cortex. *J. Neurosci.* 25: 11023-11033
- McCormick DA, Connors BW, Lighthall JW, Prince DA. 1985. Comparative electrophysiology of pyramidal and sparsely spiny stellate neurons of the neocortex. *J. Neurophysiol.* 54: 782-806
- Mechler F, Reich DS, Victor JD. 2002. Detection and discrimination of relative spatial phase by V1 neurons. *J. Neurosci.* 22: 6129-6157
- Mechler F, Ringach DL. 2002. On the classification of simple and complex cells. *Vision Res* 42: 1017-1033
- Meffin H, Hietanen MA, Cloherty SL, Ibbotson MR. in press. Spatial phase selectivity of complex cells is contrast dependent in primary visual cortex. *in press*
- Meinecke DL, Peters A. 1987. Gaba Immunoreactive Neurons in Rat Visual-Cortex. *J. Comp. Neurol.* 261: 388-404
- Mel BW, Ruderman DL, Archie KA. 1998. Translation-invariant orientation tuning in visual "complex" cells could derive from intradendritic computations. *J. Neurosci.* 18: 4325-4334
- Metin C, Godement P, Imbert M. 1988a. The primary visual cortex in the mouse: receptive field properties and functional organization. *Exp Brain Res* 69: 594-612
- Metin C, Godement P, Imbert M. 1988b. The Primary Visual-Cortex in the Mouse - Receptive-Field Properties and Functional-Organization. *Exp. Brain Res.* 69: 594-612
- Mignard M, Malpeli JG. 1991. Paths of Information-Flow through Visual-Cortex. *Science* 251: 1249-1251
- Mitchell JF, Sundberg KA, Reynolds JH. 2007. Differential attention-dependent response modulation across cell classes in macaque visual area V4. *Neuron* 55: 131-141
- Montero VM. 1993. Retinotopy of Cortical Connections Between the Striate Cortex and Extrastriate visual areas in the Rat *Exp. Brain Res.* 94: 1-15
- Mountcastle VB, Talbot WH, Sakata H, Hyvarine. 1969. Cortical Neuronal Mechanisms in Flutter-Vibration Studied in Unanesthetized Monkeys . Neuronal Periodicity and Frequency Discrimination. *J. Neurophysiol.* 32: 452-484
- Movshon JA, Thompson ID, Tolhurst DJ. 1978a. Receptive field organization of complex cells in the cat's striate cortex. *The Journal of physiology* 283: 79-99

- Movshon JA, Thompson ID, Tolhurst DJ. 1978b. Spatial summation in the receptive fields of simple cells in the cat's striate cortex. *The Journal of physiology* 283: 53-77
- Munch TA, da Silveira RA, Siegert S, Viney TJ, Awatramani GB, Roska B. 2009. Approach sensitivity in the retina processed by a multifunctional neural circuit. *Nat. Neurosci.* 12: 1308-1316
- Nelson S, Toth L, Sheth B, Sur M. 1994a. Orientation selectivity of cortical neurons during intracellular blockade of inhibition. *Science* 265: 774-777
- Nelson S, Toth L, Sheth B, Sur M. 1994b. Orientation Selectivity of Cortical-Neurons during Intracellular Blockade of Inhibition. *Science* 265: 774-777
- Niell CM, Stryker MP. 2008. Highly selective receptive fields in mouse visual cortex. *J Neurosci* 28: 7520-7536
- Niell CM, Stryker MP. 2010. Modulation of visual responses by behavioral state in mouse visual cortex. *Neuron* 65: 472-479
- Nienborg H, Hasenstaub A, Nauhaus I, Taniguchi H, Huang ZJ, Callaway EM. 2013. Contrast Dependence and Differential Contributions from Somatostatin- and Parvalbumin-Expressing Neurons to Spatial Integration in Mouse V1. *J. Neurosci.* 33: 11145-11154
- Nowak LG, Azouz R, Sanchez-Vives MV, Gray CM, McCormick DA. 2003. Electrophysiological classes of cat primary visual cortical neurons in vivo as revealed by quantitative analyses. *J Neurophysiol* 89: 1541-1566
- Nowak LG, Sanchez-Vives MV, McCormick DA. 2008. Lack of orientation and direction selectivity in a subgroup of fast-spiking inhibitory interneurons: cellular and synaptic mechanisms and comparison with other electrophysiological cell types. *Cereb Cortex* 18: 1058-1078
- Obrien DF. 1982. The Chemistry of Vision. *Science* 218: 961-966
- Ohki K, Chung S, Ch'ng YH, Kara P, Reid RC. 2005. Functional imaging with cellular resolution reveals precise micro-architecture in visual cortex. *Nature* 433: 597-603
- Ohzawa I, Sclar G, Freeman RD. 1985. Contrast Gain-Control in the Cat's Visual-System. *J. Neurophysiol.* 54: 651-667
- Payne BR, Peters A. 2002. The cat primary visual cortex. Boston University School of Medicine.
- Peter A. 1994. The organisation of the primary vision cortex in the macaque. In *Cerebral cortex, volume 10, Primary vision cortex in primates*, ed. A Peters, KS Rockland, pp. 1-35. New York: Plenum Press
- Peters A, Payne BR. 1993. Numerical Relationships between Geniculocortical Afferents and Pyramidal Cell Modules in Cat Primary Visual-Cortex. *Cereb. Cortex* 3: 69-78
- Peters A, Sethares C. 1991. Organization of Pyramidal Neurons in Area-17 of Monkey Visual-Cortex. *J. Comp. Neurol.* 306: 1-23

- Polack PO, Contreras D. 2012. Long-Range Parallel Processing and Local Recurrent Activity in the Visual Cortex of the Mouse. *J. Neurosci.* 32: 11120-11131
- Porter JT, Cauli B, Staiger JF, Lambolez B, Rossier J, Audinat E. 1998. Properties of bipolar VIPergic interneurons and their excitation by pyramidal neurons in the rat neocortex. *European Journal of Neuroscience* 10: 3617-3628
- Pouille F, Marin-Burgin A, Adesnik H, Atallah BV, Scanziani M. 2009. Input normalization by global feedforward inhibition expands cortical dynamic range. *Nat. Neurosci.* 12: 1577-1585
- Povysheva NV, Zaitsev AV, Rotaru DC, Gonzalez-Burgos G, Lewis DA, Krimer LS. 2008. Parvalbumin-positive basket interneurons in monkey and rat prefrontal cortex. *J. Neurophysiol.* 100: 2348-2360
- Price DJ, Morgan JE. 1987. Spatial Properties of Neurons in the Lateral Geniculate-Nucleus of the Pigmented Ferret. *Exp. Brain Res.* 68: 28-36
- Priebe NJ, Mechler F, Carandini M, Ferster D. 2004. The contribution of spike threshold to the dichotomy of cortical simple and complex cells. *Nat Neurosci* 7: 1113-1122
- Provencio I, Rodriguez IR, Jiang GS, Hayes WP, Moreira EF, Rollag MD. 2000. A novel human opsin in the inner retina. *J. Neurosci.* 20: 600-605
- Prusky GT, Douglas RM. 2004. Characterization of mouse cortical spatial vision. *Vision Res.* 44: 3411-3418
- Reich DS, Mechler F, Victor JD. 2001. Formal and attribute-specific information in primary visual cortex. *J. Neurophysiol.* 85: 305-318
- Reid RC, Alonso JM. 1995. Specificity of Monosynaptic Connections from Thalamus to Visual-Cortex. *Nature* 378: 281-284
- Remtulla S, Hallett PE. 1985. A Schematic Eye for the Mouse, and Comparisons with the Rat. *Vision Res.* 25: 21-31
- Ringach DL. 2002. Spatial structure and symmetry of simple-cell receptive fields in macaque primary visual cortex. *J. Neurophysiol.* 88: 455-463
- Ringach DL, Shapley RM, Hawken MJ. 2002. Orientation selectivity in macaque V1: Diversity and Laminar dependence. *J. Neurosci.* 22: 5639-5651
- Rivadulla C, Sharma J, Sur M. 2001. Specific roles of NMDA and AMPA receptors in direction-selective and spatial phase-selective responses in visual cortex. *J Neurosci* 21: 1710-1719
- Rivlin-Etzion M, Zhou KL, Wei W, Elstrott J, Nguyen PL, et al. 2011. Transgenic Mice Reveal Unexpected Diversity of On-Off Direction-Selective Retinal Ganglion Cell Subtypes and Brain Structures Involved in Motion Processing. *J. Neurosci.* 31: 8760-8769
- Rockland KS, Pandya DN. 1979. Laminar Origins and Terminations of Cortical Connections of the Occipital Lobe in the Rhesus-Monkey. *Brain Res.* 179: 3-20
- Rollag MD, Berson DM, Provencio I. 2003. Melanopsin, ganglion-cell photoreceptors,, and mammalian

- photoentrainment. *J Biol Rhythms* 18: 227-234
- Romo PA, Wang C, Zeater N, Solomon SG, Dreher B. 2011. Phase sensitivities, excitatory summation fields, and silent suppressive receptive fields of single neurons in the parastriate cortex of the cat. *J. Neurophysiol.* 106: 1688-1712
- Rosa MGP, Fritsches KA, Elston GN. 1997. The second visual area in the marmoset monkey: Visuotopic organisation, magnification factors, architectonical boundaries, and modularity. *J. Comp. Neurol.* 387: 547-567
- Rosa MGP, Krubitzer LA. 1999. The evolution of visual cortex: where is V2? *Trends Neurosci.* 22: 242-248
- Rosa MGP, Schmid LM, Pettigrew JD. 1994. Organization of the 2nd Visual Area in the Megachiropteran Bat Pteropus. *Cereb. Cortex* 4: 52-68
- Rosa MGP, Sousa APB, Gattass R. 1988. Representation of the Visual-Field in the 2nd Visual Area in the Cebus Monkey. *J. Comp. Neurol.* 275: 326-345
- Roth MM, Helmchen F, Kampa BM. 2012. Distinct Functional Properties of Primary and Posteromedial Visual Area of Mouse Neocortex. *J. Neurosci.* 32: 9716-9726
- Ruderman DL, Bialek W. 1994. Statistics of Natural Images - Scaling in the Woods. *Phys Rev Lett* 73: 814-817
- Rudy B, Fishell G, Lee S, Hjerling-Leffler J. 2011. Three Groups of Interneurons Account for Nearly 100% of Neocortical GABAergic Neurons. *Dev Neurobiol* 71: 45-61
- Runyan CA, Schummers J, Van Wart A, Kuhlman SJ, Wilson NR, et al. 2010. Response Features of Parvalbumin-Expressing Interneurons Suggest Precise Roles for Subtypes of Inhibition in Visual Cortex. *Neuron* 67: 847-857
- Runyan CA, Schummers J, Van Wart A, Kuhlman SJ, Wilson NR, et al. 2011. Response features of parvalbumin-expressing interneurons suggest precise roles for subtypes of inhibition in visual cortex. *Neuron* 67: 847-857
- Runyan CA, Sur M. 2013. Response Selectivity Is Correlated to Dendritic Structure in Parvalbumin-Expressing Inhibitory Neurons in Visual Cortex. *J. Neurosci.* 33: 11724-11733
- Sanderso KJ. 1971. Projection of Visual Field to Lateral Geniculate and Medial Interlaminar Nuclei in Cat. *J. Comp. Neurol.* 143: 101-118
- Sceniak MP, Ringach DL, Hawken MJ, Shapley R. 1999. Contrast's effect on spatial summation by macaque V1 neurons. *Nat. Neurosci.* 2: 733-739
- Schneider T, Zrenner E. 1986. The influence of phosphodiesterase inhibitors on ERG and optic nerve response of the cat. *Invest Ophthalmol Vis Sci* 27: 1395-1403
- Schuett S, Bonhoeffer T, Hubener M. 2002a. Mapping retinotopic structure in mouse visual cortex with optical imaging. *The Journal of neuroscience : the official journal of the Society for Neuroscience* 22: 6549-6559
- Schuett S, Bonhoeffer T, Hubener M. 2002b. Mapping retinotopic structure in mouse visual cortex

- with optical imaging. *J. Neurosci.* 22: 6549-6559
- Schwarz HD, Li JY. 2000. Distribution of neurons immunoreactive for calcium-binding proteins varies across areas of cat primary somatosensory cortex. *Brain Res Bull* 51: 379-385
- Sclar G, Freeman RD. 1982. Orientation Selectivity in the Cats Striate Cortex Is Invariant with Stimulus Contrast. *Exp. Brain Res.* 46: 457-461
- Shapley R, Hochstein S. 1975. Visual Spatial Summation in 2 Classes of Geniculate Cells. *Nature* 256: 411-413
- Shapley R, Perry VH. 1986. Cat and Monkey Retinal Ganglion-Cells and Their Visual Functional Roles. *Trends Neurosci.* 9: 229-235
- Sherman SM, Wilson JR, Kaas JH, Webb SV. 1976. X-Cell and Y-Cell in Dorsal Lateral Geniculate-Nucleus of Owl Monkey (*Aotus-Trivirgatus*). *Science* 192: 475-477
- Shultz D, Debanne D, Fregnac Y. 1993. Cortical Convergence of on-Pathways and Off-Pathways and Functional Adaptation of Receptive-Field Organization in Cat Area 17. *Prog Brain Res* 95: 191-205
- Sillito AM. 1975. The contribution of inhibitory mechanisms to the receptive field properties of neurones in the striate cortex of the cat. *The Journal of physiology* 250: 305-329
- Simons DJ. 1978. Response Properties of Vibrissa Units in Rat Si Somatosensory Neocortex. *J. Neurophysiol.* 41: 798-820
- Sincich LC, Horton JC. 2002. Pale cytochrome oxidase stripes in V2 receive the richest projection from macaque striate cortex. *J. Comp. Neurol.* 447: 18-33
- Singer W, Tretter F, Cynader M. 1975. Organization of Cat Striate Cortex - Correlation of Receptive-Field Properties with Afferent and Efferent Connections. *J. Neurophysiol.* 38: 1080-1098
- Skottun BC, Bradley A, Sclar G, Ohzawa I, Freeman RD. 1987. The Effects of Contrast on Visual Orientation and Spatial-Frequency Discrimination - a Comparison of Single Cells and Behavior. *J. Neurophysiol.* 57: 773-786
- Skottun BC, De Valois RL, Grosof DH, Movshon JA, Albrecht DG, Bonds AB. 1991. Classifying simple and complex cells on the basis of response modulation. *Vision Res.* 31: 1079-1086
- Smith EL, Chino YM, Ridder WH, Kitagawa K, Langston A. 1990. Orientation Bias of Neurons in the Lateral Geniculate-Nucleus of Macaque Monkeys. *Visual Neurosci* 5: 525-545
- Smith SL, Hausser M. 2010. Parallel processing of visual space by neighboring neurons in mouse visual cortex. *Nat Neurosci* 13: 1144-1149
- So YT, Shapley R. 1979. Spatial Properties of X-Cells and Y-Cells in the Lateral Geniculate-Nucleus of the Cat and Conduction Velocities of Their Inputs. *Exp. Brain Res.* 36: 533-550
- Sobotta J. 1903. Atlas and Epitome of Human Histology and Microscopic Anatomy. pp. 104. Public Domain US.

- Sohya K, Kameyama K, Yanagawa Y, Obata K, Tsumoto T. 2007. GABAergic neurons are less selective to stimulus orientation than excitatory neurons in layer II/III of visual cortex, as revealed by *in vivo* functional Ca²⁺ imaging in transgenic mice. *J Neurosci* 27: 2145-2149
- Somers DC, Nelson SB, Sur M. 1995. An Emergent Model of Orientation Selectivity in Cat Visual Cortical Simple Cells. *J Neurosci*. 15: 5448-5465
- Somogyi P, Tamas G, Lujan R, Buhl EH. 1998. Salient features of synaptic organisation in the cerebral cortex. *Brain Res Rev* 26: 113-135
- Sompolinsky H, Shapley R. 1997. New perspectives on the mechanisms for orientation selectivity. *Curr. Opin. Neurobiol.* 7: 514-522
- Spitzer H, Hochstein S. 1987. Visual Receptive-Fields of Cat Cortical Neurons Lack the Distinctive Geniculate Y-Cell Signature. *Israel J Med Sci* 23: 69-74
- Spitzer H, Hochstein S. 1988. Complex-Cell Receptive-Field Models. *Prog Neurobiol* 31: 285-309
- Stone J, Dreher B, Leventhal A. 1979. Hierarchical and Parallel Mechanisms in the Organization of Visual-Cortex. *Brain Res Rev* 1: 345-394
- Stroud AC, LeDue EE, Crowder NA. 2012. Orientation specificity of contrast adaptation in mouse primary visual cortex. *J Neurophysiol*. 108: 1381-1391
- Sur M, Sherman SM. 1982. Linear and Non-Linear W-Cells in C-Laminae of the Cats Lateral Geniculate-Nucleus. *J. Neurophysiol.* 47: 869-884
- Swadlow HA. 2003. Fast-spike interneurons and feedforward inhibition in awake sensory neocortex. *Cereb. Cortex* 13: 25-32
- Szel A, Rohlich P, Miezwieska K, Aguirre G, Vanveen T. 1993. Spatial and Temporal Differences between the Expression of Short-Wave and Middle-Wave Sensitive Cone Pigments in the Mouse Retina - a Developmental-Study. *J. Comp. Neurol.* 331: 564-577
- Tadmor Y, Tolhurst DJ. 2000. Calculating the contrasts that retinal ganglion cells and LGN neurones encounter in natural scenes. *Vision Res.* 40: 3145-3157
- Tamamaki N, Yanagawa Y, Tomioka R, Miyazaki J, Obata K, Kaneko T. 2003. Green fluorescent protein expression and colocalization with calretinin, parvalbumin, and somatostatin in the GAD67-GFP knock-in mouse. *J Comp Neurol* 467: 60-79
- Tan AY, Brown BD, Scholl B, Mohanty D, Priebe NJ. 2011. Orientation selectivity of synaptic input to neurons in mouse and cat primary visual cortex. *J Neurosci* 31: 12339-12350
- Tanaka K. 1983. Cross-Correlation Analysis of Geniculostriate Neuronal Relationships in Cats. *J. Neurophysiol.* 49: 1303-1318
- Tanaka K. 1985. Organization of Geniculate Inputs to Visual Cortical-

- Cells in the Cat. *Vision Res.* 25: 357-364
- Taniguchi H, He M, Wu P, Kim S, Paik R, et al. 2011. A resource of Cre driver lines for genetic targeting of GABAergic neurons in cerebral cortex. *Neuron* 71: 995-1013
- Tao L, Shelley M, McLaughlin D, Shapley R. 2004. An egalitarian network model for the emergence of simple and complex cells in visual cortex. *Proc Natl Acad Sci U S A* 101: 366-371
- Teich AF, Qian N. 2006. Comparison among some models of orientation selectivity. *J. Neurophysiol.* 96: 404-419
- Thomson AM, West DC, Wang Y, Bannister AP. 2002. Synaptic connections and small circuits involving excitatory and inhibitory neurons in layers 2-5 of adult rat and cat neocortex: Triple intracellular recordings and biocytin labelling in vitro. *Cereb. Cortex* 12: 936-953
- Tinsley CJ, Webb BS, Barraclough NE, Vincent CJ, Parker A, Derrington AM. 2003. The nature of V1 neural responses to 2D moving patterns depends on receptive-field structure in the marmoset monkey. *J. Neurophysiol.* 90: 930-937
- Tolhurst DJ, Dean AF. 1990. The Effects of Contrast on the Linearity of Spatial Summation of Simple Cells in the Cats Striate Cortex. *Exp. Brain Res.* 79: 582-588
- Tretter F, Cynader M, Singer W. 1975. Cat Parastriate Cortex - Primary or Secondary Visual Area. *J. Neurophysiol.* 38: 1099-1113
- Troyer TW, Krukowski AE, Priebe NJ, Miller KD. 1998. Contrast-invariant orientation tuning in cat visual cortex: Thalamocortical input tuning and correlation-based intracortical connectivity. *J. Neurosci.* 18: 5908-5927
- Tsumoto T, Eckart W, Creutzfeldt OD. 1979. Modification of Orientation Sensitivity of Cat Visual-Cortex Neurons by Removal of Gaba-Mediated Inhibition. *Exp. Brain Res.* 34: 351-363
- Umino Y, Solessio E, Barlow RB. 2008. Speed, spatial, and temporal tuning of rod and cone vision in mouse. *The Journal of neuroscience : the official journal of the Society for Neuroscience* 28: 189-198
- Usrey WM, Reid RC. 2000. Visual physiology of the lateral geniculate nucleus in two species of New World monkey: Saimiri sciureus and Aotus trivirgatus. *J. Physiol.-London* 523: 755-769
- Vaiceliunaite A, Eriskens S, Franzen F, Katzner S, Busse L. 2013. Spatial integration in mouse primary visual cortex. *J. Neurophysiol.* 110: 964-972
- Van den Bergh G, Zhang B, Arckens L, Chino YM. 2010. Receptive-field properties of V1 and V2 neurons in mice and macaque monkeys. *The Journal of comparative neurology* 518: 2051-2070
- Van Hooser SD. 2007. Similarity and diversity in visual cortex: is there a unifying theory of cortical computation? *Neuroscientist* 13: 639-656
- Van Hooser SD, Heimel JA, Chung S, Nelson SB, Toth LJ. 2005. Orientation selectivity without orientation maps

- in visual cortex of a highly visual mammal. *The Journal of neuroscience : the official journal of the Society for Neuroscience* 25: 19-28
- Van Hooser SD, Heimel JAF, Nelson SB. 2003. Receptive field properties and laminar organization of lateral geniculate nucleus in the gray squirrel (*Sciurus carolinensis*). *J. Neurophysiol.* 90: 3398-3418
- Van Hooser SD, Nelson SB. 2006. The squirrel as a rodent model of the human visual system. *Visual Neurosci* 23: 765-778
- van Kleef JP, Cloherty SL, Ibbotson MR. 2010. Complex cell receptive fields: evidence for a hierarchical mechanism. *J Physiol* 588: 3457-3470
- Veit J, Bhattacharyya A, Kretz R, Rainer G. 2014. On the Relation Between Receptive Field Structure and Stimulus Selectivity in the Tree Shrew Primary Visual Cortex. *Cereb. Cortex* 24: 2761-2771
- Vidyasagar TR, Urbas JV. 1982. Orientation Sensitivity of Cat Lgn Neurons with and without Inputs from Visual Cortical Area-17 and Area-18. *Exp. Brain Res.* 46: 157-169
- Vigneswaran G, Kraskov A, Lemon RN. 2011. Large Identified Pyramidal Cells in Macaque Motor and Premotor Cortex Exhibit "Thin Spikes": Implications for Cell Type Classification. *J. Neurosci.* 31: 14235-14242
- Volgyi B, Chheda S, Bloomfield SA. 2009. Tracer Coupling Patterns of the Ganglion Cell Subtypes in the Mouse Retina. *J. Comp. Neurol.* 512: 664-687
- Vu TQ, McCarthy ST, Owen WG. 1997. Linear transduction of natural stimuli by dark-adapted and light-adapted rods of the salamander, *Ambystoma tigrinum*. *J. Physiol.-London* 505: 193-204
- Wagor E, Mangini NJ, Pearlman AL. 1980. Retinotopic Organisation of Striate and Extrastriate Visual-Cortex in the Mouse. *J. Comp. Neurol.* 193: 187-202
- Wang KH, Majewska A, Schummers J, Farley B, Hu CC, et al. 2006. In vivo two-photon imaging reveals a role of arc in enhancing orientation specificity in visual cortex. *Cell* 126: 389-402
- Wang QX, Burkhalter A. 2007. Area map of mouse visual cortex. *J. Comp. Neurol.* 502: 339-357
- Wang Y, Gupta A, Toledo-Rodriguez M, Wu CZ, Markram H. 2002. Anatomical, physiological, molecular and circuit properties of nest basket cells in the developing somatosensory cortex. *Cereb. Cortex* 12: 395-410
- Wang Y, Toledo-Rodriguez M, Gupta A, Wu CZ, Silberberg G, et al. 2004. Anatomical, physiological and molecular properties of Martinotti cells in the somatosensory cortex of the juvenile rat. *J. Physiol.-London* 561: 65-90
- Wassle H. 2004. Parallel processing in the mammalian retina. *Nature Reviews Neuroscience* 5: 747-757
- Waters J, Larkum M, Sakmann B, Helmchen F. 2003. Supralinear Ca²⁺ influx into dendritic tufts of layer 2/3 neocortical pyramidal neurons in vitro and in vivo. *J. Neurosci.* 23: 8558-8567

- Webb BS, Tinsley CJ, Barraclough NE, Easton A, Parker A, Derrington AM. 2002. Feedback from V1 and inhibition from beyond the classical receptive field modulates the responses of neurons in the primate lateral geniculate nucleus. *Visual Neurosci* 19: 583-592
- Welagen J, Anderson S. 2011. Origins of Neocortical Interneurons in Mice. *Dev Neurobiol* 71: 10-17
- Weliky M, Bosking WH, Fitzpatrick D. 1996. A systematic map of direction preference in primary visual cortex. *Nature* 379: 725-728
- White AJR, Solomon SG, Martin PR. 2001. Spatial properties of koniocellular cells in the lateral geniculate nucleus of the marmoset *Callithrix jacchus*. *J. Physiol.-London* 533: 519-535
- White EL. 1989. Cortical Circuits. Synaptic Organisation of the Cerebral Cortex. Birkhauser, Boston.
- Wielbaard DJ, Shelley M, McLaughlin D, Shapley R. 2001. How simple cells are made in a nonlinear network model of the visual cortex. *J. Neurosci.* 21: 5203-5211
- Williams PE, Shapley RM. 2007. A dynamic nonlinearity and spatial phase specificity in macaque V1 neurons. *J. Neurosci.* 27: 5706-5718
- Winkler C, Potter A. 1914. An anatomical guide to experimental researches on the cat's brain. Amsterdam, W. Versluys.
- Woodruff A, Xu Q, Anderson SA, Yuste R. 2009. Depolarizing effect of neocortical chandelier neurons. *Front. Neural Circuits* 3, article number 15
- Woodruff A, Yuste R. 2008. Of mice and men, and chandeliers. *Plos Biol* 6: 1833-1836
- Xu XM, Callaway EM. 2009. Laminar Specificity of Functional Input to Distinct Types of Inhibitory Cortical Neurons. *J. Neurosci.* 29: 70-85
- Xu XM, Ichida JM, Allison JD, Boyd JD, Bonds AB, Casagrande VA. 2001. A comparison of koniocellular, magnocellular and parvocellular receptive field properties in the lateral geniculate nucleus of the owl monkey (*Aotus trivirgatus*). *J. Physiol.-London* 531: 203-218
- Zaitsev AV, Gonzalez-Burgos G, Povysheva NV, Kroner S, Lewis DA, Krimer LS. 2005. Localization of calcium-binding proteins in physiologically and morphologically characterized interneurons of monkey dorsolateral prefrontal cortex. *Cereb. Cortex* 15: 1178-1186
- Zaitsev AV, Povysheva NV, Gonzalez-Burgos G, Rotaru D, Fish KN, et al. 2009. Interneuron Diversity in Layers 2-3 of Monkey Prefrontal Cortex. *Cereb. Cortex* 19: 1597-1615
- Zariwala HA, Madisen L, Ahrens KF, Bernard A, Lein ES, et al. 2011. Visual tuning properties of genetically identified layer 2/3 neuronal types in the primary visual cortex of cre-transgenic mice. *Front Syst Neurosci* 4: article number 162
- Zhao XY, Chen H, Liu XR, Cang JH. 2013. Orientation-selective Responses in the Mouse Lateral Geniculate Nucleus. *J. Neurosci.* 33: 12751-12763
- Zhou FM, Hablitz JJ. 1996a. Layer I neurons of rat neocortex .1. Action potential and repetitive firing

properties. *J. Neurophysiol.* 76: 651-667

Zhou FM, Hablitz JJ. 1996b. Morphological properties of intracellularly labeled layer I neurons in rat neocortex. *J. Comp. Neurol.* 376: 198-213

Zhu W, Shelley M, Shapley R. 2009. A neuronal network model of primary visual cortex explains spatial frequency selectivity. *J Comput Neurosci* 26: 271-287

Zhuang J, Stoelzel CR, Bereshpolova Y, Huff JM, Hei XJ, et al. 2013. Layer 4 in Primary Visual Cortex of the Awake Rabbit: Contrasting Properties of Simple Cells and Putative Feedforward Inhibitory Interneurons. *J. Neurosci.* 33: 11372-11389